BRIDGING THE GAP BEFORE AND AFTER BIRTH: METHODS AND TECHNOLOGIES TO EXPLORE THE FUNCTIONAL NEURAL DEVELOPMENT IN HUMANS

EDITED BY: Marika Berchicci and Silvia Comani

PUBLISHED IN: Frontiers in Human Neuroscience

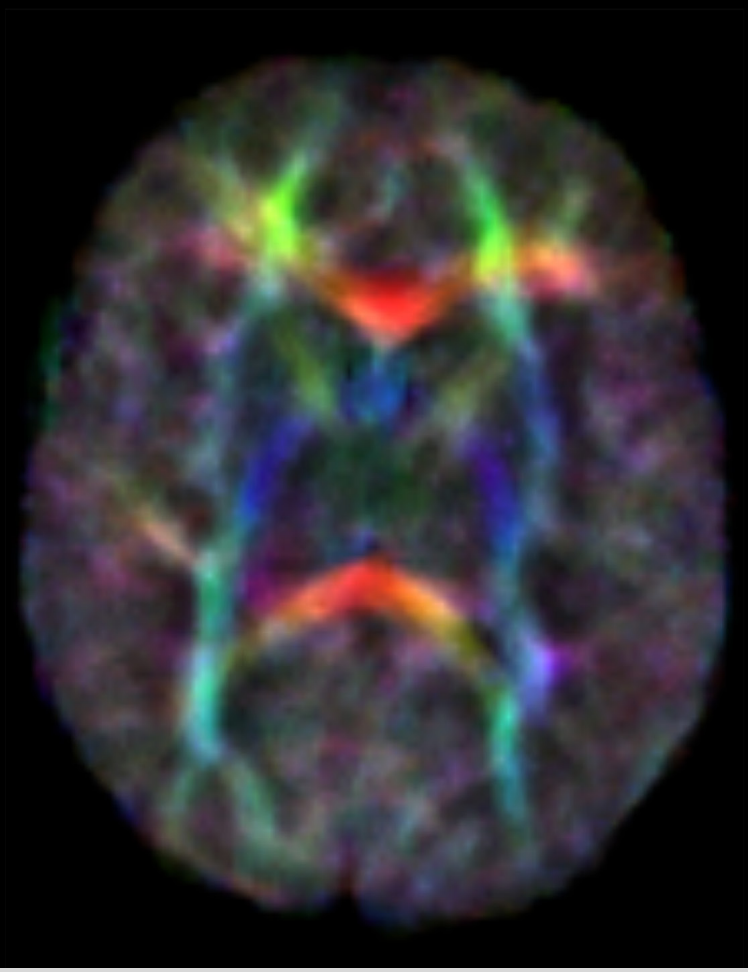

frontiers Research Topics

frontiers

ISSN 1664-8714
ISBN 978-2-88919-687-6
DOI 10.3389/978-2-88919-687-6

About Frontiers

Frontiers is more than just an open-access publisher of scholarly articles: it is a pioneering approach to the world of academia, radically improving the way scholarly research is managed. The grand vision of Frontiers is a world where all people have an equal opportunity to seek, share and generate knowledge. Frontiers provides immediate and permanent online open access to all its publications, but this alone is not enough to realize our grand goals.

Frontiers Journal Series

The Frontiers Journal Series is a multi-tier and interdisciplinary set of open-access, online journals, promising a paradigm shift from the current review, selection and dissemination processes in academic publishing. All Frontiers journals are driven by researchers for researchers; therefore, they constitute a service to the scholarly community. At the same time, the Frontiers Journal Series operates on a revolutionary invention, the tiered publishing system, initially addressing specific communities of scholars, and gradually climbing up to broader public understanding, thus serving the interests of the lay society, too.

Dedication to Quality

Each Frontiers article is a landmark of the highest quality, thanks to genuinely collaborative interactions between authors and review editors, who include some of the world's best academicians. Research must be certified by peers before entering a stream of knowledge that may eventually reach the public - and shape society; therefore, Frontiers only applies the most rigorous and unbiased reviews.

Frontiers revolutionizes research publishing by freely delivering the most outstanding research, evaluated with no bias from both the academic and social point of view.

By applying the most advanced information technologies, Frontiers is catapulting scholarly publishing into a new generation.

What are Frontiers Research Topics?

Frontiers Research Topics are very popular trademarks of the Frontiers Journals Series: they are collections of at least ten articles, all centered on a particular subject. With their unique mix of varied contributions from Original Research to Review Articles, Frontiers Research Topics unify the most influential researchers, the latest key findings and historical advances in a hot research area! Find out more on how to host your own Frontiers Research Topic or contribute to one as an author by contacting the Frontiers Editorial Office: **researchtopics@frontiersin.org**

BRIDGING THE GAP BEFORE AND AFTER BIRTH: METHODS AND TECHNOLOGIES TO EXPLORE THE FUNCTIONAL NEURAL DEVELOPMENT IN HUMANS

Topic Editors:
Marika Berchicci, University of Rome "Foro Italico", Italy
Silvia Comani, University "G. d'Annunzio" of Chieti-Pescara, Italy

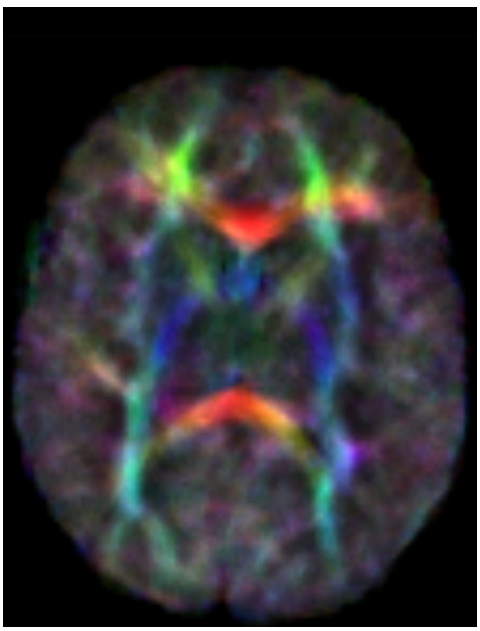

Color map of neonatal brain obtained with Diffusion Tensor Imaging (DTI)

Image taken from: Giampietri M, Bartalena L, Guzzetta A, Boldrini A and Ghirri P (2015) New techniques in the study of the brain development in newborn. Front. Hum. Neurosci. 8:1069. doi: 10.3389/fnhum.2014.01069

Infant brain damage is a serious condition that affects millions of babies each year. The period from late gestation to the first year of life is the most critical one for the development of central and autonomous nervous systems. Medical conditions such as preterm birth may compromise brain function and the end result usually is that the baby may experience long-term neurological problems related to a wide range of psychological, physical and functional complications, with consequent life-long burdens for the individuals and their families, and a high socio-economic impact for the health care system and the whole of society.

During the last years, several techniques have been employed to monitor the brain functional development in utero and after birth. As well, various analytical methods have been used to understand the functional maturation of the brain and the autonomous nervous system. However, in spite of the rapid improvement of diagnostic methods and procedures, there is still a widely recognized, severe shortage of clinically viable means for the high quality monitoring of the brain function in early life with a direct relevance to acute neurological illness and future neurocognitive outcomes.

The studies collected in this e-book document the most recent advancements in monitoring systems, analytical methods and clinical diagnostic procedures that contribute to increase our knowledge of the functional development of the human brain and autonomous nervous system during pregnancy and after birth, with the ultimate goal of reducing fetal impairment and improving healthcare in the neonatal and infant period.

Citation: Berchicci, M., Comani, S., eds. (2015). Bridging the Gap Before and After Birth: Methods and Technologies to Explore the Functional Neural Development in Humans. Lausanne: Frontiers Media. doi: 10.3389/978-2-88919-687-6

Table of Contents

frontiers in Human Neuroscience

EDITORIAL
published: 14 October 2015
doi: 10.3389/fnhum.2015.00571

Editorial: Bridging the gap before and after birth: methods and technologies to explore the functional neural development in humans

Marika Berchicci[1, 2] *and Silvia Comani*[1, 3, 4]*

[1] BIND - Behavioral Imaging and Neural Dynamics Center, University "G. d'Annunzio" of Chieti-Pescara, Chieti, Italy, [2] Department of Human Movement, Social and Health Sciences, University of Rome "Foro Italico," Rome, Italy, [3] Department of Neuroscience, Imaging and Clinical Sciences, University "G. d'Annunzio" of Chieti-Pescara, Chieti, Italy, [4] Casa di Cura Privata Villa Serena, Città Sant'Angelo, Italy

Keywords: fetus, infant, neuroimaging, brain development, autonomous nervous system, fetal heart rate

Early human development from late gestation to the neonatal period is a critical time in the individual's life span. Preterm birth or medical issues affecting the brain function during late gestation or the first months of life may lead to an avalanche of neurodevelopmental problems, including cognitive deficits and motor disability, with lifelong consequences for the individuals, their families, the health care system and the society (de Kieviet et al., 2012; March of Dimes, PMNCH, Save the Children, WHO, 2012). Despite the need for the alleviation of perinatal adversities, effective monitoring methods and clinical diagnostic procedures able to reduce fetal impairment and advance neonatal and infant healthcare are still missing.

The focus of this E-Book is on the most recent developments and findings in the field of non-invasive monitoring of the central and autonomous nervous systems in fetuses and infants. The contributed opinion, review and original research articles included in this E-Book cover different methodological, clinical, functional, and structural topics, with the purpose to disseminate the knowledge on novel perinatal diagnostic tools and procedures, and to share the findings of high quality functional assessment of the developing human brain, and of clinical studies on pathological neurodevelopment.

The fundamental requirement for a healthy functional development of the brain is the maintenance of an adequate blood flow and oxygenation. Inadequate brain perfusion is the main cause of preterm brain damage, which can be diagnosed by high-frequency ultrasound. Camfferman et al. (2015) performed an *in vitro* experiment using a microvessel flow phantom designed to mimic preterm cerebral perfusion and assess blood flow velocity. Their flow phantom allowed the visualization of the vessels, but flow velocity and vessel diameter were overestimated. Therefore, the authors solicited the development of a sonographic tool for clinical practice to study regional perfusion in preterm babies.

Conversely, fetal magnetocardiography (fMCG) is a well-established diagnostic tool for fetal surveillance. Two original research papers describe the findings of studies performed with fMCG to estimate the development of the autonomic nervous system. It is known that, around 32 weeks of gestation, four fetal behavioral states (quiet and active sleep and awakeness) can be identified by combining fetal heart rate variability (fHRV) and fetal movements. Brändle et al. (2015) confirmed these results in 55 fetuses and also showed that only quiescence and active awakeness can be found in fetuses younger than 32 weeks, respectively in the 58.5 and 41.5% of cases. Therefore, fHRV parameters can differentiate fetal behavioral states at different ages and can show the neurovegetative modulation of each state, thus offering new insights into the vegetative development *in utero*. On the other hand, Hoyer et al. (2014) proved that the use of the fMCG

Edited and reviewed by:
Srikantan S. Nagarajan, University of California, USA

***Correspondence:**
Silvia Comani
comani@unich.it

Received: *06 July 2015*
Accepted: *28 September 2015*
Published: *14 October 2015*

Citation:
Berchicci M and Comani S (2015) Editorial: Bridging the gap before and after birth: methods and technologies to explore the functional neural development in humans. Front. Hum. Neurosci. 9:571. doi: 10.3389/fnhum.2015.00571

based fetal Autonomic Brain Age Score (fABAS) may help estimating the fetal autonomic brain age, suggesting that the establishment of a fABAS score normogram is needed.

To understand the normal functional development of the fetal brain, periods of developmental vulnerability should be identified to assess the function of the fetal nervous system and open a window on novel prenatal diagnostics and prognostics. MRI has become increasingly feasible and clinically important in fetal brain studies due to its higher tissue resolution and better visualization of normal and pathological development of macroscopic anatomy or white matter microstructure and connections. Jakab et al. (2014) employed resting-state MRI (rsMRI) in 32 fetuses with no detectable morphological abnormalities to investigate the developmental changes in the functional connectivity architecture. They demonstrated that the short-range and interhemispheric connections show a sigmoid development peaking at around 26–29 gestational weeks, whereas long-range connections do not show any peak. They also observed an increasing region-specific functional connectivity from 24 to 28 gestational weeks, starting with the occipital and ending with the parietal cortex. Schöpf et al. (2014) used the same method to investigate the relationship between eye movements and brain functional activity in seven fetuses. The emergence of the visuomotor system involves the relationship of intrinsic and extrinsic components supposed to shape the subsequent development of perception. Schöpf and colleagues showed that spontaneous fetal eye movements are linked to the simultaneous networks in visual and frontal brain regions, demonstrating that the preparation of the human visuomotor system links visual and motor areas already *in utero*.

Despite the advancements in monitoring techniques and perinatal care, clinicians still have limited means to predict neurodevelopmental outcomes and plan early intervention. In their opinion article, Giampietri et al. (2015) offer a succinct and clear overview of the non-invasive techniques actually employed. The authors focused on the neonatal application of magnetic resonance imaging (MRI), claiming that, although its low predictive power, advanced MRI techniques such as diffusion tensor imaging (DTI) or spectrography could be useful in anticipating the diagnosis of brain damage and should become part of standard clinical care. The recent advances in diffusion MRI (dMRI) have also a great potential for a better understanding of neuronal connectivity impairments in preterm babies, as brilliantly exposed by Dudink et al. (2015) in their review article, or in revealing structural connectivity changes in infants and toddlers with autism spectrum disorder (ASD), as discussed by Conti et al. (2015) in their review article, suggesting a shift from hyper- to hypo-connectivity at around 3 years of age.

The development of functional connectivity patterns from infancy to childhood were studied also by Berchicci et al. (2015), who investigated the intrahemispheric properties of the sensorimotor system from 3 to 60 months of life using a prototypal magnetoencephalographic (MEG) system. In line with prior findings on the development of the adult fronto-parietal network for adaptive online task control, which involves both segregation and integration, the authors showed that this network, which provides a neurophysiological basis for the action-perception coupling, evolved with age from a more random to an adult small-world organization, more efficient for both local and global information processing. Another study regarding the development of the infant motor and motivation systems was conducted by Moon et al. (2015), who designed a contingent sucking preference study to test neonatal motivation to the mother or an unfamiliar female. Although difficult to demonstrate, electrophysiological studies showed that newborns use prenatal experiences and the motivational system to produce responses to familiar sounds. The authors demonstrated a weak neonate's contingent sucking response to the maternal voice, which was ascribed to insufficient neonates' motivation to alter their behavior, therefore pointing to the complementary value of electrophysiological and behavioral studies for very early development.

Finally, electroencephalography (EEG) is the most commonly used technique to non-invasively assess neonatal brain activity, but the main challenge in interpreting EEG signals is the quantitative characterization of the spontaneous "background activity" in sick neonates. Matic et al. (2015) applied multifactorial detrended fluctuation analysis (MF-DFA) to long-term EEG from 34 asphyxiated neonates to distinguish different grades of abnormality in EEG background activity, which could help monitoring the brain state changes occurring during long periods of time. The EEG from a normal developing neonate also presents specific characteristics. Koolen et al. (2014) used the interhemispheric synchrony (HIS) and the activation synchrony index (ASI) to analyze EEG traces from normal and abnormal neonates, and found these measures promising for diagnostic and clinical purposes. In particular, the ASI was able to correctly distinguish between normal and abnormal neonates in the 97% of cases.

REFERENCES

Berchicci, M., Tamburro, G., and Comani, S. (2015). The intrahemispheric functional properties of the developing sensorimotor cortex are influenced by maturation. *Front. Hum. Neurosci.* 9:39. doi: 10.3389/fnhum.2015.00039

Brändle, J., Preissl, H., Draganova, R., Ortiz, E., Kagan, K. O., Abele, H., et al. (2015). Heart rate variability parameters and fetal movement complement fetal behavioral states detection via magnetography to monitor neurovegetative development. *Front. Hum. Neurosci.* 9:147. doi: 10.3389/fnhum.2015.00147

Camfferman, F. A., Ecury-Goossen, G. M., La Roche, J. E., de Jong, N., van't Leven, W., Vos, H. J., et al. (2015). Calibrating Doppler imaging of preterm intracerebral circulation using a microvessel flow phantom. *Front. Hum. Neurosci.* 8:1068. doi: 10.3389/fnhum.2014.01068

Conti, E., Calderoni, S., Marchi, V., Muratori, F., Cioni, G., and Guzzetta, A. (2015). The first 1000 days of the autistic brain: a systematic review of diffusion imaging studies. *Front. Hum. Neurosci.* 9:159. doi: 10.3389/fnhum.2015.00159

de Kieviet, J. F., Zoetebier, L., van Elburg, R. M., Vermeulen, R. J., and Oosterlaan, J. (2012). Brain development of very preterm and very

low-birthweight children in childhood and adolescence: a meta-analysis. *Dev. Med. Child Neurol.* 54, 313–323. doi: 10.1111/j.1469-8749.2011.04216.x

Dudink, J., Pieterman, K., Leemans, A., Kleinnijenhuis, M., van Cappellen van Walsum, A. M., and Hoebeek, F. E. (2015). Recent advancements in diffusion MRI for investigating cortical development after preterm birth - potential and pitfalls. *Front. Hum. Neurosci.* 8:1066. doi: 10.3389/fnhum.2014.01066

Giampietri, M., Bartalena, L., Guzzetta, A., Boldrini, A., and Ghirri, P. (2015). New techniques in the study of the brain development in newborn. *Front. Hum. Neurosci.* 8:1069. doi: 10.3389/fnhum.2014.01069

Hoyer, D., Kowalski, E. M., Schmidt, A., Tetschke, F., Nowack, S., Rudolph, A., et al. (2014). Fetal autonomic brain age scores, segmented heart rate variability analysis, and traditional short term variability. *Front. Hum. Neurosci.* 8:948. doi: 10.3389/fnhum.2014.00948

Jakab, A., Schwartz, E., Kasprian, G., Gruber, G. M., Prayer, D., Schöpf, V., et al. (2014). Fetal functional imaging portrays heterogeneous development of emerging human brain networks. *Front. Hum. Neurosci.* 8:852. doi: 10.3389/fnhum.2014.00852

Koolen, N., Dereymaeker, A., Räsänen, O., Jansen, K., Vervisch, J., Matic, V., et al. (2014). Interhemispheric synchrony in the neonatal EEG revisited: activation synchrony index as a promising classifier. *Front. Hum. Neurosci.* 8:1030. doi: 10.3389/fnhum.2014.01030

March of Dimes, PMNCH, Save the Children, WHO. (2012). *Born Too Soon: The Global Action Report on Preterm Birth*. eds C. P. Howson, M. V. Kinney, and J. E. Lawn. (Geneva: World Health Organization).

Matic, V., Cherian, P. J., Koolen, N., Ansari, A. H., Naulaers, G., Govaert, P., et al. (2015). Objective differentiation of neonatal EEG background grades using detrended fluctuation analysis. *Front. Hum. Neurosci.* 9:189. doi: 10.3389/fnhum.2015.00189

Moon, C., Zernzach, R. C., and Kuhl, P. K. (2015). Mothers say "baby" and their newborns do not choose to listen: a behavioral preference study to compare with ERP results. *Front. Hum. Neurosci.* 9:153. doi: 10.3389/fnhum.2015.00153

Schöpf, V., Schlegl, T., Jakab, A., Kasprian, G., Woitek, R., Prayer, D., et al. (2014). The relationship between eye movement and vision develops before birth. *Front. Hum. Neurosci.* 8:775. doi: 10.3389/fnhum.2014.00775

Conflict of Interest Statement: The authors declare that the research was conducted in the absence of any commercial or financial relationships that could be construed as a potential conflict of interest.

frontiers in
HUMAN NEUROSCIENCE

ORIGINAL RESEARCH ARTICLE
published: 13 January 2015
doi: 10.3389/fnhum.2014.01068

Calibrating Doppler imaging of preterm intracerebral circulation using a microvessel flow phantom

Fleur A. Camfferman[1], Ginette M. Ecury-Goossen[2], Jhuresy E. La Roche[2], Nico de Jong[3,4], Willem van 't Leven[3], Hendrik J. Vos[3,4], Martin D. Verweij[4], Kazem Nasserinejad[5], Filip Cools[1], Paul Govaert[1,2] and Jeroen Dudink[2,6]*

[1] *Department of Neonatology, Universitair Ziekenhuis Brussel, Vrije Universiteit Brussel, Brussels, Belgium*
[2] *Department of Neonatology, Erasmus Medical Centre, Rotterdam, Netherlands*
[3] *Department of Biomedical Engineering, Erasmus Medical Centre, Rotterdam, Netherlands*
[4] *Department of Imaging Physics, Delft University of Technology, Delft, Netherlands*
[5] *Department of Biostatistics, Erasmus Medical Centre, Rotterdam, Netherlands*
[6] *Department of Radiology, Erasmus Medical Centre, Rotterdam, Netherlands*

Edited by:
Silvia Comani, Università degli Studi G. D'Annunzio, Italy

Reviewed by:
Narendra Reddy Dereddy, Maria Fareri Children's Hospital at Westchester Medical Center, USA
Gordon Niall Stevenson, National Health Service, UK

****Correspondence:***
Jeroen Dudink, Erasmus Medical Center, Sophia Children's Hospital, Dr. Molewaterplein 60, Rotterdam 3015 GJ, Netherlands
e-mail: j.dudink@erasmusmc.nl

Introduction: Preterm infants are born during critical stages of brain development, in which the adaptive capacity of the fetus to extra-uterine environment is limited. Inadequate brain perfusion has been directly linked to preterm brain damage. Advanced high-frequency ultrasound probes and processing algorithms allow visualization of microvessels and depiction of regional variation. To assess whether visualization and flow velocity estimates of preterm cerebral perfusion using Doppler techniques are accurate, we conducted an *in vitro* experiment using a microvessel flow phantom.

Materials and Methods: An in-house developed flow phantom containing two microvessels (inner diameter 200 and 700 μm) with attached syringe pumps, filled with blood-mimicking fluid, was used to generate non-pulsatile perfusion of variable flow. Measurements were performed using an Esaote MyLab70 scanner.

Results: Microvessel mimicking catheters with velocities as low as 1 cm/s were adequately visualized with a linear ultrasound probe. With a convex probe, velocities <2 cm/s could not be depicted. Within settings, velocity and diameter measurements were highly reproducible [intra-class correlation 0.997 (95% CI 0.996–0.998) and 0.914 (0.864–0.946)]. Overall, mean velocity was overestimated up to threefold, especially in high velocity ranges. Significant differences were seen in velocity measurements when using steer angle correction and in vessel diameter estimation ($p < 0.05$).

Conclusion: Visualization of microvessel-size catheters mimicking small brain vessels is feasible. Reproducible velocity and diameter results can be obtained, although important overestimation of the values is observed. Before velocity estimates of microcirculation can find its use in clinical practice, calibration of the ultrasound machine for any specific Doppler purpose is essential. The ultimate goal is to develop a sonographic tool that can be used for objective study of regional perfusion in routine practice.

Keywords: preterm brain, cerebral circulation, cerebral perfusion, microcirculation, flow phantom, calibration, cerebral blood flow, Doppler

INTRODUCTION

Central to normal human brain development and function is maintenance of adequate blood flow and oxygenation. This requires complex regulatory mechanisms, which at the early stages of human development exist in a vulnerable equilibrium and are notoriously difficult to monitor. Severe neonatal conditions, such as prematurity, birth trauma, infections, and congenital malformations, often compromise brain perfusion during this critical period of brain development and will grow into an avalanche of neurodevelopmental problems, including cognitive deficits, motor disability, and psychiatric diseases (Sherlock et al., 2005; Volpe, 2009) with ensuing lifelong burdens for the growing individuals and their families, and a major socio-economic impact for the health care system and the whole of society (Petrou et al., 2001).

Brain injury as a complication of preterm birth is directly or indirectly linked to low brain perfusion and oxygenation (Meek et al., 1999; Kissack et al., 2004). Although little is known about the ability of the preterm to regulate cerebral blood flow (CBF) in

Abbreviations: BMF, blood-mimicking fluid; CBF, cerebral blood flow; CD, color Doppler; ICC, intra-class correlation; ICV, internal cerebral vein; NIRS, near-infrared spectroscopy; PD, power Doppler; PI, pulsatility index; PRC, processing; PRF, pulse repetition frequency; PRS, persistence; PW, pulsed wave; PWD, pulsed wave Doppler; RI, resistance index.

response to changes in perfusion pressure, there is some evidence that the autoregulatory range is limited compared with that of adults and absent in sick infants (Greisen, 2005). Muscular walls are even absent in fragile medullary channels of the preterm brain, suggesting that some functional tools for autoregulation are not present yet (Kuban and Gilles, 1985). Consequently, extremes of systemic perfusion are transmitted unaltered to brain tissue. It is still a challenge to study neonatal organ and brain–blood perfusion systematically. A reliable, objective, repeatable, safe, and bedside method to characterize neonatal blood perfusion is needed.

Alternative methods to approximate blood flow, like blood pressure, diuresis, heart rate, and limb oxygen saturation are extensively used, but are notoriously poor surrogates of neonatal brain perfusion. Standard techniques for adult brain studies are undesirable or very difficult to apply in the neonate. CBF measured with radioactive Xenon or jugular occlusion plethysmography are disruptive to the infant and cannot be repeated frequently. MRI perfusion scans (such as arterial spin labeling) are not suited for (repeated) monitoring and require transport of often critically ill and clinically unstable infants to the radiology ward (Liem and Greisen, 2010). Now, tissue oxygen delivery can be studied using optical near-infrared spectroscopy (NIRS), a bedside and safe technique, which allows continuous monitoring. However, NIRS is not quantitative and only provides indirect information about blood flow in regions that cannot be precisely pinpointed. Although trends in CBF may be inferred from changes in cerebral oxygenation and/or blood volume, NIRS does not allow a direct measure of CBF (van Bel et al., 2008; Marin and Moore, 2011).

EEG monitoring, like NIRS, is a safe and bedside neuro monitoring tool, which gained renewed interest of clinicians and researchers because of improved hardware and software in recent years. However, changes in EEG signal reflect large neuronal electrophysiological changes in a late and often irreversible stage of brain injury evolution (Hellström-Westas, 2006).

Brain ultrasound is a widely used non-invasive and bedside tool for evaluation of neonatal brain anatomy and detection of brain injury. Color Doppler (CD) has already found a limited application in the analysis of patent ductus arteriosus and birth asphyxia. Indices like pulsatility index and resistance index have been developed and used as proxies for flow (Pezzati et al., 2002; Basu et al., 2014). Recent advances in ultrasound technique have made visualization of small diameter vessels (microcirculation) possible (Macé et al., 2011). Yet, conventional pulsed wave Doppler (PWD) is regularly used for absolute flow velocity measurements. Triplex mode imaging is used in current daily practice, in which flow information is overlaid to an anatomical B-mode image, and absolute flow velocities are measured in the PW Doppler panel (WHO, 2011). Flow information is visualized either in CD or power Doppler (PD). In CD, the color indicates average velocity in the vessel, which is sensitive to the angle of the vessel. In PD, the color indicates the total amount of Doppler energy in the echo from the vessel, which is not sensitive to the angle. The general effect is that PD should be able to detect lower flow velocities and smaller vessels, at the cost of loss of quantitative velocity information. Moreover, the additional method of directional PD gives the PD, but estimates the direction of the flow and colors it subsequently.

Although there is no general consensus on the definition of "microcirculation" in the preterm brain, it is often defined as arteriolar and venular flow. Extrapolating from descriptions of vessel anatomy in fetuses, the diameter of microvessels visualized with Doppler in cerebral white matter of a preterm infant between 24 and 30 weeks is expected to be between 50 and 100 μm (Kuban and Gilles, 1985; Anstrom et al., 2004). The large arteries of the circle of Willis of 24-week-old fetuses have diameters around 400–500 μm (Vasovic et al., 2007). High-frequency linear probes permit visualization of vessels with a diameter below 200 μm. Therefore, visualization of the brain microcirculation of the preterm infant is feasible, making this a potential tool for *in vivo*, safe, bedside, repeatable measurement of CBF. Still, one of the challenges of ultrasound is that the vessel caliber cannot be accurately measured, so that flow cannot be estimated (Kehrer et al., 2003, 2005).

Models using a flow phantom and advanced (power) Doppler technique may be of use to objectively quantify regional flow variation. To mimic preterm brain tissue, this model should depict very small vessel sizes (about 200 μm) and very low flow (<2 cm/s).

As far as we know, no studies are reported to assess the accuracy of current PW, CD, and directional PD techniques in the visualization of microperfusion. Our aim was to evaluate if velocity measurements of microvessels are reproducible and accurate using sensitive modern ultrasound techniques. The second aim was to determine which Doppler technique (color versus PD, type of probe) is best used to visualize these small vessels. To this purpose, we set up an *in vitro* experiment using a microvessel flow phantom designed to mimic preterm cerebral perfusion. We hypothesized that current ultrasound technique is sufficiently accurate to estimate flow in preterm brain microvessels.

MATERIALS AND METHODS

MICROVESSEL FLOW PHANTOM

The flow phantom (**Figure 1**) consisted of an acrylic container filled with agar-based tissue-mimicking material, built according

FIGURE 1 | The test setting. Flow phantom with a fixed ultrasound probe. BMF, blood-mimicking fluid.

to Teirlinck et al. (1998). The tissue-mimicking material contained two vessels made of polyethylene terephthalate glycol-modified (Paradigm Optics, Vancouver, WA, USA) with an inner diameter of 200 μm each, and three silicone vessels (ERIKS bv, Alkmaar, the Netherlands) with an inner diameter of 700, 1000, and 2000 μm respectively. The blood-mimicking fluid (BMF) used to run through the vessels was based on the recipe by Ramnarine et al. (1998). However, our BMF contains half the amount of dextran and glycerol compared to the original recipe. This reduces the viscosity of the fluid, which is necessary to prevent blockage of the small vessels used in this study.

We intended to simulate the internal cerebral veins (ICV) and intracerebral medullary veins of very preterm infants using this microvessel flow phantom. Based on measurements performed in daily clinical practice, the distance from the anterior fontanel to the ICV is 2.5–5 cm, and intracerebral medullary veins are located at a depth of 2 cm. Blood flow velocity in the ICV is about 5 cm/s and in medullary veins this lies around 1 cm/s (Pfannschmidt and Jorch, 1989; Deeg and Lode, 2005). ICV diameter is estimated to be 500 μm in these neonates, while the diameter of the intracerebral medullary veins is around 100 μm (Kuban and Gilles, 1985). Since capillaries for the flow phantom with a diameter of 100 and 500 μm were not available, we used the 200 and 700 μm vessels for this study.

TEST SETTING

To generate steady flow through the capillaries, we used a calibrated syringe pump (Harvard Apparatus Pump 11 Elite, Instech Laboratories, Plymouth Meeting, USA) to infuse BMF at velocities ranging from 1 to 10 cm/s. This pump can produce regular flows as low as 1.28 pL/min. To calibrate the syringe pump, we calculated expected BMF volume based on pump speed and duration of the experiment and compared this with the volume of BMF collected at the flow phantom outlet. Recording time was started at the first drop.

For each vessel size, flow settings (microliter per second) were calculated according to the following equation:

$$Q = \left(V_{\text{avg}} \times \pi r^2\right) \times 10^9 \quad (1)$$

Q is flow in microliter per second, V_{avg} is average velocity in meter per second, and r is the radius of the vessel in meter.

Measurements were obtained using an Esaote system (Mylab 70, Genova, Italy) with a linear (Esaote LA 435 Linear Array Ultrasound Probe, 6.0–18.0 MHz) and convex probe (Esaote CA123 Convex Array Ultrasound Probe, 3.3–9.0 MHz). A standard ultrasound preset was used, identical to the preset used for imaging in daily clinical practice. This standard preset was optimized for neonatal preterm microvessel visualization prior to a large local prospective cohort study. The aim of that study was to explore the feasibility of CD for monitoring of cerebral perfusion in very preterm infants at the level of microvessels (unpublished data of Raets et al. – Preterm cerebral microcirculation assessed with color Doppler: a pilot study). According to Ten Cate et al. (2013), the Esaote Ultrasound machine, as used in this experiment, proved to be more suitable for microcirculation imaging in comparison to the other ultrasound brands. This is most probably mainly caused by fundamental differences in processing the Doppler signal or internal settings inaccessible to users. Settings used in this study are summarized in **Table 1**. For the linear probe, settings included a transmit frequency of 7.7 MHz in flow visualization and 5.9 MHz in PW Doppler, a gain of 50%, and an imaging depth of 30 mm. For the convex probe, settings included a transmit frequency of 5 MHz in flow visualization and 6.3 MHz in PW Doppler, a gain of 54%, and imaging depth of 76 mm. Thermal and mechanical indices were always kept below 1.0.

The syringe pump was set to generate non-pulsatile perfusion of predefined volumes for each of the vessels (see above). Using the convex and linear probes, peak flow velocity and diameter of the capillaries were measured at 2 cm depth. Detection and diameter sizing measurements were performed using CD and directional PD. To obtain diameter measurements, a Doppler image was frozen, and diameter was estimated using a manual caliber measurement. Velocity measurements were performed in the PW Doppler panel by manually putting a marker at the extreme bound of the PW profile. Since the flow was non-pulsatile, this extreme bound was persistent over the entire measurement period (1 or more seconds) and easily identifiable. When enabled, the steering angle was aligned parallel to the capillary. The velocity measurements were repeated three times at each predefined velocity. In order to minimize bias, a single observer obtained the measurements in the presence of a second observer.

In order to prevent motion artifacts, the probes were fixed using a tripod. With set flow velocities of 5 cm/s and above, a pulsatile flow pattern was witnessed. This disturbance vanished when using a 10 mL low friction glass syringe (GASTIGHT #1010, Hamilton Company, Bonaduz, Switzerland) or a 60 mL plastic syringe instead of a 10 mL plastic syringe. Therefore, for all set flow velocities of 5 cm/s and more we used the glass syringe.

Table 1 | Ultrasound settings used in this study.

Doppler mode	Probe	Frequency (MHz)	Gain (%)	PRF (kHz)	PRS	PRC	Wall filter
PWD	Linear	5.9	53–60	0.5–10	–	6	100 Hz
	Convex	6.3	50–56	0.75–2	–	6	65 Hz
CD	Linear	7.7	50	0.37	16	M/2	1
	Convex	5	64	1.5	16	H/2	2
Directional PD	Linear	7.7	50	1–2.5	3, 4	M/2, H/2	2, 3
	Convex	5	64	1–2	3, 4, 6	L/2, M/2	2, 4

PWD, pulsed wave Doppler; CD, color Doppler mode; PD, power Doppler; PRF, pulse repetition frequency; PRS, persistence; PRC, processing.

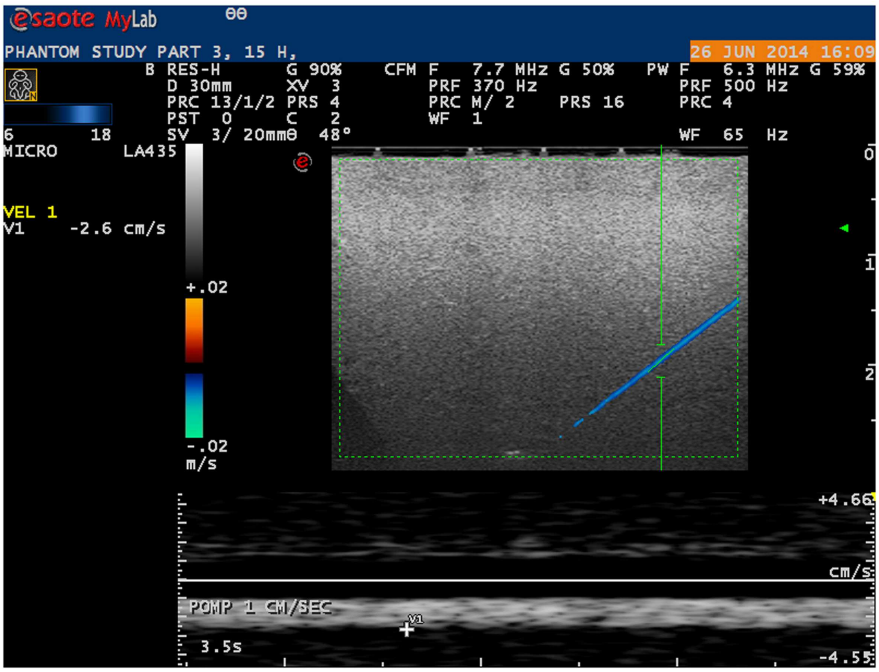

FIGURE 2 | Ultrasound image of phantom microvessel. Ultrasound image showing a 200 μm flow phantom catheter as depicted by a linear probe in color Doppler mode.

STATISTICAL ANALYSIS

To assess the reproducibility of the velocity measurements and whether velocity measured with the ultrasound corresponded with the actual set velocity, one-way random intra-class correlation (ICC) coefficient was computed with single measures. Based on bootstrap sampling, the 95% confidence interval for ICC coefficient was calculated. To compare the measured diameter with the actual diameter of the capillaries, we used the Student's one sample *t*-test. Statistically significant was assumed if two-sided *p* value was <0.05. All statistical analyses were performed in R (version 3.1.1; R Foundation for Statistical Computing, Vienna, Austria – http://www.R-project.org).

RESULTS

VELOCITY MEASUREMENTS

Microvessels mimicking catheters with a size of 200 and 700 μm with BMF velocities as low as 1 cm/s were adequately visualized using a linear probe (**Figure 2**). With a convex probe, however, velocities below 2 cm/s in the 700 μm vessel and below 3 cm/s in the 200 μm vessel could not be depicted.

Measurements of velocity and diameter proved to be highly reproducible, with an overall ICC coefficient of 0.997 (95% CI 0.996–0.998) and 0.914 (0.864–0.946), respectively.

As shown in **Table 2**, in all different settings, ICC coefficient of three consecutive velocity measurements stayed above 0.9 with a variation coefficient below 1.0, except for velocities measured in the 200 μm vessel with the convex probe.

Differences between true (pump) velocity and the peak measured Doppler velocity are shown in **Figure 3**. Overall, PWD

Table 2 | Reproducibility of velocity measurements.

Vessel diameter (μm)	Doppler mode	Probe	Steer angle correction	ICC (95% CI)	
200	Color	Linear	–	0.998 (0.991–1.000)	
			+	0.999 (0.996–0.999)	
		Convex	–	0.985 (0.643–0.989)	[a]
			+	0.991 (0.673–0.995)	[a]
	Power	Linear	–	0.997 (0.991–00.998)	
			+	0.997 (0.988–0.999)	
		Convex	–	0.915 (0.357–0.945)	[a]
			+	0.992 (0.702–0.998)	[a]
700	Color	Linear	–	0.999 (0.996–1.000)	
			+	0.999 (0.976–1.000)	
		Convex	–	0.986 (0.964–0.998)	[b]
			+	0.999 (0.992–1.000)	[b]
	Power	Linear	–	0.995 (0.933–0.997)	
			+	0.999 (0.996–0.999)	
		Convex	–	0.997 (0.991–0.999)	[b]
			+	0.999 (0.993–0.999)	[b]

Reproducibility of consecutive velocity measurements as showed by ICC (intra-class correlation) coefficients. Color, color Doppler; power, power Doppler; v, velocity.

[a] *No visualization if v ≤ 2 cm/s.*

[b] *No visualization if v = 1 cm/s.*

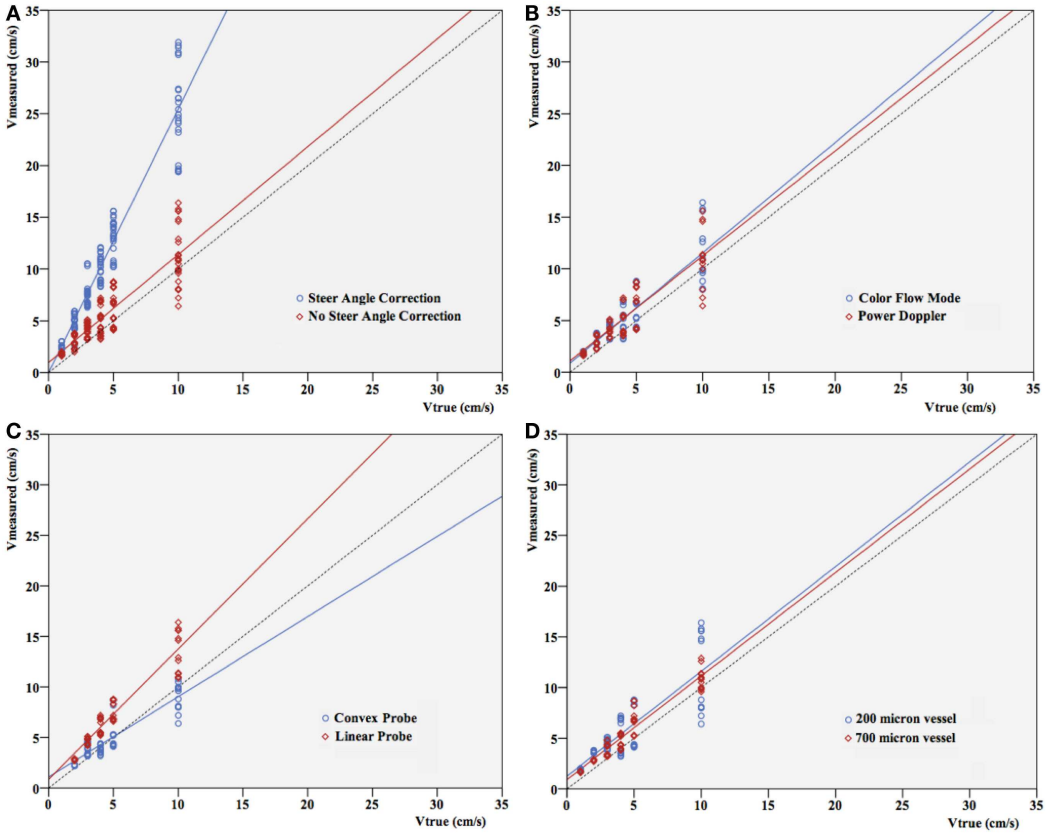

FIGURE 3 | Pump velocity versus measured Doppler velocity. Relation between true velocity (centimeter per second) and velocity measured (centimeter per second) in different settings: **(A)** with or without steer angle correction, **(B)** color Doppler versus power Doppler, **(C)** convex versus linear probe, **(D)** vessel size. Since applying steer angle correction leads to significant ($p < 0.001$) overestimation of velocity, velocities in **(B–D)** are without applying steer angle correction. The dotted line represents the line of equality.

overestimated velocity with a 1.1- to 3.5-fold overestimation. This is independent of the flow visualization method in the triplex mode, as expected (**Figure 3B**). If velocity increased, spreading of the velocities measured in the different settings seemed to be more pronounced. However, this appeared to depend almost uniquely on the highly significant differences that were seen in velocity measurements with versus without steer angle correction ($p < 0.001$). When leaving out the steer angle velocity estimates, correlation between true velocities and measured velocity ameliorated.

Overall, ICC coefficient between average velocity measured by Doppler and the true velocity was 0.352 (0.269–0.442). As shown in a Bland–Altman plot (**Figure 4**), overall agreement between true velocity (Velocity pump) and velocity estimated by Doppler was poor. However, results suggest consistent overestimation.

DIAMETER MEASUREMENTS

Student's t-test for vessel size showed significant differences in diameter estimation (p-values <0.001 and 0.005, respectively). As shown in **Figure 5**, vessel size was mostly overestimated by ultrasound.

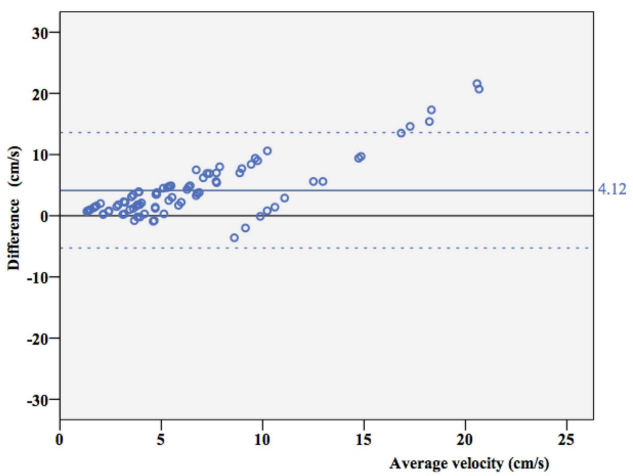

FIGURE 4 | Agreement between true velocity and Doppler velocity. Bland–Altman plot of agreement between true velocity (V_{true}) and velocity estimated by Doppler measurements ($V_{measured}$). The mean difference is 4.12 cm/s (95% CI 3.10–5.15 cm/s), dotted lines represent ± 2 SD borders.

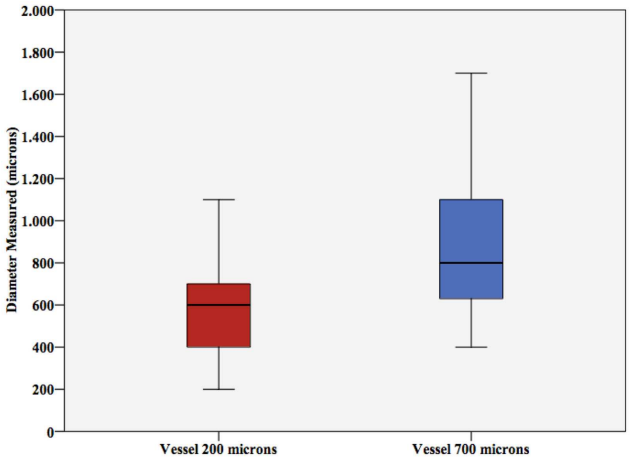

FIGURE 5 | Vessel diameter. Vessel diameter measured (±SD) for the 200 μm vessel and the 700 μm vessel. Note the significant overestimation.

DISCUSSION

In this flow phantom study, we found that Doppler ultrasound imaging is able to visualize microvessel-size catheters with low flow, mimicking cerebral microcirculation. Within the different settings, reproducible velocity and diameter results can be obtained. Our overall results showed that vessel diameter and velocity are overestimated when measured by Doppler ultrasound. This corresponds with results of previous phantom studies (Goertz et al., 2000; Raine-Fenning et al., 2008a; Schulten-Wijman et al., 2008; Xu et al., 2008). However, these studies were designed mainly to determine optimal machine settings and minimal detectable flow. To our best knowledge, this is the first *in vitro* experiment to calibrate for neonatal brain microcirculation.

Overestimation of flow velocity was observed in our study with convex as well as linear ultrasound probes. Previous publications (Guo et al., 1995; Teirlinck et al., 1998; Schulten-Wijman et al., 2008) described a similar phenomenon. Several aspects of Doppler technique and processing of the signals may contribute to this overshooting, as detailed below.

First, it might be explained by sampling inaccuracy. The flow can be assumed parabolic in the low-Reynolds number regime asserted in our measurements. In such a flow, the peak velocity is two times higher than the average flow as predicted by Eq. 1. Moreover, we manually picked the maximum Doppler velocity in the PW panel, as in current clinical practice, not the average velocity. The effect of the flow profile on such Doppler-based velocity estimation is complex, but tends to overestimate the mean velocity (Ricci et al., 2014).

A second explanation might be the way that raw ultrasound data are filtered and processed within the ultrasound machine to produce an image. Most ultrasound machines consider the mean propagation speed c in tissue to be 1540 cm/s and use this value to calculate many values, of which velocity is 1 (Zagzebski, 1996; Gill, 2012). If the true propagation speed is higher than 1540 cm/s, this may lead to overestimation of predicted velocity. Exact propagation speed of preterm brain tissue is unknown and additionally depends on several other factors, like temperature and hydration status (Kremkau et al., 1981). Also, in the process of filtering background scatter, some information might be lost or adapted, all according to the software used. At present, we are not familiar with the manufacturer's confidential post-processing algorithms to create an image from raw data. Especially, when desiring to depict smaller vessels and lower flow velocities, insight in these methods and cooperation with the manufacturer in the development of new software might be of importance.

Third, overshooting might be explained by insonation angle. Since both velocity and direction of blood flow determine Doppler shift, which is the main principle of Doppler ultrasound, insonation angle is an important determinant in calculating velocity. To make velocity quantification error as small as possible, the Doppler angle must be kept as small as possible (Zagzebski, 1996). Current study was performed in a flow phantom with an insonation angle of about 60°, which is considered the maximal insonation angle in clinical practice but still gives an important velocity estimation error. Additionally, increasing insonation angle worsens several Doppler artifacts, such as an intrinsic spectral broadening, which leads to a systematic overestimation in velocity measurements (Gill, 2012).

Pulsed wave Doppler and CD ultrasound depend on the time shift of pulsed wave echoes to calculate velocity and direction. In PD, on the other hand, the color displayed is determined by the Doppler signal power rather than the effective time shift. In theory, this makes PD more sensitive for visualization of low flow velocity (Murphy and Rubin, 1997; Martinoli et al., 1998). Yet, our study shows that both directional PD and CD are able to detect flow velocities down to 1 cm/s with the linear array, which would indicate applicability of both methods in the current framework of preterm intracerebral circulation imaging. The measured velocities with PD were independent of the CD or PD visualization method, which is expected because of the independent nature of data acquisition and processing between PW Doppler and the visualization method.

As expected, applying the steer angle artificially corrects for the angle between flow direction and ultrasound beam. Since the measured Doppler value is divided by the cosine of the angle that the sonographer sets, it should always result in larger apparent velocities in the image (Szabo, 2013). This is consistent with our findings.

Considering the specific characteristics of the linear and convex ultrasound probes and their use in clinical practice, we expected the linear probe to be more suitable for microcirculation imaging. Indeed, lower flow velocities were visualized using the linear probe in the 200 μm vessel compared to the convex probe. As seen in **Figure 3**, velocities were mainly overestimated by the linear probe while the convex probe underestimated them. Apart from that, results show no obvious superiority for this probe and its specific settings, with reference to the diameter and blood flow velocity of the microvessels.

Since B-mode ultrasound is insufficiently accurate in estimating the diameter of microvessels, we tried to approach true diameter using CD and PD. Reproducible results were obtained; however, overestimation was equally observed as in the velocity measurements. This inaccuracy in measuring diameter is a known

problem of Doppler technique. Due to the relatively long transmit pulses in Doppler, axial accuracy of CD systems is rather low, resulting in the encoding of the color sometimes beyond the true flow field (Guo et al., 1995).

Additionally, when adjusting instrument parameters, for instance, increasing the gain, overestimation of vessel diameter is more likely (Browne et al., 2004; Raine-Fenning et al., 2008b). Mitchell (1990) stated that a jet area depicted by color imaging is likely to be more dependent on instrument parameters than on vascular anatomy or physiological characteristics. However, current understanding of ultrasound technique and new *in vitro* models like this microcirculation flow model might give the opportunity to calibrate machine settings for measurement of diameter and true blood flow in near future. In a small spinoff pilot study, ultrasound settings were adjusted according to flow phantom measurements allowing accurate caliber visualization during Doppler imaging, showing the feasibility of this technique.

In conclusion, Doppler ultrasound might be an additional diagnostic tool for quantification of neonatal brain blood flow. This study shows that, before starting to use velocity estimates in patients, calibration of the ultrasound machine for that purpose is needed. The ultimate goal of this type of research is to develop a sonographic tool that can be used for objectively studying regional (3D) perfusion in routine practice.

AUTHOR CONTRIBUTIONS

Fleur A. Camfferman has written the manuscript and created figures. Ginette M. Ecury-Goossen has performed the analysis and has written the manuscript. Jhuresy E. La Roche has performed the analysis. Hendrik J. Vos provided technical support and has written the manuscript. Nico de Jong, Willem Van 'T Leven, and Martin D. Verweij provided technical support and contributed to the manuscript. Kazem Nasserinejad analyzed the data and contributed to the manuscript. Filip Cools contributed to the manuscript and the figures. Paul Govaert and Jeroen Dudink have written the manuscript, designed the experiments, and provided expert consultation. Additionally, Jeroen Dudink provided senior supervision.

REFERENCES

Anstrom, J. A., Brown, W. R., Moody, D. M., Thore, C. R., Challa, V. R., and Block, S. M. (2004). Subependymal veins in premature neonates: implications for hemorrhage. *Pediatr. Neurol.* 30, 46–53. doi:10.1016/S0887-8994(03)00404-1

Basu, S., Dewangan, S., Barman, S., Shukla, R. C., and Kumar, A. (2014). Postnatal changes in cerebral blood flow velocity in term intra-uterine growth-restricted neonates. *Paediatr. Int. Child Health* 34, 189–193. doi:10.1179/2046905514Y.0000000124

Browne, J. E., Watson, A. J., Hoskins, P. R., and Elliott, A. T. (2004). Validation of a sensitivity performance index test protocol and evaluation of colour Doppler sensitivity for a range of ultrasound scanners. *Ultrasound Med. Biol.* 30, 1475–1483. doi:10.1016/j.ultrasmedbio.2004.09.005

Deeg, K. H., and Lode, H. M. (2005). Trans-fontanellar Doppler sonography of the intracranial veins in infants – part I – normal values. *Ultraschall Med.* 26, 507–517. doi:10.1055/s-2005-858881

Gill, R. (2012). *The Physics and Technology of Diagnostic Ultrasound.* Sydney: High Frequency Publishing.

Goertz, D. E., Christopher, D. A., Yu, J. L., Kerbel, R. S., Burns, P. N., and Foster, F. S. (2000). High-frequency color flow imaging of the microcirculation. *Ultrasound Med. Biol.* 26, 63–71. doi:10.1016/S0301-5629(99)00101-5

Greisen, G. (2005). Autoregulation of cerebral blood flow in newborn babies. *Early Hum. Dev.* 81, 423–428. doi:10.1016/j.earlhumdev.2005.03.005

Guo, Z., Moreau, M., Rickey, D. W., Picot, P. A., and Fenster, A. (1995). Quantitative investigation of in vitro flow using three-dimensional colour Doppler ultrasound. *Ultrasound Med. Biol.* 21, 807–816. doi:10.1016/0301-5629(95)00007-E

Hellström-Westas, L. (2006). Continuous electroencephalography monitoring of the preterm infant. *Clin. Perinatol.* 33, 633–647. doi:10.1016/j.clp.2006.06.003

Kehrer, M., Blumenstock, G., Ehehalt, S., Goelz, R., Poets, C., and Schöning, M. (2005). Development of cerebral blood flow volume in preterm neonates during the first two weeks of life. *Pediatr. Res.* 58, 927–930. doi:10.1203/01.PDR.0000182579.52820.C3

Kehrer, M., Krägeloh-Mann, I., Goelz, R., and Schöning, M. (2003). The development of cerebral perfusion in healthy preterm and term neonates. *Neuropediatrics* 34, 281–286. doi:10.1055/s-2003-44663

Kissack, C. M., Garr, R., Wardle, S. P., and Weindling, A. M. (2004). Postnatal changes in cerebral oxygen extraction in the preterm infant are associated with intraventricular hemorrhage and hemorrhagic parenchymal infarction but not periventricular leukomalacia. *Pediatr. Res.* 56, 111–116. doi:10.1203/01.PDR.0000128984.03461.42

Kremkau, F. W., Barnes, R. W., and McGraw, C. P. (1981). Ultrasonic attenuation and propagation speed in normal human brain. *J. Acoust. Soc. Am.* 70, 29–38. doi:10.1121/1.386578

Kuban, K. C. K., and Gilles, F. H. (1985). Human telencephalic angiogenesis. *Ann. Neurol.* 17, 539–548. doi:10.1002/ana.410170603

Liem, K. D., and Greisen, G. (2010). Monitoring of cerebral haemodynamics in newborn infants. *Early Hum. Dev.* 86, 155–158. doi:10.1016/j.earlhumdev.2010.01.029

Macé, E., Montaldo, G., Cohen, I., Baulac, M., Fink, M., and Tanter, M. (2011). Functional ultrasound imaging of the brain. *Nat. Methods* 8, 662–664. doi:10.1038/nmeth.1641

Marin, T., and Moore, J. (2011). Understanding near-infrared spectroscopy. *Adv. Neonatal Care* 11, 382–388. doi:10.1097/ANC.0b013e3182337ebb

Martinoli, C., Derchi, L. E., Rizzatto, G., and Solbiati, L. (1998). Power Doppler sonography: general principles, clinical applications, and future prospects. *Eur. Radiol.* 8, 1224–1235. doi:10.1007/s003300050540

Meek, J. H., Tyszczuk, L., Elwell, C. E., and Wyatt, J. S. (1999). Low cerebral blood flow is a risk factor for severe intraventricular haemorrhage. *Arch. Dis. Child. Fetal Neonatal Ed.* 81, F15–F18. doi:10.1136/fn.81.1.F15

Mitchell, D. G. (1990). Color Doppler imaging: principles, limitations, and artifacts. *Radiology* 177, 1–10. doi:10.1148/radiology.177.1.2204956

Murphy, K. J., and Rubin, J. M. (1997). Power Doppler: it's a good thing. *Semin. Ultrasound CT MR* 18, 13–21. doi:10.1016/S0887-2171(97)90034-2

Petrou, S., Sach, T., and Davidson, L. (2001). The long-term costs of preterm birth and low birth weight: results of a systematic review. *Child Care Health Dev.* 27, 97–115. doi:10.1046/j.1365-2214.2001.00203.x

Pezzati, M., Dani, C., Biadaioli, R., Filippi, L., Biagiotti, R., Giani, T., et al. (2002). Early postnatal Doppler assessment of cerebral blood flow velocity in healthy preterm and term infants. *Dev. Med. Child Neurol.* 44, 745–752. doi:10.1017/S0012162201002870

Pfannschmidt, J., and Jorch, G. (1989). Transfontanelle pulsed Doppler measurement of blood flow velocity in the internal jugular vein, straight sinus, and internal cerebral vein in preterm and term neonates. *Ultrasound Med. Biol.* 15, 9–12. doi:10.1016/0301-5629(89)90126-9

Raine-Fenning, N. J., Nordin, N. M., Ramnarine, K. V., Campbell, B. K., Clewes, J. S., Perkins, A., et al. (2008a). Determining the relationship between three-dimensional power Doppler data and true blood flow characteristics: an in-vitro flow phantom experiment. *Ultrasound Obstet. Gynecol.* 32, 540–550. doi:10.1002/uog.6110

Raine-Fenning, N. J., Nordin, N. M., Ramnarine, K. V., Campbell, B. K., Clewes, J. S., Perkins, A., et al. (2008b). Evaluation of the effect of machine settings on quantitative three-dimensional power Doppler angiography: an in-vitro flow phantom experiment. *Ultrasound Obstet. Gynecol.* 32, 551–559. doi:10.1002/uog.6138

Ramnarine, K. V., Nassiri, D. K., Hoskins, P. R., and Lubbers, J. (1998). Validation of a new blood-mimicking fluid for use in Doppler flow test objects. *Ultrasound Med. Biol.* 24, 451–459. doi:10.1016/S0301-5629(97)00277-9

Ricci, S., Matera, R., and Tortoli, P. (2014). An improved Doppler model for obtaining accurate maximum blood velocities. *Ultrasonics* 54, 2006–2014. doi:10.1016/j.ultras.2014.05.012

Schulten-Wijman, M. J., Struijk, P. C., Brezinka, C., De Jong, N., and Steegers, E. A. (2008). Evaluation of volume vascularization index and flow index: a phantom study. *Ultrasound Obstet. Gynecol.* 32, 560–564. doi:10.1002/uog.6112

Sherlock, R. L., Anderson, P. J., Doyle, L. W., and Victorian Infant Collaborative Study G. (2005). Neurodevelopmental sequelae of intraventricular haemorrhage at 8 years of age in a regional cohort of ELBW/very preterm infants. *Early Hum. Dev.* 81, 909–916. doi:10.1016/j.earlhumdev.2005.07.007

Szabo, T. L. (2013). *Diagnostic Ultrasound Imaging: Inside Out*, 2 Edn. Oxford: Academic Press.

Teirlinck, C. J. P. M., Bezemer, R. A., Kollmann, C., Lubbers, J., Hoskins, P. R., Fish, P., et al. (1998). Development of an example flow test object and comparison of five of these test objects, constructed in various laboratories. *Ultrasonics* 36, 653–660. doi:10.1016/S0041-624X(97)00150-9

Ten Cate, D. F., Luime, J. J., van der Ven, M., Hazes, J. M., Kooiman, K., de Jong, N., et al. (2013). Very different performance of the power Doppler modalities of several ultrasound machines ascertained by a microvessel flow phantom. *Arthritis Res. Ther.* 15, R162. doi:10.1186/ar4345

van Bel, F., Lemmers, P. M., and Naulaers, G. (2008). Monitoring neonatal regional cerebral oxygen saturation in clinical practice: value and pitfalls. *Neonatology* 94, 237–244. doi:10.1159/000151642

Vasovic, L. P., Jovanovic, I. D., Ugrenovic, S. Z., and Andelkovic, Z. P. (2007). The posterior part of the human cerebral arterial circle (CAC): arterial caliber from gestational weeks 13 to 24. *J. Anat.* 211, 612–619. doi:10.1111/j.1469-7580.2007.00806.x

Volpe, J. J. (2009). Brain injury in premature infants: a complex amalgam of destructive and developmental disturbances. *Lancet Neurol.* 8, 110–124. doi:10.1016/S1474-4422(08)70294-1

World Health Organization. (2011). *Manual of Diagnostic Ultrasound.* eds H. Lutz and E Buscarini (Geneva: WHO).

Xu, X., Sun, L., Cannata, J. M., Yen, J. T., and Shung, K. K. (2008). High-frequency ultrasound Doppler system for biomedical applications with a 30-MHz linear array. *Ultrasound Med. Biol.* 34, 638–646. doi:10.1016/j.ultrasmedbio.2007.09.012

Zagzebski, J. A. (1996). *Essentials of Ultrasound Physics*, 1st Edn. Philadelphia: Mosby.

Conflict of Interest Statement: The authors declare that the research was conducted in the absence of any commercial or financial relationships that could be construed as a potential conflict of interest.

Received: 12 October 2014; accepted: 22 December 2014; published online: 13 January 2015.

Citation: Camfferman FA, Ecury-Goossen GM, La Roche JE, de Jong N, van 't Leven W, Vos HJ, Verweij MD, Nasserinejad K, Cools F, Govaert P and Dudink J (2015) Calibrating Doppler imaging of preterm intracerebral circulation using a microvessel flow phantom. Front. Hum. Neurosci. ***8****:1068. doi: 10.3389/fnhum.2014.01068*

This article was submitted to the journal Frontiers in Human Neuroscience.

frontiers in Human Neuroscience

ORIGINAL RESEARCH
published: 07 April 2015
doi: 10.3389/fnhum.2015.00147

Heart rate variability parameters and fetal movement complement fetal behavioral states detection via magnetography to monitor neurovegetative development

Johanna Brändle[1,2,3], Hubert Preissl[2], Rossitza Draganova[2], Erick Ortiz[2], Karl O. Kagan[3], Harald Abele[3], Sara Y. Brucker[1,3†] and Isabelle Kiefer-Schmidt[1,2,3†]*

[1] University Women's Hospital and Research Institute for Women's Health, University of Tuebingen, Tuebingen, Germany, [2] fMEG Center, University of Tuebingen, Tuebingen, Germany, [3] Department of Obstetrics and Gynecology, University of Tuebingen, Tuebingen, Germany

OPEN ACCESS

Edited by:
Silvia Comani,
Università degli Studi G. d'Annunzio, Italy

Reviewed by:
Kathleen M. Gustafson,
University of Kansas Medical Center, USA
Uwe Schneider,
University Hospital Jena, Germany

***Correspondence:**
Isabelle Kiefer-Schmidt,
Department of Obstetrics and Gynecology, University of Tuebingen, Calwer Street 7, Otfried-Mueller-Strasse 47, 72076 Tuebingen, Germany
isabelle.kiefer-schmidt@med.uni-tuebingen.de

[†]These authors have contributed equally to this work.

Received: 05 November 2014
Accepted: 02 March 2015
Published: 07 April 2015

Citation:
Brändle J, Preissl H, Draganova R, Ortiz E, Kagan KO, Abele H, Brucker SY and Kiefer-Schmidt I (2015) Heart rate variability parameters and fetal movement complement fetal behavioral states detection via magnetography to monitor neurovegetative development. Front. Hum. Neurosci. 9:147. doi: 10.3389/fnhum.2015.00147

Fetal behavioral states are defined by fetal movement and heart rate variability (HRV). At 32 weeks of gestational age (GA) the distinction of four fetal behavioral states represented by combinations of quiet or active sleep or awakeness is possible. Prior to 32 weeks, only periods of fetal activity and quiesence can be distinguished. The increasing synchronization of fetal movement and HRV reflects the development of the autonomic nervous system (ANS) control. Fetal magnetocardiography (fMCG) detects fetal heart activity at high temporal resolution, enabling the calculation of HRV parameters. This study combined the criteria of fetal movement with the HRV analysis to complete the criteria for fetal state detection. HRV parameters were calculated including the standard deviation of the normal-to-normal R–R interval (SDNN), the mean square of successive differences of the R–R intervals (RMSSD, SDNN/RMSSD ratio, and permutation entropy (PE) to gain information about the developing influence of the ANS within each fetal state. In this study, 55 magnetocardiograms from healthy fetuses of 24–41 weeks' GA were recorded for up to 45 min using a fetal biomagnetometer. Fetal states were classified based on HRV and movement detection. HRV parameters were calculated for each state. Before GA 32 weeks, 58.4% quiescence and 41.6% activity cycles were observed. Later, 24% quiet sleep state (1F), 65.4% active sleep state (2F), and 10.6% active awake state (4F) were observed. SDNN increased over gestation. Changes of HRV parameters between the fetal behavioral states, especially between 1F and 4F, were statistically significant. Increasing fetal activity was confirmed by a decrease in PE complexity measures. The fHRV parameters support the differentiation between states and indicate the development of autonomous nervous control of heart rate function.

Keywords: fetal behavioral states, heart rate variability (HRV), fetal magnetocardiography (fMCG), fetal maturation, autonomic nervous system (ANS)

Abbreviations: ANS, autonomic nervous system; Bpm, beats per minute; CTG, cardiotocogram, cardiotocography, fECG, fetal Electrocardiography; fHRV, fetal heart rate variability; fHRP, fetal heart rate pattern; fMCG, fetal magnetocardiography; GA, gestational age; HRV, heart rate variability; IUGR, intrauterine growth restriction; mHR, mean heart rate; PE, permutation entropy; RMSSD, root mean square of successive differences of the R–R intervals; SDNN, standard deviation of the normal-to-normal R–R intervals; SQUID, superconducting quantum interference device.

Introduction

Nijhuis et al. (1982) classified fetal behavior after 32 weeks of gestation into four states (quiet sleep 1F, active sleep 2F, quiet awake 3F, active awake 4F, see **Table 1**), based on fHRV, eye movement and body movement measured by CTG, and ultrasound (Prechtl, 1985; Drogtrop et al., 1990; Nijhuis et al., 1999). Prior to 32 weeks of GA, it is possible to distinguish activity and resting cycles (Pillai and James, 1990b). Fetal heart rate and movement is a common obstetrical marker of fetal well-being and health. Starting in the 1980s, fetal behavioral states were introduced as a concept based on fetal heart rate and movement classification and information was discovered about the development of the ANS during pregnancy.

Fetal magnetocardiography uses SQUID biomagnetometry to non-invasively record fetal heart function through the maternal abdomen. This method detects the fetal cardio electrophysiology with high temporal resolution (1 ms) superior to CTG and is less susceptible to artifacts than fECG (Peters et al., 2001). Thus, an exact detection of the fetal HRV is possible. Several research groups have confirmed the usefulness of fMCG as a new and safe technique for prenatal evaluation of fetal well-being and neurovegetative development by fHRV analysis (Van Leeuwen, 2004; Schneider et al., 2008). Most of the prior fMCG studies were conducted with small-array biomagnetometer systems, using visual classification of the data to identify fetal behavioral states. In 2008, a fetal magnetography system was installed at the MEG Center Tuebingen, dedicated for fetal monitoring. The system succeeds an earlier fetal system and provides improved signal acquisition for fetal assessment with enhanced detection of fetal signals (Lowery et al., 2006), making it possible to record fetal heart signals fMCG with high temporal resolution and fetal brain activity fMEG with high detection rates (Preissl et al., 2004). The characterization of normal fetal behavior is fundamental to neurodevelopmental research and clinical fetal evaluation. Fetal heart rate is influenced by the ANS, which matures during pregnancy. In addition several HRV parameters express the maturing influence of both ANS branches (sympathetic and parasympathetic). The SDNN measures the overall variability of the neurovegetative system. The RMSSD represents the short-term variability associated with vagal function. The SDNN/RMSSD ratio reflects sympathovagal balance (Schneider et al., 2008), and PE represents the complexity of heart beat intervals (Frank et al., 2006). Due to the high temporal resolution of the MCG, these parameters can be reliably estimated and could improve HRV analysis to enable the monitoring of the current fetal neurovegetative state, as shown in an earlier fMCG study (Schneider et al., 2008).

The focus of this study was the inclusion of fetal movement data according to the original Nijhuis criteria for fetal state classification. Additionally, HRV parameters (SDNN, RMSSD, ratio SDNN/RMSSD, PE) were simultaneously studied to gain information about the developing influence of the ANS within each fetal state. This was done by adapting the design of an earlier fMCG study (Schneider et al., 2008). An algorithm was used for an automatic fetal behavioral state detection – in order to provide a reproducible and objective approach, visual state detection was used to control and verify the results. Further interest should focus on the combination of the neurodevelopmental information obtained by both fMCG and fMEG, measuring fetal brain activity in utero, for the future, clinical applications of fetal magnetography.

Materials and Methods

Subjects

The study was performed with the fetal biomagnetometer installed at the fMEG Center in Tuebingen, Germany (Kiefer-Schmidt et al., 2013; Sonanini et al., 2014). The Ethics Committee of the Medical Faculty of the University of Tuebingen, Germany, approved the study. Written informed consent was obtained from all subjects. Fifty-five fetal magnetography recordings were obtained between 24 and 41 weeks of GA from women with uncomplicated, healthy singleton pregnancies. Subjects were divided into three GA groups: group 1 (GA 24+0 to 32+0 weeks), group 2 (GA 32+1 to 35+0 weeks), and group 3 (GA 35+1 to –41 weeks). Chromosomal abnormalities, fetal infections, and maternal diseases with negative effects on the unborn child were excluded. Only fetuses with estimated weights between the 10th and 90th percentiles for GA as determined by ultrasound were included in this study. Neonatal outcome was obtained after delivery to confirm a health child.

TABLE 1 | Criteria of the automatic state classification based on the original Nijhuis criteria.

State/fHRP	1F/fHRP1 quiet sleep	2F/fHRP2 active sleep	4F/fHRP4 active awake
Original criteria	• Quiescence which can be regularly interrupted by brief body movements (startles) • Stable heart rate, small oscillation • Isolated accelerations occur strictly related to movement	• Frequent gross body movement Heart rate with wider bandwidth than 1F • Frequent accelerations during movement	• Vigorous activity with many trunk rotations • Unstable heart rate • Large and long lasting accelerations fused into sustained tachycardia
Criteria for automatic state detection			
Baseline	<160 bpm	<160 bpm	>160 bpm possible
Oscillation bandwith	<±7.5 bpm	±7.5–±15 bpm	>±15 bpm
Accelerations	No	>15 bpm/>15 s	>30 bpm/>30 s
Movement	No	Yes	Yes

A CTG was routinely performed before every fMCG recording to confirm fetal heart rate and activity as normal for GA. Furthermore, the fetal position in relation to the sensor array was checked by ultrasound (Logiq 500 MD, GE Healthcare, Little Chalfont, Buckinghamshire, UK) prior to the recording. The study was performed in a magnetically shielded room (Vakuumschmelze, Hanau, Germany). The sensor array consisted of 156 SQUIDs (first order gradiometers) and 29 reference channels for noise detection (CTF MEGTM System, VSM Med. Tech, Coquitlam, BC, Canada). Subjects were seated comfortably in an upright position and asked to lean forward against the concave sensor array, modeled especially for the pregnant abdomen. Four coils fixed on elastic belts were positioned around the maternal abdomen to mark fetal head position with respect to the sensor array and to detect maternal movement during the measurement. The mothers were asked to relax during the recording and to move as little as possible. A choice of relaxing music was offered and transferred via air-conducting lines from a music player outside the room to a headphone. The duration of the recording depended on maternal comfort and was set to a maximum of 45 min. Subsequently, the ultrasound examination was repeated to check fetal position.

Data Acquisition

The recordings were performed at a sampling rate of 1220.7 Hz. Datasets with low signal-to-noise ratios for fetal heart signals and data with more than 3% artifacts or missed heartbeats were excluded from the analysis. All data were filtered with a bandpass of 1–80 Hz using the 8th order Butterworth filter with zero-phase distortion. Maternal heart signals were attenuated using a signal space projection technique and the fetal R-waves were identified using the Hilbert transform technique. The time between two R-waves was defined as a beat-to-beat interval and used to calculate fetal mHR. Classical parameters of fHRV representing the time domain (SDNN, RMSSD, SDNN/RMSSD ratio) and a non-linear fHRV measure (PE) were calculated for each state, 1F through 4F, and each gestational group in a moving window of 256 bpm. As a preprocessing step, a shifting window with a fixed size of 256 heartbeats was standardized in accordance with recommended standards (Malik, 1996; Grimm et al., 2003). The HRV parameters calculated were: SDNN – the standard deviation of normal-to-normal beats – representing the overall variability of sympathetic and vagal oscillations in the short data windows; RMSSD – the root mean square of successive differences, reflecting vagal control; the SDNN/RMSSD ratio – relating overall variability to its short-term variability shared in the time domain as a measure of sympathovagal balance (Schneider et al., 2008); and PE, representing the complexity of heart rate series (Frank et al., 2006). Fetal heart rate over time was plotted in bpm as a cardiogram in a CTG-like fashion. The fMCG signal measures fetal movement as changes in the orientation of fetal heart vectors with respect to the sensor array. This detection of fetal movement is orientated solely on the fetal heart vector and therefore only gross fetal movements such as trunk rotations are discernible. The resulting variation in signal amplitude was plotted as an actogram showing the fluctuation of the baseline over time. Any deviation >25% from baseline was considered to represent fetal movement. The cardiogram and the actogram were recorded simultaneously and plotted together as an actocardiogram, plotted in **Figure 1**. We developed an algorithm for automatic state classification based on the Nijhuis criteria (**Table 1**), taking into account the occurrence of fetal movement and the fHRP. All datasets were additionally classified by visual inspection of the actocardiograms by an observer with experience in the analysis of CTG and actocardiograms. A second observer with experience further independently analyzed the actocardiograms. If disagreement occurred, consensus was achieved by revision. Due to the low occurrence of the 3F state (Schneider et al., 2008), only the 1F, 2F, and 4F states were included in the present analysis. Prior to GA 32 weeks (group 1), only active and quiet states were distinguished, corresponding to the algorithm criteria of 1F for quiescence and 2F for activity (Pillai and James, 1990b).

Statistics

Statistics were performed with SPSS 18.0 for Windows (IBM, Armonk, NY, USA). A one-way ANOVA was used for the statistical analysis of fetal behavioral states (independent variable) and parameters of HRV (dependent variable; **Figures 3** and **4**). To improve the design of **Figures 3** and **4,** all data were plotted on a logarithmic axis. A value of $p < 0.05$ was considered statistically significant. *Post hoc* analysis of the difference between the individual states and three age groups employed the Mann–Whitney *U* test. After correction for multiple comparisons (Bonferroni), $p < 0.0167$ was considered significant for the *post hoc* analysis. The correlation of fHRV parameters with GA was analyzed by Spearman's rank correlation.

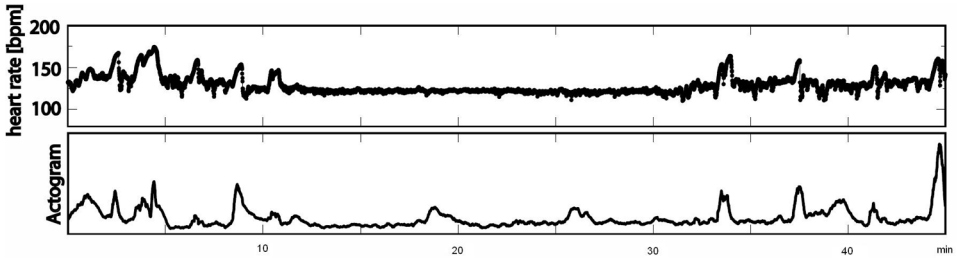

FIGURE 1 | Example of an actocardiogram in 38 weeks of GA measured over 45 min (first line: cardiogram in bpm; second line: actogram).

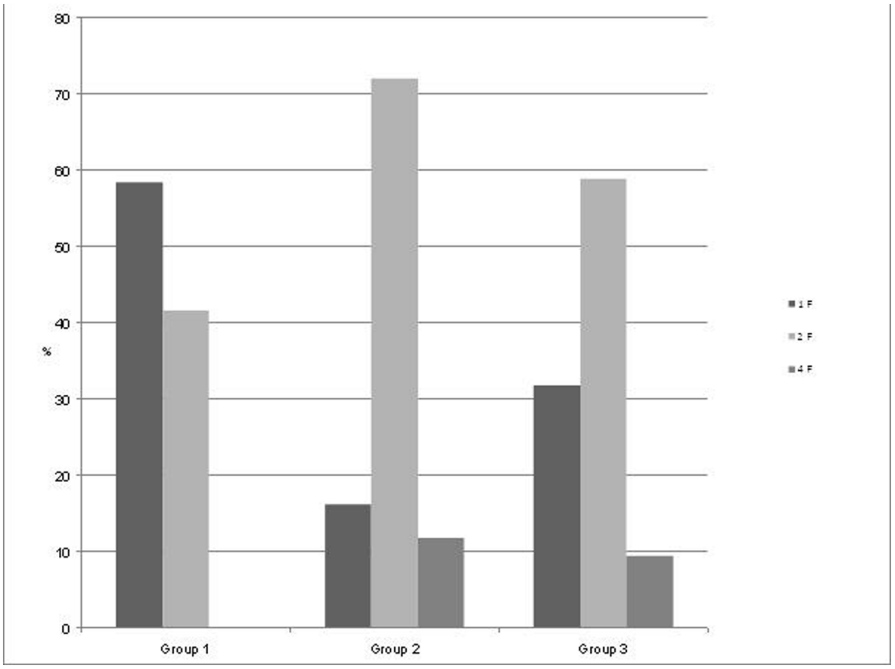

FIGURE 2 | Distribution of the fetal behavioral states in percent of total recording time per GA group. Group 1: GA 24+0 to 32+0 weeks), Group 2: GA 32+1 to 35+0 weeks, and Group 3: GA 35+1 to 41 weeks.

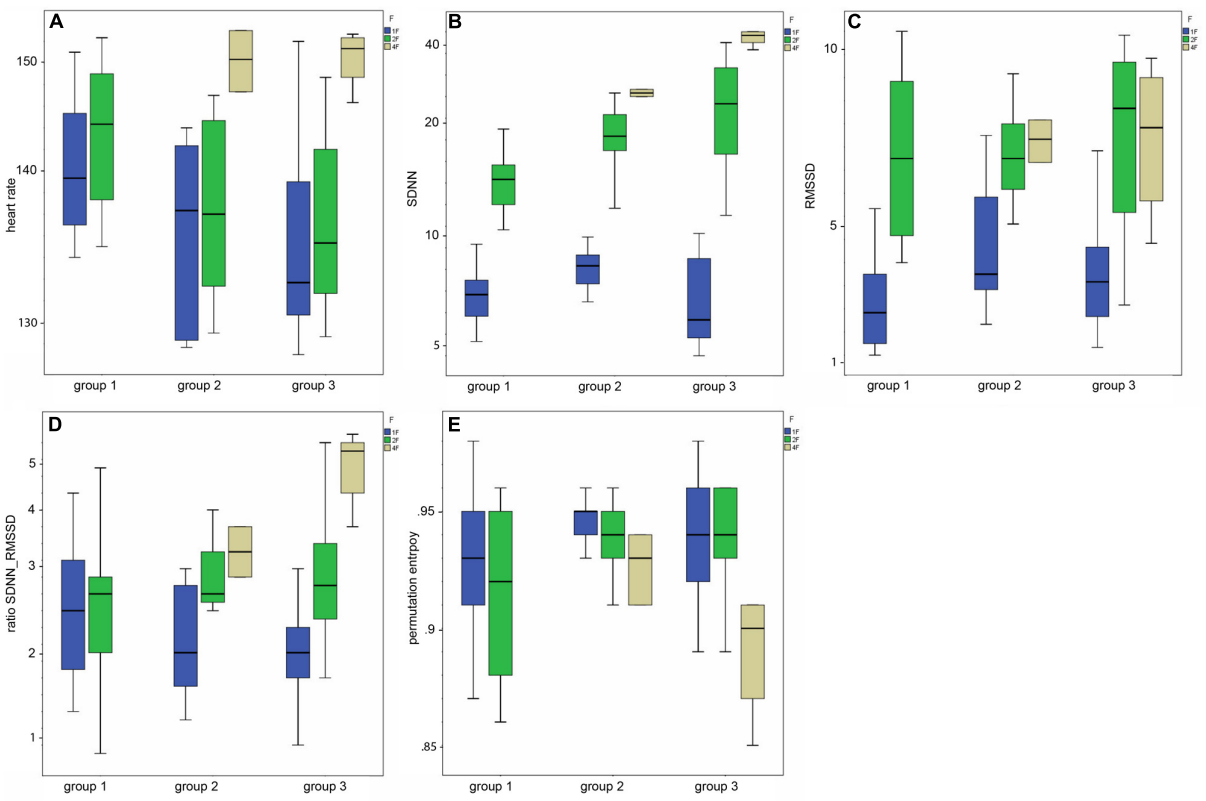

FIGURE 3 | (A–E) Box-and-whiskers plots of the HRV parameters by fetal behavioral state (1F, 2F, 4F) and GA group (group 1–3).

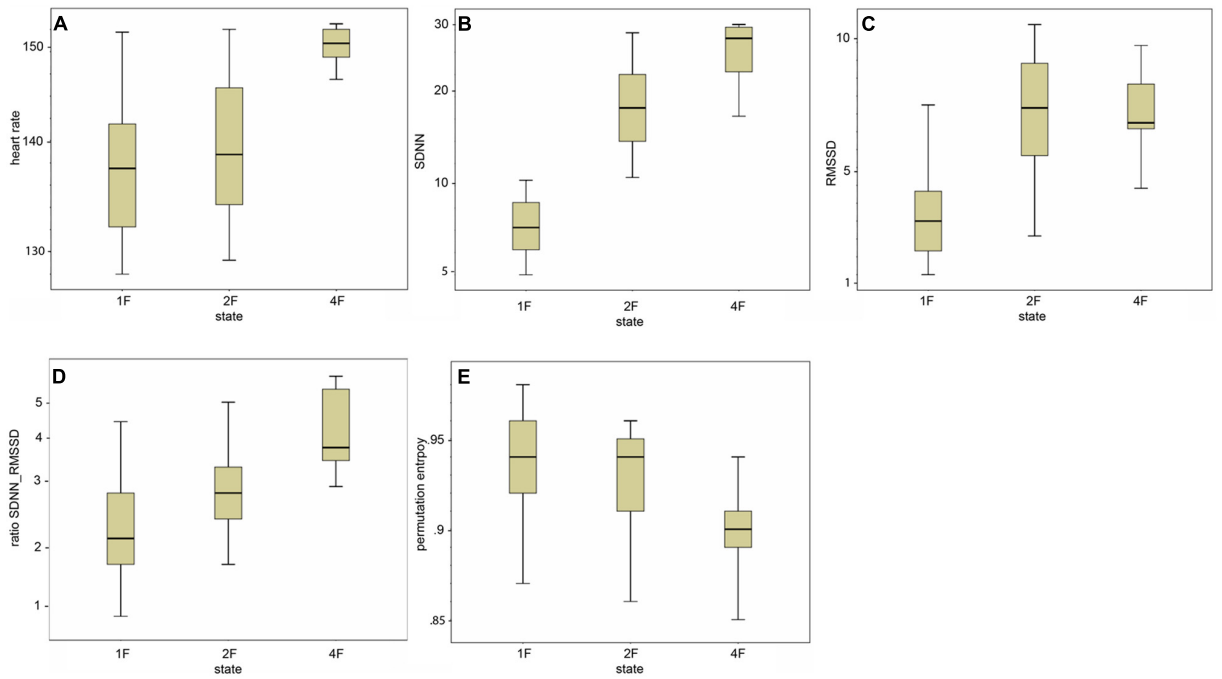

FIGURE 4 | (A–E) Box-and-whiskers plots of the distribution of the individual HRV parameter per fetal behavioral state (1F, 2F, 4F).

Results

Starting at 24 weeks of GA, we performed measurements in 55 pregnant women (mean age 33 years) with a mean recording time of 32.5 min (range 10–45 min) divided into three groups by GA (group 1, $n = 18$; group 2, $n = 15$; and group 3, $n = 22$) as seen in **Figure 2**. State detection was possible in all 55 datastets (automatic state classification: $n = 49$; visual classification: $n = 6$). In 89% of all cases automatic state classification was used successfully. Only in 11% ($n = 6$) the algorithm failed and visual inspection was needed for classification. In this visual classification the two observers disagreed in two cases an a consensus was achieved by revision. In group 1 (GA < 32 weeks), fetuses were in the resting state and in activity cycles during 58.4 and 41.6% of the recording time, respectively. Group 2 (GA 32–35 weeks), exhibited 1F, 2F, and 4F during 16.2, 72, and 11.8% of the recording time. In the late gestation group 3, the occurrence of 1F increased to 31.8%, 2F decreased to 58.8% and 4F remained almost unchanged at 9.4% (**Figure 2**).

Parameters of fHRV and GA

Mean heart rate was stable between group 1 (144 bpm) and group 2 (145 bpm), but decreased to 141 bpm in group 3 (corr: −0.363, $p < 0.001$), as demonstrated in **Figure 3A**. This shift was significant ($\chi^2 = 12.48$; $p < 0.005$) between the GA groups in general and between group 1 and 3 in the *post hoc* analysis.

The SDNN showed an increasing trend with GA for state 2F and 4F, as seen in **Figure 3B**, but did not attain statistical significance between the age groups in general ($\chi^2 = 5.43$, $p = 0.066$). The increase was significant from group 1 to group 2, but not between the other age groups. There was no significant correlation between GA and SDNN in general (corr: 0.181; $p = 0.081$).

The RMSSD showed no clear decrease or increase across the GA groups, nor was the correlation between RMSSD and GA statistically significant (corr: 0.103; $p = 0.323$; **Figure 3C**).

The SDNN/RMSSD ratio (**Figure 3D**) showed a decreasing trend between group 1 and 2, group 2 and 3, and group 1 and 3 (corr: 0.026; $p = 0.805$).

PE did not show any significant changes between the GA groups (corr: 0.179; $p = 0.059$; **Figure 3E**). The decrease did not attain statistical significance as an overall main effect between all three groups ($\chi^{sup2} = 3.52$, $p = 0.172$).

Table 2 indicates the results of the *post hoc* analysis for each fHRV parameter between the age groups. **Figures 3A–E** shows the distribution of the HRV parameters by GA group. **Table 3** indicates the distribution of the fHRP parameter in the age groups.

Parameters of fHRV and Fetal Behavioral States

Classical fHRV parameters were calculated for each recording in relation to the different fetal behavioral states. **Figures 4A–E** shows the distribution of the HRV parameters by fetal behavioral state. As shown in **Table 4**, mHR increased from 1F to 2F, from 1F to 4F, and from 2F to 4F in each GA group. This main effect was statistically significant between the states for all fetuses in general ($\chi^2 = 31.87$, $p < 0.001$) and for the changes in behavioral state from 1F to 4F and from 2F to 4F. The SDNN increased significantly with the fetal behavioral state ($\chi^2 = 95.42$, $p < 0.001$).

TABLE 2 | *Post hoc* analysis (*U* = Mann–Whitney test) of the HRV parameters and the age groups.

Group	mHR	SDNN	RMSSD	SDNN/RMSSD ratio	PE
1–2	0.032 ($U = 199.0$)	**0.009 ($U = 174.0$)**	0.217 ($U = 246.0$)	0.041 ($U = 0.707$)	0.165 ($U = 225.0$)
1–3	**0.001($U = 350.0$)**	0.101 ($U = 517.0$)	0.306 ($U = 573.0$)	0.330 ($U = 0.902$)	0.080 ($U = 506.5$)
2–3	0.400($U = 373.0$)	0.941 ($U = 425.0$)	0.931 ($U = 415.0$)	0.990 ($U = 1.5$)	0.831 ($U = 394.5$)

Statistically significant p-values are in bold type.

TABLE 3 | Distribution of the measured parameters of fHRP divided in groups regarding GA [Mean (STD)].

Group 1	Rest:	Active:	
Mean HR	142.76 (5.10)	148.72 (7.36)	
SDNN	7.48 (0.82)	18.77 (4.38)	
RMSSD	3.23 (1.13)	13.15 (9.78)	
Ratio SDNN/RMSSD	2.55 (0.82)	1.99 (1.26)	
Perm. entropy	0.93 (0.03)	0.92 (0.03)	
Group 2	**1F:**	**2F:**	**4F:**
Mean HR	136.34 (6.80)	141.02 (6.77)	156.92 (10.63)
SDNN	8.84 (1.22)	22.59 (3.93)	26.99 (10.39)
RMSSD	4.57 (1.44)	7.82 (3.57)	6.99 (2.04)
Ratio SDNN/RMSSD	2.10 (0.58)	3.33 (1.04)	4.06 (1.17)
Perm. Entropy	0.95 (0.02)	0.94 (0.02)	0.93 (0.03)
Group 3	**1F:**	**2F:**	**4F:**
Mean HR	134.21 (7.45)	137.83 (6.03)	150.82 (4.97)
SDNN	7.43 (1.57)	25.43 (4.87)	34.04 (10.83)
RMSSD	4.29 (1.14)	8.83 (3.46)	7.29 (4.55)
Ratio SDNN/RMSSD	1.84 (0.59)	3.28 (1.28)	5.41 (2.21)
PE	0.95 (0.02)	0.94 (0.02)	0.90 (0.03)

From 1F to 2F and from 1 F to 4F the increase attained statistical significance (**Figure 4B**). The RMSSD increased significantly with the behavioral state in general ($\chi^2 = 54.19$, $p < 0.001$) and from 1F to 2F and 1F to 4F, as seen in **Figure 4C**. The SDNN/RMSSD ratio increased significantly in general as a main effect ($\chi^2 = 1.76$, $p < 0.001$) and from 1F to 2F and 1F to 4F (**Figure 4D**). PE decreased significantly from 1F to 4F and 2F to 4F, but not from 1F to 2F (**Figure 4E**).

Discussion

Fetal Behavioral States

Behavioral states in mature normal fetuses were primarily investigated by ultrasound relating to the original Nijhuis criteria, namely fHRPs, eye movement, and general body movement (Nijhuis et al., 1982). Between 36 and 42 weeks of GA, fetal behavioral states 1F, 2F, and 4F were reported as occurring 30.2, 57.5, and 9.5% of the time (Pillai and James, 1990a), respectively. This is in good agreement with our findings for the corresponding GA group 3 with 31.8% 1F, 58.8% 2F, and 9.4% 4F. Relating to the same gestational period, a fMCG study (Lange et al., 2009) visually classified fHRPs and found respective relative durations of 27.5, 42.5, and 20% for 1F, 2F, and 4F. The remaining 10% for 3F and the fact that the study used only fetal heart rate to classify fetal behavioral states without taking fetal movement into account might explain the differences in findings compared with our current study. Another fMCG study (Schneider et al., 2008) investigated fHRPs in the same GA groups as we did in our study and detected more 1F and 4F, but less 2F compared to our results in fetuses over 32 weeks of GA. Nevertheless, that study reported changes in fetal behavioral states with increasing GA from group 2 to group 3 that were similar to those observed in our present study, i.e., an increase in 1F (28–43.9% vs. 16.2–31.8% in our study) and decreases in 2F (50–42.1% vs. 72–58.8% in our study) and 4F (22.4–14% vs. 11.8–9.4% in our study). We aimed to describe fetal behavioral states more accurately by additionally taking into account fetal movement as one of the original Nijhuis criteria defining these states. The strong concordance between the behavioral state frequencies in mature fetuses beyond 36 weeks of GA and traditional studies of fetal behavioral state based on all Nijhuis criteria support our approach (Pillai and James, 1990a; Nijhuis, 1993). This indicates that this is a valid approach for fetal state detection. The advantage of an automatic state detection is to be objective and reproducible. As this algorithm was newly applied but not established yet, we double-checked the data visually and preferred in case of discrepancy the visual detected state. More data of a comparison between both methods is necessary to validate the automatic state detection.

During early gestation, only quiet vs. active states were distinguishable, representing the premature fetus. With progressing gestation, heart rate patterns became more defined, and matched fetal movement. The frequencies of fetal behavioral states developed as expected (Pillai and James, 1990a; Schneider et al., 2008). These results confirm that, as the ANS matures, the fetus develops the ability to synchronize HRV and body movement and to develop fetal behavioral states.

Heart Rate Variability

Our further goal was to assess neurovegetative modulation by comparing established parameters of fetal HRV, namely SDNN, RMSSD, SDNN/RMSSD ratio, and PE, with the fetal behavioral states 1F, 2F, and 4F across three GA groups. The total values of the HRV parameters were in accordance with an MCG study based on visual classification of fHRPs to identify behavioral states (Schneider et al., 2008), although the individual values were spread out over a wide range and clustered more clearly within the three GA groups as demonstrated in **Figure 3**. In our study, the SDNN showed an increasing trend with GA, indicating the increasing modulation of autonomous

TABLE 4 | *Post hoc* analysis (*U* = Mann–Whitney test) of the HRV parameter and the fetal behavioral states.

State changes	mHR	SDNN	RMSSD	SDNN/RMSSD ratio	PE
1F–2F	0.057 ($U = 1444.0$)	**0.000 ($U = 1.00$)**	**0.000 ($U = 406.0$)**	**0.000 ($U = 0.002$)**	0.721 ($U = 1717.0$)
1F–4F	**0.000 ($U = 37.0$)**	**0.000 ($U = 13.0$)**	**0.000 ($U = 128.0$)**	**0.000 ($U = 0.101$)**	**0.016 ($U = 206.0$)**
2F–4F	**0.000 ($U = 67.0$)**	0.030 ($U = 314.0$)	0.713 ($U = 466.0$)	0.042 ($U = 0.674$)	**0.009 ($U = 273.5$)**

Statistically significant p-values are shown in bold type.

nervous control. Schneider et al. (2008) confirmed a slight increase based on higher values for 2F and 4F in fetuses over 32 weeks of GA. Moreover, as previously reported (Zhuravlev et al., 2002; Schneider et al., 2008), the SDNN/RMSSD ratio showed a decreasing trend with GA, indicating that the level of vegetative control increased toward term. However, both RMSSD and PE showed no clear changes with progressing gestation either in our data or in previous studies (Schneider et al., 2008). However, there were changes in parameters between the behavioral states. We observed increases in SDNN and RMSSD between the quiet sleep state (1F) to the two active states (2F and 4F; **Figures 4B–C**). Whereas the SDNN reflects the overall increase in variability in vegetative function with fetal activity, the RMSSD represents the progressive vagal influence on short-term-variability. Maturation of the ANS more strongly emphasized the sympathetic branches, as indicated by the increase in SDNN/RMSSD ratio with fetal state. The changes in RMSSD from 2F to 4F were inverse to the changes in SDNN; a slight decrease was visible but not statistically significant. This finding was confirmed by prior studies showing the same shift in fetuses over 35 weeks of GA (Schneider et al., 2008; Lange et al., 2009). Moreover, earlier studies also reported an inverse change in SDNN/RMSSD ratio and PE, with the lowest ratio in the 1F state being observed for the linear parameters and the highest for PE. Notably, our data revealed differences in SDNN and RMSSD between the 1F and 2F states and in PE between the 2F and 4F states. All parameters showed significant shifts between 1F and 4F. These changes are in agreement with earlier reports of high linear fHRV parameters and low complexity measures in high fetal activity (Frank et al., 2006; Schneider et al., 2008).

The fHRV parameters may help to differentiate between fetal behavioral states and indicate the neurovegetative modulation within each state, thus offering greater insight into the vegetative development in utero. This confirms other studies pointing to the SDNN as a distinguishing parameter (Frank et al., 2006; Lange et al., 2009), including a more recent study indicating large state-dependent changes in SDNN (Wallwitz et al., 2012). mHR declined from the youngest to the oldest GA group, which reflects the known decrease in baseline heart rate toward term. MHR clearly increased with fetal activity as seen toward 4F, the behavioral state characterized by long lasting heart rate accelerations and possibly sustained tachycardia (Nijhuis et al., 1982). We conclude that developmental changes in HRV indicate how the autonomous nervous system matures the fetus's ability to develop behavioral states. These findings were evident for fetal age itself from the clear findings between the states but not with GA in our study. The findings from our data are in agreement with earlier studies in this field (Schneider et al., 2008; Lange et al., 2009). In contrast, studies investigating parameters over the course of pregnancy (Van Leeuwen et al., 1999; Lange et al., 2005) revealed an increase in linear parameters and complexity measures with GA, but it remains unclear whether the underlying state development is a bias influencing this change in parameters. However, in our study there was no subdivision into age groups for the analysis of the parameter changes between the behavioral states nor did we perform a subanalysis of the behavioral states across age groups due to the limited number of cases. Schneider et al. (2008) showed changes for SDNN, RMSSD, and PE that were similar to those in our study in general, but they were able to further elucidate that the shifts in the parameters from 1F to 2F concerned all fetal age groups, whereas the changes from 2F to 4F or from 1F to 2F became evident only during the later stages of gestation, mostly after 35 weeks. According to the standard criteria for fetal behavioral states, the increasing maturation of the fetal ANS causes fetal heart rate and movement to become increasingly synchronized. This synchronization is a known marker of fetal well-being and is used in the clinical monitoring of pregnant women. It is well known that fetal HRV can be affected by a number of factors, including GA, maternal medication, or fetal pathology (Van Leeuwen et al., 1999; Lange et al., 2005, 2009; Lowery et al., 2008). Cases of high-risk pregnancy, e.g., IUGR or preeclampsia, showed lower levels of fetal movement, absence of fetal heart rate synchronization, and movement, or decelerations in fetal heart rate (Schneider et al., 2006, 2009). Therefore, the combination of fetal actocardiogram and HRV parameters could be helpful in indicating fetal distress with the aid of fetal magnetography. The use of fHRV parameters enhances the possibilities to monitor fetal autonomous nervous development making the combination of fMCG and fMEG expedient in future neurodevelopmental studies. This could serve as a starting point for the implementation of fetal magnetography as a multimodal tool for fetal assessment.

Acknowledgments

We thank Magdalene Weiss from the fMEG-Center Tuebingen for her substantial work for this study. The study was approved by the Ethics Committee of the University of Tuebingen (No.476/2008MPG1). This study was supported by the Deutsche Forschungsgemeinschaft (DFG BI 195/50 and KI 1306/3-1), The University of Tuebingen (E.05.00303 and E.05.0259.1), and the Landesstiftung Baden-Wuerttemberg, Germany.

References

Drogtrop, A. P., Ubels, R., and Nijhuis, J. G. (1990). The association between fetal body movements, eye movements and heart rate patterns in pregnancies between 25 and 30 weeks of gestation. *Early. Hum. Dev.* 23, 67–73. doi: 10.1016/0378-3782(90)90129-7

Frank, B., Pompe, B., Schneider, U., and Hoyer, D. (2006). Permutation entropy improves fetal behavioural state classification based on heart rate analysis from biomagnetic recordings in near term fetuses. *Med. Biol. Eng. Comput.* 44, 179–187. doi: 10.1007/s11517-005-0015-z

Grimm, B., Haueisen, J., Huotilainen, M., Lange, S., Van Leeuwen, P., Menendez, T., et al. (2003). Recommended standards for fetal magnetocardiography. *Pacing Clin. Electrophysiol.* 26, 2121–2126. doi: 10.1046/j.1460-9592.2003.00330.x

Kiefer-Schmidt, I., Raufer, J., Brandle, J., Munssinger, J., Abele, H., Wallwiener, D., et al. (2013). Is there a relationship between fetal brain function and the fetal behavioral state? A fetal MEG-study. *J. Perinat. Med.* 41, 605–612. doi: 10.1515/jpm-2013-0022

Lange, S., Van Leeuwen, P., Geue, D., Hatzmann, W., and Gronemeyer, D. (2005). Influence of gestational age, heart rate, gender and time of day on fetal heart rate variability. *Med. Biol. Eng. Comput.* 43, 481–486. doi: 10.1007/BF02344729

Lange, S., Van Leeuwen, P., Schneider, U., Frank, B., Hoyer, D., Geue, D., et al. (2009). Heart rate features in fetal behavioural states. *Early. Hum. Dev.* 85, 131–135. doi: 10.1016/j.earlhumdev.2008.07.004

Lowery, C. L., Eswaran, H., Murphy, P., and Preissl, H. (2006). Fetal magnetoencephalography. *Semin. Fetal Neonatal. Med.* 11, 430–436. doi: 10.1016/j.siny.2006.09.002

Lowery, C. L., Govindan, R. B., Murphy, P., and Eswaran, H. (2008). Assessing cardiac and neurological maturation during the intrauterine period. *Semin. Perinatol.* 32, 263–268. doi: 10.1053/j.semperi.2008.04.006

Malik, M. (1996). Heart rate variability. standards of measurement, physiological interpretation, and clinical use. task force of the European society of cardiology and the North American society of pacing and electrophysiology. *Eur. Heart. J.* 17, 354–381. doi: 10.1093/oxfordjournals.eurheartj.a014868

Nijhuis, I. J., Ten Hof, J., Nijhuis, J. G., Mulder, E. J., Narayan, H., Taylor, D. J., et al. (1999). Temporal organization of fetal behavior from 24-weeks gestation onward in normal and complicated pregnancies. *Dev. Psychobiol.* 34, 257–268. doi: 10.1002/(SICI)1098-2302(199905)34:2<257::AID-DEV2>3.0.CO;2-V

Nijhuis, J. G. (1993). "Fetal behavioral states," in *Ultrasound in Obstetrics and Gynecology*, eds F. A. Chervenak, G. C. Isaacson, and S. Campbell (Boston, MA: Brown & Co.), 447–455.

Nijhuis, J. G., Prechtl, H. F., Martin, C. B. Jr., and Bots, R. S. (1982). Are there behavioural states in the human fetus? *Early Hum. Dev.* 6, 177–195. doi: 10.1016/0378-3782(82)90106-2

Peters, M., Crowe, J., Pieri, J. F., Quartero, H., Hayes-Gill, B., James, D., et al. (2001). Monitoring the fetal heart non-invasively: a review of methods. *J. Perinat. Med.* 29, 408–416. doi: 10.1515/JPM.2001.057

Pillai, M., and James, D. (1990a). Behavioural states in normal mature human fetuses. *Arch. Dis. Child* 65, 39–43. doi: 10.1136/adc.65.1_Spec_No.39

Pillai, M., and James, D. (1990b). The development of fetal heart rate patterns during normal pregnancy. *Obstet. Gynecol.* 76, 812–816. doi: 10.1097/00006250-199011000-00017

Prechtl, H. F. (1985). Ultrasound studies of human fetal behaviour. *Early. Hum. Dev.* 12, 91–98. doi: 10.1016/0378-3782(85)90173-2

Preissl, H., Lowery, C. L., and Eswaran, H. (2004). Fetal magnetoencephalography: current progress and trends. *Exp. Neurol.* 190(Supp. 1), S28–S36. doi: 10.1016/j.expneurol.2004.06.016

Schneider, U., Fiedler, A., Liehr, M., Kahler, C., and Schleussner, E. (2006). Fetal heart rate variability in growth restricted fetuses. *Biomed. Tech.* (*Berl.*). 51, 248–250. doi: 10.1515/BMT.2006.048

Schneider, U., Frank, B., Fiedler, A., Kaehler, C., Hoyer, D., Liehr, M., et al. (2008). Human fetal heart rate variability-characteristics of autonomic regulation in the third trimester of gestation. *J. Perinat. Med.* 36, 433–441. doi: 10.1515/JPM.2008.059

Schneider, U., Schleussner, E., Fiedler, A., Jaekel, S., Liehr, M., Haueisen, J., et al. (2009). Fetal heart rate variability reveals differential dynamics in the intrauterine development of the sympathetic and parasympathetic branches of the autonomic nervous system. *Physiol. Meas.* 30, 215–226. doi: 10.1088/0967-3334/30/2/008

Sonanini, A., Stingl, K., Preissl, H., Brandle, J., Hoopmann, M., Kagan, O., et al. (2014). Fetal behavioral states are stable over daytime - evidence by longitudinal and cross-sectional fetal biomagnetic recordings. *J. Perinat. Med.* 42, 307–314. doi: 10.1515/jpm-2013-0180

Van Leeuwen, P. (2004). Fetal magnetocardiography: time intervals and heart rate variability. *Neurol. Clin. Neurophysiol.* 2004, 46.

Van Leeuwen, P., Lange, S., Bettermann, H., Gronemeyer, D., and Hatzmann, W. (1999). Fetal heart rate variability and complexity in the course of pregnancy. *Early. Hum. Dev.* 54, 259–269. doi: 10.1016/S0378-3782(98)00102-9

Wallwitz, U., Schneider, U., Nowack, S., Feuker, J., Bauer, S., Rudolph, A., et al. (2012). Development of integrative autonomic nervous system function: an investigation based on time correlation in fetal heart rate patterns. *J. Perinat. Med.* doi: 10.1515/jpm-2012-0074 [Epub ahead of print].

Zhuravlev, Y. E., Rassi, D., Mishin, A. A., and Emery, S. J. (2002). Dynamic analysis of beat-to-beat fetal heart rate variability recorded by SQUID magnetometer: quantification of sympatho-vagal balance. *Early Hum. Dev.* 66, 1–10. doi: 10.1016/S0378-3782(01)00225-0

Conflict of Interest Statement: The authors declare that the research was conducted in the absence of any commercial or financial relationships that could be construed as a potential conflict of interest.

frontiers in
HUMAN NEUROSCIENCE

ORIGINAL RESEARCH ARTICLE
published: 25 November 2014
doi: 10.3389/fnhum.2014.00948

Fetal autonomic brain age scores, segmented heart rate variability analysis, and traditional short term variability

Dirk Hoyer[1]*, Eva-Maria Kowalski[1,2], Alexander Schmidt[1] Florian Tetschke[1], Samuel Nowack[1], Anja Rudolph[1,3], Ulrike Wallwitz[1,3], Isabelle Kynass[1,3], Franziska Bode[1,3], Janine Tegtmeyer[1,3], Kathrin Kumm[1,3], Liviu Moraru[1], Theresa Götz[1], Jens Haueisen[2], Otto W. Witte[1], Ekkehard Schleußner[3] and Uwe Schneider[3]

[1] *Biomagnetic Center, Hans Berger Department of Neurology, Jena University Hospital, Friedrich Schiller University, Jena, Germany*
[2] *Institute of Biomedical Engineering and Informatics, Ilmenau University of Technology, Ilmenau, Germany*
[3] *Department of Obstetrics, Jena University Hospital, Friedrich Schiller University, Jena, Germany*

Edited by:
Silvia Comani, Università degli Studi "G. d'Annunzio", Italy

Reviewed by:
Dirk Cysarz, Witten/Herdecke University, Germany
Kathleen M. Gustafson, University of Kansas Medical Center, USA

***Correspondence:**
Dirk Hoyer, Biomagnetic Center, Hans Berger Department of Neurology, Jena University Hospital, Friedrich Schiller University, Erlanger Allee 101, D-07747 Jena, Germany
e-mail: Dirk.Hoyer@med.uni-jena.de

Disturbances of fetal autonomic brain development can be evaluated from fetal heart rate patterns (HRP) reflecting the activity of the autonomic nervous system. Although HRP analysis from cardiotocographic (CTG) recordings is established for fetal surveillance, temporal resolution is low. Fetal magnetocardiography (MCG), however, provides stable continuous recordings at a higher temporal resolution combined with a more precise heart rate variability (HRV) analysis. A direct comparison of CTG and MCG based HRV analysis is pending. The aims of the present study are: (i) to compare the fetal maturation age predicting value of the MCG based fetal Autonomic Brain Age Score (fABAS) approach with that of CTG based Dawes-Redman methodology; and (ii) to elaborate fABAS methodology by segmentation according to fetal behavioral states and HRP. We investigated MCG recordings from 418 normal fetuses, aged between 21 and 40 weeks of gestation. In linear regression models we obtained an age predicting value of CTG compatible short term variability (STV) of R^2 = 0.200 (coefficient of determination) in contrast to MCG/fABAS related multivariate models with R^2 = 0.648 in 30 min recordings, R^2 = 0.610 in active sleep segments of 10 min, and R^2 = 0.626 in quiet sleep segments of 10 min. Additionally segmented analysis under particular exclusion of accelerations (AC) and decelerations (DC) in quiet sleep resulted in a novel multivariate model with R^2 = 0.706. According to our results, fMCG based fABAS may provide a promising tool for the estimation of fetal autonomic brain age. Beside other traditional and novel HRV indices as possible indicators of developmental disturbances, the establishment of a fABAS score normogram may represent a specific reference. The present results are intended to contribute to further exploration and validation using independent data sets and multicenter research structures.

Keywords: prenatal diagnosis, fetal autonomic brain age, magnetocardiography, cardiotocography

INTRODUCTION

Prenatal risk factors can permanently change the fetal brain development and are associated with diseases in later age. Adverse influences during fetal development that became permanently programmed can increase the postnatal risk for cardiovascular, metabolic, hyperkinetic, cognitive, learning and behavioral disorders (e.g., Barker, 1998, 2002; Barker et al., 2002; O'Keeffe et al., 2003; Van den Bergh et al., 2005).

Prenatal functional diagnosis is limited and requires innovative concepts. In that context, the fetal autonomic (neuro-vegetative) control plays a key role since it provides valuable information about several control systems that are mediated by the autonomic nervous system. The associated heart rate patterns (HRP) are one of the few signals that can be obtained non-invasively from the fetus, and hence, heart rate variability (HRV) analysis is uniquely suited to assess the fetal functional autonomic brain development. Fetal HRP provide quantitative information about sympathetic and vagal activation, fetal behavioral states, and fetal movements (Nijhuis et al., 1982; Van Leeuwen et al., 1999; David et al., 2007; Hoyer et al., 2009; Schmidt et al., 2014).

In order to obtain normal values of maturation indices in healthy fetuses and deviations due to risk factors, a sophisticated analysis of fetal HRP is required. Finally, the association between prenatal and postnatal autonomic control and disturbances needs to be investigated in that context.

Antepartum cardiotocography (CTG) is a predominant established method that contributes to fetal surveillance and risk assessment both antenatal and during labor based on the analysis of fetal HRP age (Nijhuis et al., 2000; Pardey

et al., 2002; Serra et al., 2008, 2009). FIGO (International Federation of Gynaecology and Obstetrics) risk score as well as the fluctuation indices short term variability (STV) and long term variability (LTV) are realized in Dawes-Redman methodology (Pardey et al., 2002). The fetal HRP displayed in CTG depends on gestational age, fetal activity and a variety of other factors, but classification of recordings primarily aimed on distinguishing the healthy from the distressed fetus rather than precisely assessing maturation. Hence, the resulting question to be followed in this study is, to which extent CTG methodology allows a fetal autonomic brain age assessment in comparison to the higher quality MCG methodology.

Universal characteristics of evolution and development in non-living and living nature are increasing fluctuation amplitude, increasing complexity and pattern formation. Those characteristics similarly apply in the phylogenetic and the ontogenetic development. The fetal HRP reflect corresponding characteristics of the maturating fetal autonomic brain activity. All of those characteristics can be interpreted as reflecting autonomous influences of the sympathetic and parasympathetic nervous systems, influenced by the superordinate medullary centers. In a previous study, using continuous magnetocardiographic (MCG) recordings at 1 ms temporal resolution, we designed a resulting "fetal autonomic brain age score" (fABAS; Hoyer et al., 2013b).

However, a certain part of variance could not be explained by the score and the question arises how and to which extent a more sophisticated model may improve the performance. In that context, segmentation of the measured HRP under consideration of behavioral states as well as of the particular exclusion of acceleration (AC) and deceleration (DC) patterns may provide information about different aspects of autonomic modulations in more detail.

The aims of the present study are: (i) to compare the fetal maturation age predicting value of the MCG based fABAS approach with that of Dawes-Redman methodology; and (ii) to elaborate fABAS methodology by segmentation of the recordings according to behavioral states and HRP.

MATERIALS AND METHODS

SUBJECTS AND DATA AQUISITION

From the study database of the Biomagnetic Center, Department of Neurology, and Department of Obstetrics, both Jena University Hospital, recordings of 418 normal singleton fetuses, aged between 21 and 40 weeks of gestation (WGA), healthy according to standard obstetric observation methods, single recording in a non-stress situation were included. The study was approved by the Local Ethics Committee of the Friedrich Schiller University. All women signed a written, informed consent form.

All measurements were taken in a magnetically shielded room at the Biomagnetic Center, Department of Neurology, Jena University Hospital using the vector-magnetograph ARGOS 200 (ATB, Chieti, Italy). Pregnant women were positioned supine or with a slight twist to either side to prevent compression of the inferior vena cava. The dewar was positioned as close as possible above the fetal heart determined by sonographic localization, but without contact to the maternal abdominal wall. The MCG signal was recorded over a period of 30 min with a sampling rate of 1024 Hz. The fetal heart beats were detected using a newly developed independent component analysis based strategy (Schmidt et al., 2014). The fetal body movements were reconstructed from the fMCG signal (for details see Schmidt et al., 2014).

CTG COMPATIBLE ANALYSIS ACCORDING TO DAWES-REDMAN

In the present work the heart beat intervals (MCG sampling period $\approx$1 ms) were integrated over 3.75 s epochs in order to obtain a CTG compatible signal of the identical recording. Analyzable 1 min sections were considered as those that contain neither large decelerations nor more than 50% artifacts (not detected beats/beat intervals; Pardey et al., 2002).

- STV is calculated as mean difference between consecutive heart beat interval epochs in all analyzable 1 min sections. The results of all analyzed 1 min sections are averaged.
- LTV is calculated as fluctuation range of heart beat interval epochs in analyzable 1 min sections. The fluctuation range is calculated as a sum between maximal deviation above baseline and maximal deviation below baseline. The fluctuation ranges of all analyzed 1 min sections are averaged.

Furthermore, the Dawes-Redman criteria for normality from 26 WGA upwards, that require up to 60 min recordings, were formally applied to the 30 min recordings of the fetuses aged at least 26 WGA (n = 313). The following criteria have to be met (adapted from Pardey et al., 2002):

- The recording must contain at least one episode of high variation.
- STV >3.0 ms, but if it is <4.5 ms LTV averaged across all episodes of high variation must be >3rd percentile for WGA.
- No evidence of a high-frequency sinusoidal rhythm.
- At least one AC, or a fetal movement rate of $\geq$20 per hour and a LTV averaged across all episodes of high variation >10th percentile for WGA.
- At least one fetal movement or three AC.
- No DC of >20 lost beats if the recording is <30 min, no more than one DC of 21–100 lost beats if it is >30 min, and no DC at all >100 lost beats.
- The basal fetal heart rate must be 116–160 beats/min if the recording is <30 min.
- LTV within 3 SD of its estimated value or (a) STV >5.0 ms; (b) an episode of high variation with $\geq$0.5 fetal movements per minute; (c) the basal fHR $\geq$120 beats/min; and (d) the signal loss <30%.
- The final epoch of the recording must not be part of a DC.
- No suspected artifacts at the end of the recording if the recording is <60 min.

In that context, an AC is defined as an increase in heart rate for more than 15 s with a minimum deviation from baseline exceeding 10 bpm. A DC is defined as a decrease below the baseline for more than 30 s and a deviation >20 bpm or 60 s and >10 bpm, respectively (Pardey et al., 2002).

Table 1 | Heart rate variability indices.

Parameter	Meaning, Interpretation	Calculation
Dawes-Redman		
STV	**Short Term Variability** Integrative sympatho-vagal modulations, fluctuation periods of seconds	Mean difference between consecutive heart beat interval epochs of 3.75 s, w/o DC and artifacts <50%
LTV	**Long Term Variability** Fluctuation periods of minutes	Mean fluctuation range of heart beat interval epochs in 1 min sections, w/o DC and artifacts <50%
fABAS		
AMP	**Fluctuation range** of heart beat intervals, overall sympatho-vagal modulations	20–95 inter-quantile distance of detrended NN interval series
gMSE3	**Complexity** of sympatho-vagal rhythms	Generalized Mutual Information at coarse graining level 3 of beat interval series, see Hoyer et al. (2013a)
skewness	**Asymmetry**, contribution of vagal and sympathetic activity with their different time constants, decline of DC and formation of AC	skewness of instantaneous heart rate series
pNN5	**Fast, vagal** Mainly vagally modulated rhythms	Percentage of differences between adjacent NN intervals that are >5 ms.
lnVLF/LF	**Baseline fluctuation** in relation to sympatho-vagal modulations	Ratio between very low (0.02–0.08 Hz) and low (0.08–0.2 Hz) frequency band power
Pattern segmented		
gMSE3 w/o DC gMSE3 basic	**w/o DC** - parameters under exclusion of DC	Mean of parameter of subsegments without DC
skewness w/o DC skewness basic		
pNN5 w/o DC pNN5 basic	**basic** - parameters of basic rhythm	Mean of parameter of subsegments w/o DC and w/o AC
lnVLF/LF w/o DC lnVLF/LF basic		

** Segmented analysis of fluctuation range (AMP) was not performed due to lacking significance in quiet sleep. Partly adapted from Hoyer et al. (2013b), further details in TaskForce (1996), Pardey et al. (2002), Hoyer et al. (2013a).*

MCG BASED HEART RATE VARIABILITY ANALYSIS—FETAL AUTONOMIC BRAIN AGE SCORE

The fABAS was previously proposed by the authors using a calculation precision of ≈1 ms according to the MCG sampling rate (Hoyer et al., 2013b). Fetal autonomic brain age score based on particular HRV parameters that were selected according to universal developmental characteristics, namely increasing fluctuation amplitude (assessed by AMP), increasing complexity (assessed by gMSE3), and pattern formation (assessed by skewness, pNN5, lnVLF/LF, see **Table 1**). In that previous work, the fetal age was predicted by multivariate linear regression models (forward procedure: stepwise inclusion of variables while $P(F) < 0.05$; backward procedure: stepwise exclusion of variables while $P(F) > 0.1$) for each sleep state independently. The resulting models for quiet and active sleep were considered fABAS. While [gMSE3, skewness, VLF/LF, pNN5] contributed in the quiet sleep model, [AMP, skewness, gMSE3, pNN5, VLF/LF] contributed in the active sleep model. Here, an additional model was built for the entire 30 min recordings that can include only one or several behavioral states. The resulting additional model constitutes a third branch of fABAS. Furthermore, the linear regression models were supplemented with quadratic term regression models that were built using the same HRV parameters.

SLEEP STATE SEGMENTATION

From the entire 30 min recordings 10 min segments according to quiet and active sleep related HRP I, HRP II were selected following a consensus decision by three independent obstetricians according to an advanced version of standard criteria (Nijhuis et al., 1982; Schneider et al., 2009; Hoyer et al., 2013b).

- HRP I (quiet state, correlated to quiet sleep 1F): stable fetal heart rate (fHR) (variation of visually determined floating baseline <10 bpm/3 min) with a small oscillation bandwidth (< ±5 bpm from floating baseline fHR), isolated (maximum 2 per 10 min) AC (>15 bpm over >15 s) and a floating baseline fHR that does not exceed 160 bpm.
- HRP II (active state, correlated to active sleep 2F): fluctuating fHR with an oscillation bandwidth exceeding +/− 5 bpm from floating baseline, frequent (at least 3 per 10 min) AC (>15 bpm, >15 s), and the fHR exceeding 160 bpm only during AC.
- HRP III (active state, correlated to active awakeness 4F): fHR patterns with long-lasting AC exceeding 160 bpm, frequently fused into a sustained tachycardia.

Based on the classification results we selected 10 min sections of quiet sleep ($n = 137$) and active sleep ($n = 344$). Consequently, in 63 of the 418 recordings, sections of both, HRP I and HRP

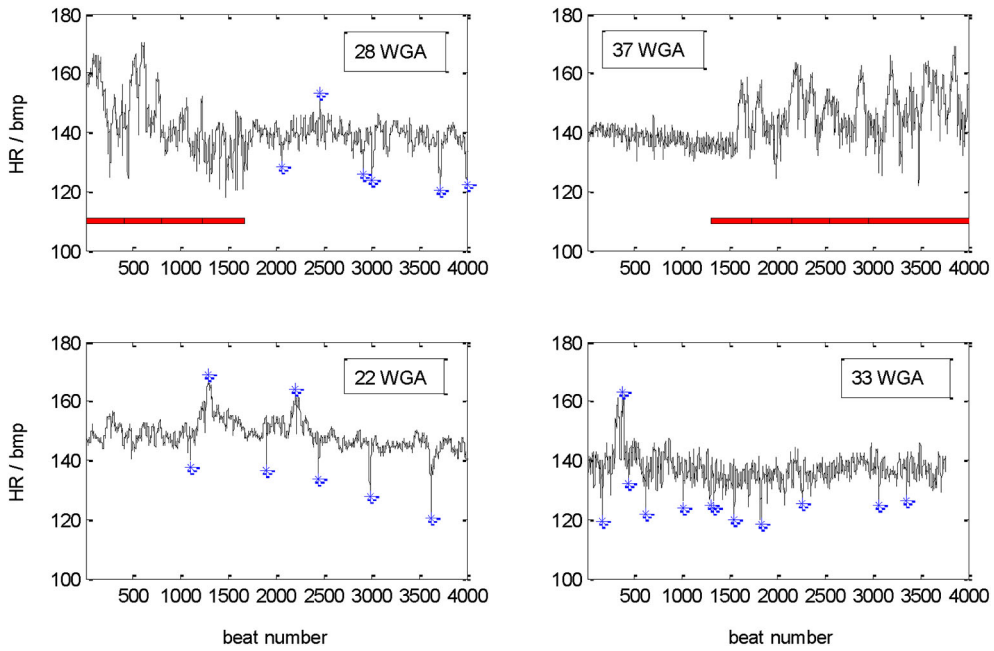

FIGURE 1 | Tachograms of 30 min recordings of four different fetuses. Upper part: changes between sections of active (marked by red horizontal bar) and quiet sleep related heart rate patterns in a younger (28 WGA) and an older (37 WGA) fetus. Lower part: quiet sleep related heart rate patterns at 22 and 33 WGA. DC and AC (>10 bpm deviation from floating baseline, marked by blue *) are identified in the quiet sleep sections only.

II, were classified. Active awakeness classified recordings were not analyzed because of their small sample size ($n = 29$).

PATTERN SEGMENTATION–PARTIAL EXCLUSION OF HEART RATE ACCELERATIONS AND DECELERATIONS

In addition, periods without DC and segments of basic activity (with neither DC nor AC), respectively, were analyzed in the HRP I segments. The methodology of the here proposed MCG based segmented HRV analysis is different from the CTG—Dawes-Redman methodology used above. In the present context, the definitions of AC and DC were modified according to the following rules:

- Sections without DC were identified in moving 3 min windows (shifted by 1 min over 10 min segment) if there were no deviations below the baseline (estimated for each 3 min window) > 10 bpm;
- Sections of basic activity were identified in moving 3 min windows (shifted by 1 min over 10 min segment) if there were no deviations below or above the baseline (estimated for each 3 min window) > 10 bpm.

The baseline was estimated according to original Dawes-Redman methodology (Pardey et al., 2002). From all identified windows the HRV parameters were calculated and averaged.

This kind of pattern segmentation was performed for all significantly age predicting HRV parameters of fABAS (see **Table 1**).

The example recordings shown in **Figure 1** demonstrate the diversity of the recorded pattern. In the upper part a change between active and quiet state in a premature age of 28 WGA is compared with a clear change from quiet to active state in the mature age of 37 WGA. In the part underneath, recordings classified as quiet sleep at 22 and 33 WGA are shown. Please notice partly unstable baseline, AC and DC are marked in the quiet sleep section. There are neither periods of incorrect heart beat detections (beat intervals) nor periods of dropouts.

STATISTICAL ANALYSIS

The predictive value of the HRV parameters was assessed by univariate and multivariate, linear and quadratic term regression models over the entire investigated maturation period (corrected coefficient of determination R^2). The cases were weighted to approximate equal distribution over gestational age. $P < 0.05$ was considered significant. Since most of the predictors were significant, only non-significant results are marked by "n.s.". For better reading, predictors with $R^2 > 0.3$ were marked by bold letters. All statistical analyses were carried out using IBM SPSS Statistics 21.

RESULTS

30 MIN RECORDINGS

Traditional STV and LTV were calculated from analyzable periods according to CTG methodology like outlined above. Short term variability predicted the maturation age with a low coefficients of determination ($R^2 = 0.200$, 206, linear and quadratic model, **Table 2**). The Dawes-Redman criteria were met with increasing frequency between 26 and 32 WGA and were consistently met from 32 WGA onwards (**Figure 2**).

From the fABAS related HRV parameters, AMP, skewness, and pNN5 and provided strong univariate linear age predictors

Table 2 | Analyses of 30 min recordings: univariate and multivariate, linear and quadratic term regression models, coefficients of determination R^2, parameters selected according to CTG (Dawes-Redman related (Pardey et al., 2002)) and MCG based fABAS related (Hoyer et al., 2013b), $R^2 > 0.3$ in bold, all cases significant.

Parameter	30 min recording	
	Linear	Quadratic
CTG compatible		
STV (ms)	0.200	0.206
LTV (ms)	0.085	0.116
fMCG based, fABAS related		
Time domain		
AMP	**0.312**	**0.321**
skewness	**0.458**	**0.502**
pNN5	**0.347**	**0.367**
Power spectra		
lnVLF/LF	0.034	0.060
Complexity		
gMSE3	0.226	0.231
Multivariate model, fABAS		
[AMP, skewness, pNN5, lnVLF/LF, gMSE3]	**0.648**	**0.656**
Multivariate model, fABAS + STV		
[AMP, skewness, pNN5, lnVLF/LF, gMSE3, STV]	**0.649**	**0.657**

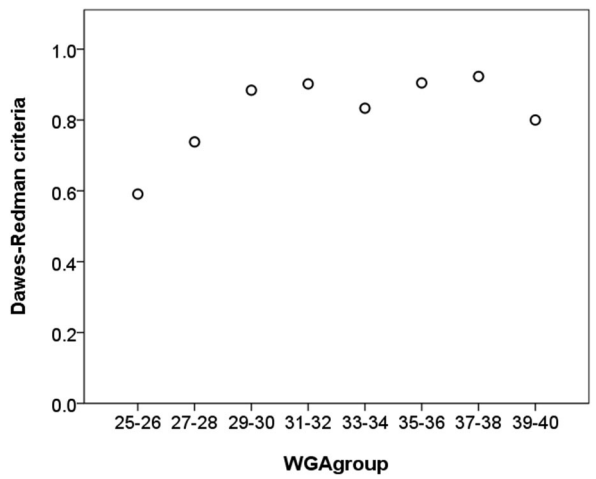

FIGURE 2 | Relative frequency of recordings that meet the Dawes-Redman criteria (1 = 100%) vs. chronological age (in weeks GA) of 30 min recordings. In absolute values, 134 of 167 cases met the criteria in the subset of ≤32 WGA and 130 of 146 in the subset of >32 WGA, respectively.

(R^2 = 0.312, 0.458, 0.347). They were partly improved by including a quadratic term (R^2 = 0.321, 0.502, 0.367). In the multivariate models all parameters significantly contributed leading to R^2 = 0.648 and R^2 = 0.656, respectively (**Table 2**, **Figure 3**). In contrast, STV and LTV did not provide additional predictive value to the multivariate models.

SEGMENTED RECORDINGS

Active sleep 10 min segments

In the active sleep data, AMP (R^2 = 0.392 and 0.430, linear and quadratic), skewness (R^2 = 0.352 and 0.431) and pNN5

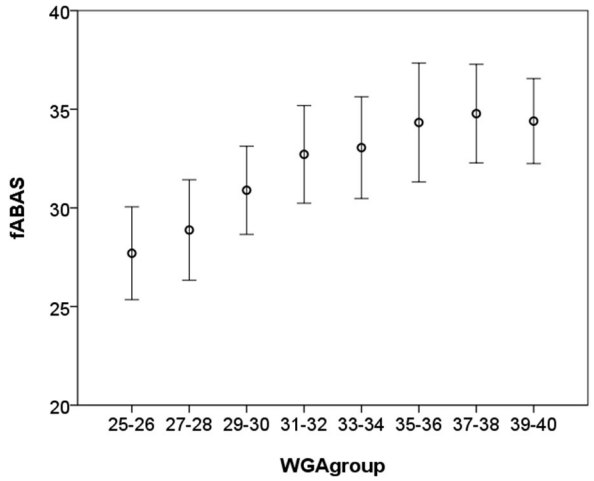

FIGURE 3 | Fetal autonomic brain age score [AMP, skewness, pNN5, lnVLF/LF, gMSE3] vs. chronological age (in WGA) of 30 min recordings, mean ± standard deviation.

Table 3 | Analyses of 10 min segments in active sleep: linear and quadratic regression models, coefficients of determination R^2, parameters selected according to fABAS (Hoyer et al., 2013b), $R^2 > 0.3$ in bold.

Predictor	R^2	
	Linear	Quadratic
Time domain		
AMP	**0.392**	**0.430**
Skewness	**0.352**	**0.431**
pNN5	**0.350**	**0.376**
Power spectra		
lnVLF/LF	0.098	0.103
Complexity		
gMSE3	0.128	0.130
Multivariate model	-	-
[AMP, Skewness, gMSE3, pNN5, lnVLF/LF]	**0.610**	**0.636**

(R^2 = 0.350 and 0.376) clearly predicted the fetal maturation age. In the multivariate models, additionally gMSE3 and lnVLF/LF contributed leading to R^2 = 0.610 and 0.636 in the linear and quadratic, respectively, models (**Table 3**).

Quiet sleep 10 min segments

In the quiet sleep data, gMSE3 (R^2 = 0.542 and 0.565), but also pNN5 (R^2 = 0.320 and 0.338) and skewness (R^2 = 0.316 and 0.320) were stronger predictors than lnVLF/LF (R^2 = 0.147 and 0.159). AMP did not provide predictive value. The stepwise built multivariate model included [skewness, gMSE3, pNN5] (R^2 = 0.626 and 0.641; **Table 4**).

Further pattern segmentation in quiet sleep

Further pattern segmentation, namely the exclusion of DC and AC removed the predictive value of skewness. This result is consistent with the fact that skewness mainly reflects asymmetries due to DC and AC which are important maturation characteristics. Other aspects of behavior are basic activity, i.e., the basic rhythm

Table 4 | Analyses of 10 min segments in quiet sleep: additional pattern segmentation (without decelerations: w/o DC; basic activity, neither DC nor AC: basic), linear and quadratic regression models, coefficients of determination R^2, parameters according to Table 2, $R^2 > 0.3$ in bold.

Predictor	R^2	
	Linear	Quadratic
Time domain		
AMP	n.s.	n.s.
Skewness	**0.316**	**0.320**
skewness w/o DC	0.123	0.127
skewness basic	0.032	0.038
pNN5	**0.320**	**0.338**
pNN5 w/o DC	**0.396**	**0.451**
pNN5 basic	**0.374**	**0.428**
Power spectra		
lnVLF/LF	0.147	0.159
lnVLF/LF w/o DC	0.192	0.201
lnVLF/LF basic	0.195	0.206
Complexity		
gMSE3	**0.542**	**0.565**
gMSE3 w/o DC	**0.609**	**0.627**
gMSE3 basic	**0.632**	**0.657**
Multivariate model, fABAS indices		
[Skewness, gMSE3, pNN5]	**0.626**	**0.641**
Multivariate model, pattern segmented		
[Skewness, gMSE3, gMSE3w/oDC, gMSE3basic]	**0.706**	**0.714**

containing neither AC nor DC, and activity under exclusion of DC. Concerning those aspects, the predictive value of pNN5, gMSE3 and lnVLF/LF was increased. The gMSE3 related indices were the strongest univariate predictors (gMSE, gMSEw/oDC, gMSE3basic: $R^2 = 0.542$, 0.609. 0.632 in the linear models, and $R^2 = 0.565$, 0.627. 0.657 in the quadratic models, see **Table 4**).

The stepwise built multivariate model resulted on the inclusion of [skewness, gMSE3, gMSEw/oDC, gMSE3basic] with $R^2 = 0.706$ in the linear and $R^2 = 0.714$ quadratic model. This result indicates a relevant advantage compared to the consideration of data that are classified as quiet sleep as a total without further pattern segmentation.

DISCUSSION

Traditional HRV indices reflect: (i) vagal activity during quiet sleep; (ii) sympathetic activity during active sleep; and (iii) integrative control in longer recordings with changing states. In a recent study, we have demonstrated a strong relationship between those HRV indices and fetal maturation age (Hoyer et al., 2009). Compared to those traditional HRV indices, we newly developed a fABAS based on universal developmental characteristics assessing maturation age with a high precision in active and quiet sleep (Hoyer et al., 2013b). In this study we show that fABAS based methodology significantly improves fetal maturation age assessment compared to established CTG. Those results are based on our comprehensive database obtained from MCG measurements.

The particular aims of the present study were: (i) to compare the fetal maturation age predicting value of the MCG based fABAS approach with that of CTG (Dawes-Redman) compatible STV; and (ii) to elaborate fABAS methodology by segmentation according to behavioral states (overall recording, active and quiet sleep segments) and HRP.

30 MIN RECORDINGS

The maturation age predicting value of STV ($R^2 = 0.200$, linear model) was significantly lower in comparison to fABAS.

Interestingly, using the indices of fABAS applied to the entire 30 min recordings, the maturation age was clearly predictable ($R^2 = 0.648$, linear model), although the signals were very heterogeneous due to the occurrence of only one or several behavioral states. The increased R^2 in the quadratic models, moreover, may reflect the saturating maturation after 32 WGA mainly expressed in skewness (see **Figure 3**). This characteristic curve is in line with previous results of power spectral analysis (Van Leeuwen et al., 2003).

ACTIVE AND QUIET SLEEP 10 MIN SEGMENTS

The predictive value of the fABAS related models in active and quiet sleep ($R^2 = 0.610$, 0.626, linear models) was slightly lower in comparison to the 30 min recordings. However, it should be noticed that state dependent aspects of autonomic control, such as vagal and sympathetic dominance, provided an almost similar predictive value. Saturating maturation after 32 WGA considered in quadratic models of vagal HRV (pNN5) in quiet sleep and mainly sympathetic/overall HRV (AMP, skewness) in active sleep may have also contributed to increased R^2 in the quadratic models.

FURTHER PATTERN SEGMENTATION IN QUIET SLEEP

Further segmentation in quiet sleep focused on the differential contribution of basic activity and AC as well as DC of at least 10 bpm deviation from baseline. The resulting independent factors of the novel model, namely skewness, gMSE3, gMSE3w/oDC, gMSE3basic, may highlight the role of complex adjustments between sympatho-vagally mediated fluctuations in connection with AC and DC patterns. The predictive value ($R^2 = 0.706$, linear model) was clearly higher than that of fABAS. This result indicates that the essential universal developmental characteristics, namely increasing complexity and pattern formation which go hand in hand with fetal development, also apply for the particular pattern during quiet sleep. Furthermore, the result implies that a consideration of the respective physiological pattern in detail, might even improve the maturation assessment. Therefore, fABAS may serve as classification tool for the general condition, whereas further pattern segmentation provides a more detailed focus on an observed abnormality.

Fetal autonomic brain age score indices in combination with the novel pattern segmentation based on our comprehensive MCG database can serve as a representative norm-sample of the normal fetal autonomic maturation age (see **Figures 3**, **4**). With that it will be easy to detect even minor deviations from the normal fetal development.

METHODOLOGICAL ISSUES

In principle, the application of the Dawes-Redman criteria and LTV as a traditional CTG methodology to MCG based HRV

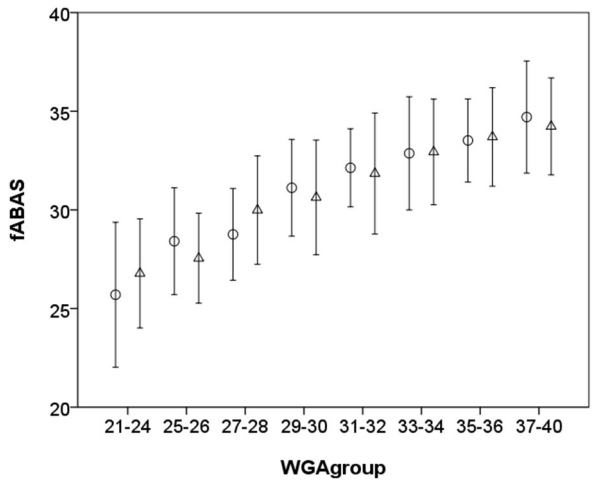

FIGURE 4 | Fetal autonomic brain age score [Skewness, gMSE3, pNN5] for quiet sleep segments ∘ and [AMP, Skewness, gMSE3, pNN5, lnVLF/LF] for active sleep segments △ vs. chronological age (in WGA), mean ± standard deviation, notice that 21–24 WGA and 37–40 WGA, respectively, are merged due to the small number of samples.

analysis was possible. During a period of 60 min, which is recommended for the application of the Dawes-Redman criteria, at least one active pattern is statistically expected to occur. However, since only 30 min recordings were analyzed, a number of subjects did not meet the criteria. Recordings of 60 min length would allow direct consideration of FIGO Dawes-Redman criteria. Even longer observations would furthermore lead to a better evaluation of sleep state dynamics. However, due to patient compliance and the possibly increasing number of artifacts in longer measurements, the performance in shorter recordings is of particular interest.

The segmentation according to behavioral state classification is the result of a consensus decision of three experts based on HRP that furthermore slightly change with maturation age between 21–40 WGA. This classification is not always unequivocal, but it reflects the heterogeneity of recordings and the state of the art.

The present results are mainly representative for the investigated 30 min recordings and 10 min segments. A next necessary step would be the validation and improvement of the presented methodology in recordings from different measurement sites.

For a fair evaluation of the here proposed methodology and search for the optimum, other HRV indices should also be taken into consideration. The here presented methodology allows the inclusion of further precise MCG HRV indices as well of FIGO recommended CTG compatible indices.

In the subsequent steps, multifactorial models are required to consider both, maturation age and developmental disorders.

CONCLUSION

Heart rate variability indices selected according to fABAS using 30 min fMCG recordings and segmented HRV analysis provide a promising tool for the estimation of the fetal autonomic brain age that is superior to CTG based indices. Resulting normograms of normal autonomic brain maturation may constitute significant references for the identification of developmental disturbances. The presented methodology is intended to contribute to further exploration and validation with regard to the early identification of developmental disorders using independent data sets in multicenter studies.

ACKNOWLEDGMENTS

This work was supported by the German Research Foundation (Deutsche Forschungsgemeinschaft, HO 1634 12-2, Schn 775/2-3) and the Curie Intra-European Fellowship IEF-2009-237290. We thank Stefan Claus for editing the manuscript.

REFERENCES

Barker, D. J. (1998). In utero programming of chronic disease. *Clin. Sci. (Lond)* 95, 115–128. doi: 10.1042/cs19980019

Barker, D. J. (2002). Fetal programming of coronary heart disease. *Trends Endocrinol. Metab.* 13, 364–368. doi: 10.1016/s1043-2760(02)00689-6

Barker, D. J., Eriksson, J. G., Forsén, T., and Osmond, C. (2002). Fetal origins of adult disease: strength of effects and biological basis. *Int. J. Epidemiol.* 31, 1235–1239. doi: 10.1093/ije/31.6.1235

David, M., Hirsch, M., Karin, J., Toledo, E., and Akselrod, S. (2007). An estimate of fetal autonomic state by time-frequency analysis of fetal heart rate variability. *J. Appl. Physiol. (1985)* 102, 1057–1064. doi: 10.1152/japplphysiol.00114.2006

Hoyer, D., Heinicke, E., Jaekel, S., Tetschke, F., Di Pietro Paolo, D., Haueisen, J., et al. (2009). Indices of fetal development derived from heart rate patterns. *Early Hum. Dev.* 85, 379–386. doi: 10.1016/j.earlhumdev.2009.01.002

Hoyer, D., Nowack, S., Bauer, S., Tetschke, F., Rudolph, A., Wallwitz, U., et al. (2013a). Fetal development of complex autonomic control evaluated from multiscale heart rate patterns. *Am. J. Physiol. Regul. Integr. Comp. Physiol.* 304, R383–R392. doi: 10.1152/ajpregu.00120.2012

Hoyer, D., Tetschke, F., Jaekel, S., Nowack, S., Witte, O. W., Schleußner, E., et al. (2013b). Fetal functional brain age assessed from universal developmental indices obtained from neuro-vegetative activity patterns. *PLoS One* 8:e74431. doi: 10.1371/journal.pone.0074431

Nijhuis, J. G., Prechtl, H. F., Martin, C. B. Jr., and Bots, R. S. (1982). Are there behavioural states in the human fetus?. *Early Hum. Dev.* 6, 177–195. doi: 10.1016/0378-3782(82)90106-2

Nijhuis, I. J., ten Hof, J., Mulder, E. J., Nijhuis, J. G., Narayan, H., Taylor, D. J., et al. (2000). Fetal heart rate in relation to its variation in normal and growth retarded fetuses. *Eur. J. Obstet. Gynecol. Reprod. Biol.* 89, 27–33. doi: 10.1016/s0301-2115(99)00162-1

O'Keeffe, M. J., O'Callaghan, M., Williams, G. M., Najman, J. M., and Bor, W. (2003). Learning, cognitive and attentional problems in adolescents born small for gestational age. *Pediatrics* 112, 301–317. doi: 10.1542/peds.112.2.301

Pardey, J., Moulden, M., and Redman, C. W. (2002). A computer system for the numerical analysis of nonstress tests. *Am. J. Obstet. Gynecol.* 186, 1095–1103. doi: 10.1067/mob.2002.122447

Schmidt, A., Schneider, U., Witte, O. W., Schleussner, E., and Hoyer, D. (2014). Developing fetal motor-cardiovascular coordination analysed from multi-channel magnetocardiography. *Physiol. Meas.* 35, 1943–1959. doi: 10.1088/0967-3334/35/10/1943

Schneider, U., Schleussner, E., Fiedler, A., Jaekel, S., Liehr, M., Haueisen, J., et al. (2009). Fetal heart rate variability reveals differential dynamics in the intrauterine development of the sympathetic and parasympathetic branches of the autonomic nervous system. *Physiol. Meas.* 30, 215–226. doi: 10.1088/0967-3334/30/2/008

Serra, V., Bellver, J., Moulden, M., and Redman, C. W. (2009). Computerized analysis of normal fetal heart rate pattern throughout gestation. *Ultrasound Obstet. Gynecol.* 34, 74–79. doi: 10.1002/uog.6365

Serra, V., Moulden, M., Bellver, J., and Redman, C. W. (2008). The value of the short-term fetal heart rate variation for timing the delivery of growth-retarded fetuses. *BJOG* 115, 1101–1117. doi: 10.1111/j.1471-0528.2008.01774.x

TaskForce. (1996). Heart rate variability: standards of measurement, physiological interpretation and clinical use. Task Force of the European Society of Cardiology

and the North American Society of Pacing and Electrophysiology. *Circulation* 93, 1043–1065. doi: 10.1161/01.CIR.93.5.1043

Van den Bergh, B. R., Mulder, E. J., Mennes, M., and Glover, V. (2005). Antenatal maternal anxiety and stress and the neurobehavioural development of the fetus and child: links and possible mechanisms. A review. *Neurosci. Biobehav. Rev.* 29, 237–258. doi: 10.1016/j.neubiorev.2004.10.007

Van Leeuwen, P., Geue, D., Lange, S., Hatzmann, W., and Gronemeyer, D. (2003). Changes in the frequency power spectrum of fetal heart rate in the course of pregnancy. *Prenat. Diagn.* 23, 909–916. doi: 10.1002/pd.723

Van Leeuwen, P., Lange, S., Bettermann, H., Grönemeyer, D., and Hatzmann, W. (1999). Fetal heart rate variability and complexity in the course of pregnancy. *Early Hum. Dev.* 54, 259–269. doi: 10.1016/s0378-3782(98)00102-9

Conflict of Interest Statement: The authors declare that the research was conducted in the absence of any commercial or financial relationships that could be construed as a potential conflict of interest.

Received: 11 September 2014; accepted: 07 November 2014; published online: 25 November 2014.

*Citation: Hoyer D, Kowalski E-M, Schmidt A, Tetschke F, Nowack S, Rudolph A, Wallwitz U, Kynass I, Bode F, Tegtmeyer J, Kumm K, Moraru L, Götz T, Haueisen J, Witte OW, Schleußner E and Schneider U (2014) Fetal autonomic brain age scores, segmented heart rate variability analysis, and traditional short term variability. Front. Hum. Neurosci. **8**:948. doi: 10.3389/fnhum.2014.00948*

This article was submitted to the journal Frontiers in Human Neuroscience.

frontiers in
HUMAN NEUROSCIENCE

ORIGINAL RESEARCH ARTICLE
published: 22 October 2014
doi: 10.3389/fnhum.2014.00852

Fetal functional imaging portrays heterogeneous development of emerging human brain networks

András Jakab[1]*, Ernst Schwartz[1], Gregor Kasprian[2], Gerlinde M. Gruber[3], Daniela Prayer[2], Veronika Schöpf[2†] and Georg Langs[1,4†]

[1] *Computational Imaging Research Lab, Department of Biomedical Imaging and Image-guided Therapy, Medical University of Vienna, Vienna, Austria*
[2] *Division for Neuroradiology and Musculoskeletal Radiology, Department of Biomedical Imaging and Image-guided Therapy, Medical University of Vienna, Vienna, Austria*
[3] *Department of Systematic Anatomy, Center for Anatomy and Cell Biology, Medical University of Vienna, Vienna, Austria*
[4] *Computer Science and Artificial Intelligence Lab, Massachusetts Institute of Technology, Cambridge, MA, USA*

Edited by:
Marika Berchicci, University of Rome "Foro Italico," Italy

Reviewed by:
Emmanuel Carrera, Hôpitaux Universitaires de Genève, Switzerland
Lajos R. Kozák, Semmelweis University Budapest, Hungary

****Correspondence:***
András Jakab, Computational Imaging Research Lab, Department of Biomedical Imaging and Image-guided Therapy, Medical University of Vienna, Währinger Gürtel 18-20, Vienna, Austria
e-mail: andras.jakab@meduniwien.ac.at

†Veronika Schöpf and Georg Langs have contributed equally to this work.

The functional connectivity architecture of the adult human brain enables complex cognitive processes, and exhibits a remarkably complex structure shared across individuals. We are only beginning to understand its heterogeneous structure, ranging from a strongly hierarchical organization in sensorimotor areas to widely distributed networks in areas such as the parieto-frontal cortex. Our study relied on the functional magnetic resonance imaging (fMRI) data of 32 fetuses with no detectable morphological abnormalities. After adapting functional magnetic resonance acquisition, motion correction, and nuisance signal reduction procedures of resting-state functional data analysis to fetuses, we extracted neural activity information for major cortical and subcortical structures. Resting fMRI networks were observed for increasing regional functional connectivity from 21st to 38th gestational weeks (GWs) with a network-based statistical inference approach. The overall connectivity network, short range, and interhemispheric connections showed sigmoid expansion curve peaking at the 26–29 GW. In contrast, long-range connections exhibited linear increase with no periods of peaking development. Region-specific increase of functional signal synchrony followed a sequence of occipital (peak: 24.8 GW), temporal (peak: 26 GW), frontal (peak: 26.4 GW), and parietal expansion (peak: 27.5 GW). We successfully adapted functional neuroimaging and image post-processing approaches to correlate macroscopical scale activations in the fetal brain with gestational age. This *in vivo* study reflects the fact that the mid-fetal period hosts events that cause the architecture of the brain circuitry to mature, which presumably manifests in increasing strength of intra- and interhemispheric functional macro connectivity.

Keywords: fetal functional MRI, fetal brain connectivity, prenatal development, connectome, fetal brain development

INTRODUCTION

Human brain development is a finely orchestrated process that relies on the sequential execution of genetic programs, complex cellular interactions, and the formation and resolution of transient organs (Price et al., 2006; Kostovic and Judas, 2010). The protracted telencephalon maturation and the evolutionary expansion of the neocortex are prerequisites for our intellectual capacity (Clancy et al., 2001; Preuss, 2009), and many highly developed cognitive abilities are linked to features that are unique to humans (Bystron et al., 2008; Fjell et al., 2013). Early brain development encompasses the rapid growth of the size of the cerebral cortex and the increase in its cellular variability, associated with the expansion of transient fetal structures, including the subventricular zone and the subplate (Molnár et al., 2006; Rakic, 2009). When compared to the developmental trajectories of great apes, the growth rate of the human brain diverges during mid-gestation, and further expansion of white matter volume is observed in early postnatal life (Rilling, 2014). Specific areas, such as the association areas of the neocortex and areas related to language processing, exhibit exceptionally large subplate zones in humans (Rakic, 2009), and these differences are also mirrored in the cortical expansion during childhood and protracted myelination, which is completed in adulthood (Geschwind, 1964; Hill et al., 2010).

In contrast to our knowledge on brain circuit formation and histogenesis from post mortem studies and functional examinations in early childhood (Johnson, 2001; Price et al., 2006; Huang et al., 2009; Judas et al., 2013), to date, we have only a limited understanding of emerging neural activity during human fetal development. The complex connectional architecture of neural ensembles is a fundamental characteristic of the adult brain, and

Abbreviations: BOLD, blood oxygen level dependent contrast; CSF, cerebrospinal fluid; fMRI, functional magnetic resonance imaging; FOV, field of view; FWHM, full width at half maximum; GW, gestational week; ICA, independent component analysis; MRI, magnetic resonance imaging; NBS, network-based statistics; ROI, region of interest; SSE, sum of squares for error; TE, echo time; TR, repetition time.

we are beginning to understand how its variability across individuals is linked to cognitive ability (van den Heuvel et al., 2009), or neuropsychiatric disorders (Greicius, 2008). Some functional networks in the fronto-parietal and ventrolateral frontal cortex seem to be specific to humans (Mantini et al., 2013; Neubert et al., 2014), and the functional variability across the adult cortex correlates with cortical expansion from the primate to human brain (Mueller et al., 2013). To understand normal fetal functional brain development, it is of vital importance to identify critical periods of developmental vulnerability in which harmful environmental agents can manifest as a deterioration of mental capability or cause psychiatric diseases (Rice and Barone, 2000). In these phases of interest, functional assessment of the fetal nervous system would open a novel window on prenatal diagnostics and prognostics (Jakob and Beckmann, 1986; Paul et al., 2007; Schlotz and Phillips, 2009).

Studying fetal behavior with ultrasound has been adopted as a marker for neural development in clinical practice, offering an indirect view of the underlying functional processes (Pugash et al., 2008; Morokuma et al., 2013). MRI in the fetal brain has become increasingly feasible and clinically important due to its higher tissue resolution and better visualization of normal and pathological development of macroscopic anatomy or white matter microstructure and connections (Glenn and Barkovich, 2006; Kasprian et al., 2008; Jokhi and Whitby, 2011). Advanced imaging techniques, such as spectroscopy, serve as indicators of naturally changing metabolite levels during gestation (Kok et al., 2001), and characterize impaired development caused by primary brain malformation, hypoxic-ischemic injury, infection, or a combination of those factors (Mailath-Pokorny et al., 2012). BOLD fMRI has probed macroscopic-scale intrinsic neural activations across the entire life span (Buckner et al., 2013), and has an unsurpassed role in recent population-wide neuroimaging endeavors (Nooner et al., 2012; Uğurbil et al., 2013; Yan et al., 2013). Initial fetal investigation of spontaneous, intrinsic functional activity and functional brain connectivity has established intra-lobar activations (Schöpf et al., 2012) and cross-hemispheric connections in normally developing fetuses (Thomason et al., 2013).

In this paper, we provide a comprehensive view of the developing functional networks in the fetal brain. We capture this process by examining changes in the whole-brain functional connectivity architecture (Achard et al., 2006; Rubinov and Sporns, 2010; Zalesky et al., 2010) during gestation. We measured thalamo-cortical, cortico-cortical, intra-hemispheric, and inter-hemispheric functional connections, and organized them into a whole-brain graph (Fransson, 2005; Bullmore and Sporns, 2009). The graph-based method (Rubinov and Sporns, 2010) detected regional and temporal heterogeneity of functional connectivity development across the cortex before birth, reflecting the possible sequence of maturation in cortical areas.

MATERIALS AND METHODS

ETHICS AND SAFETY OF FETAL MRI ACQUISITIONS

Based on the follow-up studies of infants or children who had been exposed to MR imaging *in utero*, no gross abnormality, disease, or disability likely to be related to MR exposure could be demonstrated (Kok et al., 2004). The study protocol was approved by the local ethics committee, the mothers gave written, informed consent prior to the examination, and research was conducted according to the principles expressed in the Declaration of Helsinki.

STUDY POPULATION

This cross-sectional study included thirty-two singleton fetuses (16 female, 16 male) between GWs 21–37 (mean: 29.2; SD: 4.9) with normal brain development. The distribution of the gestational ages was the following. Second trimester (<26th GW): eight fetuses, early third trimester (26–29th GW): eight fetuses, 29–37th GW: 16 fetuses. Between May 2010 and August 2012, fMRI was performed for 200 fetuses. From of this cohort 141 scans were excluded due to image artifacts, uncontrollable fetal or maternal motion. After retaining the technically successful scans, the next exclusion criterion was the presence of brain abnormalities. Brain abnormalities were confirmed with the use of structural MRI in 27 of the cases. Therefore, 32 scans were retained for further analysis, which had no confirmed brain abnormalities. In the remaining study cohort, the indication for the mothers to undergo fetal MRI included: gastrointestinal pathology (two subjects); maternal clinical conditions (nine subjects); micrognathia or clefts (three subjects); renal and urogenital pathology (six subjects); thoracic pathology (one subject); asymmetry of the lateral ventricles (LVs; six subjects); and pathologies of the diaphragm (five subjects). Our final investigations were restricted to the 32 subjects who were proven negative for these suspected anomalies.

IMAGE ACQUISITION

Functional magnetic resonance imaging was carried out on a 1.5 T clinical scanner (Philips Medical Systems, Best, Netherlands) using a sensitivity encoding (SENSE) cardiac coil with five elements, utilizing single-shot gradient-recalled echo-planar imaging (EPI). The pregnant women were examined in the supine or left decubitus position (feet first), and no contrast agents or sedatives were administered. The MRI scans were acquired between May 2010 and August 2012. All investigations were scheduled between 7 and 9 am. Image matrix size was 144 × 144, with an FOV of 250 mm × 250 mm, a TE/TR of 50/1000 ms, and a flip angle of 90°. The resting-state scan comprised 50 image volumes with slices obtained perpendicular to the fetal brainstem, 10–30 slices were acquired and scan time was 1 min. The fMRI examinations followed the diagnostic (e.g., T2-weighted anatomical) scans, utilizing institutional protocols similar to those of previous reports (Schöpf et al., 2012).

IMAGE PROCESSING

The next paragraphs introduce an optimized work-flow for processing fetal functional images, which required effort in the direction of adapting conventional toolboxes and further extending them by fetal-specific developments. An overview of post-processing steps is given in **Figure 1**.

SPATIAL NORMALIZATION OF FUNCTIONAL MR IMAGES TO GESTATIONAL WEEK-SPECIFIC BRAIN TEMPLATES

A practical way to interrogate the developing fetal neuroanatomy is to pool image datasets of the study cohort according to GW and

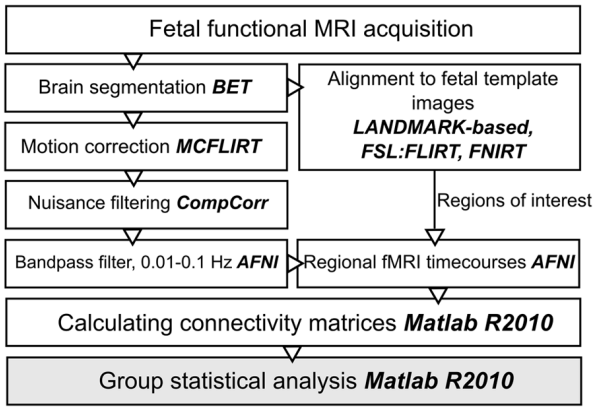

FIGURE 1 | Work diagram of the fMRI processing steps. The names of the respective image processing toolboxes are given in bold. BET, brain extraction tool; FLIRT, FSL linear registration tool; FNIRT, FSL non-linear registration tool; CompCor, component based noise correction method; AFNI, analysis of functional neuroimages.

use templates that depict the mean anatomical configuration of each GW. During the spatial normalization, we used the reference template images provided by Rueckert (2012) which are high-resolution representations of the changing fetal brain from the 23rd to the 37th GW. Template creation procedure described in: (Serag et al., 2012), while the fetal templates were accessed from Rueckert (2012).

Temporally averaged images of the fMRI data guided the registrations to achieve overlap with the T2-weighted templates. Each fMRI image was anatomically aligned to the respective GW-specific template image using the following procedure. We ensured proper orientation and coarse initial alignment by a landmark-based registration procedure using 12 manually annotated corresponding anatomical locations in the source and target images (**Figure 2**). We then relied on a two-step, intensity-based image registration in the FSL software (version 5.0, Linux 64-bit platform; Jenkinson et al., 2012): a linear, affine registration (FLIRT tool) followed by the non-linear matching of images (FNIRT algorithm), thereby coping effectively with the inter-individual anatomical differences. All further image processing steps, such as motion correction, noise reduction, band-pass filtering, and time-course extraction, were performed in the native space of the fMRI images, and the transformations were only used to propagate anatomically defined regions of interest into the subject's space or propagate results through up-sampling to a reference space to aid visualization. Therefore, the possible confounding factor of image interpolation only affected the ROI system, and not the actual fMRI data.

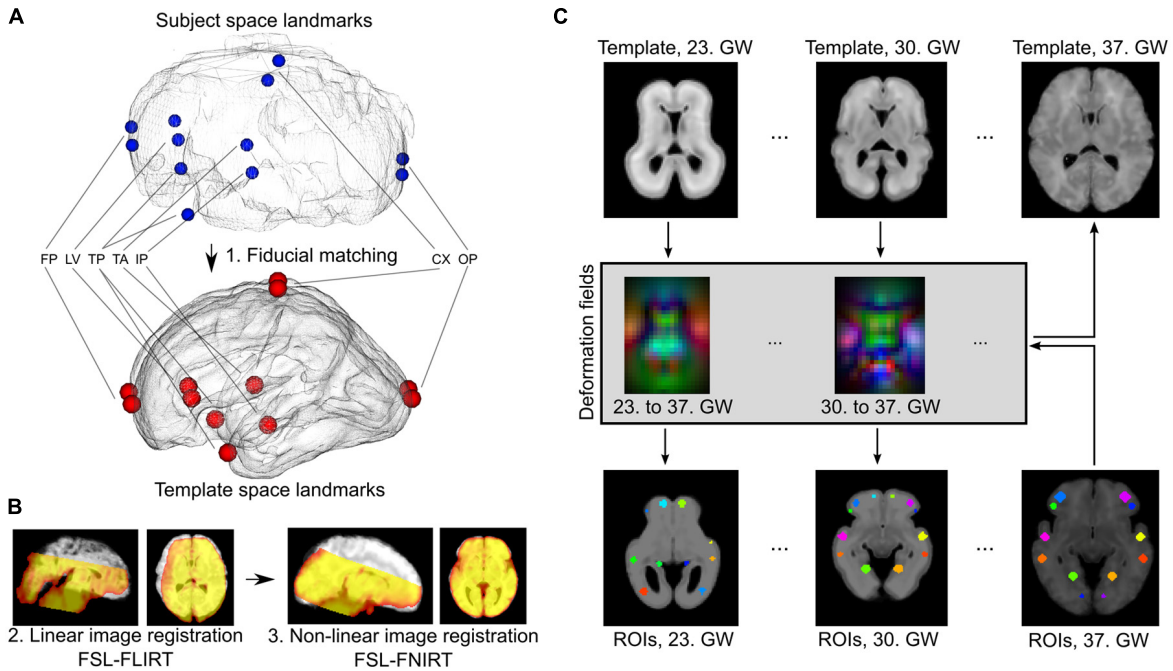

FIGURE 2 | Registration of fetal fMRI data to anatomical standard images and ROI propagation across developmental phases. **(A)** Landmark-based initial registration was used to match the averaged BOLD fMRI images of fetuses and GW specific fetal template brains. FP, fontal pole; LV, lateral ventricles, frontal horn; TP, temporal pole; TA, thalamic adhesion (midline); IP, midline point of the interpeduncular cleft in the midbrain; CX, topmost point of the convexities; OP, occipital pole. **(B)** Second step of the fetal to standard image registration, carried out with intensity-based algorithms: linear (FLIRT) and non-linear (FNIRT) registrations in the FSL software. **(C)** Establishing GW-specific regions with a longitudinal label propagation approach. First row: for each GW from the 23rd to the 37th, a high-resolution anatomical template was used, between which pair-wise non-linear transformations were calculated (second row). These transformations were used to transform the ROI system into any GW (third and fourth rows).

REGION OF INTEREST DEFINITION, FINDING CORRESPONDENCES ACROSS DEVELOPMENTAL STAGES

A ROI definition is critical when analyzing whole-brain structural or functional connectivity by node-based approaches, as it has a profound influence on network topology (Kelly et al., 2012). Conventionally, it is possible to obtain data-driven parcellations of a given territory or use anatomical priors to define gross landmarks. In the current study, we chose to use the latter. The 37th GW's high-resolution template image was visualized to facilitate the localization of crucial areas that are commonly depicted in adult neuroimaging atlases, such as in the Harvard-Oxford Cortical atlas (Desikan et al., 2006). The labels either matched large surface structures (precentral, postcentral gyrus), or subdivisions of areas with known and assumed diverging connectivity profiles (anterior, lateral, posterior thalamus), or structures that corresponded to functionally defined regions (e.g., the calcarine cortex of the visual system).

As the formation of cortico-cortical and cortico-subcortical circuits is not complete by the mid-fetal period, we placed anatomical regions onto the border of the subplate and the hypothesized future cortical plate position to capture presumably valuable signal from this region as well. In the reference ROI system, the ROI shape was spherical, mainly because little information is available about the volumetric extent of fetal cortical domains in the reference space. In 34.4% of the cases, the field of MR acquisitions did not cover the entire supratentorial area and the fetal cortex, and had limited cranio-caudal brain coverage. Examples for the ROI system, the ROI system matched to individual fetuses and the anatomical reference nomenclature is described in detail in **Figure 3**.

Our assumption was that the ROI system can be propagated into a developmental ensemble of brain reference images. Thus, ROI definition is only performed for the image having the best overall quality (i.e., in the 37th GW reference images, the secondary and tertiary sulci can guide the observer). Pair-wise registrations between the high-resolution templates were created in order to generate a collection of non-linear deformation fields that would feasibly match each GW's space with the 37th GW's template image. The non-linear registration was performed using "FNIRT" algorithm in FSL, with the registration parameters optimized to tackle the small scale of fetal brains. We illustrated this procedure in **Figure 2**. The correspondence between anatomical locations after the deformation in each GW template was checked by an observer with experience in neuroanatomy (András Jakab). The robustness of the ROI propagation method was visually checked by comparing the locations of ROIs with identifiable sulcal structures, such as the lateral, central, or parieto-occipital sulcus.

CORRECTING THE CONFOUNDING EFFECTS OF FETAL HEAD MOTION AND NON-NEURONAL MRI SIGNAL

Significant head rotations and translations can occur during fMRI experiments due to the frequent, spontaneous fetal movements and maternal breathing. Excessive motion in terms of amplitude and duration served as exclusion criteria for fetuses. This decision relied on the subjective observer-driven selection in addition to other imaging artifacts, similar to the approach in previous works (Schöpf et al., 2012). After removing subjects, minor head motion was detectable in almost every case and displacements were estimated and corrected with the MCFLIRT algorithm in FSL (Oakes et al., 2005). This processing step comprised the rigid-body registration of images to the mid-scan frame and removal of those frames that showed excessive motion estimates ("scrubbing" frames with root mean square displacement larger than 2 mm; Power et al., 2012). As displacement induces spurious effects in signal intensity temporal characteristics, we used the motion parameters (translation and rotation) as first-level explanatory variables in signal filtering, as recommended in the literature (Weissenbacher et al., 2009).

Furthermore, the variability of motion patterns can be influenced by gestational age. Hence we included per-subject motion as a covariate in higher-level analysis. This explanatory variable in the general linear model (GLM) putatively diminishes the effect of variable fetal motion among subjects at different developmental stages. We provide an example for typical fetal motion patterns, the effect of motion correction and the relationship to head motion to gestational age in **Figure 4**.

The observed signal during fMRI experiments is known to be coupled with the underlying neural activity due to the BOLD phenomenon (Logothetis and Wandell, 2004). In contrast to the intuitive notion of *structural or axonal connection* in neuroimaging studies, a *functional connection* or co-activation between remote brain areas is assumed when the MR signal fluctuations in the low frequency range are correlated in the temporal domain (Lowe et al., 1998; Greicius et al., 2003). Functional connectivity is thus a purely statistical approach inherently prone to confounding factors, i.e., rhythmic variations in the MR signal not explained by the large-scale activation of neurons. The majority of studies employ a model in which confounding factors are attributed to image noise caused by circulation (Shmueli et al., 2007), respiration (Birn et al., 2008), head motion (Power et al., 2012), or MR equipment-related noise. During nuisance signal reduction, the neural signal is the residual after first-level regression analyses in which we use the time-courses of known non-neural origin and other nuisance variables. Here we adapted the CompCor approach to reduce noise (Behzadi et al., 2007). According to the CompCor noise reduction model, principal MRI signal components from the white matter, CSF, or other "noise" image voxels are used. Time-courses of nuisance signals were derived using anatomical priors, while voxels having the largest SD of signal intensity were segmented as noise voxels. The first five principal components (PCs) of these signals were entered into the confound regression procedure. We illustrate the nuisance confound regression procedure in **Figure 5**. A detailed description of the utilized fetal noise signal model is provided in the Supplementary Material.

PORTRAYING THE DEVELOPING FETAL BRAIN CONNECTOME AS A COMPLEX GRAPH

We built undirected, weighted graphs representing intrinsic functional connectivity, with the set of longitudinally propagated brain regions as nodes. Connectivity value for a network edge was

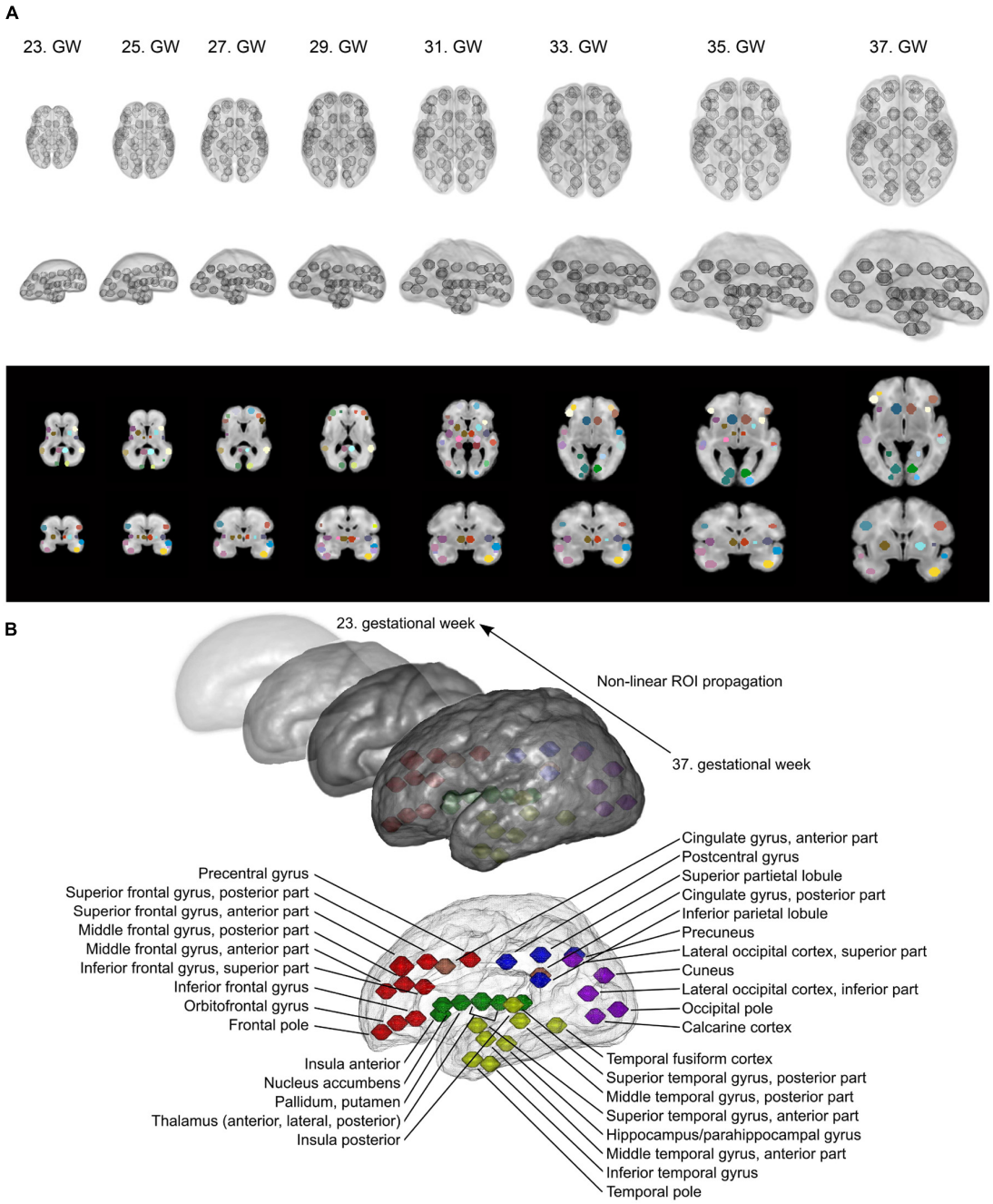

FIGURE 3 | Fetal brain atlas used for fMRI time-course calculation: ROI system and anatomical nomenclature. (A) Illustration of the region propagation procedure. Using high-resolution anatomical templates, we marked 90 anatomically relevant regions on the fetal cortical surface, which was then propagated through the investigated gestational period. Three-dimensional renderings and cross-sectional anatomical images with ROIs are shown. **(B)** Anatomical nomenclature of the ROI system. Correspondence to major lobes or systems is marked with different colors: red = frontal lobe; blue = parietal lobe; purple = occipital lobe; yellow = temporal lobe; green = subcortical; pink = limbic/cingulate gyrus.

defined using the Z-transformed Pearson product-moment correlation coefficient between brain regions. No thresholding or binning of the network was performed. We used the adaptation of graph theoretical measures to weighted nets, as implemented by the Brain Connectivity Toolbox for Matlab (BCT, version: 2012. 12. 04) and described in (Rubinov and Sporns, 2010).

TESTING HYPOTHESES ON COMPLEX NETWORKS: APPLICATION TO FETAL NEURODEVELOPMENT

To test our hypothesis about the developing brain, we modeled the temporal changes of brain connections as the effect of gestational time (gestational days) on the variance of individual connections, $S_{i,j}$. Prior to this model, all connections were evaluated against

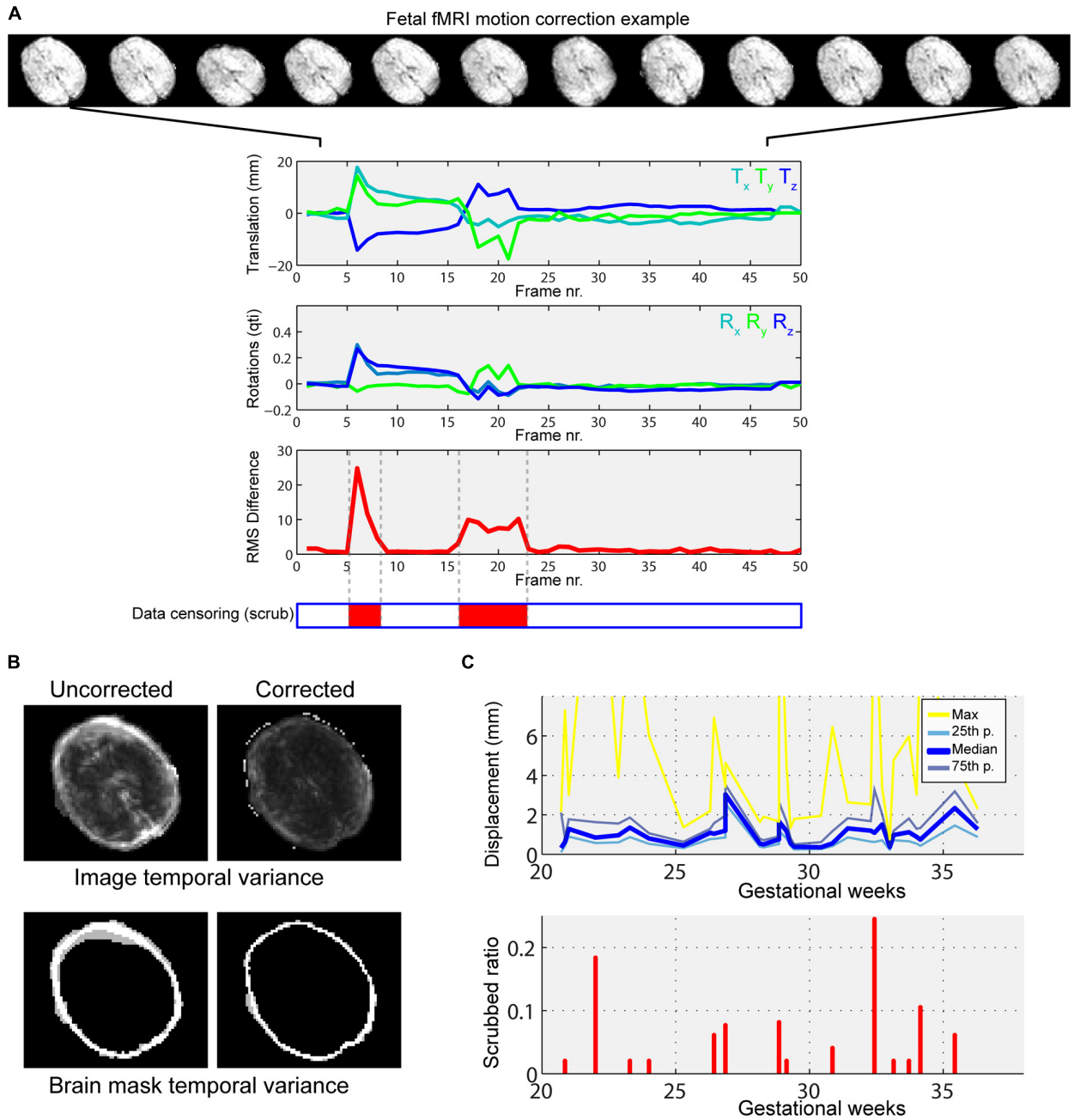

FIGURE 4 | Illustration of typical fetal in-scanner head motion patterns, correlation with gestational age. (A) Fetal head motion during MR scanning is estimated by frame-to-frame linear registrations. We illustrate a fetus with excessive head movements, as indicated by the large peaks in the translation and rotational components. Total displacement was used to censor periods of the scan with large motion (middle panel, red markings). **(B)** The motion correction procedure reduces the temporal variance of peripheral brain voxels, as shown in the cross-sectional panels. Such regions of high, spurious temporal variance give rise to nuisance signals in the functional connectivity patterns. **(C)** Depiction of gestational age-dependent changes of head motion. Top: median, 25th percentile, 75th percentile and maximum displacements of the fetal head vs. GWs. Bottom: the ratio of censored data vs. GWs. In our study cohort, fetal in-scanner head motion does not show correlation with gestational age.

simulated random brain graphs where the intrinsic functional connectivity were assumed to be explained by the spatial closeness of network edges and the consequent sharing of possible nuisance sources. This procedure is detailed in the Supplementary Material.

The application of univariate GLMs to each putative neuronal link (i.e., graph edge) raises the problem of mass multiple comparisons: in general, we cannot simply assume that such links are independent observations. Furthermore, correcting for the family-wise error rate (FWER) with the false discovery rate procedure

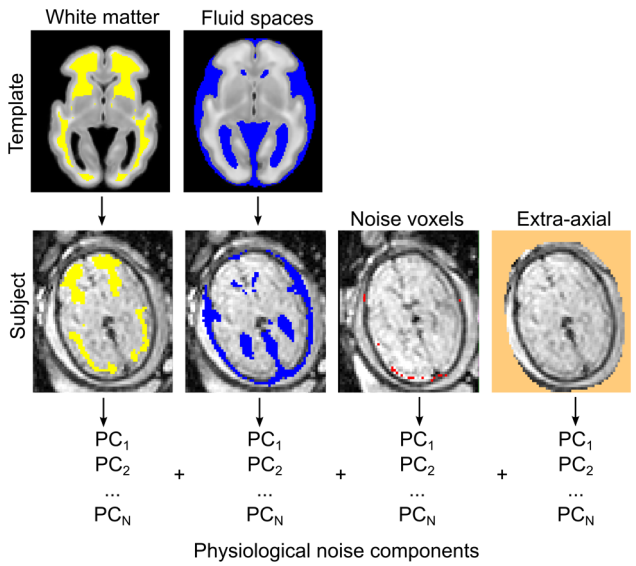

FIGURE 5 | Estimating physiological noise components for the correction of fetal fMRI signal using an adaptation of the CompCor approach. Top row: white matter and CSF components are segmented from the GW-specific anatomical templates. Segmentations are transformed to individual subjects **(bottom row)** while the voxels with highest temporal variation, and other, extra-axial structures, are calculated from the data. These voxels are used to perform the component-based filtering of the nuisance signal, according to the CompCor method described by Behzadi et al. (2007). PCs, principal components.

would inherently result in a loss of statistical power due to the large number of univariate measurements, which, in our case, would mean 2415 individual connections ($n_{i,j} = 70$, therefore the number of total connections is $\frac{70^2-70}{2}$).

The network-based statistics (NBS) method was utilized to tackle the multiple comparisons problem, as described by Zalesky et al. (2010) and implemented in the NBS Toolbox for Matlab R2012. This approach has the advantage of exploiting the internal connectional structure of brain graphs during the correction step for multiple comparisons, and potentially offers a substantial gain in statistical power. For the GLMs in our study, we provide the test statistics (F-test) for each connection in the graph and also for nodes where the test results were averaged over each edge connected with the node.

DETERMINING LOCAL AND GLOBAL GROWTH CHARACTERISTICS

We aimed to determine the trend of overall functional network development (statistical threshold: $F > 5$, NBS-adjusted value) as well as for regional sub-networks. Thus, regional growth characteristics including, but not restricted to the connections in the frontal, parietal, temporal, and occipital lobes, short- and long-range connections, and thalamus connections were evaluated separately. The sub-network of a brain lobe was defined as all the connections that involve regions from that lobe.

Short- and long-range connections were defined by taking the Euclidean distance measures from the ROI-to-ROI distance matrix. For sampling short-range connections, the lowest 25th percentile of the distance matrix was used, while, for long-range connections, we used the highest 75 percentile. This categorization of short- versus long-range connections remained fixed during the gestation, and it was based on the Euclidean distances measured at the 37th week of gestation. We further evaluated the distribution of connectivity lengths across the gestation period.

We fitted two models on the observed network strength values over time: linear (first degree polynomial), and non-linear, sigmoid functions:

$$f(x)_{sub} = \frac{1}{1 + e^{-\frac{x+a}{b}}} c + d$$

where $f(x)_{sub}$ was the predicted value for the mean connectivity strength of the sub-network using the sigma model, x was the predictor variable (gestational age), and a, b, c, and d were the estimated coefficients. Using least squares fitting with robust estimation of outliers in the Curve Fitting Toolbox in Matlab R2012, we determined the goodness of fit for each selected sub-network and the global network. The least absolute residuals (LARs) approach was employed to estimate the statistical outliers during the regression procedure. The two models, i.e., linear and non-linear, were compared by their adjusted R-squared and SSE values. For sigmoid functions, it is possible to determine an inflation point, which is the x value (or the gestational age) that corresponds to the maximum point of its first derivative. Growth characteristics were further evaluated for global brain volumetric changes, head motion, signal intensity, and signal temporal variation.

A bootstrap sampling approach was utilized to test the statistical robustness of curve-fitting for each analyzed brain region. During bootstrapping, 50% of the observations were randomly selected, and the fitting of the linear and sigmoid functions was repeated over 1000 iterations. Two-sample t-tests were performed to compare the goodness of fit between linear and sigmoid fitting.

RESULTS

FETAL FUNCTIONAL MRI: DATA QUALITY AND AGE-RELATED CHANGES

Fetal fMRI is a challenging imaging modality, hindered by potential imaging artifacts. We give examples for fetal fMRI from our study database in **Figure 6**. After removing fMRI time frames with excessive fetal head motion, 46.4 ± 7.8 frames per subject were retained for analysis, while zero to nine frames were removed per case. The ratio of removed (censored) fMRI frames is illustrated in **Figure 4**. Motion correction reduced the image variance in the peripheral brain regions, which is commonly associated by movement artifacts (an example is provided in **Figure 4B**.). Head movement during the examinations (root mean squared displacement of brain voxels by translations and rotations) was not correlated with gestational age [mm, average: 0.643 ± 0.459 (range: 0.158–2.01); linear fit, $R^2 = 0.139$, $p = 0.448$; Illustration: **Figure 4C**].

Next, we describe the potential age-dependent characteristics in our measurement, which may serve as confounding factors. The following quantitative parameters of fetuses changed over the course of gestation. Segmented fetal brain volumes showed significant linear growth [cm^3, average: 266.7 ± 108.5 (range: 77–469.1); linear fit, $R^2 = 0.86$, $p < 0.001$], and this correlation was similar to

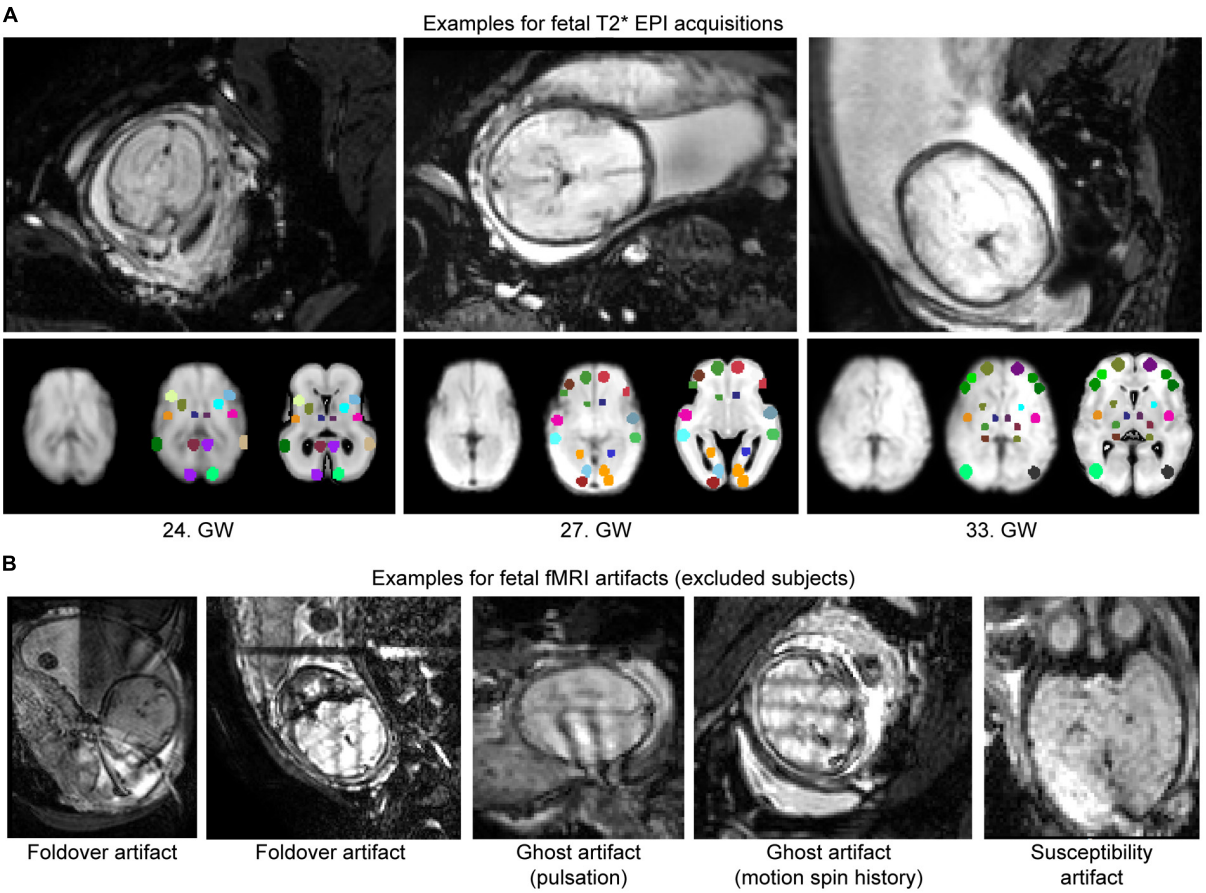

FIGURE 6 | Examples for fetal fMRI and the most common imaging artifacts. (A) Fetal fMRI with full FOV. Bottom panels: standardized functional image, ROI system warped to the standardized image and the fetal atlas systems illustrated. We provide 1–1 examples from the GWs 24, 27, and 33. **(B)** Fetal fMRI is a challenging imaging modality with many artifacts to expect. We illustrate this by excluded subjects' cross-sectional images. Examples for fold-over artifact, ghost artifact and susceptibility artifacts are shown.

the increase in the total size of brain ROI over time [cm^3, average: 6.954 ± 2.859 (range: 2.2–11.3); linear fit, $R^2 = 0.856$, $p < 0.001$]. BOLD signal intensities decreased from the 21st to the 37th GW [signal intensity, average: 236.6 ± 66.4 (range: 127.7–387.9); linear fit, $R^2 = -0.207$, $p = 0.256$]. This characteristic change in BOLD signal intensity can be attributed to the slight decrease in water content in fetal brain tissues during gestation and the consequent change of spin relaxivity (Chung et al., 2000). The temporal variation of the filtered and nuisance-corrected BOLD signal decreased over time [signal intensity variation, 6.378 ± 4.532 (1.02–19.06); linear fit, $R^2 = -0.3057$, $p = 0.088$], although this decrease was not significant.

EMERGING INTRINSIC FUNCTIONAL NETWORKS

Network-based statistical inference analysis was performed for 2415 different functional connections (i.e., upper triangle of the brain connectivity matrix; Zalesky et al., 2010). Permutation testing revealed that 850 were different from a random graph, and the intrinsic functional connectivity values of 114 region pairs significantly correlated with gestational age after correcting for multiple comparisons. A linear and a non-linear growth model were tested for the relationship between gestational age and functional connectivity. The variation of each statistical parameter was quantified in terms of the uncertainty calculated during a bootstrapping sampling procedure.

The mean intrinsic functional connectivity of the entire brain network showed a significant increase over gestation (linear model, R^2-adjusted: 0.623 ± 0.0467; SSE: 0.93 ± 0.16; sigmoid model, R^2-adjusted: 0.66 ± 0.063; SSE: 0.875 ± 0.167), and the sigmoid function described the relationship between GW and connectivity more powerfully (difference of SSEs, $p < 0.001$). Until the 25th GW, the mean network connectivity remained close to zero (average connectivity strength range from the 21st–26th GW: −0.163–0.0525). The inflation point of the non-linear strengthening of functional connections was estimated at 26.59 ± 1.19 weeks. The period of connection development in which the connection strengthening rate is larger than 90% of the mean inflation rate was defined as the "expansion period." This interval was calculated from the first derivative of the fitting function. The expansion period of the total functional connectivity network was observed between GWs 25.58–28.69. We illustrate the increase of functional connectivity in **Figure 7B**.

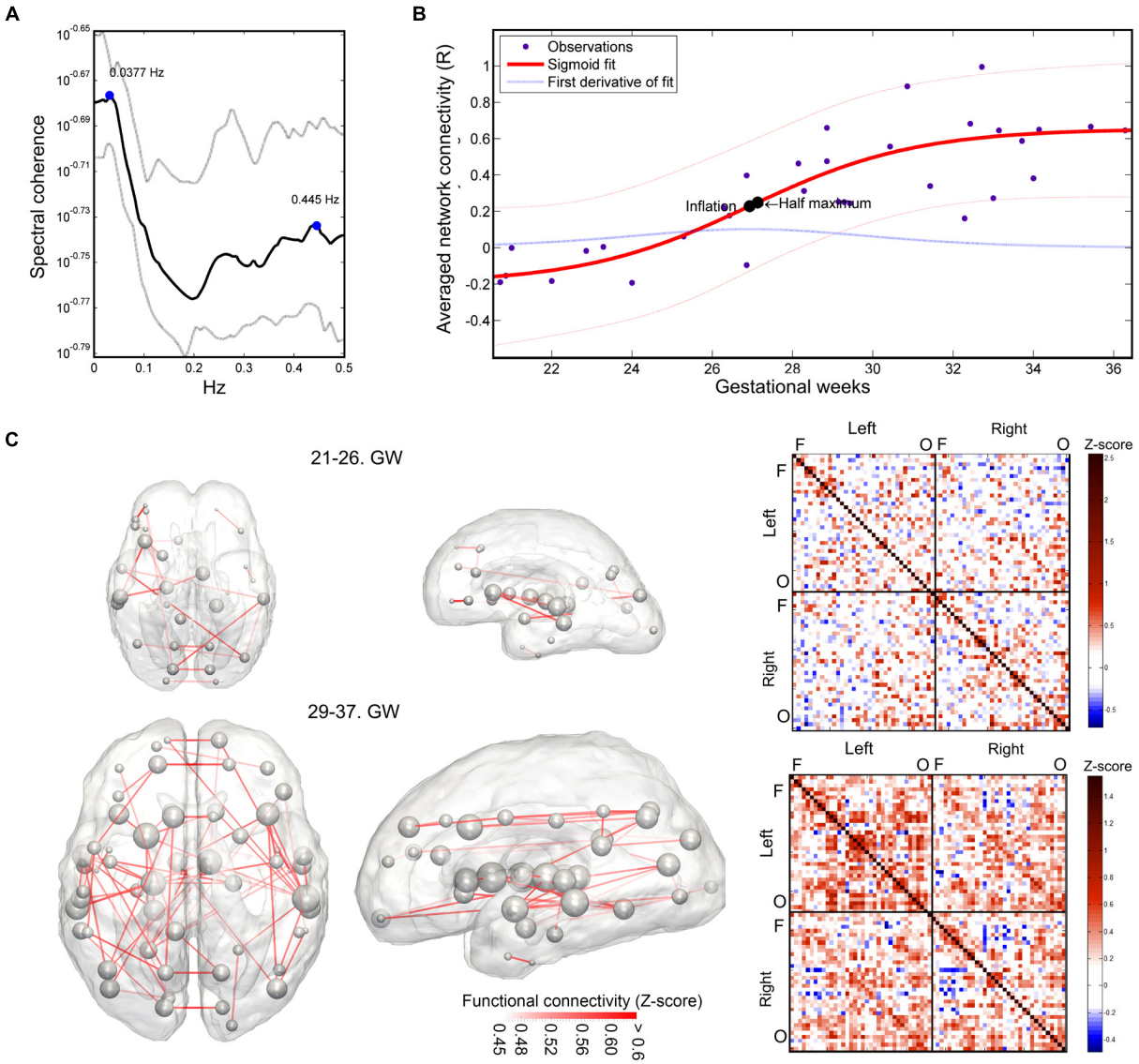

FIGURE 7 | Results of the functional connectivity analysis: spectral coherence of time-courses, developmental trajectory of developing fetal intrinsic functional connectivity. (A) Spectral coherence analysis of fetal fMRI time-courses. The mean coherence plot (black line) was derived for all pairs of fetal functional time-courses at all GWs. Gray line depicts the interquartile range of observation across subjects. The plot is dominated by two peaks, representing low-frequency synchronicity at 0.0377 Hz and possible noise correlation at 0.445 Hz. Bold line: mean coherence, dotted lines: SD. **(B)** Development of the fetal functional brain connectome, gestational age-dependent distribution of functional connections. We illustrate the sigmoid curve-fitting on individual average network connectivity strength measurements. Each point in the graph refers to the mean intrinsic functional connectivity of a fetus, which calculation was restricted to the values that were found to be significantly associated with gestational age. Half-inflation point of the curve is found at the 27th GW and it depicts the gestational age in which the maximum increase of intrinsic functional connectivity is found. **(C)** Developmental expansion of the fetal functional brain connectome, visualization as matrices and 3D graphs. Two stages of the development are depicted: prior to the presumed expansion of functional connectivities (21st–26th GWs) and after this period. This dichotomy was defined using the average intrinsic functional connectivity values **(B)**. The transparence of each edge in the 3D visualization (left images) refers to the population mean of the intrinsic functional connectivity (Z-score). The size of nodes in the network depiction is proportional to the sum of connectivity values over all edges that are connected to them. Group-mean network edges were visualized using a threshold of $Z = 0.45$. Graphs were overlaid on anatomical templates from the 23rd and 37th GWs. The mean connectivity networks are also visualized as connectivity matrices, Fs, frontal regions, Os, occipital regions.

Using this concept of expansion, we provide visualizations of the mean fetal functional network structure for pre- and post-expansion periods, and calculated the connectivity values for each of these states of functional connectivity development in **Figure 7C**.

The average intrinsic functional connectivity values in the fetal brain graphs during the expansion period (GW 26–29) were significantly higher than before the 26th GW (pre-expansion: -0.0696 ± 0.0834; expansion: 0.234 ± 0.148; $p = 0.000173$). This difference was also significant for values before and after

the expansion state (pre-expansion: −0.0696 ± 0.0834; post-expansion: 0.385 ± 0.159; $p = 0.036$). Our results are summarized in **Table 1**. Between the 21st and 26th GWs, the mean functional network architecture is dominated by occipital and temporal connections, while frontal, parietal, or interhemispheric connections are sparser. After the expansion period (29–37th GW), we observed the increase of functional connectivity strength in the parietal and frontal lobes and long-range correlations between the frontal and temporal lobes.

HETEROGENEOUS AND REGION-SPECIFIC DEVELOPMENTAL CHARACTERISTICS

After separating the entire connectivity network into regions according to brain lobes, we evaluated the developmental trajectories of within-lobe, interhemispheric, and thalamo-cortical connections. Here we use the term "connectivity strength" for the average intrinsic functional connectivity values of a given group of network edges. The estimation of expansion periods revealed a sequential order for how regional functional connectivity becomes increasingly strong. The non-linear sigmoid expansion better described the regional increase of intrinsic network connectivity strength (**Table 2**). The correlation between the gestational time and the connectivity observations was high, with adjusted *R*-squared values ranging from 0.45 (thalamus connections) to 0.64 (interhemispheric connections).

The inflation time shows a heterogeneous pattern across the fetal cortex. The inflation time of the occipital connections was the earliest (R^2-adjusted: 0.47 ± 0.08, inflation point: 24.83 ± 1.59 GW), while the inflation time for the parietal connections was the latest in the sequence (R^2-adjusted: 0.55 ± 0.07, inflation point: 27.48 ± 0.79 GW). The occipital expansion of functional connectivity was followed by the temporal, frontal, and parietal lobes. Thalamus-cortex interconnections displayed trends of development similar to that of the overall network (expansion of overall network: 26.59 ± 1.19 GW; expansion of thalamic connections: 26.31 ± 1.75 GW).

COMPARING SHORT- AND LONG-RANGE CONNECTIVITY

A further distinction was made according to the region-to-region physical (Euclidean) distances: short- and long-range connections were analyzed separately. Maximum strengthening of all short-range connections occurred at the 27.69 ± 0.94 GW, although we were unable to determine the same for long-range functional coherence where linear strengthening was discovered (SSE of linear model: 0.53 ± 0.1; SSE of non-linear model: 1.47 ± 0.3, $p < 0.0001$). Numeric data of the revealed order of development are summarized in **Table 2**. We provide a visualization of the core regional networks, the developmental curves and the estimated sequence of functional connectivity inflation in **Figure 8**.

After the 26th GW, the proportion of long-range connections becomes significantly higher, as reflected by the larger Euclidean region-to-region distances within the reference network (**Table 1**).

The sigmoid strengthening described the functional connectivity of short-range connections significantly better than the linear, but this observation did not hold for long-range connections. Instead, it appears that long-range connectivities gradually increase from the beginning of the observed gestational period.

SPECTRAL COHERENCE ANALYSIS OF FETAL FUNCTIONAL MRI SIGNALS FROM THE CORTICAL PLATE

Magnitude-squared spectral coherence of BOLD recordings characterized low frequency synchrony of intrinsic signal fluctuations in the fetal brain. Prominent frequency peaks of signal synchronicity were found at 0.0377 ± 0.0599 Hz and 0.427 ± 0.068 Hz, and peak heights were 0.255 ± 0.096 and 0.219 ± 0.047, respectively. This pattern remained consistent at all observed gestational ages. Similar to adult fMRI measurements, it can be assumed that the lower frequency peak corresponds to the neural component, while the higher frequency component is likely to be explained by cardiac effects on the signal (calculated frequency, beats per minute: 144 ± 28, range: 120–216). We illustrated the average spectrum of time-courses and the spectral coherence in **Figure 7A**.

DISCUSSION

CHARACTERISTICS OF THE DEVELOPING FETAL FUNCTIONAL CONNECTOME

In this work, we have employed fMRI to portray the development of the fetal functional brain connectome. The rate of signal synchronicity increase is highest at the transition from the second to the third trimester, with the peak around the 26th GW. MRI

Table 1 | Prenatal development of intrinsic functional connectivity and changes in the region-to-region Euclidean distances.

	Average network connectivity, region-to-region distances (mm)	Average functional connectivity strength of network
Pre-expansion (GW 21–26; $n = 8$)	24.726 ± 1.922 (21.232–27.186)	−0.0696 ± 0.0834 (−0.163–0.0525)
Expansion (GW 26–29; $n = 8$)	27.28 ± 1.608 (25.344–30.526)	0.234 ± 0.148 (−0.0669–0.38)
Post-expansion (GW 29–37; $n = 16$)	26.612 ± 1.459 (23.106–28.626)	0.385 ± 0.159 (0.147–0.6094)
Difference: pre-expansion vs. expansion	Increase: 2.554; $p = 0.0121$	Increase: 0.304; $p = 1.7296e-4$
Difference: post-expansion vs. expansion	Increase: 1.885; $p = 0.0135$	Increase: 0.151; $p = 0.036$

Functional connectivity refers to the Pearson product moment correlation coefficient of the signal time-courses of two brain regions. The average functional connectivity strength is the average correlation coefficient of the network edges that were found to be significantly correlated with gestational age. For optimal comparison, the reported Euclidean distances were fixed for each network edge and these values reflect the distances found at the 37th week of gestation.

Table 2 | Regional characteristics of prenatal intrinsic functional connectivity development: results of the regression analysis.

	Linear model			Sigmoid model				Linear vs. sigmoid
	R^2	Adjusted R^2	SSE	R^2	Adjusted R^2	SSE	Inflation time	
Overall network	0.639 ± 0.045	0.624 ± 0.047	0.93 ± 0.161	0.66 ± 0.064	0.613 ± 0.073	0.878 ± 0.168	26.589 ± 1.196	Sigmoid, $p < 0.0001$
Occipital connections	0.513 ± 0.059	0.492 ± 0.061	1.378 ± 0.219	0.538 ± 0.071	0.473 ± 0.08	1.312 ± 0.251	24.826 ± 1.589	Sigmoid, $p < 0.0001$
Frontal connections	0.563 ± 0.062	0.544 ± 0.065	1.187 ± 0.194	0.649 ± 0.06	0.6 ± 0.069	0.954 ± 0.153	26.434 ± 0.477	Sigmoid, $p < 0.0001$
Temporal connections	0.505 ± 0.054	0.484 ± 0.056	1.601 ± 0.254	0.541 ± 0.063	0.477 ± 0.071	1.468 ± 0.269	25.993 ± 0.929	Sigmoid, $p < 0.0001$
Parietal connections	0.566 ± 0.081	0.547 ± 0.084	1.381 ± 0.31	0.602 ± 0.058	0.547 ± 0.066	1.297 ± 0.22	27.477 ± 0.786	Sigmoid, $p < 0.0001$
Thalamocortical and subcortical connections	0.504 ± 0.0548	0.483 ± 0.057	1.967 ± 0.317	0.519 ± 0.067	0.453 ± 0.077	1.919 ± 0.312	26.31 ± 1.75	Sigmoid, $p < 0.0001$
Short-range connectivity	0.509 ± 0.048	0.488 ± 0.05	1.642 ± 0.251	0.557 ± 0.065	0.495 ± 0.075	1.471 ± 0.251	27.69 ± 0.942	Sigmoid, $p < 0.0001$
Long-range connectivity	0.673 ± 0.052	0.657 ± 0.054	0.532 ± 0.104	0.545 ± 0.07	0.481 ± 0.08	1.471 ± 0.293	25.647 ± 1.445	Linear, $p < 0.0001$
Interhemispheric connections	0.663 ± 0.044	0.649 ± 0.046	0.904 ± 0.144	0.687 ± 0.046	0.643 ± 0.053	0.853 ± 0.132	26.416 ± 1.014	0.084

Two models were tested, we evaluated whether connectivity development was better described with a linear or a non-linear sigmoid growth model. Variance during the bootstrapping analysis is given by the SD. Group comparisons were performed using two-sample, two-sided Student t-tests, assuming equal variances.

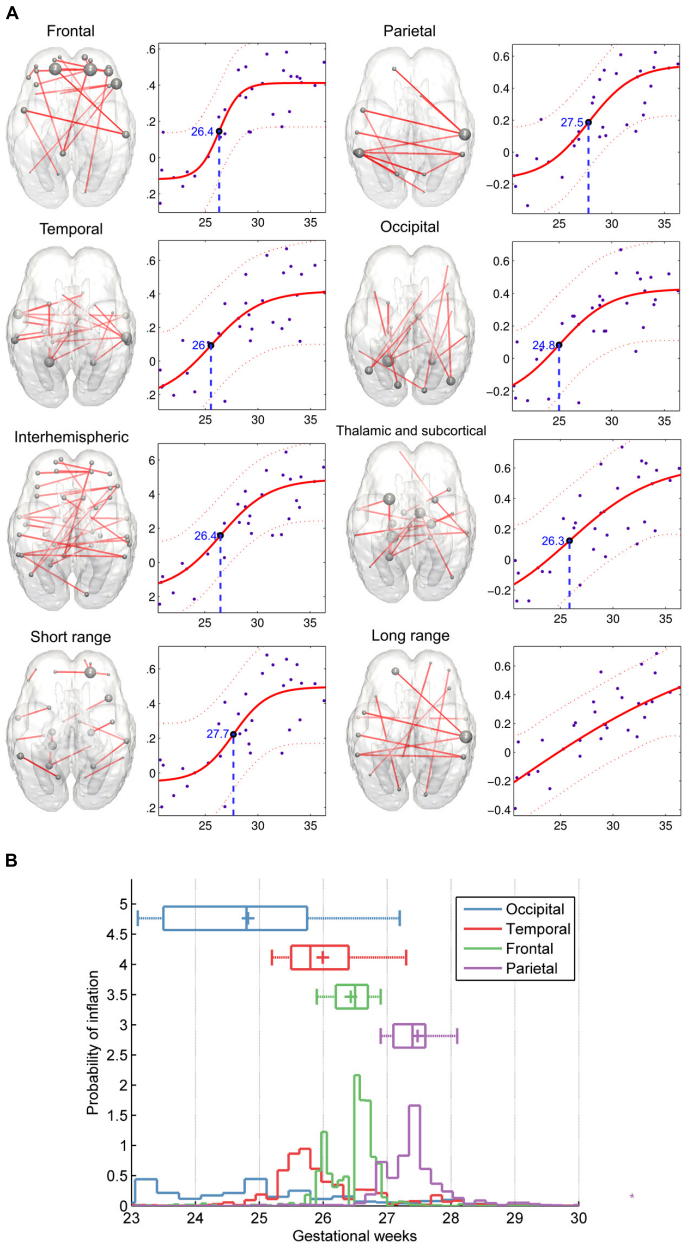

FIGURE 8 | Region-specific development of functional connectivity in the fetal brain. (A) In these visualizations, a regional sub-network was defined to include all connections within a brain lobe, and these were restricted for the edges which connectivity values showed significant correlation with gestational age. Plots depict significant age effects on functional connectivity within each sub-network. Components of sub-networks are depicted as graphs, overlaid onto a 25th-GW brain template model. In this form of visualization, graph edges refer to a functional connection (*Z*-score) between two areas, while the brain areas are represented as nodes. Node size refers to the sum of its connections, weighted by the functional connectivity. **(B)** Regional timing of functional brain connectivity expansion during the late second and third trimester, variability of the observed inflation times during the bootstrapping procedure. According to the hypothesis that functional connectivities exhibit non-linear growth characteristics rather than a linear trend during the mid-fetal period, it is possible to determine the gestational age of inflation by sampling. 50% of the measurement points were sampled randomly during this procedure, and the relative probability estimates of the inflation points of the fitted functions are depicted against the gestational age. The distribution of sampled connections indicates a sequence of occipital, temporal, frontal, and parietal development of intrinsic functional connectivity values.

signal fluctuations were first synchronized in the occipital lobe (e.g., primary visual cortex), followed by the temporal, frontal (including the motor cortex), and parietal lobes. When looking for the optimal characteristics to describe the increase of intrinsic functional connectivity, observations followed a non-linearly increasing trend, the only exception to which were the long-range connections. The proportion of short- and long-range connections was not homogeneous in the evaluated course of

gestation: after the expansion period (26th to 29th week), more long-range connections could be observed.

PRENATAL DEVELOPMENT OF FUNCTIONAL BRAIN CONNECTIVITY FOLLOWS POSTERO-ANTERIOR TIMING

The heterogeneous timing of network development across the cortex relates to findings regarding the network variability across adult subjects. Mueller and co-authors found that parietal regions—in particular the association cortex—exhibit high variability compared to primary regions, such as the sensorimotor system (Mueller et al., 2013). The timing suggests that the regions with high inter-individual variability are those regions whose connectivity structure is developed relatively late during gestation. Similarly, these late-developing regions are phylogenetically young cortical areas that exhibit the strongest cortical expansion during late evolution, when comparing the macaque and human cortex (Hill et al., 2010). Buckner and Krienen (2013) discuss the timing of primary cortical areas and subsequent areas, such as the association cortex, relating the complex long-range networks with relatively weak organizational coherence across individuals to the rapid expansion of the corresponding cortical areas during evolution. Although we do not answer the question of whether this is mirrored during early individual brain development, the results suggest that the fetal brain appears to exhibit timing patterns similar to those of cortical evolution.

EMERGENCE OF FETAL NEURAL ACTIVITY: BIOLOGICAL BACKGROUND

The second and third trimester of gestation is critical for the healthy development of cerebral pathways and for the normal functioning of the newborn brain. Here, we interpret findings in the context of major events of telencephalon development within this time frame. Cortical neurons begin to receive their first afferent inputs from the thalamus through a multiple-step process that involves the establishment and resolution of transient connections through the subplate (Price et al., 2006; Kostovic and Judas, 2010). The subplate constitutes a distinct layer of the fetal cortex (Kostovic and Molliver, 1974) and contains a heterogeneous set of early post-migratory neurons, which show the most advanced and mature electrophysiological characteristics compared to other neurons of the fetal brain (Moore et al., 2009). Experimental data indicate an essential role of GABAergic subplate neurons in the generation of early synchronized network activity, and thus, in the establishment of normal neuronal circuits and a regular columnar architecture of the developing cortical plate (Zhang and Poo, 2001; Lopez-Bendito and Molnar, 2003; Kanold, 2009; Luhmann et al., 2009; Judas et al., 2013). Electrical discharges in the human cortex can be demonstrated *in vitro* (Penn and Shatz, 1999; Moore et al., 2009). Moreover, correlates of spontaneous network activity can be identified by early human preterm electrophysiology.

The maturation of thalamocortical afferentation is accompanied by the evolution of a more complex electroencephalography pattern (Vanhatalo and Kaila, 2006), including delta brushes from the 28–30th GWs onward (Khazipov and Luhmann, 2006). Thus, early cortical maturation occurs mainly independent of sensory input, and is driven by spontaneous activity, amplified through subplate neurons (Luhmann et al., 2009). Due to the high water content in the extracellular matrix and the low number of neurons, the subplate displays distinct MRI features, as described *in vitro* and *in vivo* (Maas et al., 2004; Prayer et al., 2006). A spatial and temporal regional morphological variation during development has been described. In the dorsolateral cortical areas, receiving massive cortico-cortical and thalamocortical input, the subplate shows the thickest dimensions, whereas it is diminished in size in the mesocortical regions (Kostovic et al., 2002). There is a developmental peak between 27 and 30 GWs, followed by a stage of dissolution after 30 GWs. Thus, the morphologic dimensions of the fetal subplate mirror the dynamics and grade of the regional connectivity of somatosensory and association cortices. This spatiotemporal anatomic trajectory is in accordance with the results of our functional imaging-based global effects analysis (**Figure 4**). The rapid and significant increase in connectivity between 24 and 31 GWs, with a half-inflation point at 27 GWs correlates with the period of maximum growth of the human fetal subplate and increasing synaptogenesis in the cortical plate. We were able to describe a stage of stabilization of the connectome after 31 GWs, which parallels the process of subplate dissolution and the consolidation of existing networks. The general hierarchy of myelination starts with sensory pathway myelination before the motor and association pathways (Flechsig, 1920). Although myelination mainly occurs postnatally, we were able to demonstrate that functional connections develop first in the occipital and temporal areas at around the 25th GW, whereas the frontal lobe connectivity evolves later. This is consistent with recent neuroimaging and neuropathology data showing an earlier maturation of the optic and acoustic radiations, compared to the frontal lobe pathways traveling through the anterior limb of the internal capsule (Yakovlev and Lecours, 1967; Kinney et al., 1988; Dubois et al., 2008). Trivedi et al. (2009) used diffusion tensor magnetic resonance imaging to demonstrate the region-specific maturation of the fetal brain, concluding that diffusion anisotropy quantifies the microstructural orderedness that reflects the peaking activity of neuronal migration. Coherent with the functional developmental timing in our study, they revealed an initial occipital and temporal increase and peaking of anisotropy.

Moreover, we reported that long-range and interhemispheric connectivity shows a linear increase during development, as opposed to the rapid dynamics of short-range connectivity within certain brain lobes. As long-range association pathways as well as commissural pathways follow a steady and linear developmental trajectory, the dynamics of our functional imaging-based connectome seems to reflect the divergent properties of these processes.

RELATIONSHIP TO PREVIOUS FINDINGS

In utero fMRI came to the forefront only in the last decade to assess stimulation-related activity (Gowland and Fulford, 2004; Jardri et al., 2008) or activation in resting conditions (Schöpf et al., 2012). To date, only a small number of studies have employed this method for the portrayal of functional ontogenesis in normal or pathological circumstances.

A possible way to extend our knowledge in this field is to adapt imaging techniques that are widely used in humans after birth. In this regard, *in vivo* neuroimaging techniques, such as diffusion tensor MR imaging (DTI, Johansen-Berg and Rushworth,

2009; Dennis et al., 2013; Yoshida et al., 2013) or BOLD fMRI have already contributed to significant findings in human developmental neuroscience. The analysis of fetal functional neuroimaging data as an emerging network can be viewed as an extension of previous single-subject or group-based analytical approaches (Schöpf et al., 2012; Thomason et al., 2013).

Observations of fetal behavior *in utero* (Joseph, 2000; Morokuma et al., 2013) outline a fine-tuned arrangement of how functioning neural ensembles emerge that serve basic capacities, like somatomotor functioning, auditory responses, plasticity, or regulatory mechanisms (D'Elia et al., 2001; Partanen et al., 2013a). Evidence for the emergence of fetal auditory processing and simple learning capacities mostly comes from electrophysiological measurements (Holst et al., 2005; Partanen et al., 2013b) or task-related functional imaging (Jardri et al., 2012).

Similarly, fMRI of the immature neonatal brain is restrictive for the characterization of *typical* development: observations are mostly limited to the 26–40th weeks of gestation when the prerequisites for sensory-driven processing are assumed to be already in place (Doria et al., 2010).

Our findings of increasing interhemispheric intrinsic functional connectivity are in line with previously performed studies utilizing prenatal MR imaging, with a notable difference that previous works reported qualitative findings on the emerging activity, or used linear growth models for selected connections (Schöpf et al., 2012; Thomason et al., 2013). The sequence of functional connectivity increase was recently reported to follow a medial–lateral and posterior–anterior trajectory, which is partially supported by our observation of an occipital-temporal-frontal course of network emergence. Using ICA to map the temporo-spatial components of prenatal brain activity, Schöpf et al. (2012) revealed consistent bilateral occipital networks as early as the 22nd GW. Further reproducible components were observed bilaterally in the frontal lobe and unilaterally in the temporal lobe, and, notably, parietal networks were absent. In our developmental model, the pre-expansion period before the 26th week was characterized by bilateral occipital, unilateral temporal connections, and the presence of inter-hemispheric long-range synchrony between non-homotopic areas. The low-frequency MRI signal fluctuations were found to be the most coherent in the 0.01–0.1 Hz range, which matches the commonly assigned filter intervals in adult studies and other prenatal fMRI analyses. In this work, we relied on a more intricate representation of the developing brain activity, compared to previous works on prenatal data: a graph model and network-based inference approach was chosen to capture the overall network properties in a statistically sound framework. In addition, a careful preprocessing pipeline was used to lessen physiological noise and confound the effects of fetal head motion (Power et al., 2012).

The analysis of the developing functional connectome and macroscopic-scale network architecture was previously elucidated using imaging data from immature neonates. According to a report by Doria et al. (2010) preterm neonates seem to exhibit distributed functional connectivity networks at birth. A longitudinal study by Smyser et al. (2010) discovered a variety of network components that resembled their adult counterparts as early as the 26th GW. A consistent component in similar studies is the *default mode network*, whose prenatal existence has been questioned (Lee et al., 2013). This interrogation of developing resting-state functional networks suggests that the period of the most rapid synaptogenesis triggers spontaneous brain activity that is organized into networks, and such networks are similar in spatial extent to those observed in newborns.

By measuring the signal intensity changes coupled with blood oxygenation levels, fMRI indirectly characterizes the time-course of slowly fluctuating neural activation (Logothetis and Wandell, 2004). Physiological measurements suggest that fMRI activations are neuronally driven and more strongly coupled to dendritic activity than action potentials (Lauritzen, 2005). The known mid-gestational shifts of electrical activity in the human cortex correlate with the reported periods of functional connectivity expansion, although a definitive conclusion cannot yet be drawn due to the limitations of *in vivo* imaging technology. Spontaneous brain activity in preterm neonates remains questionable as a model for normal, *in utero* development (Damaraju et al., 2010); a more faithful description about the electrophysiological maturation in healthy subjects would be optimal to explicate our findings on functional activity. So far, such an investigation on normally developing human subjects is not feasible and this problem remains unsolved.

STUDY LIMITATIONS

A number of factors limit the experimental support of our work to describe emerging brain function in human fetuses. Here we report three major categories of possible limitations in fetal fMRI studies: (1) origin of fMRI signals in the developing brain, (2) fetal head motion and age-related confounds, and (3) finding optimal anatomical correspondences during gestation and ROI system creation.

Colonnese and Khazipov (2012) advised a more careful interpretation of pre- and perinatal fMRI studies on the grounds that the coupling of the BOLD signal and neuronal activity is immature or unknown. The relationship between the MRI signal and the underlying neural activity is the topic of extensive debate. However, there is converging evidence that functional connectivity can be explained or predicted by mono- and polysynaptic cortico-cortical interconnections (Honey et al., 2009). Furthermore, spontaneous low-frequency activations in the fetal sensory areas are possibly driven by mechanisms different than that in the adult brain, serving the development of the cortex and not endogenous processing.

Fetal in-scanner head motion is a challenging issue in fMRI, and here in our study this was the primary criteria for excluding otherwise normally developing fetuses. For fMRI experiments with long TR, fetal motion can occur between slices as well, requiring special algorithms for motion correction. In our study, we did not reveal significant dependency of fetal motion patterns with gestational age, although in a larger, unfiltered cohort, this can be expected. Therefore we suggest including total subject-level head displacement as a higher level explanatory variable in group comparisons. As head motion causes not only voxel displacement but signal intensity changes as well, it is important

to include motion confound variables in the nuisance regression step.

Here we summarize the following age-related confounds that can hinder the interpretation of our current results. First, fetal brain size significantly grows during gestation, therefore any trend in functional connectivity increase can be a result of merely observing larger ROI. Another consequence of the brain growth is that ROIs are naturally closer to each other in a young brain and this may result in a bias toward stronger short-range connections. In our study, fMRI signal variance did not show significant correlation with gestational age. A further critical step in resting-state fMRI analysis is the nuisance correction, where nuisance means both predictable and random sources of image noise. Here, the steps for MR image analysis were adapted for fetal functional imaging to ensure that maturing macroscopic-scale neural activity contributes to the observed signal intensity fluctuations. Although the current strategy is to obtain noise signals from areas where no neurons reside, the spurious effects of non-neuronal origin cannot be excluded, and, furthermore, monitoring of possible physiological noise sources would be desirable. We experienced a high exclusion rate of clinical cases on the grounds of excessive movement or other artifacts, greatly reducing the data available for analysis.

A possible limiting factor comes from the fact that our study relied on a manually defined ROI system. Localization in the fetal cortex is not directly possible by anatomical atlases, but rather, via the transfer of adult landmarks based on non-linear matching of geometry. This limits the spatial correspondence between subjects. It is possible that the propagation of cortical loci through similarity-based transformations introduces a bias toward later gestational ages when the convoluted surface is more ideal for localization and inter-subject correspondences are better. A possible solution to this problem is the use of functional data-driven parcellation of the cortex, such as demonstrated by Craddock et al. (2012) on the group level. It is possible to use group level ICA to reveal spatially coherent networks within the resting-state fMRI data. Although the transformation of our fetal fMRI data into one reference space for group ICA may suffer from interpolation artifacts due to the large volumetric and anatomical differences.

OUTLOOK AND CONCLUSION

Understanding the formation of functioning neural ensembles in the human brain is particularly important for a model of healthy development, and such a functional, developmental model could be a standard to which pathological conditions can be compared. The assessment of the critical late gestational sculpting of fetal brain activity and macroscopic-scale functional circuitry is feasible with *in utero* neuroimaging. The optimization of imaging sequences and post-processing is crucial and must include strategies to address fetal head motion and non-neuronal sources of fMRI signal. The use of functional connectivity on a ROI basis will allow future investigations on disease development and its correlation to healthy characteristics of connectivity development curves, as shown in this work.

AUTHOR CONTRIBUTIONS

András Jakab has written the manuscript, designed the experiments, performed the analysis and created figures. Ernst Schwartz has performed the analysis and contributed to the manuscript. Gerlinde M. Gruber has acquired data and contributed to the manuscript. Gregor Kasprian has written the manuscript and provided expert consultation. Daniela Prayer has acquired data, written manuscript and provided expert consultation, Veronika Schöpf, Georg Langs has written the manuscript, designed the experiments, provided senior supervision.

ACKNOWLEDGMENTS

This work was supported by the Austrian National Bank Anniversary Fund (FETALMORPHO) to Gregor Kasprian, the EU FP7 projects KHRESMOI to Georg Langs, the Austrian Science Fund (P23205-B09) to Veronika Schöpf. András Jakab is supported by the European Union FP7 Marie Curie IEF Research grant FABRIC – exploring the Formation and Adaptation of the Brain Connectome," grant no. 2012-PIEF-GA-33003.

SUPPLEMENTARY MATERIAL

The Supplementary Material for this article can be found online at: http://www.frontiersin.org/journal/10.3389/fnhum.2014.00852/abstract

REFERENCES

Achard, S., Salvador, R., Whitcher, B., Suckling, J., and Bullmore, E. (2006). A resilient, low-frequency, small-world human brain functional network with highly connected association cortical hubs. *J. Neurosci.* 26, 63–72. doi: 10.1523/JNEUROSCI.3874-05.2006

Behzadi, Y., Restom, K., Liau, J., and Liu, T. T. (2007). A component based noise correction method (CompCor) for BOLD and perfusion based fMRI. *Neuroimage* 37, 90–101. doi: 10.1016/j.neuroimage.2007.04.042

Birn, R. M., Murphy, K., and Bandettini, P. A. (2008). The effect of respiration variations on independent component analysis results of resting state functional connectivity. *Hum. Brain Mapp.* 29, 740–750. doi: 10.1002/hbm.20577

Buckner, R. L., and Krienen, F. M. (2013). The evolution of distributed association networks in the human brain. *Trends Cogn. Sci. (Regul. Ed.)* 17, 648–665. doi: 10.1016/j.tics.2013.09.017

Buckner, R. L., Krienen, F. M., and Yeo, B. T. T. (2013). Opportunities and limitations of intrinsic functional connectivity MRI. *Nat. Neurosci.* 16, 832–837. doi: 10.1038/nn.3423

Bullmore, E., and Sporns, O. (2009). Complex brain networks: graph theoretical analysis of structural and functional systems. *Nat. Rev. Neurosci.* 10, 186–198. doi: 10.1038/nrn2575

Bystron, I., Blakemore, C., and Rakic, P. (2008). Development of the human cerebral cortex: boulder committee revisited. *Nat. Rev. Neurosci.* 9, 110–122. doi: 10.1038/nrn2252

Chung, H. W., Chen, C. Y., Zimmerman, R. A., Lee, K. W., Lee, C. C., and Chin, S. C. (2000). T2-Weighted fast MR imaging with true FISP versus HASTE: comparative efficacy in the evaluation of normal fetal brain maturation. *AJR Am. J. Roentgenol.* 175, 1375–1380. doi: 10.2214/ajr.175.5.1751375

Clancy, B., Darlington, R. B., and Finlay, B. L. (2001). Translating developmental time across mammalian species. *Neuroscience* 105, 7–17. doi: 10.1016/S0306-4522(01)00171-3

Colonnese, M., and Khazipov, R. (2012). Spontaneous activity in developing sensory circuits: implications for resting state fMRI. *Neuroimage* 62, 2212–2221. doi: 10.1016/j.neuroimage.2012.02.046

Craddock, R. C., James, G. A., Holtzheimer, P. E. III, Hu, X. P., and Mayberg, H. S. (2012). A whole brain fMRI atlas generated via spatially constrained spectral clustering. *Hum. Brain Mapp.* 33, 1914–1928. doi: 10.1002/hbm.21333

Damaraju, E., Phillips, J. R., Lowe, J. R., Ohls, R., Calhoun, V. D., and Caprihan, A. (2010). Resting-state functional connectivity differences in premature children. *Front. Syst. Neurosci.* 4:23. doi: 10.3389/fnsys.2010.00023

D'Elia, A., Pighetti, M., Moccia, G., and Santangelo, N. (2001). Spontaneous motor activity in normal fetuses. *Early Hum. Dev.* 65, 139–147. doi: 10.1016/S0378-3782(01)00224-9

Dennis, E. L., Jahanshad, N., McMahon, K. L., de Zubicaray, G. I., Martin, N. G., Hickie, I. B., et al. (2013). Development of brain structural connectivity between ages 12 and 30: a 4-tesla diffusion imaging study in 439 adolescents and adults. *Neuroimage* 64, 671–684. doi: 10.1016/j.neuroimage.2012.09.004

Desikan, R. S., Ségonne, F., Fischl, B., Quinn, B. T., Dickerson, B. C., Blacker, D., et al. (2006). An automated labeling system for subdividing the human cerebral cortex on MRI scans into gyral based regions of interest. *Neuroimage* 31, 968–980. doi: 10.1016/j.neuroimage.2006.01.021

Doria, V., Beckmann, C. F., Arichi, T., Merchant, N., Groppo, M., Turkheimer, F. E., et al. (2010). Emergence of resting state networks in the preterm human brain. *Proc. Natl. Acad. Sci. U.S.A.* 107, 20015–20020. doi: 10.1073/pnas.1007921107

Dubois, J., Dehaene-Lambertz, G., Perrin, M., Mangin, J. F., Cointepas, Y., Duchesnay, E., et al. (2008). Asynchrony of the early maturation of white matter bundles in healthy infants: quantitative landmarks revealed noninvasively by diffusion tensor imaging. *Hum. Brain Mapp.* 29, 14–27. doi: 10.1002/hbm.20363

Fjell, A. M., Westlye, L. T., Amlien, I., Tamnes, C. K., Grydeland, H., Engvig, A., et al. (2013). High-expanding cortical regions in human development and evolution are related to higher intellectual abilities. *Cereb. Cortex* doi: 10.1093/cercor/bht201 [Epub ahead of print].

Flechsig, P. E. (1920). *Anatomie des Menschlichen Gehirns und Rückenmarks auf Myelogenetischer Grundlage.* Leipzig: G. Thieme.

Fransson, P. (2005). Spontaneous low-frequency BOLD signal fluctuations: an fMRI investigation of the resting-state default mode of brain function hypothesis. *Hum. Brain Mapp.* 26, 15–29. doi: 10.1002/hbm.20113

Geschwind, N. (1964). "The development of the brain and the evolution of language," in *Monograph Series on Language and Linguistics*, ed. C. I. J. M. Stuart (Washington, DC: Georgetown University Press).

Glenn, O. A., and Barkovich, A. J. (2006). Magnetic resonance imaging of the fetal brain and spine: an increasingly important tool in prenatal diagnosis, part 1. *AJNR Am. J. Neuroradiol.* 27, 1604–1611.

Gowland, P., and Fulford, J. (2004). Initial experiences of performing fetal fMRI. *Exp. Neurol.* 190(Suppl. 1), 22–27. doi: 10.1016/j.expneurol.2004.06.022

Greicius, M. (2008). Resting-state functional connectivity in neuropsychiatric disorders. *Curr. Opin. Neurol.* 21, 424–430. doi: 10.1097/WCO.0b013e328306f2c5

Greicius, M. D., Krasnow, B., Reiss, A. L., and Menon, V. (2003). Functional connectivity in the resting brain: a network analysis of the default mode hypothesis. *Proc. Natl. Acad. Sci. U.S.A.* 100, 253–258. doi: 10.1073/pnas.0135058100

Hill, J., Inder, T., Neil, J., Dierker, D., Harwell, J., and Van Essen, D. (2010). Similar patterns of cortical expansion during human development and evolution. *Proc. Natl. Acad. Sci. U.S.A.* 107, 13135–13140. doi: 10.1073/pnas.1001229107

Holst, M., Eswaran, H., Lowery, C., Murphy, P., Norton, J., and Preissl, H. (2005). Development of auditory evoked fields in human fetuses and newborns: a longitudinal MEG study. *Clin. Neurophysiol.* 116, 1949–1955. doi: 10.1016/j.clinph.2005.04.008

Honey, C. J., Sporns, O., Cammoun, L., Gigandet, X., Thiran, J. P., Meuli, R., et al. (2009). Predicting human resting-state functional connectivity from structural connectivity. *Proc. Natl. Acad. Sci. U.S.A.* 106, 2035–2040. doi: 10.1073/pnas.0811168106

Huang, H., Xue, R., Zhang, J., Ren, T., Richards, L. J., Yarowsky, P., et al. (2009). Anatomical characterization of human fetal brain development with diffusion tensor magnetic resonance imaging. *J. Neurosci.* 29, 4263–4273. doi: 10.1523/JNEUROSCI.2769-08.2009

Jakob, H., and Beckmann, H. (1986). Prenatal developmental disturbances in the limbic allocortex in schizophrenics. *J. Neural Transm.* 65, 303–326. doi: 10.1007/BF01249090

Jardri, R., Houfflin-Debarge, V., Delion, P., Pruvo, J. P., Thomas, P., and Pins, D. (2012). Assessing fetal response to maternal speech using a noninvasive functional brain imaging technique. *Int. J. Dev. Neurosci.* 30, 159–161. doi: 10.1016/j.ijdevneu.2011.11.002

Jardri, R., Pins, D., Houfflin-Debarge, V., Chaffiotte, C., Rocourt, N., Pruvo, J. P., et al. (2008). Fetal cortical activation to sound at 33 weeks of gestation: a functional MRI study. *Neuroimage* 42, 10–18. doi: 10.1016/j.neuroimage.2008.04.247

Jenkinson, M., Beckmann, C. F., Behrens, T. E., Woolrich, M. W., and Smith, S. M. (2012). FSL. *Neuroimage* 62, 782–790. doi: 10.1016/j.neuroimage.2011.09.015

Johansen-Berg, H., and Rushworth, M. F. S. (2009). Using diffusion imaging to study human connectional anatomy. *Annu. Rev. Neurosci.* 32, 75–94. doi: 10.1146/annurev.neuro.051508.135735

Johnson, M. H. (2001). Functional brain development in humans. *Nat. Rev. Neurosci.* 2, 475–483. doi: 10.1038/35081509

Jokhi, R. P., and Whitby, E. H. (2011). Magnetic resonance imaging of the fetus. *Dev. Med. Child Neurol.* 53, 18–28. doi: 10.1111/j.1469-8749.2010.03813.x

Joseph, R. (2000). Fetal brain behavior and cognitive development. *Dev. Rev.* 20, 81–98. doi: 10.1006/drev.1999.0486

Judas, M., Sedmak, G., and Kostovic, I. (2013). The significance of the subplate for evolution and developmental plasticity of the human brain. *Front. Hum. Neurosci.* 7:423. doi: 10.3389/fnhum.2013.00423

Kanold, P. O. (2009). Subplate neurons: crucial regulators of cortical development and plasticity. *Front. Neuroanat.* 3:16. doi: 10.3389/neuro.05.016.2009

Kasprian, G., Brugger, P. C., Weber, M., Krssák, M., Krampl, E., Herold, C., et al. (2008). In utero tractography of fetal white matter development. *Neuroimage* 43, 213–224. doi: 10.1016/j.neuroimage.2008.07.026

Kelly, C., Biswal, B. B., Craddock, R. C., Castellanos, F. X., and Milham, M. P. (2012). Characterizing variation in the functional connectome: promise and pitfalls. *Trends Cogn. Sci. (Regul. Ed.)* 16, 181–188. doi: 10.1016/j.tics.2012.02.001

Khazipov, R., and Luhmann, H. J. (2006). Early patterns of electrical activity in the developing cerebral cortex of humans and rodents. *Trends Neurosci.* 29, 414–418. doi: 10.1016/j.tins.2006.05.007

Kinney, H. C., Brody, B. A., Kloman, A. S., and Gilles, F. H. (1988). Sequence of central nervous system myelination in human infancy. II. Patterns of myelination in autopsied infants. *J. Neuropathol. Exp. Neurol.* 47, 217–234. doi: 10.1097/00005072-198805000-00003

Kok, R. D., de Vries, M. M., Heerschap, A., and van den Berg, P. P. (2004). Absence of harmful effects of magnetic resonance exposure at 1.5 T in utero during the third trimester of pregnancy: a follow-up study. *Magn. Reson. Imaging* 22, 851–854. doi: 10.1016/j.mri.2004.01.047

Kok, R. D., van den Bergh, A. J., Heerschap, A., Nijland, R., and van den Berg, P. P. (2001). Metabolic information from the human fetal brain obtained with proton magnetic resonance spectroscopy. *Am. J. Obstet. Gynecol.* 185, 1011–1015. doi: 10.1067/mob.2001.117677

Kostovic, I., and Judas, M. (2010). The development of the subplate and thalamocortical connections in the human foetal brain. *Acta Paediatr.* 99, 1119–1127. doi: 10.1111/j.1651-2227.2010.01811.x

Kostovic, I., Judas, M., Rados, M., and Hrabac, P. (2002). Laminar organization of the human fetal cerebrum revealed by histochemical markers and magnetic resonance imaging. *Cereb. Cortex* 12, 536–544. doi: 10.1093/cercor/12.5.536

Kostovic, I., and Molliver, M. (1974). New interpretation of laminar development of cerebral-cortex-synaptogenesis in different layers of neopallium in human fetus. *Anat. Rec.* 178:395.

Lauritzen, M. (2005). Reading vascular changes in brain imaging: is dendritic calcium the key? *Nat. Rev. Neurosci.* 6, 77–85. doi: 10.1038/nrn1589

Lee, W., Morgan, B. R., Shroff, M. M., Sled, J. G., and Taylor, M. J. (2013). The development of regional functional connectivity in preterm infants into early childhood. *Neuroradiology* 55(Suppl. 2), 105–111. doi: 10.1007/s00234-013-1232-z

Logothetis, N. K., and Wandell, B. A. (2004). Interpreting the BOLD signal. *Annu. Rev. Physiol.* 66, 735–769. doi: 10.1146/annurev.physiol.66.082602.092845

Lopez-Bendito, G., and Molnar, Z. (2003). Thalamocortical development: how are we going to get there? *Nat. Rev. Neurosci.* 4, 276–289. doi: 10.1038/nrn1075

Lowe, M., Mock, B., and Sorenson, J. (1998). Functional connectivity in single and multislice echoplanar imaging using resting-state fluctuations. *Neuroimage* 7, 119–132. doi: 10.1006/nimg.1997.0315

Luhmann, H. J., Kilb, W., and Hanganu-Opatz, I. L. (2009). Subplate cells: amplifiers of neuronal activity in the developing cerebral cortex. *Front. Neuroanat.* 3:19. doi: 10.3389/neuro.05.019.2009

Maas, L. C., Mukherjee, P., Carballido-Gamio, J., Veeraraghavan, S., Miller, S. P., Partridge, S. C., et al. (2004). Early laminar organization of the human cerebrum demonstrated with diffusion tensor imaging in extremely premature infants. *Neuroimage* 22, 1134–1140. doi: 10.1016/j.neuroimage.2004.02.035

Mailath-Pokorny, M., Kasprian, G., Mitter, C., Schöpf, V., Nemec, U., and Prayer, D. (2012). Magnetic resonance methods in fetal neurology. *Semin. Fetal Neonatal Med.* 17, 278–284. doi: 10.1016/j.siny.2012.06.002

Mantini, D., Corbetta, M., Romani, G. L., Orban, G. A., and Vanduffel, W. (2013). Evolutionarily novel functional networks in the human brain? *J. Neurosci.* 33, 3259–3275. doi: 10.1523/JNEUROSCI.4392-12.2013

Molnár, Z., Métin, C., Stoykova, A., Tarabykin, V., Price, D. J., Francis, F., et al. (2006). Comparative aspects of cerebral cortical development. *Eur. J. Neurosci.* 23, 921–934. doi: 10.1111/j.1460-9568.2006.04611.x

Moore, A. R., Filipovic, R., Mo, Z., Rasband, M. N., Zecevic, N., and Antic, S. D. (2009). Electrical excitability of early neurons in the human cerebral cortex during the second trimester of gestation. *Cereb. Cortex* 19, 1795–1805. doi: 10.1093/cercor/bhn206

Morokuma, S., Fukushima, K., Otera, Y., Yumoto, Y., Tsukimori, K., Ochiai, M., et al. (2013). Ultrasound evaluation of fetal brain dysfunction based on behavioral patterns. *Brain Dev.* 35, 61–67. doi: 10.1016/j.braindev.2012.01.007

Mueller, S., Wang, D., Fox, M. D., Yeo, B. T., Sepulcre, J., Sabuncu, M. R., et al. (2013). Individual variability in functional connectivity architecture of the human brain. *Neuron* 77, 586–595. doi: 10.1016/j.neuron.2012.12.028

Neubert, F., Mars, R., Thomas, A., Sallet, J., and Rushworth, M. S. (2014). Comparison of Human ventral frontal cortex areas for cognitive control and language with areas in monkey frontal cortex. *Neuron* 81, 700–713. doi: 10.1016/j.neuron.2013.11.012

Nooner, K. B., Colcombe, S., Tobe, R., Mennes, M., Benedict, M., Moreno, A., et al. (2012). The NKI-Rockland sample: a model for accelerating the pace of discovery science in psychiatry. *Front. Neurosci.* 6:152. doi: 10.3389/fnins.2012.00152

Oakes, T., Johnstone, T., Ores Walsh, K., Greischar, L., Alexander, A., Fox, A., et al. (2005). Comparison of fMRI motion correction software tools. *Neuroimage* 28, 529–543. doi: 10.1016/j.neuroimage.2005.05.058

Partanen, E., Kujala, T., Naatanen, R., Liitola, A., Sambeth, A., and Huotilainen, M. (2013a). Learning-induced neural plasticity of speech processing before birth. *Proc. Natl. Acad. Sci. U.S.A.* 110, 15145–15150. doi: 10.1073/pnas.1302159110

Partanen, E., Kujala, T., Tervaniemi, M., and Huotilainen, M. (2013b). Prenatal music exposure induces long-term neural effects. *PLoS ONE* 8:e78946. doi: 10.1371/journal.pone.0078946

Paul, L. K., Brown, W. S., Adolphs, R., Tyszka, J. M., Richards, L. J., Mukherjee, P., et al. (2007). Agenesis of the corpus callosum: genetic, developmental and functional aspects of connectivity. *Nat. Rev. Neurosci.* 8, 287–299. doi: 10.1038/nrn2107

Penn, A. A., and Shatz, C. J. (1999). Brain waves and brain wiring: the role of endogenous and sensory-driven neural activity in development. *Pediatr. Res.* 45, 447–458. doi: 10.1203/00006450-199904010-00001

Power, J. D., Barnes, K. A., Snyder, A. Z., Schlaggar, B. L., and Petersen, S. E. (2012). Spurious but systematic correlations in functional connectivity MRI networks arise from subject motion. *Neuroimage* 59, 2142–2154. doi: 10.1016/j.neuroimage.2011.10.018

Prayer, D., Kasprian, G., Krampl, E., Ulm, B., Witzani, L., Prayer, L., et al. (2006). MRI of normal fetal brain development. *Eur. J. Radiol.* 57, 199–216. doi: 10.1016/j.ejrad.2005.11.020

Preuss, T. M. (2009). "The cognitive neuroscience of human uniqueness," in, *The Cognitive Neurosciences*, ed. M. S. Gazzaniga (Cambridge, MA: MIT Press), 49–64.

Price, D. J., Kennedy, H., Dehay, C., Zhou, L., Mercier, M., Jossin, Y., et al. (2006). The development of cortical connections. *Eur. J. Neurosci.* 23, 910–920. doi: 10.1111/j.1460-9568.2006.04620.x

Pugash, D., Brugger, P. C., Bettelheim, D., and Prayer, D. (2008). Prenatal ultrasound and fetal MRI: the comparative value of each modality in prenatal diagnosis. *Eur. J. Radiol.* 68, 214–226. doi: 10.1016/j.ejrad.2008.06.031

Rakic, P. (2009). Evolution of the neocortex: a perspective from developmental biology. *Nat. Rev. Neurosci.* 10, 724–735. doi: 10.1038/nrn2719

Rice, D., and Barone, S. (2000). Critical periods of vulnerability for the developing nervous system: evidence from humans and animal models. *Environ. Health Perspect.* 108(Suppl. 3), 511–533. doi: 10.1289/ehp.00108s3511

Rilling, J. K. (2014). Comparative primate neuroimaging: insights into human brain evolution. *Trends Cogn. Sci. (Regul. Ed.)* 18, 46–55. doi: 10.1016/j.tics.2013.09.013

Rubinov, M., and Sporns, O. (2010). Complex network measures of brain connectivity: uses and interpretations. *Neuroimage* 52, 1059–1069. doi: 10.1016/j.neuroimage.2009.10.003

Rueckert, D. (2012). *A Multi-channel 4D Probabilistic Atlas of the Developing Fetal Brain.* Available at: http://biomedic.doc.ic.ac.uk/brain-development/index.php?n=Main.Fetal (accessed November 1, 2013).

Schlotz, W., and Phillips, D. I. W. (2009). Fetal origins of mental health: evidence and mechanisms. *Brain Behav. Immun.* 23, 905–916. doi: 10.1016/j.bbi.2009.02.001

Schöpf, V., Kasprian, G., Brugger, P. C., and Prayer, D. (2012). Watching the fetal brain at "rest." *Int. J. Dev. Neurosci.* 30, 11–17. doi: 10.1016/j.ijdevneu.2011.10.006

Serag, A., Aljabar, P., Ball, G., Counsell, S. J., Boardman, J. P., Rutherford, M. A., et al. (2012). Construction of a consistent high-definition spatio-temporal atlas of the developing brain using adaptive kernel regression. *Neuroimage* 59, 2255–2265. doi: 10.1016/j.neuroimage.2011.09.062

Shmueli, K., van Gelderen, P., de Zwart, J. A., Horovitz, S. G., Fukunaga, M., Jansma, J. M., et al. (2007). Low-frequency fluctuations in the cardiac rate as a source of variance in the resting-state fMRI BOLD signal. *Neuroimage* 38, 306–320. doi: 10.1016/j.neuroimage.2007.07.037

Smyser, C. D., Inder, T. E., Shimony, J. S., Hill, J. E., Degnan, A. J., Snyder, A. Z., et al. (2010). Longitudinal analysis of neural network development in preterm infants. *Cereb. Cortex* 20, 2852–2862. doi: 10.1093/cercor/bhq035

Thomason, M. E., Dassanayake, M. T., Shen, S., Katkuri, Y., Alexis, M., Anderson, A. L., et al. (2013). Cross-hemispheric functional connectivity in the human fetal brain. *Sci. Transl. Med.* 5:173ra24.

Trivedi, R., Gupta, R. K., Husain, N., Rathore, R. K., Saksena, S., Srivastava, S., et al. (2009). Region-specific maturation of cerebral cortex in human fetal brain: diffusion tensor imaging and histology. *Neuroradiology* 51, 567–576. doi: 10.1007/s00234-009-0533-8

Uğurbil, K., Xu, J., Auerbach, E. J., Moeller, S., Vu, A. T., Duarte-Carvajalino, J. M., et al. (2013). Pushing spatial and temporal resolution for functional and diffusion MRI in the human connectome project. *Neuroimage* 80, 80–104. doi: 10.1016/j.neuroimage.2013.05.012

van den Heuvel, M. P., Stam, C. J., Kahn, R. S., and Hulshoff Pol, H. E. (2009). Efficiency of functional brain networks and intellectual performance. *J. Neurosci.* 29, 7619–7624. doi: 10.1523/JNEUROSCI.1443-09.2009

Vanhatalo, S., and Kaila, K. (2006). Development of neonatal EEG activity: from phenomenology to physiology. *Semin. Fetal Neonatal Med.* 11, 471–478. doi: 10.1016/j.siny.2006.07.008

Weissenbacher, A., Kasess, C., Gerstl, F., Lanzenberger, R., Moser, E., and Windischberger, C. (2009). Correlations and anticorrelations in resting-state functional connectivity MRI: a quantitative comparison of preprocessing strategies. *Neuroimage* 47, 1408–1416. doi: 10.1016/j.neuroimage.2009.05.005

Yakovlev, P. I., and Lecours, A. (1967). "The myelogenetic cycles of regional maturation of the brain," in *Regional Development of the Brain in Early Life*, ed. A. Minkowski (Oxford: Blackwell), 3–70.

Yan, C., Craddock, R. C., Zuo, X., Zang, Y., and Milham, M. P. (2013). Standardizing the intrinsic brain: towards robust measurement of inter-individual variation in 1000 functional connectomes. *Neuroimage* 80, 246–262. doi: 10.1016/j.neuroimage.2013.04.081

Yoshida, S., Oishi, K., Faria, A., and Mori, S. (2013). Diffusion tensor imaging of normal brain development. *Pediatr. Radiol.* 43, 15–27. doi: 10.1007/s00247-012-2496-x

Zalesky, A., Fornito, A., and Bullmore, E. T. (2010). Network-based statistic: identifying differences in brain networks. *Neuroimage* 53, 1197–1207. doi: 10.1016/j.neuroimage.2010.06.041

Zhang, L. I., and Poo, M. M. (2001). Electrical activity and development of neural circuits. *Nat. Neurosci.* 4(Suppl.), 1207–1214. doi: 10.1038/nn753

Conflict of Interest Statement: The authors declare that the research was conducted in the absence of any commercial or financial relationships that could be construed as a potential conflict of interest.

Received: 01 July 2014; paper pending published: 30 July 2014; accepted: 03 October 2014; published online: 22 October 2014.

Citation: Jakab A, Schwartz E, Kasprian G, Gruber GM, Prayer D, Schöpf V and Langs G (2014) Fetal functional imaging portrays heterogeneous development of emerging human brain networks. Front. Hum. Neurosci. ***8****:852. doi: 10.3389/fnhum.2014.00852 This article was submitted to the journal Frontiers in Human Neuroscience.*

frontiers in
HUMAN NEUROSCIENCE

ORIGINAL RESEARCH ARTICLE
published: 02 October 2014
doi: 10.3389/fnhum.2014.00775

The relationship between eye movement and vision develops before birth

Veronika Schöpf[1]*, Thomas Schlegl[2], Andras Jakab[2], Gregor Kasprian[1], Ramona Woitek[1], Daniela Prayer[1] and Georg Langs[2,3]*

[1] *Division of Neuro- and Musculoskeletal Radiology, Department of Biomedical Imaging and Image-guided Therapy, Medical University of Vienna, Vienna, Austria*
[2] *Computational Imaging Research Laboratory, Department of Biomedical Imaging and Image-guided Therapy, Medical University of Vienna, Vienna, Austria*
[3] *Computer Science and Artificial Intelligence Lab, Massachusetts Institute of Technology, Cambridge, MA, USA*

Edited by:
Silvia Comani, Università degli Studi "G. d'Annunzio," Italy

Reviewed by:
Christos Papadelis, Boston Children's Hospital – Harvard Medical School, USA
Xiaobing Li, Nanjing Medical University Suzhou Hospital, China

****Correspondence:***
Georg Langs, Computational Imaging Research Laboratory, Department of Biomedical Imaging and Image-guided Therapy, Medical University of Vienna, Währinger Gürtel 18-20, 1090 Vienna, Austria
e-mail: georg.langs@meduniwien.ac.at; Veronika Schöpf, Division of Neuro- and Musculoskeletal Radiology, Department of Biomedical Imaging and Image-guided Therapy, Medical University of Vienna, Währinger Gürtel 18-20, 1090 Vienna, Austria
e-mail: veronika.schoepf@meduniwien.ac.at

While the visuomotor system is known to develop rapidly after birth, studies have observed spontaneous activity in vertebrates in visually excitable cortical areas already before extrinsic stimuli are present. Resting state networks and fetal eye movements were observed independently *in utero*, but no functional brain activity coupled with visual stimuli could be detected using fetal fMRI. This study closes this gap and links *in utero* eye movement with corresponding functional networks. BOLD resting-state fMRI data were acquired from seven singleton fetuses between gestational weeks 30–36 with normal brain development. During the scan time, fetal eye movements were detected and tracked in the functional MRI data. We show that already *in utero* spontaneous fetal eye movements are linked to simultaneous networks in visual- and frontal cerebral areas. In our small but in terms of gestational age homogenous sample, evidence across the population suggests that the preparation of the human visuomotor system links visual and motor areas already prior to birth.

Keywords: functional connectivity, development, eye movement, ICA, *in utero* fMRI

INTRODUCTION

Postnatal sensory development is critical (Lewis and Maurer, 2005), as external stimuli shape the cortical architecture and its initial genetic roadmap (Bengoetxea et al., 2012). The nervous structures responsible for initial stimulus processing and evidence from animal studies suggest that already before the onset of vision, genetic factors, and spontaneous activity form the basis for subsequent topographic refinement of functional networks driven by experience. Vaidya and Gordon (2013) suggested that both genetic and experience-dependent maturational processes shape intrinsic connectivity networks.

Spontaneous neuronal activity is suspected to affect initial organization necessary for subsequent formation of more mature networks (Katz and Shatz, 1996). Recently, spontaneous retinal activity was described in mice *in vivo*, but the extent to which corresponding structured information is transmitted through the sensory system is still unknown (Ackman et al., 2012). Comparable activity has not yet been observed in humans. While substantial work exists on postnatal visual development in children, little is known about the events during the prenatal stimulus scarce period, when intrinsic activity is expected to dominate. Responses to visual stimuli were reported from as early as the 28th gestational week using neural electromagnetic activity measures acquired with magnetic resonance encephalography (MEG; Eswaran et al., 2004). *In utero* resting state networks (Schöpf et al., 2012; Thomason et al., 2013), and fetal eye movements (Birnholz, 1981; Woitek et al., 2013) were observed independently, but no visual stimulus response could be located in fetal functional magnetic resonance imaging (fMRI; Fulford et al., 2003). It is well established that resting-state fMRI is a powerful tool to study the organization of functional brain networks (Rosazza et al., 2012). The analysis of fMRI is not trivial and often requires data driven algorithms, such as independent component analysis [e.g., Schöpf et al. (2010a,b)]. The emergence of the visuomotor system is particularly informative regarding the precursory period of post-natal vision. It involves the relationship of intrinsic and extrinsic components suspected to shape the subsequent development of perception. The interaction of active eye movements and vision remains central in adult perception. In this work we investigated the relationship between eye movements and functional activity *in utero*, to identify the corresponding functional networks present before birth.

Even-though the questions where functional visual activity occurs *in utero*, and how primary visual areas do respond to extrinsic stimuli are not yet answered, voxel based morphometry studies in congenitally blind subjects hint at brain areas that change due

to the processing of extrinsic stimuli. While congenitally blind subjects exhibit lower cortical volume in both frontal areas (BA 44, 45) and visual areas (BA 17, 18; Ptito et al., 2008), compared to a control population, functional connectivity between frontal areas (parts of BA 44, 45, and 47) and occipital areas is stronger in early blind (Liu et al., 2007). This suggests an ambiguous relationship between associated intrinsic and extrinsic processing systems (Golland et al., 2007). It might indicate that an initial abundance in connectivity between such areas as those implicated for language and visual processing is pruned after vision onset. While this then results in a clearer separation between the two systems, the network as a whole is relevant during initial organization of functional architecture.

Here we use data driven methodology to first show that there exists a link between spontaneous eye movements and functional networks in the occipital brain regions associated with vision. Furthermore, we detected stable functional networks involving both occipital and frontal regions.

MATERIALS AND METHODS

SUBJECTS

Seven singleton fetuses between gestational weeks (GW) 30–36 [mean: 32.86 (SD 1.81); mean age of mothers at MRI: 32.29 years (3.99 SD)] with no pathological brain development were scanned after informed consent was obtained from the mothers. The ethics committee of the Medical University of Vienna approved the study.

IMAGE ACQUISITION

Magnetic resonance imaging was performed on a 1.5 T unit (Philips Medical Systems, Best, The Netherlands) using a SENSE (sensitivity encoding) cardiac coil with five elements. The pregnant women were examined in supine position, and neither contrast agents nor sedatives were administered. Measurements were performed using single-shot gradient-recalled echo-planar imaging (EPI). Fifteen axial slices with slice thickness of 3 mm were acquired with a matrix size of 144 × 144, FOV of 250 × 250 mm and TE/TR of 50/1000 ms and a flip angle of 90°. Axial slices were positioned perpendicular to the fetal brainstem. Two experienced neuroradiologists (GK and DP) evaluated the MR images.

TRACKING OF EYE MOVEMENTS RELATIVE TO HEAD AXIS

We tracked the movements of both fetal eyes computationally based on the fMRI data (see **Figure 1**). First, we identified the MR slice that contained the eyes, and then pixels were classified by means of a random forest classifier (Breiman, 2001) to assign each pixel a probability of being part of an eye. Based on this probability map, eye center locations were estimated, and the segmentation of the eye was refined by mathematical morphology operations. The lens was detected along the eye border, and the view direction was calculated as the direction from eye center to the lens center. The head axis was defined as the symmetry axis between the two eyes. Relative eye angles were calculated as the difference between each eye angle (left and right) and the head central axis. Eye positions and relative eye angles were calculated for each frame in the MRI sequence resulting in a sequence of relative angles for the both eyes for each fMRI frame (see **Figure 2**).

Based on the eye tracking sequences we create regressors and event indicators defined as explanatory variables that reflect the onset of eye movement. Eye movement events are defined as the time points when the eye movement is initiated. We obtain these points by marking peaks of the derivative of the absolute value of the first derivative of the relative eye angles. These are time points when the change of relative eye angle accelerates. We discard peaks below a value of 1.4, and used the time points of the remaining peaks as event-indicators. For each eye this vector is then convolved with a standard hemodynamic response function corresponding to the TR of the fMRI sequence to obtain the final explanatory vector for each eye.

$$e :\leftrightarrow (d(|d(\alpha_1)/dt|)/dt > t) \vee (d(|d(\alpha_2)/dt|)/dt > t)$$

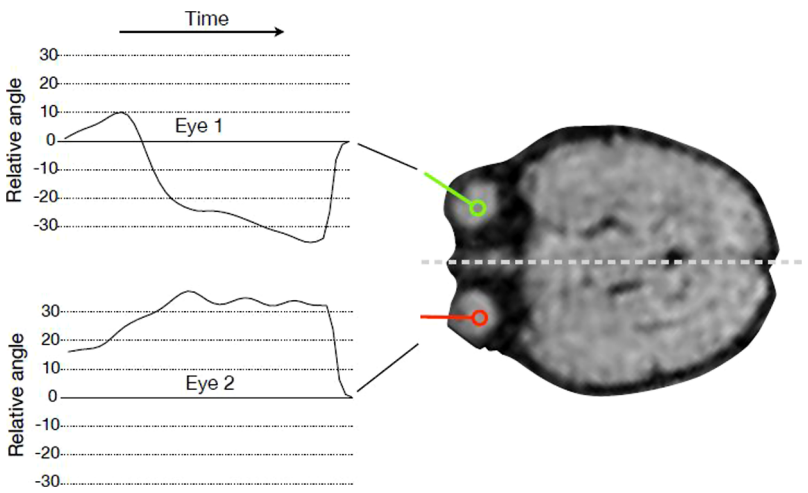

FIGURE 1 | Tracking eye movements over time. For every time point in the fMRI sequence, the angle of gaze direction relative to head orientation was recorded for every subject and both eyes.

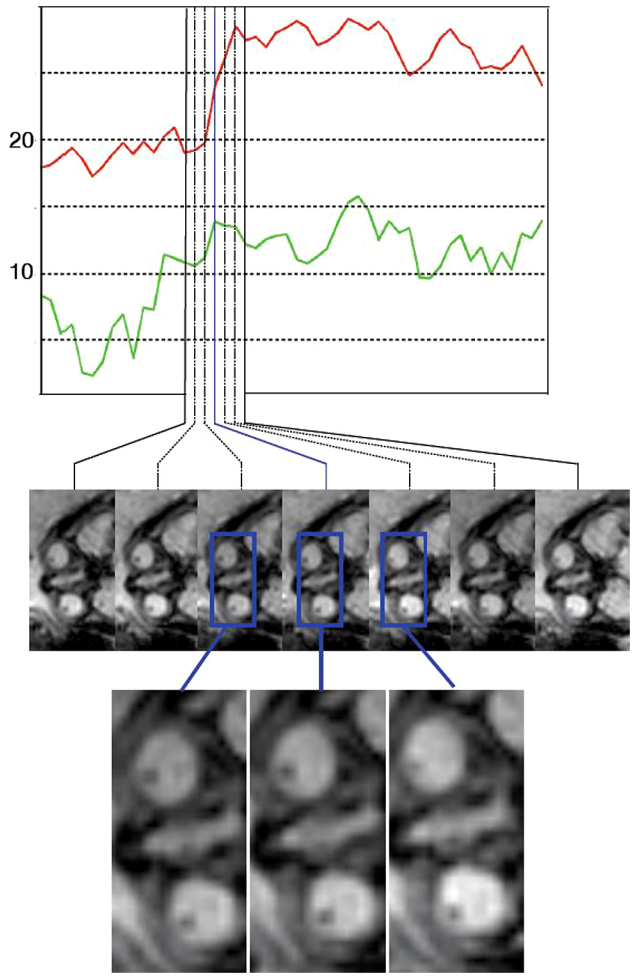

FIGURE 2 | An example of an eye movement sequence. The top plot shows the measures eye angles relative to the head axis (red for eye 1 and green for eye 2). The images below show the imaging data depicting the eyes at the corresponding time points. The eye movements are in the range of 5–7° in this sequence, and therefore qualitative analysis by a reader is difficult.

Description of main movement regressor: eye movement onset left/right jointly.

MOTION CORRECTION AND REGISTRATION

Image preprocessing was performed with FSL (FMRIB's Software Library, www.fmrib.ox.ac.uk/fsl) including motion correction as implemented in MCFLIRT version 5.5 (Oakes et al., 2005).

NUISANCE REGRESSORS

To lessen the confounding effects of non-neural signal fluctuations, we used a GLM based procedure to orthogonalize the fMRI signal to nuisance signals. Typically, such signals are originating from fetal head or maternal respiratory motion, and physiological noise, such as cardiac effects. We utilized the CompCor approach (Behzadi et al., 2007) which uses anatomical priors and principal component analysis to define non-neural signal. Fetal specific atlases were used to derive the CSF and WM compartments. We used CompCor regressors from an eroeded white matter mask, and from a region surrounding the cortical surface, including the CSF and the skull. For each region average signal and the most dominant six principal components were used as regressors. Furthermore derived nuisance regressors from the head and eye tracking information: (1,2) head position, (3,4) change of head position (x,y), (5) head angle, (6) change of head angle. The measurements from head tracking were convolved with a Gaussian filter, with SD 2.

ANALYSIS

Single subject independent component analysis was performed using probabilistic ICA as implemented in Multivariate Exploratory Linear Decomposition Optimized into Independent Components (MELODIC) version 3.10, a part of FSL (FMRIB's Software Library, www.fmrib.ox.ac.uk/fsl), using FastICA (Beckmann and Smith, 2004). The number of sources was estimated from the data by maximizing the Laplacian approximation to the Bayesian evidence of the model order (Minka, 2000; Beckmann and Smith, 2004). For the optimization of the non-Gaussian sources, contrast function, and convergence thresholds, as suggested by Hyvärinen et al. (2001), were used. Estimated component maps were divided by the SD of the residual noise and thresholded by fitting a mixture model to the intensity values histogram (Beckmann and Smith, 2004). Cross correlation coefficients of the derived independent components with all eye movement parameters were calculated.

RESULTS

To investigate if the networks active at movement onsets are stable, and can be detected from the data regardless of the eye movement, we performed ICA on the fMRI data. On average 13 independent components were estimated per subject (SD 4.03). Correlation of single-subject component time courses with the eye movement regressor was calculated. The independent component with maximum correlation coefficients for each subjects were evaluated [mean correlation coefficient: 0.33 (SD 0.07)]. The networks showing the highest correlation with fetal eye movement (see **Figure 3**) include association related areas as the angular gyrus, the inferior parietal gyrus, the superior frontal gyrus, as well as a primary visual area the medial occipital gyrus and motion associated function.

DISCUSSION

The present results indicate a relationship between fetal eye movements and activation in visual brain areas, motor areas, and orbitofrontal areas *in utero*. The observed functional networks correlating to visuomotor activity may offer a new perspective of the time period in which the orbitofrontal prepares for extrinsic sensory processing. The presence and relationship of the reported functional networks between visual and frontal areas in fetuses may prepare the developing brain for the processing of visual patterns as a precursor for the subsequent postnatal stimulus driven development of visual perception. Although observations are

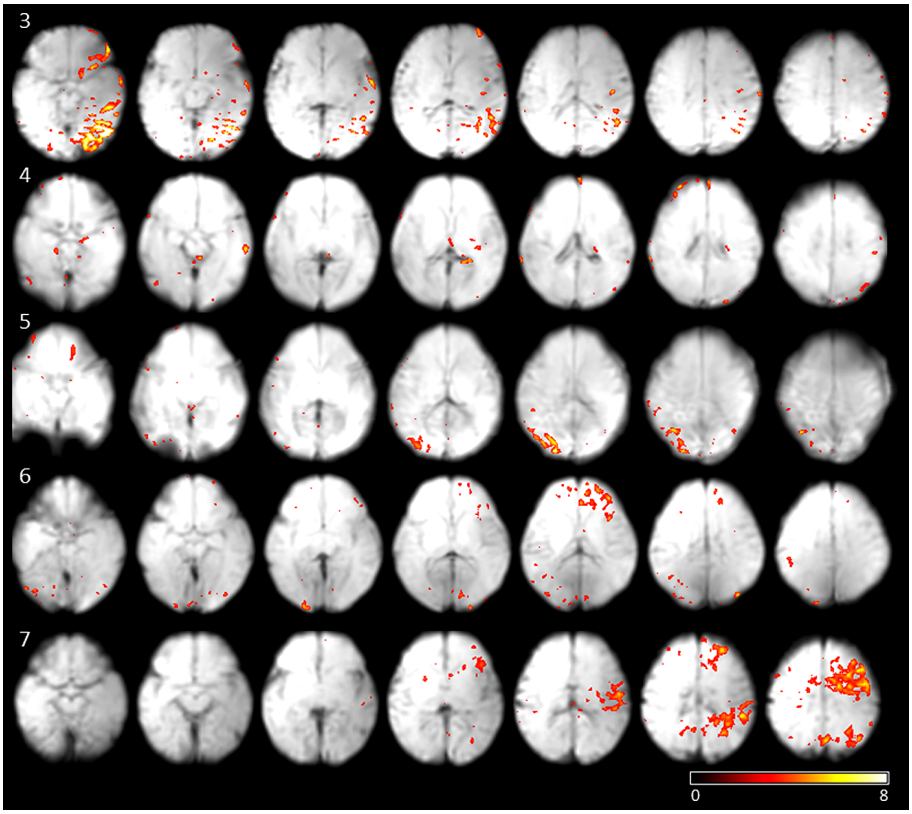

FIGURE 3 | Results of subjects 3–7 of the independent components with the maximum correlation coefficients with the eye movement on-set regressor derived from eye tracking. Maps are overlaid on individual mean EPIs.

based on a limited number of subjects, the results were consistent across the population.

FETAL EYE MOVEMENTS

Previous work on *in utero* fMRI provides insight in the developing brain ranging from stimulus processing (Schöpf et al., 2011) to intrinsic resting-state activity (Schöpf et al., 2012; Thomason et al., 2013). The observation of brain networks *in utero* suffers from the uncertainty of the status of the fetus at rest or asleep, which cannot be controlled. According to the categorization of fetal behavioral states from Romanini and Rizzo (1995), periods of "quiet sleep" or "quiet awake" can only be differentiated upon fetal eye movement. Four fetal eye movement patterns were initially characterized based on early ultrasound observations (Birnholz, 1981): Type I eye movements were described as single, transient deviations consisting of a bulb deviation, and a slower return back to the resting position, single but prolonged eye movements as Type II, complex sequences of eye movements to different directions without periodicity as Type III, and repetitive nystagmoid eye movements as Type IV. Additionally splitting of Type I eye movements into Type Ia (fast deviation, slower reposition) and Type Ib (fast deviation, equally fast reposition) was based on eye movement observation during MRI measurements (Woitek et al., 2013). It has already been shown that MRI sequences provide a valuable tool for visualizing and categorizing fetal eye movements (Brémond-Gignac et al., 1997; Woitek et al., 2013). While this method was initially developed to serve as an indicator for ocular development and as an indirect biomarker to detect malformations affecting the brainstem, our study investigates for the first time the networks responsible for the processing of eye movement *in utero*, enabling the purest form of a natural self induced stimulus, eye movement.

FUNCTIONAL SENSORI MOTOR NETWORKS *IN UTERO*

We did not observe activations in the frontal eye field, which is known to be related to saccadic eye movements. As saccades are very fast (20–400 ms), we do not expect them to be correlated with the MRI tracked motion events due to the limited temporal resolution of the MRI eye tracking.

Slow pursuit or gazing movements (looking at directions intentionally or following a moving object) are controlled with involvement of deep-parieto-occipital cortex. Although we cannot confirm on intentional focusing *in utero,* we do see parietal–occipital activity in four out of seven cases. It is known from studies on macaques that the parieto-occipital cortex shows activation during self-generated eye movements (Law et al., 1998) and plays a crucial role in encoding extrapersonal visual space (Galletti et al., 1995). As we did not provide the fetus with visual

stimuli, the activation we observed in the parietal–occipital area might hint at the generator of intrinsic eye movements in human fetuses.

There is only little motor activity and little involvement of the supplementary motor cortex or the typical frontal eye field (see below). These results are in line with findings in macaques reporting on fetal eye motion mainly governed by brainstem and midbrain processes. They suggest supratentorial control of eye motion gaining functional importance during brain development.

The networks we observed in fetuses differ from those known in the adult brain, and do not include a number of regions typically associated with eye movements in adults. Instead, they include areas identified with extrinsic stimulus processing (V1 in subjects 3,4,5,6) and motor control (subjects 3,4,6,7). So far no visual stimulus fMRI response activity *in utero* could be located (Fulford et al., 2003).

THE FETAL- VERSUS THE ADULT BRAIN

Most experiments investigating sensory systems *in utero*, as for example visual and auditory systems, were constituted based on block length and stimulus sequences of adult paradigm settings, which might be a poor fit for fetal function and could explain the non-detection of activity patterns in, e.g., the primary sensory areas [for a review see Schöpf et al. (2011)]. The lack of previous localizations in primary sensory areas as a response to sensory stimuli strongly indicates that conventional fMRI paradigms used in adult settings do not capture the fetal brain settings. In light of (Dehorter et al., 2012) proposition that the developing brain is not a small adult brain but that the voltage- and transmitter-gated currents act like network driven patterns following a developmental sequence, the present results point to endogenous activity in the developing cortex as modulating the formation of functional units in the sensorimotor system. Instead of linking primary sensory activity to external stimuli, they evidence a link to spontaneous eye motion as part of the sensorimotor system. The function of these early patterns is to enable heterogeneous neurons to fire and wire together and prepare for subsequent stimulus driven development rather than to code specific modalities at this point.

Colonnese et al. (2010) already observed the change of functional units and a switch to mature visual response shortly before delivery in humans based on recordings from the visual cortex of preterm human infants. They proposed a "bursting" period of visual responsiveness during which weak retinal information is amplified by endogenous network oscillations, which in turn enable a primitive form of vision. Colonnese et al. (2010) concluded that an intrinsic program that is able to switch cortical responses in anticipation of patterned vision operates early visual developmental processing.

LIMITATIONS

A constraining factor of the presented work is the limited sample size. According to this issue results are based on a single subject level analysis. As the sample was very homogenous with regard to gestational age this setting was chosen specifically to abstain from technical nuisance introduction emerging from registration to a template, which could influence the quality of single eye movement trackings. On the other hand, this homogeneity of developmental age does not allow for the analysis of eye movement related networks across gestational development, which will be of interest in future investigation. Furthermore, an important open question regarding our understanding of the hemodynamic developmental trajectory across *in utero* development, could be addressed by model driven data analysis.

ACKNOWLEDGMENTS

This work was supported by the Austrian National Bank Anniversary Fund (FETALMORPHO) to Gregor Kasprian, the EU FP7 projects KHRESMOI and VISCERAL to Georg Langs, the Austrian Science Fund (P23205-B09) to Veronika Schöpf. Andras Jakab is supported by the European Union FP7 Marie Curie IEF Research grant FABRIC – "exploring the Formation and Adaptation of the Brain Connectome," grant no. 2012-PIEF-GA-33003.

REFERENCES

Ackman, J. B., Burbridge, T. J., and Crair, M. C. (2012). Retinal waves coordinate patterned activity throughout the developing visual system. *Nature* 490, 219–225. doi: 10.1038/nature11529

Beckmann, C. F., and Smith, S. M. (2004). Probabilistic independent component analysis for functional magnetic resonance imaging. *IEEE Trans. Med. Imaging* 23, 137–152. doi: 10.1109/TMI.2003.822821

Behzadi, Y., Restom, K., Liau, J., and Liu, T. T. (2007). A component based noise correction method (CompCor) for BOLD and perfusion based fMRI. *Neuroimage* 37, 90–101. doi: 10.1016/j.neuroimage.2007.04.042

Bengoetxea, H., Ortuzar, N., Bulnes, S., Rico-Barrio, I., Lafuente, J. V., and Argandoña, E. G. (2012). Enriched and deprived sensory experience induces structural changes and rewires connectivity during the postnatal development of the brain. *Neural Plast.* 2012, 305693. doi: 10.1155/2012/305693

Birnholz, J. C. (1981). The development of human fetal eye movement patterns. *Science* 213, 679–681. doi: 10.1126/science.7256272

Breiman, L. (2001). Random forests. *Mach. Learn.* 45, 5–32. doi: 10.1023/A:1010933404324

Brémond-Gignac, D. S., Benali, K., Deplus, S., Cussenot, O., Ferkdadji, L., Elmaleh, M., et al. (1997). In utero eyeball development study by magnetic resonance imaging. *Surg. Radiol. Anat.* 19, 319–322. doi: 10.1007/BF01637602

Colonnese, M. T., Kaminska, A., Minlebaev, M., Milh, M., Bloem, B., Lescure, S., et al. (2010). A conserved switch in sensory processing prepares developing neocortex for vision. *Neuron* 67, 480–498. doi: 10.1016/j.neuron.2010.07.015

Dehorter, N., Vinay, L., Hammond, C., and Ben-Ari, Y. (2012). Timing of developmental sequences in different brain structures: physiological and pathological implications. *Eur. J. Neurosci.* 35, 1846–1856. doi: 10.1111/j.1460-9568.2012.08152.x

Eswaran, H., Lowery, C. L., Wilson, J. D., Murphy, P., and Preissl, H. (2004). Functional development of the visual system in human fetus using magnetoencephalography. *Exp. Neurol.* 190(Suppl.), S52–S58. doi: 10.1016/j.expneurol.2004.04.007

Fulford, J., Vadeyar, S. H., Dodampahala, S. H., Moore, R. J., Young, P., Baker, P. N., et al. (2003). Fetal brain activity in response to a visual stimulus. *Hum. Brain Mapp.* 20, 239–245. doi: 10.1002/hbm.10139

Galletti, C., Battaglini, P. P., and Fattori, P. (1995). Eye position influence on the parieto-occipital area PO (V6) of the macaque monkey. *Eur. J. Neurosci.* 7, 2486–2501. doi: 10.1111/j.1460-9568.1995.tb01047.x

Golland, Y., Bentin, S., Gelbard, H., Benjamini, Y., Heller, R., Nir, Y., et al. (2007). Extrinsic and intrinsic systems in the posterior cortex of the human brain revealed during natural sensory stimulation. *Cereb. Cortex* 17, 766–777. doi: 10.1093/cercor/bhk030

Hyvärinen, A., Karhunen, J., and Oja, E. (2001). *Independent Component Analysis.* Toronto, ON: John Wiley & Sons.

Katz, L. C., and Shatz, C. J. (1996). Synaptic activity and the construction of cortical circuits. *Science* 274, 1133–1138. doi: 10.1126/science.274.5290.1133

Law, I., Svarer, C., Rostrup, E., and Paulson, O. B. (1998). Parieto-occipital cortex activation during self-generated eye movements in the dark. *Brain* 121 1, 2189–2200. doi: 10.1093/brain/121.11.2189

Lewis, T. L., and Maurer, D. (2005). Multiple sensitive periods in human visual development: evidence from visually deprived children. *Dev. Psychobiol.* 46, 163–183. doi: 10.1002/dev.20055

Liu, Y., Yu, C., Liang, M., Li, J., Tian, L., Zhou, Y., et al. (2007). Whole brain functional connectivity in the early blind. *Brain* 130, 2085–2096. doi: 10.1093/brain/awm121

Minka, T. (2000). *Automatic Choice of Dimensionality for PCA*. Technical Report 514. Cambridge, MA: MIT Media Lab Vision and Modeling Group.

Oakes, T. R., Johnstone, T., Ores Walsh, K. S., Greischar, L. L., Alexander, A. L., Fox, A. S., et al. (2005). Comparison of fMRI motion correction software tools. *Neuroimage* 28, 529–543. doi: 10.1016/j.neuroimage.2005.05.058

Ptito, M., Schneider, F. C. G., Paulson, O. B., and Kupers, R. (2008). Alterations of the visual pathways in congenital blindness. *Exp. Brain Res.* 187, 41–49. doi: 10.1007/s00221-008-1273-4

Romanini, C., and Rizzo, G. (1995). Fetal behaviour in normal and compromised fetuses. An overview. *Early Hum. Dev.* 43, 117–131. doi: 10.1016/0378-3782(95)01667-8

Rosazza, C., Minati, L., Ghielmetti, F., Mandelli, M. L., and Bruzzone, M. G. (2012). Functional connectivity during resting-state functional MR imaging: study of the correspondence between independent component analysis and region-of-interest-based methods. *AJNR Am. J. Neuroradiol.* 33, 180–187. doi: 10.3174/ajnr.A2733

Schöpf, V., Kasess, C. H., Lanzenberger, R., Fischmeister, F., Windischberger, C., and Moser, E. (2010a). Fully exploratory network ICA (FENICA) on resting-state fMRI data. *J. Neurosci. Methods* 192, 207–213. doi: 10.1016/j.jneumeth.2010.07.028

Schöpf, V., Windischberger, C., Kasess, C., Lanzenberger, R., and Moser, E. (2010b). Group ICA of resting-state data: a comparison. *MAGMA* 23, 317–325. doi: 10.1007/s10334-010-0212-0

Schöpf, V., Kasprian, G., Brugger, P., and Prayer, D. (2012). Watching the fetal brain at "rest". *Int. J. Dev. Neurosci.* 30, 11–17. doi: 10.1016/j.ijdevneu.2011.10.006

Schöpf, V., Kasprian, G., and Prayer, D. (2011). Functional imaging in the fetus. *Top. Magn. Reson. Imaging* 22, 113–118. doi: 10.1097/RMR.0b013e3182699283

Thomason, M. E., Dassanayake, M. T., Shen, S., Katkuri, Y., Alexis, M., Anderson, A. L., et al. (2013). Cross-hemispheric functional connectivity in the human fetal brain. *Sci. Transl. Med.* 5, 173ra24. doi: 10.1126/scitranslmed.3004978

Vaidya, C. J., and Gordon, E. M. (2013). Phenotypic variability in resting-state functional connectivity: current status. *Brain Connect.* 3, 99–120. doi: 10.1089/brain.2012.0110

Woitek, R., Kasprian, G., Lindner, C., Stuhr, F., Weber, M., Schöpf, V., et al. (2013). Fetal eye movements on magnetic resonance imaging. *PLoS ONE* 8:e77439. doi: 10.1371/journal.pone.0077439

Conflict of Interest Statement: The authors declare that the research was conducted in the absence of any commercial or financial relationships that could be construed as a potential conflict of interest.

Received: 24 July 2014; paper pending published: 30 August 2014; accepted: 11 September 2014; published online: 02 October 2014.

Citation: Schöpf V, Schlegl T, Jakab A, Kasprian G, Woitek R, Prayer D and Langs G (2014) The relationship between eye movement and vision develops before birth. Front. Hum. Neurosci. ***8****:775. doi: 10.3389/fnhum.2014.00775*

This article was submitted to the journal Frontiers in Human Neuroscience.

frontiers in
HUMAN NEUROSCIENCE

OPINION ARTICLE
published: 20 January 2015
doi: 10.3389/fnhum.2014.01069

New techniques in the study of the brain development in newborn

Matteo Giampietri[1]*, Laura Bartalena[1], Andrea Guzzetta[2], Antonio Boldrini[1] and Paolo Ghirri[1]

[1] Department of Maternal and Child Health, Division of Neonatology and Neonatal Intensive Care Unit, S. Chiara Hospital, University of Pisa, Pisa, Italy
[2] Department of Developmental Neuroscience, Stella Maris Scientific Institute, Pisa, Italy
*Correspondence: giampimg@gmail.com

Edited by:
Marika Berchicci, Università degli Studi di Roma "Foro Italico", Italy

Reviewed by:
Noa Ofek-Shlomai, Hebrew University of Jerusalem, Israel

Keywords: magnetic resonance imaging, cranial ultrasound, neurodevelopmental outcome, diffusion tensor imaging (DTI), tractography

In the last few decades, the survival rates of preterm babies and full-term babies with severe diseases have increased due to advances in perinatal care. Understandably however, higher survival rates have not been accompanied by an overall reduction of morbidity, so that limitation of long-term neurodevelopmental abnormalities remains a major challenge of early care (Plaisier et al., 2014). The possibility to better predict the outcome of newborns at neurodevelopmental risk is essential to inform early intervention, to allow best allocation of resources, and to minimize long-term consequences. Unfortunately, clinicians continue to possess limited ability to predict neurodevelopmental outcomes, mainly relying, in most settings, on early findings at cranial ultrasound (cUS).

Recent studies (Smyser et al., 2012) have proven the power of magnetic resonance imaging (MRI) superior to other neuroimaging modalities, including cUS, in detecting cerebral injury. Neonatal MRI provides non-invasive, high-resolution images in less than 1 h; scans are performed without sedation eliminating the risk and the costs associated to it and are not associated to radiation exposure, as for computerized tomography (CT). The application of MRI in the neonatal population is rapidly increasing, making MRI one of the key diagnostic tools for the assessment of early brain development and injury.

In specific clinical groups, such as for example very preterm infants, cerebral MRI should become part of standard clinical care and should be systematically performed at term equivalent age (TEA). Accurate assessment of cortical folding at TEA provides an important marker for structural brain growth and maturation. Myelination of the posterior limb of the internal capsule (PLIC) at around 36–38 weeks gestation, identifiable on T1 but also on T2-weighted images, is another important maturational hallmark, since its presence and symmetry are very powerful in predicting motor outcome. MR imaging is superior to cUS also in detecting diffuse white matter (WM) injury. Indeed, although cystic periventricular leukomalacia is seen less often, diffuse non-cystic types of WM injury, including punctate WM lesions and diffuse excessive high signal intensity, are most frequent and are considered the leading cause of disturbed brain growth, connectivity, and functionality. The predictive power of conventional MRI in this domain remains relatively low, as it is not sensitive enough to analyze changes in microstructure; however, it is greatly enhanced by the use of advanced MR techniques targeting the WM, such as diffusion tensor imaging (DTI), that can help analyzing brain growth in extremely preterm babies in the absence of evident WM abnormalities (Ramenghi et al., 2009).

Diffusion tensor imaging (DTI) is a relatively new MR modality that assesses water diffusion in biological tissues at microstructural level. The diffusion tensor describes an ellipsoid in space characterized by the diffusion eigenvalues (λ_1,λ_2,λ_3) in the three orthogonal directions and their corresponding eigenvectors. In brain WM, axial diffusivity (λ_1) is oriented along the direction of the main tracts and radial diffusivity (λ_2 and λ_3) is oriented perpendicular to these tracts. Average diffusivity (D_{av}) reflects the mean of these eigenvalues and it is an indicator of brain maturation and/or injury. D_{av} decreases with increasing age probably for decreasing water content and increasing complexity of WM structures with myelination. Fractional anisotropy (FA) reflects the variance of the eigenvalues, ranging from 0 (isotropic diffusion) to 1 (anisotropic). The diffusion is mainly anisotropic because the water molecules preferentially move in the direction of fascicles of axons (Adams et al., 2010). In the white and gray matter, there is similar water content but different D_{av} value probably because the WM is less restrictive to water motion. Brain water content decreases with increasing gestational age and this mostly increases the WM anisotropy values. This increase has also been attributed to changes in WM structure associated with histologic maturation, and it takes place at different rates in different brain areas [the main areas analyzed are in commissural tracts, the corpus callosum (CC), and in projection tracts, the corticospinal tracts (CSTs)]. Developmental changes in anisotropy of cerebral cortex reflect changes in its microstructure, such as the arborization of basal dendrites of cortical neurons, the innervation of the cortical plate by thalamocortical and cortico-cortical fibers, all processes which are important basis of later functional connectivity (Huppi and Dubois, 2006). Because there are strongly preferred directions of diffusion, it is possible to create color maps of neonatal brain with diffusion tensor post-processing techniques. The color maps are based on major orientation with red representing right–left, green representing antero–posterior, and blue representing superior–inferior anatomical directions (De Bruïne et al., 2013) (**Figure 1**).

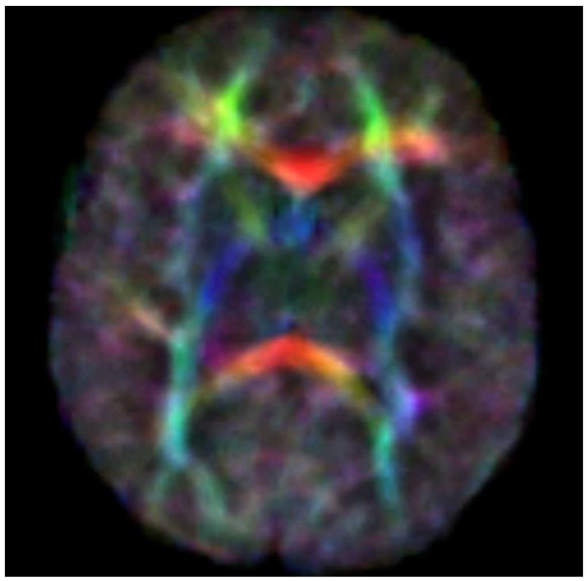

FIGURE 1 | Color anisotropy maps.

Preterm birth can cause white matter injuries (WMIs) and consequently can cause change in FA and diffusivity. Decreased FA in the CC of preterm babies scanned at TEA is rather common and implies less efficient transmission between the hemispheres and may lead to language problems and cognitive dysfunctions. Regions with increased FA in a preterm baby may be attributed to a loss or to an impairment of WM instead of improved WM maturation (Li et al., 2014). Disorders of motor function can be tested in clinical practice with DTI. In children with congenital hemiparesis, there are different diffusion characteristics of CSTs compared to healthy one. There is an increasing FA asymmetry and a decrease in FA value in the affected pyramidal tract.

A recent extension of DTI is tractography, which is a powerful tool that offers the possibility of non-invasive identification of specific WM pathways and connections in the brain. The general principle is to connect adjacent image voxels following water diffusion. Directional coherence of the fibers in a pathway is used to determine the presence or absence of connectivity between two regions of the brain. Tracking of the fiber-trajectories is terminated when they turn of too much degrees between two successive voxels. The main regions of interest include the CSTs, the CC, and optic radiations (OR). The primary goal should be to understand the normal relationship between structural and functional networks of these structures but there are few data in preterm babies (Brown et al., 2014). Preterm birth correlates with reduced connectivity, and it is very difficult to establish normal value for all gestational ages. Maturation does not occur simultaneously in the brain infact, for example, connectivity increases earlier in the occipital lobe and then in the frontal area. The postnatal age and WMI are additional confounding factors of diffusion metrics (Pannek et al., 2014). Nevertheless, the primary difference between DTI and conventional imaging is the capability of DTI to often detect injury earlier. This could anticipate the diagnosis of brain damage and might offer advantages in the future for deciding early intervention or administration of neuroprotective agents. Further studies will be needed to confirm whether these new techniques may predict neurodevelopmental outcome and whether they are equally applicable to all the pathways of the central nervous system.

REFERENCES

Adams, E., Chau, V., Poskitt, K. J., Grunau, R. E., Synnes, A., and Miller, S. P. (2010). Tractography-based quantification of corticospinal tract development in premature newborns. *J. Pediatr.* 156, 882–888. doi:10.1016/j.jpeds.2009.12.030

Brown, C. J., Miller, S. P., Booth, B. G., Andrews, S., Chau, V., Poskitt, K. J., et al. (2014). Structural network analysis of brain development in young preterm neonates. *Neuroimage* 101, 667–680. doi:10.1016/j.neuroimage.2014.07.030

De Bruïne, F. T., Van Wezel-Meijler, G., Leijser, L. M., Steggerda, S. J., Van Den Berg-Huysmans, A. A., Rijken, M., et al. (2013). Tractography of white-matter tracts in very preterm infants: a 2-year follow-up study. *Dev. Med. Child Neurol.* 55, 427–433. doi:10.1111/dmcn.12099

Huppi, P. S., and Dubois, J. (2006). Diffusion tensor imaging of brain development. *Semin. Fetal Neonatal Med.* 11, 489–497. doi:10.1016/j.siny.2006.07.006

Li, K., Sun, Z., Han, Y., Gao, L., Yuan, L., and Zeng, D. (2014). Fractional anisotropy alterations in individuals born preterm: a diffusion tensor imaging meta-analysis. *Dev. Med. Child Neurol.* doi:10.1111/dmcn.12618

Pannek, K., Scheck, S. M., Colditz, P. B., Boyd, R. N., and Rose, S. E. (2014). Magnetic resonance diffusion tractography of the preterm infant brain: a systematic review. *Dev. Med. Child Neurol.* 56, 113–124. doi:10.1111/dmcn.12250

Plaisier, A., Govaert, P., Lequin, M. H., and Dudink, J. (2014). Optimal timing of cerebral MRI in preterm infants to predict long-term neurodevelopmental outcome: a systematic review. *AJNR Am. J. Neuroradiol.* 35, 841–847. doi:10.3174/ajnr.A3513

Ramenghi, L. A., Rutherford, M., Fumagalli, M., Bassi, L., Messner, H., Counsell, S., et al. (2009). Neonatal neuroimaging: going beyond the pictures. *Early Hum. Dev.* 85(10 Suppl.), S75–S77. doi:10.1016/j.earlhumdev.2009.08.022

Smyser, C. D., Kidokoro, H., and Inder, T. E. (2012). Magnetic resonance imaging of the brain at term equivalent age in extremely premature neonates: to scan or not to scan? *J. Paediatr. Child Health* 48, 794–800. doi:10.1111/j.1440-1754.2012.02535.x

Conflict of Interest Statement: The authors declare that the research was conducted in the absence of any commercial or financial relationships that could be construed as a potential conflict of interest.

Received: 11 November 2014; accepted: 23 December 2014; published online: 20 January 2015.

Citation: Giampietri M, Bartalena L, Guzzetta A, Boldrini A and Ghirri P (2015) New techniques in the study of the brain development in newborn. Front. Hum. Neurosci. ***8****:1069. doi: 10.3389/fnhum.2014.01069*

This article was submitted to the journal Frontiers in Human Neuroscience.

frontiers in
HUMAN NEUROSCIENCE

MINI REVIEW ARTICLE
published: 21 January 2015
doi: 10.3389/fnhum.2014.01066

Recent advancements in diffusion MRI for investigating cortical development after preterm birth—potential and pitfalls

J. Dudink[1]*†, K. Pieterman[1†], A. Leemans[2], M. Kleinnijenhuis[3], A. M. van Cappellen van Walsum[4] and F. E. Hoebeek[5]

[1] *Department of Neonatology, Pediatric Intensive Care and Pediatric Radiology, Erasmus Medical Center - Sophia Children's Hospital, Rotterdam, Netherlands*
[2] *Image Sciences Institute, University Medical Center Utrecht, Utrecht, Netherlands*
[3] *Oxford Centre for Functional Magnetic Resonance Imaging of the Brain, University of Oxford, Oxford, UK*
[4] *Department of Anatomy, Donders Institute for Brain, Cognition, and Behaviour, Radboud University Medical Center, Nijmegen, Netherlands*
[5] *Department of Neuroscience, Erasmus Medical Center Rotterdam, Rotterdam, Netherlands*

Edited by:
Silvia Comani, Università degli Studi G. d'Annunzio, Italy

Reviewed by:
Zoltan Nagy, University of Zurich, Switzerland
Jan Buijs, Maxima Medisch Centrum, Netherlands

****Correspondence:***
J. Dudink, Department of Neonatology, Pediatric Intensive Care and Pediatric Radiology, Erasmus Medical Center - Sophia Children's Hospital, Wytemaweg 80, 3015 CN Rotterdam, Netherlands
e-mail: j.dudink@erasmusmc.nl

† These authors have contributed equally to this work.

Preterm infants are born during a critical period of brain maturation, in which even subtle events can result in substantial behavioral, motor and cognitive deficits, as well as psychiatric diseases. Recent evidence shows that the main source for these devastating disabilities is not necessarily white matter (WM) damage but could also be disruptions of cortical microstructure. Animal studies showed how moderate hypoxic-ischemic conditions did not result in significant neuronal loss in the developing brain, but did cause significantly impaired dendritic growth and synapse formation alongside a disturbed development of neuronal connectivity as measured using diffusion magnetic resonance imaging (dMRI). When using more advanced acquisition settings such as high-angular resolution diffusion imaging (HARDI), more advanced reconstruction methods can be applied to investigate the cortical microstructure with higher levels of detail. Recent advances in dMRI acquisition and analysis have great potential to contribute to a better understanding of neuronal connectivity impairment in preterm birth. We will review the current understanding of abnormal preterm cortical development, novel approaches in dMRI, and the pitfalls in scanning vulnerable preterm infants.

Keywords: diffusion magnetic resonance imaging, DTI, cortical imaging technique, prematurity, cortical development, cortical development and plasticity, diffusion MRI

INTRODUCTION

During the final trimester of pregnancy, the human brain rapidly develops by a complex interplay of genetic, epigenetic and environmental factors. Preterm infants are born during this period that is critical for neuronal connectivity, brain growth and cortical maturation, which together puts them at risk for functional impairments that are likely to persist into later life (Saigal and Doyle, 2008; Volpe, 2009). In particular the development of the cerebral cortex is imperative for the social and emotional well-being (e.g., Salmaso et al., 2014). Histological studies in both animals and humans have demonstrated that white and gray matter develop in close relation, and that isolated white matter (WM) injury sparing the cerebral cortex is uncommon (Govaert et al., 2006; Pierson et al., 2007; Sizonenko et al., 2007; Volpe, 2009; Okabayashi et al., 2011). Diffusion-MRI (dMRI) is a valuable tool to study brain development *in vivo*, and is based on its ability to characterize diffusion patterns of water molecules within the brain (Basser et al., 1994). As these patterns are directly related to brain microstructure, different models have been developed to characterize the diffusion signal in detail. The diffusion tensor (DT) model has been commonly used for this purpose, and represents the diffusion characteristics within each voxel as an ellipsoid (Basser et al., 1994; Jones and Leemans, 2011). Using only six parameters, this model is able to provide a quantitative description of the diffusion characteristics representing neuroanatomy. The ellipsoidal shape is more elongated (cigar-shaped) in regions with highly aligned and densely packed tissue components, such as the corpus callosum, representing *anisotropic* diffusion. In contrast, the DT shape resembles a sphere in brain regions with less aligned fiber tissue, wherein the diffusion pattern is called *isotropic*. Several studies have pointed out that the DT model is less adequate in representing complex fiber orientations within a single voxel (Tournier et al., 2004, 2011; Jeurissen et al., 2013), which is furthermore reflected by the fact that diffusion tensor imaging (DTI) has been predominantly used to characterize large WM bundles such as the corpus callosum and pyramidal tract but hardly to study "complex" brain regions containing crossing fibers and more dispersedly organized microstructure such as gray matter (Martinussen et al., 2005; Pannek et al., 2014).

Present-day, neuroimaging studies resulted in the development of acquisition and processing pipelines designed to derive

more detailed information about the precise diffusion characteristics within each voxel. These advances increase the applicability of dMRI to regions of more complex microstructure such as the cerebral cortex. Several higher-order models to fit the diffusion data have been developed recently, including models designed to study cortical microstructure, such as *neurite orientation dispersion and density imaging* (NODDI; Zhang et al., 2012). This mini-review will briefly outline these and other recent developments regarding cortical imaging and discuss related challenges and pitfalls.

INSIGHTS IN IMPAIRED CORTICAL DEVELOPMENT FROM HUMAN AND ANIMAL SPECIMEN STUDIES

For long, histological substrates of brain damage following preterm birth were most prominently characterized by large, focal WM lesions, adjacent to the ventricles, known as periventricular leukomalacia (PVL). Although cystic changes of WM are most prominent in PVL, several studies have outlined that relative sparing of the cerebral cortex is implausible in this type of WM injury. Andiman et al. (2010) histologically assessed the cortical microstructure in specimens of human tissue collected following focal periventricular WM injury possibly induced by preterm birth, and observed a significant reduction in pyramidal neuron density in layer V of the overlying cerebral cortex, indicating cell death of cortical neurons in focal WM injury (Andiman et al., 2010). A commonly used middle cerebral artery stroke model in mice showed comparable histological features, such as the histological abnormalities in layer V of the cortex. This included both morphological alterations of cell components and signs of neuronal necrosis (de Oliveira et al., 2014). In addition, subcortical nuclei were also affected in PVL cases, showing significant neuronal loss in thalamus, globus pallidus and the cerebellar dentate nucleus (Pierson et al., 2007). These findings exemplify that opposed to isolated WM injury, impaired neurodevelopment in preterm infants represents a complex interplay between gray and WM damage, leading to structural changes throughout the entire brain (Tymofiyeva et al., 2012; Ball et al., 2013a).

With the improved spatial resolution of state-of-the-art radiological techniques (e.g., ultra-high field MRI) the neonatal care specialists also encounter diffuse anatomical anomalies that affect both cortical and subcortical structures. Often these subtle aberrations are found in preterm children that suffered from hypoxia, ischemia or inflammation. Although the extent of such anatomical aberrations seems limited when visualized using conventional imaging, both human imaging and histology studies have demonstrated that these changes in the preterm brain can nevertheless significantly impact on long-term functional outcome (Ment et al., 2009). Moreover, using an experimental sheep model it was recently shown that the cortical development was severely affected following mild levels of ischemia, which evoked non-cystic and thus diffuse WM alteration (Dean et al., 2013). Using *ex vivo* high-field diffusion MRI it was also shown that normal cortical development was impeded, i.e., the physiological decrease in cortical anisotropy resulting from emerging cellular complexity during development was less pronounced in sheep exposed to moderate ischemia.

In contrast to focal WM changes such as PVL, the number of cortical neurons was not reduced in this type of WM damage, but Golgi-staining showed that ischemia induced a significant reduction of dendritic branching in the cerebral cortex, which could well explain the observed differences in anisotropy compared to age-matched controls. These results indicate that disrupted cortical development in moderate ischemia does not have to be linked to drastic effects like neuronal loss, but can also evoke "milder" effects like morphological aberrations (Dean et al., 2013).

Results of such translational studies of impaired cortical development are very useful, as they contribute to ensuring correct interpretation of *in vivo* human imaging results. By combining histology with MR-imaging in animal models and specimen studies, histological features of disrupted cortical development can be correlated to MR abnormalities seen in preterm born infants. Histology of the human cortex has been used as validation of normal brain cortical architecture (Kleinnijenhuis et al., 2013b; White et al., 2013), as well as to assess how histopathological findings correlate to cortical dMRI (Hulst and Geurts, 2011; Kolasinski et al., 2012; Gao et al., 2013; Leigland et al., 2013). These insights can be expected to help develop reliable, non-invasive, *in vivo* neuroimaging biomarkers for early prediction of impaired neurodevelopment.

MRI STUDIES OF IMPAIRED CORTICAL DEVELOPMENT IN HUMANS

The shift to more subtle radiologic abnormalities in both cortex and WM demands new ways to assess structure and development of the preterm brain. dMRI can provide additional insights in the characteristics of the preterm brain by mapping the diffusion pattern of water molecules. Because tissue components hinder the random motion of water molecules, dMRI measurements are directly related to underlying tissue microstructure (Basser and Jones, 2002; Mori and Van Zijl, 2002). Analysis of preterm brain damage using dMRI can thereby contribute to a better understanding of injury-mechanisms underlying impaired neurodevelopment, by revealing alterations in neuronal organization and extracellular matrix composition (Basser and Jones, 2002; Mori and Van Zijl, 2002).

Conventional T1 imaging has been used to assess the impact of preterm birth on cortical development. This sequence is particularly suitable for assessment of cortical volume and surface area, hence it provides good contrast between white and gray matter in combination with high spatial resolution. Studies making use of this have shown that cortical volume and surface area are substantially affected by preterm birth. Phillips et al. (2011) showed that in early childhood, cortical thickness was significantly higher and surface area significantly lower among preterm born infants than in term born controls (Phillips et al., 2011). This indicates that the normal pattern of cortical maturation—a combination of cortical thinning and surface area expansion—is substantially delayed or disrupted by preterm birth. The importance of these findings is highlighted by the fact that impaired cortical growth between 24 weeks and term-equivalent age is directly related to neurocognitive abilities in later life (Rathbone et al., 2011). The degree of cortical folding seems directly related to the extent of

WM connectivity (Melbourne et al., 2014), which is particularly relevant because studies in ex-preterm adolescents and adults show that characteristic changes in cortical folding, thickness and volume persist in later life (Martinussen et al., 2005; Nagy et al., 2011; Skranes et al., 2013).

ADVANCED DIFFUSION WEIGHTED IMAGING TECHNIQUES

Cortical diffusion MRI can help to determine *in vivo* how changes in cortical folding and thickness are related to cortical changes at a cellular level. Advances in dMRI, such as more widespread application of high-angular resolution diffusion imaging (HARDI), enable a more reliable assessment of cortical microstructure (Tuch et al., 2002). Benefits of HARDI acquisition arise from a substantial increase in number of diffusion-encoding directions, providing a more reliable and extensive characterization of the 3d diffusion profile. Next to an increase in angular resolution, increased spatial resolution is desirable, because it facilitates more reliable differentiation among cortical regions, underlying WM and surrounding cerebrospinal fluid. Higher-order processing algorithms of HARDI-data provide more detailed information than the tradition DT model, as these models aim at extracting the diffusion characteristics from each voxel more extensively.

The structure of the neocortex dramatically increases in complexity during development (McKinstry et al., 2002; Ball et al., 2013b). During developmental stages characterized by high densities of radial glial fibers, the DT model might be an adequate model for describing diffusion in the cortex (**Figure 1**). Furthermore, structural development of the cortex can be detected with the DT model (Neil et al., 1998; McKinstry et al., 2002), but the model's specificity is limited, because multiple features of the microstructure have similar effects on tensor characteristics (Vos et al., 2011, 2012). For example, the decrease in anisotropy observed over cortical development is thought to results from emerging dendritic arborization (Dean et al., 2013), but the same anisotropy decrease could also result from, for instance a reduction in radial glial fibers (Sizonenko et al., 2007). Most likely, these different changes happen concurrently and therefore it is essential to distinguish these contributions and other microstructural features, not only with postmortem techniques, but also with *in vivo* methods such as diffusion MRI.

As mentioned above, appealing alternatives to the DT model are available to capture more of the cortical complexity. The limitation of the DT model of describing diffusion behavior as an ellipsoid can be overcome by fitting models that allow more peaks in the modeled diffusion profile (Frank, 2002; Jansons and Alexander, 2003; Tuch et al., 2003; Tournier et al., 2004; Wedeen et al., 2005). By making use of high-angular resolution data, it is possible to fit more complex models which include multiple fibers. Such models have been widely adopted for resolving crossing fiber populations in WM tractography (Jeurissen et al., 2011, 2014; Pannek et al., 2014; Tax et al., 2014a). Likewise, complex cortical fiber arrangements emerging during gestation should also be reflected in the fiber orientation distributions derived from these data. Metrics specific to various cortical fiber populations might then be derived for application of this method in WM of the preterm brain (Raffelt et al., 2012; Dell'Acqua et al., 2013). Although radial and tangential components in the fiber orientation distribution have been *ex vivo* demonstrated (**Figure 2**) in adult human (Kleinnijenhuis et al., 2013a) and animal cortex (Dyrby et al., 2011), the performance of these models under such anisotropic conditions is uncertain (Parker et al., 2013). Furthermore, because scan time increases linearly with the number of directions, *in vivo* application of these elaborate sampling schemes in preterm newborns is particularly challenging.

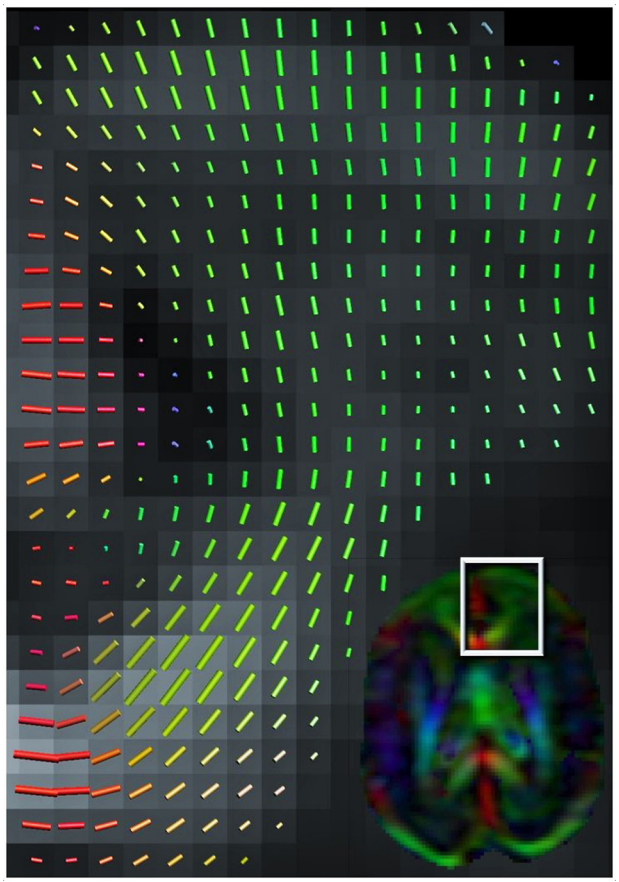

FIGURE 1 | Color-coded orientation map of a preterm infant's brain (born at 26 weeks of gestation and scanned at 30 weeks gestation at 1.5 Tesla MRI scanner) calculated from diffusion tensor imaging. Each pixel contains information about the eigenvector (Green color signifies preferential diffusion in the antero-posterior direction; Red in the latero-lateral direction; Blue in the superior-inferior direction) and extent of diffusion anisotropy (intensity of color) which summarizes the information obtained from each 3 × 3-matrix tensor. The cortex at 30 weeks gestation still has a clear radial organization (shown in close-up).

An innovation that could also be valuable for investigating the cortex in preterm infants is the estimation of quantitative measures of tissue microstructure. This approach surpasses the measures obtained from the DT model, as it can directly inform on the fraction, size and shape of various tissue compartments. Whereas extracellular water is—although hindered in its path—free to diffuse throughout the extracellular space, intracellular water is restricted within the bounds of the

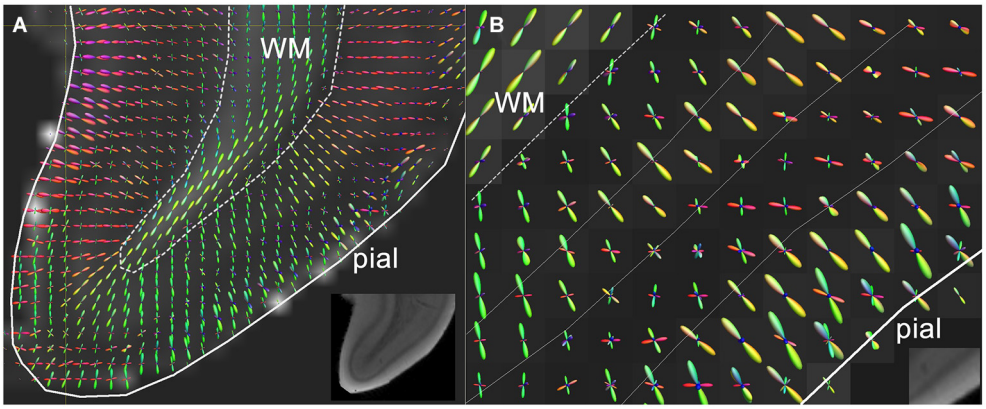

FIGURE 2 | (A) High resolution diffusion-MRI of sub-cortical white matter and cortical gray matter of the adult human primary visual cortex. High angular and spatial resolution data (768 directions at 300 micrometers isotropic resolution) was used to generate orientation distribution functions (ODF's) for each voxel. The spikes of the ODF are color-coded and represent the different directions of orientation within a single voxel. The ODF's in the cortex are mainly orientated perpendicular to the cortical surface, and represent its radial organization, whereas underlying white matter is arranged corticofugally. **(B)** Close-up of the cortex in a neighboring slice, showing that the ODF's are able to discern different layers of the cortex based on differences in microstructural characteristics between different laminae. The fractional anisotropy image is used as a backdrop image. Greyscale insets represent the anatomical GRE reference images showing cortical layers including the stria of Gennari. Adapted from Kleinnijenhuis et al. (2011).

cell. Sensitization to these different water pools is achieved by varying the b-value (or diffusion time), where higher b-values represent to some extent the intracellular signal, increasing the specificity to the tissue structures (e.g., Assaf and Basser, 2005). This simple principle has been used in several investigations of the preterm brain (Dudink et al., 2008; Ferizi et al., 2014; Pannek et al., 2014; Riffert et al., 2014). The diffusion kurtosis tensor (Jensen et al., 2005) is a somewhat more elaborate model that allows separation of the Gaussian and non-Gaussian contribution to the diffusion attenuation, assumed to represent the extracellular and intracellular spaces. A recent report demonstrates a marked decrease of radial kurtosis in the third trimester (Jeon, 2014), suggesting that it is a sensitive measure for disruption of radial glial fibers. Although the diffusion kurtosis isolates non-Gaussianity in the signal, it does not inform on the source of this non-Gaussianity. This is particularly relevant for the developing cortex, because non-Gaussianity can also result from fiber dispersion. The biophysical multi-compartment model NODDI (Zhang et al., 2012) is able to account for and inform on fiber dispersion, by explicitly including it in the signal model. The main parameters that can be estimated from the NODDI model are intracellular volume fraction and the orientation dispersion index. The first reports applying this model to the preterm brain (Eaton-Rosen, 2014; Kunz et al., 2014), suggest an increase in orientation dispersion during the third trimester, while the intracellular fiber volume fraction does not change.

DATA QUALITY AND PATIENT SAFETY

Although present-day and future innovations of dMRI offer new ways to increase understanding of disturbed cortical development in preterm infants, obtaining good quality images is particularly challenging in this patient group. For example, higher heart- and breathing rates in preterm infants and tendency of head movement during scanning can easily result in poor data quality, as dMRI sequences are motion-sensitive and artifact-prone. These matters are particularly relevant when studying cortical microstructure using these techniques, as certain types of distortions are more pronounced along the rim of brain tissue (Jones and Cercignani, 2010). Awareness of acquisition and processing steps determining data quality is therefore essential. To start with, fine-tuning of MR acquisition to the specific characteristic of the preterm brain and infant is desirable. Neonatal scanning hardware, such as neonatal coils, MR-compatible incubators, fixation pillows and noise-reducing earplugs have the potential to increase image quality and patient safety during scanning (Pannek et al., 2012). Furthermore, as neonatal dMRI data are highly sensitive to cardiac pulsation artifacts, the introduction of pulse triggering might benefit dMRI data quality considerably (Kozák et al., 2013). Still, extensive assessment of data quality is essential to ensure reliability of images. An approach combining visual inspection of raw diffusion data with software-based quality checks seems essential to ensure data reliability, as certain types of artifacts can hardly be seen on the diffusion data themselves (Tournier et al., 2011; Heemskerk et al., 2013). Dependent on the extent of quality loss, datasets need to be excluded from analysis or optimized using artifact and motion correction software in order to prevent inclusion of erroneous diffusion metrics in study results (Chang et al., 2005; Veraart et al., 2013; Collier et al., 2014; Plaisier et al., 2014; Tax et al., 2014b). This especially holds true for advanced neonatal diffusion MRI sequences, as complex acquisition and processing pipelines are accompanied with many pitfalls (Jones and Cercignani, 2010; Kersbergen et al., 2014).

CONCLUSION

High resolution dMRI has great potential to improve understanding of cortical neuronal connectivity impairment in children

born preterm. During the fetal period, axons from and to the cortical plate also start to form, and tends to align in the early phase of development. This radial structure forms the basis for the columnar organization of the fetal cortex (Sidman and Rakic, 1973; Rakic, 2002). As advances in neonatal imaging hardware and software will reduce traditional limitations of dMRI, future neonatal dMRI studies could go as far as study normal and abnormal maturation of columnar organization of our neocortex (Mountcastle, 1997). Next to that, HARDI-based imaging studies in animals and adults have shown that it is possible to discern different cortical regions based on the unique diffusion-"fingerprint" of different cortical regions. Likely, these advances will eventually result in the development of microstructure-based atlases, which can be used to study developmental patterns and eventual plasticity of individual cortical regions that are defined using microstructure (Schnell et al., 2009; Nagy et al., 2013; Wu et al., 2014; Aggarwal et al., 2015). Validation of these new techniques using histology is essential to ensure good correlation between microstructure and imaging.

ACKNOWLEDGMENTS

The research of A. Leemans is supported by VIDI Grant 639.072.411 from the Netherlands Organisation for Scientific Research (NWO). The research of F. E. Hoebeek is supported by ZON-MW TOP-GO (10.066) and NWO-VIDI 864.11.016. The research of K. Pieterman is supported by a KNAW Ter Meulen Grant.

REFERENCES

Aggarwal, M., Nauen, D. W., Troncoso, J. C., and Mori, S. (2015). Probing region-specific microstructure of human cortical areas using high angular and spatial resolution diffusion MRI. *Neuroimage* 105, 198–207. doi: 10.1016/j.neuroimage.2014.10.053

Andiman, S. E., Haynes, R. L., Trachtenberg, F. L., Billiards, S. S., Folkerth, R. D., Volpe, J. J., et al. (2010). The cerebral cortex overlying periventricular leukomalacia: analysis of pyramidal neurons. *Brain Pathol.* 20, 803–814. doi: 10.1111/j.1750-3639.2010.00380.x

Assaf, Y., and Basser, P. J. (2005). Composite hindered and restricted model of diffusion (CHARMED) MR imaging of the human brain. *Neuroimage* 27, 48–58. doi: 10.1016/j.neuroimage.2005.03.042

Ball, G., Boardman, J. P., Aljabar, P., Pandit, A., Arichi, T., Merchant, N., et al. (2013a). The influence of preterm birth on the developing thalamocortical connectome. *Cortex* 49, 1711–1721. doi: 10.1016/j.cortex.2012.07.006

Ball, G., Srinivasan, L., Aljabar, P., Counsell, S. J., Durighel, G., Hajnal, J. V., et al. (2013b). Development of cortical microstructure in the preterm human brain. *Proc. Natl. Acad. Sci. U S A* 110, 9541–9546. doi: 10.1073/pnas.1301652110

Basser, P. J., and Jones, D. K. (2002). Diffusion-tensor MRI: theory, experimental design and data analysis—a technical review. *NMR Biomed.* 15, 456–467. doi: 10.1109/iembs.2002.1106328

Basser, P. J., Mattiello, J., and Lebihan, D. (1994). MR diffusion tensor spectroscopy and imaging. *Biophys. J.* 66, 259–267. doi: 10.1016/s0006-3495(94)80775-1

Chang, L. C., Jones, D. K., and Pierpaoli, C. (2005). RESTORE: robust estimation of tensors by outlier rejection. *Magn. Reson. Med.* 53, 1088–1095. doi: 10.1002/mrm.20426

Collier, Q., Veraart, J., Jeurissen, B., Den Dekker, A. J., and Sijbers, J. (2014). Iterative reweighted linear least squares for accurate, fast and robust estimation of diffusion magnetic resonance parameters. *Magn. Reson. Med.* doi: 10.1002/mrm.25351. [Epub ahead of print].

Dean, J. M., Mcclendon, E., Hansen, K., Azimi-Zonooz, A., Chen, K., Riddle, A., et al. (2013). Prenatal cerebral ischemia disrupts MRI-defined cortical microstructure through disturbances in neuronal arborization. *Sci. Transl. Med.* 5:168ra167. doi: 10.1126/scitranslmed.3004669

Dell'Acqua, F., Simmons, A., Williams, S. C., and Catani, M. (2013). Can spherical deconvolution provide more information than fiber orientations? Hindrance modulated orientational anisotropy, a true-tract specific index to characterize white matter diffusion. *Hum. Brain Mapp.* 34, 2464–2483. doi: 10.1002/hbm.22080

de Oliveira, J. L., Crispin, P., Duarte, E. C., Marloch, G. D., Gargioni, R., Trentin, A. G., et al. (2014). Histopathology of motor cortex in an experimental focal ischemic stroke in mouse model. *J. Chem. Neuroanat.* 57–58, 1–9. doi: 10.1016/j.jchemneu.2014.03.002

Dudink, J., Larkman, D. J., Kapellou, O., Boardman, J. P., Allsop, J. M., Cowan, F. M., et al. (2008). High b-value diffusion tensor imaging of the neonatal brain at 3T. *AJNR Am. J. Neuroradiol.* 29, 1966–1972. doi: 10.3174/ajnr.a1241

Dyrby, T. B., Baaré, W. F., Alexander, D. C., Jelsing, J., Garde, E., and Søgaard, L. V. (2011). An ex vivo imaging pipeline for producing high-quality and high-resolution diffusion-weighted imaging datasets. *Hum. Brain Mapp.* 32, 544–563. doi: 10.1002/hbm.21043

Eaton-Rosen, Z. (2014). "Cortical maturation in the preterm period revealed using a multi-component diffusion-weighted MR model," in *Proceedings of the International Society for Magnetic Resonance in Medice*, 0080.

Ferizi, U., Schneider, T., Panagiotaki, E., Nedjati-Gilani, G., Zhang, H., Wheeler-Kingshott, C. A., et al. (2014). A ranking of diffusion MRI compartment models with in vivo human brain data. *Magn. Reson. Med.* 72, 1785–1792. doi: 10.1002/mrm.25080

Frank, L. R. (2002). Characterization of anisotropy in high angular resolution diffusion-weighted MRI. *Magn. Reson. Med.* 47, 1083–1099. doi: 10.1002/mrm.10156

Gao, Y. R., Choe, A. S., Stepniewska, I., Li, X., Avison, M. J., and Anderson, A. W. (2013). Validation of DTI tractography-based measures of primary motor area connectivity in the squirrel monkey brain. *Plos One* 8:e75065. doi: 10.1371/journal.pone.0075065

Govaert, P., Lequin, M., Korsten, A., Swarte, R., Kroon, A., and Barkovich, A. J. (2006). Postnatal onset cortical dysplasia associated with infarction of white matter. *Brain Res.* 1121, 250–255. doi: 10.1016/j.brainres.2006.08.093

Heemskerk, A. M., Leemans, A., Plaisier, A., Pieterman, K., Lequin, M. H., and Dudink, J. (2013). Acquisition guidelines and quality assessment tools for analyzing neonatal diffusion tensor MRI data. *AJNR Am. J. Neuroradiol.* 34, 1496–1505. doi: 10.3174/ajnr.a3465

Hulst, H. E., and Geurts, J. J. G. (2011). Gray matter imaging in multiple sclerosis: what have we learned? *BMC Neurol.* 11:153. doi: 10.1186/1471-2377-11-153

Jansons, K. M., and Alexander, D. C. (2003). Persistent angular structure: new insights from diffusion MRI data. Dummy version. *Inf. Process. Med. Imaging.* 18, 672–683. doi: 10.1007/978-3-540-45087-0_56

Jensen, J. H., Helpern, J. A., Ramani, A., Lu, H., and Kaczynski, K. (2005). Diffusional kurtosis imaging: the quantification of non-gaussian water diffusion by means of magnetic resonance imaging. *Magn. Reson. Med.* 53, 1432–1440. doi: 10.1002/mrm.20508

Jeon, T. (2014). "Microstructural development of human brain cerebral cortex from early 3rd trimester to around the birth with diffusion kurtosis imaging," in *Proceedings of the International Society for Magnetic Resonance in Medice*, 1742.

Jeurissen, B., Leemans, A., Jones, D. K., Tournier, J. D., and Sijbers, J. (2011). Probabilistic fiber tracking using the residual bootstrap with constrained spherical deconvolution. *Hum. Brain Mapp.* 32, 461–479. doi: 10.1002/hbm.21032

Jeurissen, B., Leemans, A., Tournier, J. D., Jones, D. K., and Sijbers, J. (2013). Investigating the prevalence of complex fiber configurations in white matter tissue with diffusion magnetic resonance imaging. *Hum. Brain Mapp.* 34, 2747–2766. doi: 10.1002/hbm.22099

Jeurissen, B., Tournier, J. D., Dhollander, T., Connelly, A., and Sijbers, J. (2014). Multi-tissue constrained spherical deconvolution for improved analysis of multi-shell diffusion MRI data. *Neuroimage* 103, 411–426. doi: 10.1016/j.neuroimage.2014.07.061

Jones, D. K., and Cercignani, M. (2010). Twenty-five pitfalls in the analysis of diffusion MRI data. *NMR Biomed.* 23, 803–820. doi: 10.1002/nbm.1543

Jones, D. K., and Leemans, A. (2011). Diffusion tensor imaging. *Methods Mol. Biol.* 711, 127–144. doi: 10.1007/978-1-61737-992-5_6

Kersbergen, K. J., Leemans, A., Groenendaal, F., Van Der Aa, N. E., Viergever, M. A., De Vries, L. S., et al. (2014). Microstructural brain development between 30 and 40 weeks corrected age in a longitudinal cohort of extremely preterm infants. *Neuroimage* 103C, 214–224. doi: 10.1016/j.neuroimage.2014.09.039

Kleinnijenhuis, M., Barth, M., Zerbi, V., Sikma, K.-J., Küsters, B., Slump, C. H., et al. (2011). "Layer-specific diffusion weighted imaging in human primary visual cortex *in vitro*," in *Organization for Human Brain Mapping* (Quebec City, Canada), 2509.

Kleinnijenhuis, M., Zerbi, V., Küsters, B., Slump, C. H., Barth, M., and Van Cappellen Van Walsum, A. M. (2013a). Layer-specific diffusion weighted imaging in human primary visual cortex in vitro. *Cortex* 49, 2569–2582. doi: 10.1016/j.cortex.2012.11.015

Kleinnijenhuis, M., Zhang, H., Wiedermann, D., Küsters, B., Norris, D. G., and Van Cappellen Van Walsum, A.-M. (2013b). "Detailed laminar characteristics of the human neocortex revealed by NODDI and histology," in *Organization for Human Brain Mapping* (Seattle, WA), 3815.

Kolasinski, J., Stagg, C. J., Chance, S. A., Deluca, G. C., Esiri, M. M., Chang, E. H., et al. (2012). A combined post-mortem magnetic resonance imaging and quantitative histological study of multiple sclerosis pathology. *Brain* 135, 2938–2951. doi: 10.1093/brain/aws242

Kozák, L. R., Dávid, S., Rudas, G., Vidnyánszky, Z., Leemans, A., and Nagy, Z. (2013). Investigating the need of triggering the acquisition for infant diffusion MRI: a quantitative study including bootstrap statistics. *Neuroimage* 69, 198–205. doi: 10.1016/j.neuroimage.2012.11.063

Kunz, N., Zhang, H., Vasung, L., O'brien, K. R., Assaf, Y., Lazeyras, F., et al. (2014). Assessing white matter microstructure of the newborn with multi-shell diffusion MRI and biophysical compartment models. *Neuroimage* 96, 288–299. doi: 10.1016/j.neuroimage.2014.03.057

Leigland, L. A., Budde, M. D., Cornea, A., and Kroenke, C. D. (2013). Diffusion MRI of the developing cerebral cortical gray matter can be used to detect abnormalities in tissue microstructure associated with fetal ethanol exposure. *Neuroimage* 83, 1081–1087. doi: 10.1016/j.neuroimage.2013.07.068

Martinussen, M., Fischl, B., Larsson, H. B., Skranes, J., Kulseng, S., Vangberg, T. R., et al. (2005). Cerebral cortex thickness in 15-year-old adolescents with low birth weight measured by an automated MRI-based method. *Brain* 128, 2588–2596. doi: 10.1093/brain/awh610

McKinstry, R. C., Mathur, A., Miller, J. H., Ozcan, A., Snyder, A. Z., Schefft, G. L., et al. (2002). Radial organization of developing preterm human cerebral cortex revealed by non-invasive water diffusion anisotropy MRI. *Cereb. Cortex* 12, 1237–1243. doi: 10.1093/cercor/12.12.1237

Melbourne, A., Kendall, G. S., Cardoso, M. J., Gunny, R., Robertson, N. J., Marlow, N., et al. (2014). Preterm birth affects the developmental synergy between cortical folding and cortical connectivity observed on multimodal MRI. *Neuroimage* 89, 23–34. doi: 10.1016/j.neuroimage.2013.11.048

Ment, L. R., Hirtz, D., and Huppi, P. S. (2009). Imaging biomarkers of outcome in the developing preterm brain. *Lancet Neurol.* 8, 1042–1055. doi: 10.1016/s1474-4422(09)70257-1

Mori, S., and Van Zijl, P. C. (2002). Fiber tracking: principles and strategies—a technical review. *NMR Biomed.* 15, 468–480. doi: 10.1002/nbm.781

Mountcastle, V. B. (1997). The columnar organization of the neocortex. *Brain* 120(Pt. 4), 701–722. doi: 10.1093/brain/120.4.701

Nagy, Z., Alexander, D. C., Thomas, D. L., Weiskopf, N., and Sereno, M. I. (2013). Using high angular resolution diffusion imaging data to discriminate cortical regions. *PLoS One* 8:e63842. doi: 10.1371/journal.pone.0063842

Nagy, Z., Lagercrantz, H., and Hutton, C. (2011). Effects of preterm birth on cortical thickness measured in adolescence. *Cereb. Cortex* 21, 300–306. doi: 10.1093/cercor/bhq095

Neil, J. J., Shiran, S. I., McKinstry, R. C., Schefft, G. L., Snyder, A. Z., Almli, C. R., et al. (1998). Normal brain in human newborns: apparent diffusion coefficient and diffusion anisotropy measured by using diffusion tensor MR imaging. *Radiology* 209, 57–66. doi: 10.1148/radiology.209.1.9769812

Okabayashi, S., Uchida, K., Nakayama, H., Ohno, C., Hanari, K., Goto, I., et al. (2011). Periventricular leucomalacia (PVL)-like lesions in two neonatal cynomolgus monkeys (Macaca fascicularis). *J. Comp. Pathol.* 144, 204–211. doi: 10.1016/j.jcpa.2010.06.006

Pannek, K., Guzzetta, A., Colditz, P. B., and Rose, S. E. (2012). Diffusion MRI of the neonate brain: acquisition, processing and analysis techniques. *Pediatr. Radiol.* 42, 1169–1182. doi: 10.1007/s00247-012-2427-x

Pannek, K., Scheck, S. M., Colditz, P. B., Boyd, R. N., and Rose, S. E. (2014). Magnetic resonance diffusion tractography of the preterm infant brain: a systematic review. *Dev. Med. Child Neurol.* 56, 113–124. doi: 10.1111/dmcn.12250

Parker, G. D., Marshall, D., Rosin, P. L., Drage, N., Richmond, S., and Jones, D. K. (2013). A pitfall in the reconstruction of fibre ODFs using spherical deconvolution of diffusion MRI data. *Neuroimage* 65, 433–448. doi: 10.1016/j.neuroimage.2012.10.022

Phillips, J. P., Montague, E. Q., Aragon, M., Lowe, J. R., Schrader, R. M., Ohls, R. K., et al. (2011). Prematurity affects cortical maturation in early childhood. *Pediatr. Neurol.* 45, 213–219. doi: 10.1016/j.pediatrneurol.2011.06.001

Pierson, C. R., Folkerth, R. D., Billiards, S. S., Trachtenberg, F. L., Drinkwater, M. E., Volpe, J. J., et al. (2007). Gray matter injury associated with periventricular leukomalacia in the premature infant. *Acta Neuropathol.* 114, 619–631. doi: 10.1007/s00401-007-0295-5

Plaisier, A., Pieterman, K., Lequin, M. H., Govaert, P., Heemskerk, A. M., Reiss, I. K., et al. (2014). Choice of diffusion tensor estimation approach affects fiber tractography of the fornix in preterm brain. *AJNR Am. J. Neuroradiol.* 35, 1219–1225. doi: 10.3174/ajnr.A3830

Raffelt, D., Tournier, J. D., Rose, S., Ridgway, G. R., Henderson, R., Crozier, S., et al. (2012). Apparent fibre density: a novel measure for the analysis of diffusion-weighted magnetic resonance images. *Neuroimage* 59, 3976–3994. doi: 10.1016/j.neuroimage.2011.10.045

Rakic, P. (2002). Evolving concepts of cortical radial and areal specification. *Prog. Brain Res.* 136, 265–280. doi: 10.1016/s0079-6123(02)36023-0

Rathbone, R., Counsell, S. J., Kapellou, O., Dyet, L., Kennea, N., Hajnal, J., et al. (2011). Perinatal cortical growth and childhood neurocognitive abilities. *Neurology* 77, 1510–1517. doi: 10.1212/WNL.0b013e318233b215

Riffert, T. W., Schreiber, J., Anwander, A., and Knösche, T. R. (2014). Beyond fractional anisotropy: extraction of bundle-specific structural metrics from crossing fiber models. *Neuroimage* 100, 176–191. doi: 10.1016/j.neuroimage.2014.06.015

Saigal, S., and Doyle, L. W. (2008). An overview of mortality and sequelae of preterm birth from infancy to adulthood. *Lancet* 371, 261–269. doi: 10.1016/s0140-6736(08)60136-1

Salmaso, N., Jablonska, B., Scafidi, J., Vaccarino, F. M., and Gallo, V. (2014). Neurobiology of premature brain injury. *Nat. Neurosci.* 17, 341–346. doi: 10.1038/nn.3604

Schnell, S., Saur, D., Kreher, B. W., Hennig, J., Burkhardt, H., and Kiselev, V. G. (2009). Fully automated classification of HARDI in vivo data using a support vector machine. *Neuroimage* 46, 642–651. doi: 10.1016/j.neuroimage.2009.03.003

Sidman, R. L., and Rakic, P. (1973). Neuronal migration, with special reference to developing human brain: a review. *Brain Res.* 62, 1–35. doi: 10.1016/0006-8993(73)90617-3

Sizonenko, S. V., Camm, E. J., Garbow, J. R., Maier, S. E., Inder, T. E., Williams, C. E., et al. (2007). Developmental changes and injury induced disruption of the radial organization of the cortex in the immature rat brain revealed by in vivo diffusion tensor MRI. *Cereb. Cortex* 17, 2609–2617. doi: 10.1093/cercor/bhl168

Skranes, J., Løhaugen, G. C., Martinussen, M., Håberg, A., Brubakk, A. M., and Dale, A. M. (2013). Cortical surface area and IQ in very-low-birth-weight (VLBW) young adults. *Cortex* 49, 2264–2271. doi: 10.1016/j.cortex.2013.06.001

Tax, C. M., Jeurissen, B., Vos, S. B., Viergever, M. A., and Leemans, A. (2014a). Recursive calibration of the fiber response function for spherical deconvolution of diffusion MRI data. *Neuroimage* 86, 67–80. doi: 10.1016/j.neuroimage.2013.07.067

Tax, C. M., Otte, W. M., Viergever, M. A., Dijkhuizen, R. M., and Leemans, A. (2014b). REKINDLE: Robust extraction of kurtosis INDices with linear estimation. *Magn. Reson. Med.* doi: 10.1002/mrm.25165. [Epub ahead of print].

Tournier, J. D., Calamante, F., Gadian, D. G., and Connelly, A. (2004). Direct estimation of the fiber orientation density function from diffusion-weighted MRI data using spherical deconvolution. *Neuroimage* 23, 1176–1185. doi: 10.1016/j.neuroimage.2004.07.037

Tournier, J. D., Mori, S., and Leemans, A. (2011). Diffusion tensor imaging and beyond. *Magn. Reson. Med.* 65, 1532–1556. doi: 10.1002/mrm.22924

Tuch, D. S., Reese, T. G., Wiegell, M. R., Makris, N., Belliveau, J. W., and Wedeen, V. J. (2002). High angular resolution diffusion imaging reveals intravoxel white matter fiber heterogeneity. *Magn. Reson. Med.* 48, 577–582. doi: 10.1002/mrm.10268

Tuch, D. S., Reese, T. G., Wiegell, M. R., and Wedeen, V. J. (2003). Diffusion MRI of complex neural architecture. *Neuron* 40, 885–895. doi: 10.1016/s0896-6273(03)00758-x

Tymofiyeva, O., Hess, C. P., Ziv, E., Tian, N., Bonifacio, S. L., McQuillen, P. S., et al. (2012). Towards the "baby connectome": mapping the structural connectivity of the newborn brain. *PLoS One* 7:e31029. doi: 10.1371/journal.pone.0031029

Veraart, J., Sijbers, J., Sunaert, S., Leemans, A., and Jeurissen, B. (2013). Weighted linear least squares estimation of diffusion MRI parameters: strengths, limitations and pitfalls. *Neuroimage* 81, 335–346. doi: 10.1016/j.neuroimage.2013.05.028

Volpe, J. J. (2009). Brain injury in premature infants: a complex amalgam of destructive and developmental disturbances. *Lancet Neurol.* 8, 110–124. doi: 10.1016/s1474-4422(08)70294-1

Vos, S. B., Jones, D. K., Jeurissen, B., Viergever, M. A., and Leemans, A. (2012). The influence of complex white matter architecture on the mean diffusivity in diffusion tensor MRI of the human brain. *Neuroimage* 59, 2208–2216. doi: 10.1016/j.neuroimage.2011.09.086

Vos, S. B., Jones, D. K., Viergever, M. A., and Leemans, A. (2011). Partial volume effect as a hidden covariate in DTI analyses. *Neuroimage* 55, 1566–1576. doi: 10.1016/j.neuroimage.2011.01.048

Wedeen, V. J., Hagmann, P., Tseng, W. Y., Reese, T. G., and Weisskoff, R. M. (2005). Mapping complex tissue architecture with diffusion spectrum magnetic resonance imaging. *Magn. Reson. Med.* 54, 1377–1386. doi: 10.1002/mrm.20642

White, N. S., Leergaard, T. B., D'Arceuil, H., Bjaalie, J. G., and Dale, A. M. (2013). Probing tissue microstructure with restriction spectrum imaging: histological and theoretical validation. *Hum. Brain Mapp.* 34, 327–346. doi: 10.1002/hbm.21454

Wu, D., Reisinger, D., Xu, J., Fatemi, S. A., van Zijl, P. C., Mori, S., et al. (2014). Localized diffusion magnetic resonance micro-imaging of the live mouse brain. *Neuroimage* 91, 12–20. doi: 10.1016/j.neuroimage.2014.01.014

Zhang, H., Schneider, T., Wheeler-Kingshott, C. A., and Alexander, D. C. (2012). NODDI: practical in vivo neurite orientation dispersion and density imaging of the human brain. *Neuroimage* 61, 1000–1016. doi: 10.1016/j.neuroimage.2012.03.072

Conflict of Interest Statement: The authors declare that the research was conducted in the absence of any commercial or financial relationships that could be construed as a potential conflict of interest.

Received: 27 October 2014; accepted: 22 December 2014; published online: 21 January 2015.

Citation: Dudink J, Pieterman K, Leemans A, Kleinnijenhuis M, van Cappellen van Walsum AM and Hoebeek FE (2015) Recent advancements in diffusion MRI for investigating cortical development after preterm birth—potential and pitfalls. Front. Hum. Neurosci. ***8****:1066. doi: 10.3389/fnhum.2014.01066*

This article was submitted to the journal Frontiers in Human Neuroscience.

frontiers in Human Neuroscience

MINI REVIEW
published: 26 March 2015
doi: 10.3389/fnhum.2015.00159

The first 1000 days of the autistic brain: a systematic review of diffusion imaging studies

Eugenia Conti[1,2], *Sara Calderoni*[1], *Viviana Marchi*[1,2], *Filippo Muratori*[1,2], *Giovanni Cioni*[1,2] *and Andrea Guzzetta*[1,2]*

[1] Department of Developmental Neuroscience, Stella Maris Scientific Institute, IRCCS Stella Maris Foundation, Pisa, Italy,
[2] Department of Clinical and Experimental Medicine, University of Pisa, Pisa, Italy

There is overwhelming evidence that autism spectrum disorder (ASD) is related to altered brain connectivity. While these alterations are starting to be well characterized in subjects where the clinical picture is fully expressed, less is known on their earlier developmental course. In the present study we systematically reviewed current knowledge on structural connectivity in ASD infants and toddlers. We searched PubMed and Medline databases for all English language papers, published from year 2000, exploring structural connectivity in populations of infants and toddlers whose mean age was below 30 months. Of the 264 papers extracted, four were found to be eligible and were reviewed. Three of the four selected studies reported higher fractional anisotropy values in subjects with ASD compared to controls within commissural fibers, projections fibers, and association fibers, suggesting brain hyper-connectivity in the earliest phases of the disorder. Similar conclusions emerged from the other diffusion parameters assessed. These findings are reversed to what is generally found in studies exploring older patient groups and suggest a developmental course characterized by a shift toward hypo-connectivity starting at a time between two and four years of age.

Keywords: autism, diffusion MRI, structural connectivity, toddlers, hyperconnectivity, neurodevelopment

OPEN ACCESS

Edited by:
Silvia Comani, Università degli Studi "G. d'Annunzio", Italy

Reviewed by:
Jürgen Hänggi, University of Zurich, Switzerland
Jeroen Dudink, Erasmus MC-Sophia, Netherlands

***Correspondence:**
Andrea Guzzetta, SMILE Laboratory, Department of Developmental Neuroscience, Stella Maris Scientific Institute, IRCCS Stella Maris Foundation, Viale del Tirreno 331, Calambrone 56128, Pisa, Italy; Department of Clinical and Experimental Medicine, University of Pisa, Via Savi, 10-56126 Pisa, Italy
aguzzetta@fsm.unipi.it

Received: *15 December 2014*
Accepted: *07 March 2015*
Published: *26 March 2015*

Citation:
Conti E, Calderoni S, Marchi V, Muratori F, Cioni G and Guzzetta A (2015) The first 1000 days of the autistic brain: a systematic review of diffusion imaging studies. Front. Hum. Neurosci. 9:159. doi: 10.3389/fnhum.2015.00159

Introduction

Autism spectrum disorders (ASD) are a heterogeneous group of neurodevelopmental diseases affecting 1 in 68 children in the USA (Centers for Disease Control and Prevention [CDC], 2014), characterized by impairment in socio-communicative abilities, as well as restricted and stereotyped behaviors (American Psychiatric Association, 2013). The age at which clinical diagnosis is generally made ranges between 3 and 4 years, although converging evidence from both retrospective and prospective studies suggests that symptoms of ASD usually emerge in the first 2 years of life (Zwaigenbaum et al., 2013; Chawarska et al., 2014). This might suggest the diagnosis of ASD to be difficult within the first 1000 days, even if the symptoms emerge earlier, supporting the need for reliable early biological markers of the disorder.

An overwhelming number of studies have been performed in the last decade addressing the possible brain abnormalities associated with ASD. Increasing evidence suggests that in the phase when symptoms of ASD are fully expressed, i.e., in school-aged children or older, their neurobiological underpinnings consist of a disruption in structural and functional connectivity

Abbreviations: ASD, autism spectrum disorders; FA, fractional anisotropy; HD-EEG, high-density electroencephalography; HR, high risk; MD, mean diffusivity.

(reviewed in Vissers et al., 2012). Although the results are highly heterogeneous, both in terms of techniques used and clinical characteristics of the samples, a strong consensus now exists on the presence of an overall hypo-connectivity of long-range connecting tracts as a robust biological hallmark of the disease (Just et al., 2012; Aoki et al., 2013).

While the neurobiological underpinnings of ASD at a time when the clinical picture is well expressed are starting to be understood, much less is known on the preceding developmental course. This certainly reflects the course of symptoms, as the diagnosis is usually not considered stable before 30 months and infants diagnosed as being in the spectrum earlier are not rarely found to have grown out of the diagnosis later on (Turner et al., 2006). Precocious neuroanatomical correlates of ASD have been firstly detected by structural MRI studies reporting an increased brain volume (Sparks et al., 2002; Hazlett et al., 2005; Courchesne et al., 2011), stemming from both gray and white matter increase (Xiao et al., 2014), particularly in frontal and temporal regions (Schumann et al., 2010; Calderoni et al., 2012), or from an elevated extra-axial (extra-parenchymal) accumulation of cerebrospinal fluid (Shen et al., 2013). Furthermore, early anomalies of cortical development in key brain areas of ASD patients were also suggested by altered cortical thickness in superior/inferior frontal gyrus and superior temporal sulcus (Raznahan et al., 2013), or within central, intraparietal, and frontal medial sulci through sulcal shape analyses (Auzias et al., 2014).

Morphological anomalies described in ASD infants have been proposed as a correlate of the atypical organization of brain connectivity (Zhang and Sejnowski, 2000; Lewis and Elman, 2008). Indeed, the first years of postnatal life represent a crucial time period of brain development characterized in typical development by both axonal pruning and synaptogenesis to build up and strengthen cortical networks. Prospective studies in high-risk infants, recruiting newborns siblings of ASD children, have been recently set-up in several centers, often encompassing neuro-structural and neuro-functional measures of brain development and supporting the concept of ASD as a disorder of connectivity emerging during the first months of life (Bosl et al., 2011; Wolff et al., 2012).

A fuller understanding of the neurobiological transformations of the first 30 months of life, i.e., the first 1000 days, in children who will develop ASD is of utmost importance in order to support early clinical diagnosis and to allow for a prompt start of early behavioral interventions. In this paper, we aim to review current knowledge on the anomalies of brain structural connectivity in subjects with ASD in the first 30 months of life, age before which the diagnosis is still considered unstable (Landa, 2008). We in particular collected all studies focused on infants and toddlers with ASD exploring diffusion MRI and/or tractography.

Methods

To review the literature, we queried PubMed and Medline using the following search terms: (ASD OR Autism OR 'ASD*' OR Asperger) AND (Infant* OR Toddler*) AND ('Structural connectivity' OR MRI OR DTI OR 'diffusion imaging' OR tractography). Criteria for inclusion in the study were established prior to the literature search. Inclusion was limited to papers published between January, 2000 and February, 2015, and was restricted to peer-reviewed English language articles. Reviews were not included in the selection, but were used to collect original studies. We screened all the selected papers in order to include studies in which mean age of the ASD sample was below 30 months. Studies focussing only on ASD subjects with known etiology (e.g., Fragile-X syndrome, tuberous sclerosis) were not included.

After duplicates removal, the search strategy yielded a total of 264 records. All abstracts were independently reviewed by three of the authors (EC, SC, and VM) and conflicting judgements were solved by consensus. During the review process 223 papers were excluded based on clear failure to meet the inclusion criteria. Forty-one papers were evaluated in full-text, of which 18 were review papers. Of the remaining 23, only four met the inclusion criteria and were included in this review (Ben Bashat et al., 2007; Wolff et al., 2012; Lewis et al., 2014; Xiao et al., 2014). All four were case-control studies, and only one of them was longitudinal (Wolff et al., 2012). Information on sample demographics, MRI characteristics and study design are reported in **Table 1**.

Mean age of the ASD group across the studies varied between 6 and 29 months. In particular Wolff et al. (2012) assessed a longitudinal cohort of high-risk subjects (ASD siblings) at 6, 12, and 24 months. Subjects were grouped retrospectively, according to the diagnosis at 2 years, into high-risk positive (HR+; siblings who obtained scores over ASD cut off at ADOS (Lord et al., 2000) evaluation) and high-risk negative (HR–; siblings who obtained scores below ASD cut off at ADOS evaluation; **Table 1**). In the remaining three studies (Ben Bashat et al., 2007; Lewis et al., 2014; Xiao et al., 2014), the ASD populations were more homogeneous with mean age ranging from 24 to 29 months. Lewis et al. (2014) analyzed a population of ASD siblings with small age range (24.5 months $\pm$ 0.73). They compared HR+ and HR− with subjects with typical development. Xiao et al. (2014) compared ASD subjects (29.92 months $\pm$ 5.54) with age-matched toddlers with developmental delay (DD). Lastly, Ben Bashat et al. (2007) analyzed ASD and typically developing subjects; while the ASD sample was entirely composed of toddlers (29 months $\pm$ 7), typical subjects encompassed a wider age range, i.e., 4 months–23 years.

MRI methodology used in the studies was heterogeneous. Ben Bashat et al. (2007) were the only to use a 1.5T MRI scanner with diffusion at six directions and a *b*-value of 6000. The remaining three studies utilized a 3T MRI scanner, and diffusion acquisition was based on either 25 (Wolff et al., 2012; Lewis et al., 2014) or 30 directions (Xiao et al., 2014) with a *b*-value of 1000. Post-processing analyses were similarly, heterogeneous. Lewis et al. (2014) used a novel approach based on the assessment of network efficiency. By using diffusion data the authors obtained measures of the length and strength of connections between anatomical regions and thus calculated efficiency of sets of connections (networks), rather than considering each connection independently, obtaining measures of local and global nodal efficiency. The remaining three papers used more conventional approaches FA, MD, and

TABLE 1 | Study characteristics.

Study (Design)	Groups (Mean in months ± SD)	Methods	Diffusion indexes	↑FA in ASD ($p < 0.05$)	↓FA in ASD ($p < 0.05$)	Other diffusion indexes $p < 0.05$
Ben Bashat et al. (2007) (Case control)	ASD: $n = 7$ (29 ± 7) TD: $n = 41$ (38 ± 13)	DTI Whole-brain ROI analysis	FA Probability Displacement	CC (genu and splenium); left PLIC; left external capsule; left forceps minor; left CST	n/a	↑ **Probability in ASD:** bilateral forceps minor; left external capsule; left PLIC; blateral ALIC; bilateral CST ↓ **Displacement in ASD:** blateral forceps minor; left external capsule; left PLIC; blateral ALIC; left CST
Wolff et al. (2012) (Longitudinal)	**6 months** HR+: $n = 28$ (6.8 ± 0.8) HR–: $n = 64$ (6.7 ± 0.8) **12 months** HR+: $n = 17$ (12.7 ± 0.7) HR–: $n = 49$ (12.7 ± 0.6) **24 months** HR+: $n = 17$ (24.5 ± 0.6) HR–: $n = 33$ (24.7 ± 0.8)	DTI ROI analysis	FA AD RD	↑**FA in HR+ (6 months):** CC (body); left Fornix; left ILF; bilateral PLIC; left UF	↓**FA in HR+ (24 months):** left ALIC; left anterior thalamic radiation	No significant differences in AD and RD
Xiao et al. (2014) (Case control)	ASD: $n = 50$ (29.9 ± 5.54) DD: $n = 28$ (28.2 ± 4.4)	DTI VB analysis	FA MD	↑**FA in ASD:** CC; posterior cingulate; limbic lobe	n/a	↓ **MD in ASD:** CC; posterior cingulate; left limbic lobe; left Insula
Lewis et al. (2014) (Case control)	HR+: $n = 31$ (24.5 ± 0.7) HR–: $n = 82$ (24.7 ± 0.9) LR: $n = 23$ (24.5 ± 0.6)	DTI Whole-brain Network analysis	Local and Global Efficiency			↑ **Local efficiency in ASD:** bilateral T and O lobes (inferior and medial regions), and predominately in the RH for lateral regions, extending to the supramarginal gyrus; the left T and O lobes, extending into the precuneus, and in several posterior regions in the RH ↓ **Global efficiency in ASD:** bilateral T and O lobes, extending in the RH to the angular and supramarginal gyri. The left pars triangularis and medial orbital gyrus; bilateral T lobes, extending in the left hemisphere to the O cortex, and in the RH to the angular and supramarginal gyri

AD, axial diffusivity; ALIC, anterior limb of internal capsule; CC, corpus callosum; CST, cortico-spinal tract; DD, developmental delay; FA, fractional anisotropy; HR–, high-risk subjects, negative; HR+, high risk subjects, positive; ILF, inferior longitudinal fasciculus; LR, low risk subjects; MD, mean diffusivity; O, occipital; PLIC, posterior limb of internal capsule; RD, radial diffusivity; RH, right hemisphere; T, temporal; TD, typical developing group; UF, uncinate fasciculus.

probability and displacement diffusion indexes, with two studies using a ROI-based analysis (Ben Bashat et al., 2007; Wolff et al., 2012) and one using a voxel-based analysis (Xiao et al., 2014).

Results

Findings are reported as grouped in (i) FA, which is currently the most common index explored in diffusion studies, and (ii) all other diffusion indexes.

Fractional Anisotropy

Three of the four studies measured FA values. Findings are discussed according to the identified connections as grouped into commissural fibers, projection fibers, (thalamocortical, corticofugal, and cerebellar), and association fibers (long and short range) (Catani et al., 2012). As FA is widely explored in most diffusion studies, in order to put our results into a developmental perspective, we compared the three selected studies with those exploring structural connectivity in older subjects, and in particular in ASD groups were the mean age was between 30 and 60 months (**Figure 1**).

Commissural fibers (corpus callosum, anterior commissure, posterior commissure, forceps major, and minor). In three (Ben Bashat et al., 2007; Wolff et al., 2012; Xiao et al., 2014) of the four selected papers commissural fibers were explored. In all cases, significantly higher FA values were found in infants and toddlers with ASD as opposed to control subjects. In particular, Xiao et al. (2014) showed higher FA values in the splenium of the corpus callosum, while Ben Bashat et al. (2007) also in the genu, and in the left forceps minor. Wolff et al. (2012) reported significant differences within the body of corpus callosum at 6 months of age, which were not observed at 12 and 24 months. The comparison with studies exploring older subjects (mean age 30–60 months), showed similar findings in an ASD group with mean age of around 38 months, with higher FA values in the ASD group in the genu and the body of the corpus callosum (Weinstein et al., 2011),

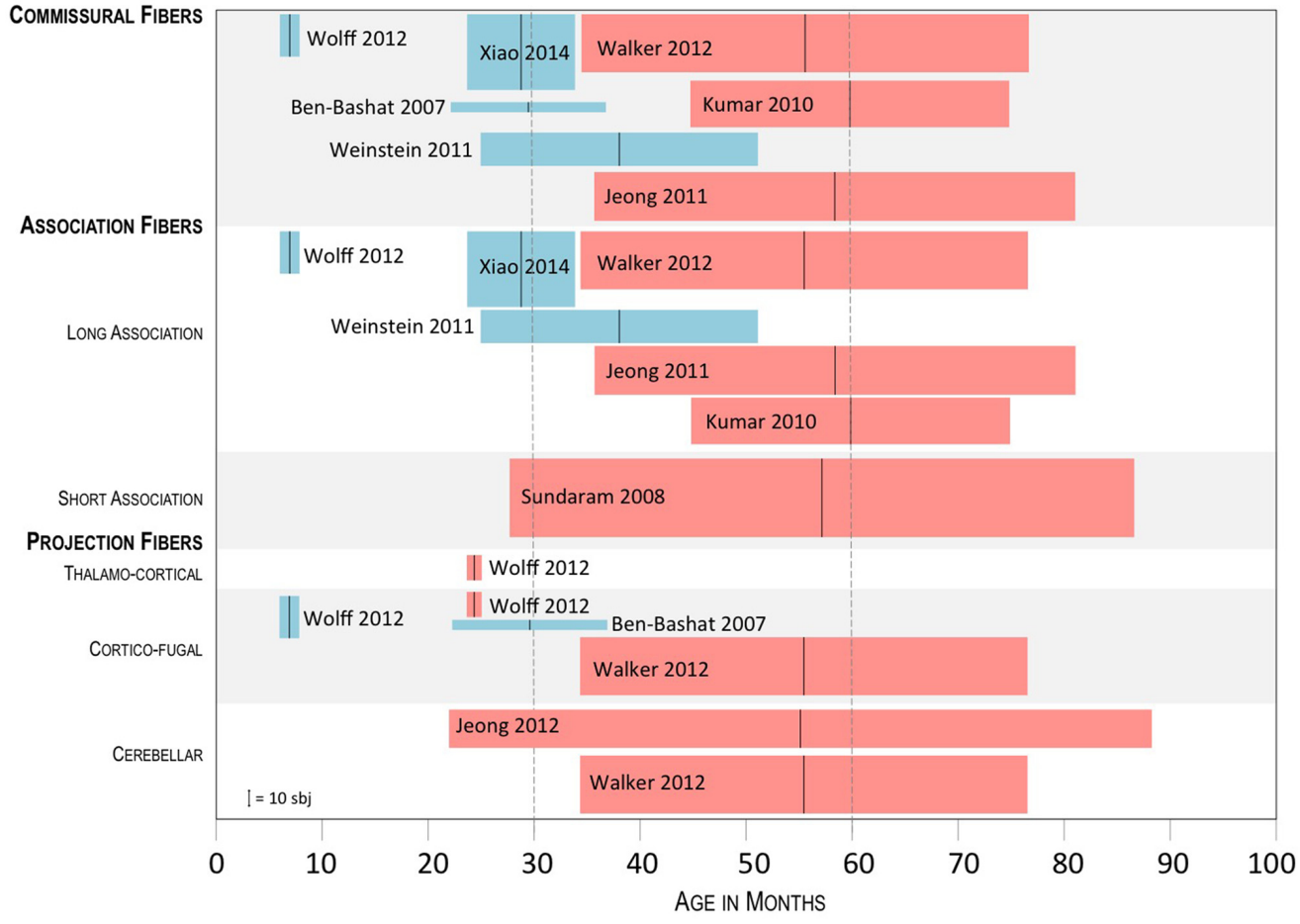

FIGURE 1 | Summary of the results of studies exploring FA in ASD subject groups whose mean age was below 60 months. Tracts showing a significant difference between ASD and controls are shown, with blue boxes indicating higher FA in ASD and red boxes indicating lower FA in ASD. The black vertical bar in the middle of the boxplots shows the mean age of the ASD group; the lateral sides of the boxplots, show the SD; height of the boxplots represents the sample size, as referred to in the lower left corner.

and reverse results in three further studies exploring groups of subjects with mean age between 56 and 60 months, with lower FA values in the ASD group in all parts of the corpus callosum (Kumar et al., 2010; Jeong et al., 2011; Walker et al., 2012).

Association fibers (long: arcuate fasciculus, cingulum, uncinate fasciculus, inferior fronto-occipital fasciculus, fornix; short: U-shape fibers). In two of the four selected papers association fibers were explored (Wolff et al., 2012; Xiao et al., 2014). Again, in both cases, significantly higher FA values were found in infants and toddlers with ASD as opposed to control subjects. In particular, Xiao et al. (2014) found higher FA values in the cingulum and the limbic lobe, while Wolff et al. (2012), found higher FA values in the left fornix and uncinate fasciculus at 6 months, which were not observed later, at 12 and 24 months. The comparison with studies exploring older subjects, showed higher FA values in ASD subjects with mean age of 38 months (Weinstein et al., 2011), in particular within the left superior longitudinal and arcuate fasciculus. In other four studies, focussed on children ranging from 56 to 60 months, lower FA values were reported in the superior temporal gyrus (Walker et al., 2012), uncinate fasciculus and arcuate fasciculus (Kumar et al., 2010; Jeong et al., 2011), inferior-frontal-occipital fasciculus, superior longitudinal fasciculus, and cingulum (Kumar et al., 2010), and short intra-lobar frontal fibers (Sundaram et al., 2008).

Projection fibers (internal capsule; external capsule; cerebellar tracts; corona radiata corticofugal fibers, thalamocortical fibers). In two of the four selected papers projection fibers were explored (Ben Bashat et al., 2007; Wolff et al., 2012). In both cases, significantly higher FA values were found in infants and toddlers with ASD as opposed to control subjects, except for Wolff et al. (2012) who reported increased FA values at 6 months of age within the right posterior limb of internal capsule and interestingly decreased FA values within the left anterior thalamic radiation at 24 months. Ben Bashat et al. (2007) reported increased FA values in left posterior limb of internal capsule, in left external capsule and in left cortico-spinal tract. Studies exploring older subjects found lower FA values in ASD subjects in cortico-spinal tract, pons, and posterior limb of internal capsule (Walker et al., 2012). Significant differences in the cerebellar tracts were only found in two studies assessing children with mean age between 30 and 60 months. Interestingly, they both found lower FA values in ASD subjects within the cerebellum (Walker et al., 2012) and the dento-rubrothalamic projection (Jeong et al., 2012).

Other Diffusion Indexes

Three of the four papers explored diffusion indexes different from FA. The most innovative approach was the one by Lewis et al. (2014) who explored network efficiency between nodes, either local or global. They found decreased local and global efficiency over temporal, parietal, and occipital lobes in high-risk infants later classified as ASD, as compared to both low- and high-risk infants not classified as ASD. The frontal lobes showed only a reduction in global efficiency in Broca's area. The reductions in nodal local and nodal global efficiency in ASD infants were interpreted not simply as indexes of hypo-connectivity, but rather as the result of more limited local connectivity and less direct connections to other brain regions. Ben Bashat et al. (2007) calculated probability and displacement values using q-space analysis for the diffusion data set, according to their own previous papers, claiming them as better indicators of white matter pathology than conventional FA (Assaf et al., 2002; Ben Bashat et al., 2005). Hyper-connectivity, reflected in significantly increased probability along with reduced displacement values, was detected in several brain regions. In particular, significant increase in probability values (and decrease in displacement values) were reported in the left forceps minor, left external capsule, left posterior limb of the internal capsule and bilaterally in the anterior limb of the internal capsule and cortico-spinal tract. Finally, Xiao et al. (2014) calculated MD values in ASD toddlers showing a reduction in the same regions where FA was increased, including the corpus callosum, cingulum, and limbic lobe. Overall, these results support evidence of hyper-connectivity in infants and toddlers with autism and are in contrast with the decreased, restricted diffusion reported in previous studies in older children and adolescents.

Discussion

Evidence from the reviewed studies suggests that white matter atypical diffusion properties are a consistent finding in the early phases of ASD, and can precede the full-blown expression of the clinical picture. All three studies exploring brain FA, the most commonly investigated diffusion measure (Basser and Pierpaoli, 1996), extensively reported higher values in ASD subjects compared to controls. Along the same lines, the majority of the other diffusion measures explored, including MD, probability, and displacement values, points toward an increased directional restriction of water diffusion in several brain tracts. Interestingly, these findings are opposite to what reported in an overwhelming body of literature showing a widespread reduction of FA and increase in MD in children, adolescents and young adults with ASD (Aoki et al., 2013).

While these latter reports have been considered by most as supporting the underconnectivity theory of ASD, firstly formulated from functional MRI studies (Just et al., 2004), recent studies have underlined the importance of not over-interpreting diffusion data as direct indices of structural connectivity, particularly in consideration of the methodological limits expressed by diffusion tensor imaging (Jones et al., 2013; Castellanos et al., 2014). Indeed, the significance of diffusion indices as to brain connectivity is increasingly matter of debate, and it is strongly encouraged that more advanced approaches, such as the HARDI (high angular resolution diffusion imaging), are applied in order to minimize the limitations of DTI, including a better resolution of crossing and kissing fibers (Bloy et al., 2012).

The relationship between structural and functional connectivity is not fully understood in subjects with ASD, and particularly so in infants and toddlers, since no study to date has specifically addressed this issue (Uddin et al., 2013). Initially, based on fMRI studies, local regions of hyper-connectivity described in high functioning ASD subjects were interpreted as

related to islands of preserved capacities (Wass, 2011). More recently, however, functional hyper-connectivity has been interpreted as reflecting diffuse and less specialized, rather than more efficient, brain networks in older subjects (Just et al., 2012).

The few functional connectivity studies performed in infants and toddlers with ASD do not clarify this issue. In the only EEG study assessing connectivity in infants with ASD, Orekhova et al. (2014) demonstrated elevated alpha range connectivity, particularly in frontal and central areas, by applying High Density-EEG in high-risk infants aged around 14 months (range 12–17), who were later diagnosed with ASD. Conversely, in older ASD patients aged around 29 months (range 12–46), Dinstein et al. (2011) reported significant weaker functional connectivity in putative language areas, as assessed by sleep fMRI inter-hemispheric synchronization.

Irrespective of its connotations, the issue remains about the time of development at which, as compared to control subjects, white matter properties begin to shift from increased FA to decreased FA. Overall, studies in this review suggest a time between 2 and 4 years of age as the phase when this shift is most likely starting to occur. The first structures showing an inversion of FA distribution are the thalamocortical projections, which were found to have significantly lower FA values in ASD toddlers already at 24 months of age (Wolff et al., 2012). Around the same age, a decreased local and global efficiency over temporal, parietal and occipital lobes in ASD toddlers was found and interpreted as the result of connectivity disruption (Lewis et al., 2014). A more widespread shift of FA, involving in particular commissural and long-association fibers, is likely to occur at a slightly older age, as shown by the global persistence of increased FA in study cohorts with mean age up to 38 months (Ben Bashat et al., 2007; Weinstein et al., 2011; Xiao et al., 2014). In most papers assessing populations of older children, starting from those with mean age of around 5 years, higher FA is generally not found, with few exceptions. One of them is the report by Billeci et al. (2012) who found a widespread FA increase in the white matter of ASD young children aged around 5.5 years, particularly at the level of corpus callosum, cingulum, internal capsule, and arcuate fasciculus. In their study, however, the regression analysis of FA vs. age showed that FA increase was mainly attributable to the subgroup of younger patients, with the older ones indeed showing an FA reduction.

While interpreting the findings of the papers included in this review, the heterogeneity in the quality of the studies needs to be mentioned. For instance, number of diffusion directions used ranged from 6 in one study to 25 or 30 in the other three. Also, movement artifacts are likely to have affected differentially the findings, as only two of the four studies (Ben Bashat et al., 2007; Xiao et al., 2014) used sedation during scanning, which is known to significantly reduce motion artifacts as compared to natural sleep scanning. Given the low number of studies collected, however, it would be hard to properly ponder the contribution of the methodological differences among the studies as to the interpretation of the findings.

Overall, the results of this review describe a developmental trajectory of white matter diffusion properties in ASD infants compatible with the early signs of enlarged head circumference and macrocephaly extensively reported in the literature (Courchesne et al., 2011). Converging evidence from head-circumference, neuroimaging, and post-mortem studies supports the view that the brains of ASD individuals are larger than controls from at least 2 years of age, particularly at the level of the frontal and temporal lobes (Courchesne et al., 2011; Muratori et al., 2012). This finding tends to disappear within the preschool age and eventually results in significant undergrowth during adolescence. This trajectory greatly parallels the developmental course in diffusion indices emerging from this review and is compatible with the proposed interpretation of early overgrowth as an epiphenomenon of abnormal connectivity resulting from a lack of physiological synaptic pruning (Frith, 2003).

Despite the growing interest in the literature in understanding the neuro-structural underpinnings of ASD at the onset of clinical symptoms, or before, available data are still not exhaustive. To date, studies are still scarce and are highly heterogeneous in terms of sample size, control groups and MRI analysis. A possible strategy to face this limitation would be the partaking of large, longitudinal ASD data repositories within the scientific community, which would provide priceless information about the early neurostructural markers of the disorder. The increasing application of this and other methodological strategies, including the use of higher-order diffusion imaging such as HARDI, is likely to rapidly and exponentially widen in the near future our knowledge on the developmental trajectory of early brain connectivity in ASD.

Acknowledgment

SC was partially supported by the Italian Ministry of Health and Tuscany Region with the grant 'GR-2010-2317873.'

References

American Psychiatric Association. (2013). *Diagnostic and Statistical Manual of Mental Disorders*, 5th Edn. Arlington, VA: American Psychiatric Publishing. doi: 10.1176/appi.books.9780890425596

Aoki, Y., Abe, O., Nippashi, Y., and Yamasue, H. (2013). Comparison of white matter integrity between autism spectrum disorder subjects and typically developing individuals: a meta-analysis of diffusion tensor imaging tractography studies. *Mol. Autism* 4, 25. doi: 10.1186/2040-2392-4-25

Assaf, Y., Ben-Bashat, D., Chapman, J., Peled, S., Biton, I. E., Kafri, M., et al. (2002). High b-value q-space analyzed diffusion-weighted MRI: application to multiple sclerosis. *Magn. Reson. Med.* 47, 115–126. doi: 10.1002/mrm.10040

Auzias, G., Viellard, M., Takerkart, S., Villeneuve, N., Poinso, F., Fonseca, D. D., et al. (2014). Atypical sulcal anatomy in young children with autism spectrum disorder. *Neuroimage Clin.* 4, 593–603. doi: 10.1016/j.nicl.2014.03.008

Basser, P. J., and Pierpaoli, C. (1996). Microstructural and physiological features of tissues elucidated by quantitative-diffusion-tensor MRI. *J. Magn. Reson. B* 111, 209–219. doi: 10.1006/jmrb.1996.0086

Ben Bashat, D., Ben Sira, L., Graif, M., Pianka, P., Hendler, T., Cohen, Y., et al. (2005). Normal white matter development from infancy to adulthood: comparing diffusion tensor and high b value diffusion weighted MR images. *J. Magn. Reson. Imaging* 21, 503–511. doi: 10.1002/jmri.20281

Ben Bashat, D., Kronfeld-Duenias, V., Zachor, D. A., Ekstein, P. M., Hendler, T., Tarrasch, R., et al. (2007). Accelerated maturation of white matter in young

children with autism: a high b value DWI study. *Neuroimage* 37, 40–47. doi: 10.1016/j.neuroimage.2007.04.060

Billeci, L., Calderoni, S., Tosetti, M., Catani, M., and Muratori, F. (2012). White matter connectivity in children with autism spectrum disorders: a tract-based spatial statistics study. *BMC Neurol.* 12:148. doi: 10.1186/1471-2377-12-148

Bloy, L., Ingalhalikar, M., Batmanghelich, N. K., Schultz, R. T., Roberts, T. P., and Verma, R. (2012). An integrated framework for high angular resolution diffusion imaging-based investigation of structural connectivity. *Brain Connect.* 2, 69–79. doi: 10.1089/brain.2011.0070

Bosl, W., Tierney, A., Tager-Flusberg, H., and Nelson, C. (2011). EEG complexity as a biomarker for autism spectrum disorder risk. *BMC Med.* 9:18. doi: 10.1186/1741-7015-9-18

Calderoni, S., Retico, A., Biagi, L., Tancredi, R., Muratori, F., and Tosetti, M. (2012). Female children with autism spectrum disorder: an insight from mass-univariate and pattern classification analyses. *Neuroimage* 59, 1013–1022. doi: 10.1016/j.neuroimage.2011.08.070

Castellanos, F. X., Cortese, S., and Proal, E. (2014). Connectivity. *Curr. Top. Behav. Neurosci.* 16, 49–77. doi: 10.1007/978-3-662-45758-0_244

Catani, M., Dell'acqua, F., Bizzi, A., Forkel, S. J., Williams, S. C., Simmons, A., et al. (2012). Beyond cortical localization in clinico-anatomical correlation. *Cortex* 48, 1262–1287. doi: 10.1016/j.cortex.2012.07.001

Centers for Disease Control and Prevention [CDC]. (2014). Prevalence of autism spectrum disorder among children aged 8 years — autism and developmental disabilities monitoring network, 11 Sites, United States, 2010. *Surveill Summ.* 63, 1–21.

Chawarska, K., Shic, F., Macari, S., Campbell, D. J., Brian, J., Landa, R., et al. (2014). 18-month predictors of later outcomes in younger siblings of children with autism spectrum disorder: a baby siblings research consortium study. *J. Am. Acad. Child Adolesc. Psychiatry* 53, 1317–1327. doi: 10.1016/j.jaac.2014.09.015

Courchesne, E., Campbell, K., and Solso, S. (2011). Brain growth across the life span in autism: age-specific changes in anatomical pathology. *Brain Res.* 1380, 138–145. doi: 10.1016/j.brainres.2010.09.101

Dinstein, I., Pierce, K., Eyler, L., Solso, S., Malach, R., Behrmann, M., et al. (2011). Disrupted neural synchronization in toddlers with autism. *Neuron* 70, 1218–1225. doi: 10.1016/j.neuron.2011.04.018

Frith, C. (2003). What do imaging studies tell us about the neural basis of autism? *Novartis Found. Symp.* 251, 149–166. doi: 10.1002/0470869380.ch10

Hazlett, H. C., Poe, M., Gerig, G., Smith, R. G., Provenzale, J., Ross, A., et al. (2005). Magnetic resonance imaging and head circumference study of brain size in autism: birth through age 2 years. *Arch. Gen. Psychiatry* 62, 1366–1376. doi: 10.1001/archpsyc.62.12.1366

Jeong, J. W., Chugani, D. C., Behen, M. E., Tiwari, V. N., and Chugani, H. T. (2012). Altered white matter structure of the dentatorubrothalamic pathway in children with autistic spectrum disorders. *Cerebellum* 11, 957–971. doi: 10.1007/s12311-012-0369-3

Jeong, J. W., Kumar, A. K., Sundaram, S. K., Chugani, H. T., and Chugani, D. C. (2011). Sharp curvature of frontal lobe white matter pathways in children with autism spectrum disorders: tract-based morphometry analysis. *AJNR Am. J. Neuroradiol.* 32, 1600–1606. doi: 10.3174/ajnr.A2557

Jones, D. K., Knosche, T. R., and Turner, R. (2013). White matter integrity, fiber count, and other fallacies: the do's and don'ts of diffusion MRI. *Neuroimage* 73, 239–254. doi: 10.1016/j.neuroimage.2012.06.081

Just, M. A., Cherkassky, V. L., Keller, T. A., and Minshew, N. J. (2004). Cortical activation and synchronization during sentence comprehension in high-functioning autism: evidence of underconnectivity. *Brain* 127, 1811–1821. doi: 10.1093/brain/awh199

Just, M. A., Keller, T. A., Malave, V. L., Kana, R. K., and Varma, S. (2012). Autism as a neural systems disorder: a theory of frontal-posterior underconnectivity. *Neurosci. Biobehav. Rev.* 36, 1292–1313. doi: 10.1016/j.neubiorev.2012.02.007

Kumar, A., Sundaram, S. K., Sivaswamy, L., Behen, M. E., Makki, M. I., Ager, J., et al. (2010). Alterations in frontal lobe tracts and corpus callosum in young children with autism spectrum disorder. *Cereb. Cortex* 20, 2103–2113. doi: 10.1093/cercor/bhp278

Landa, R. J. (2008). Diagnosis of autism spectrum disorders in the first 3 years of life. *Nat. Clin. Pract. Neurol.* 4, 138–147. doi: 10.1038/ncpneuro0731

Lewis, J. D., and Elman, J. L. (2008). Growth-related neural reorganization and the autism phenotype: a test of the hypothesis that altered brain growth leads to altered connectivity. *Dev. Sci.* 11, 135–155. doi: 10.1111/j.1467-7687.2007.00634.x

Lewis, J. D., Evans, A. C., Pruett, J. R., Botteron, K., Zwaigenbaum, L., Estes, A., et al. (2014). Network inefficiencies in autism spectrum disorder at 24 months. *Transl. Psychiatry* 4:e388. doi: 10.1038/tp.2014.24

Lord, C., Risi, S., Lambrecht, L., Cook, E. H. Jr., Leventhal, B. L., DiLavore, P. C., et al. (2000). The autism diagnostic observation schedule-generic: a standard measure of social and communication deficits associated with the spectrum of autism. *J. Autism Dev. Disord.* 30, 205–223. doi: 10.1023/A:1005592401947

Muratori, F., Calderoni, S., Apicella, F., Filippi, T., Santocchi, E., Calugi, S., et al. (2012). Tracing back to the onset of abnormal head circumference growth in Italian children with autism spectrum disorder. *Res. Autism Spectr. Disord.* 6, 442–449. doi: 10.1016/j.rasd.2011.07.004

Orekhova, E. V., Elsabbagh, M., Jones, E. J., Dawson, G., Charman, T., Johnson, M. H., et al. (2014). EEG hyper-connectivity in high-risk infants is associated with later autism. *J. Neurodev. Disord.* 6:40. doi: 10.1186/1866-1955-6-40

Raznahan, A., Wallace, G. L., Antezana, L., Greenstein, D., Lenroot, R., Thurm, A., et al. (2013). Compared to what? Early brain overgrowth in autism and the perils of population norms. *Biol. Psychiatry* 74, 563–575. doi: 10.1016/j.biopsych.2013.03.022

Schumann, C. M., Bloss, C. S., Barnes, C. C., Wideman, G. M., Carper, R. A., Akshoomoff, N., et al. (2010). Longitudinal magnetic resonance imaging study of cortical development through early childhood in autism. *J. Neurosci.* 30, 4419–4427. doi: 10.1523/JNEUROSCI.5714-09.2010

Shen, M. D., Nordahl, C. W., Young, G. S., Wootton-Gorges, S. L., Lee, A., Liston, S. E., et al. (2013). Early brain enlargement and elevated extra-axial fluid in infants who develop autism spectrum disorder. *Brain* 136, 2825–2835. doi: 10.1093/brain/awt166

Sparks, B. F., Friedman, S. D., Shaw, D. W., Aylward, E. H., Echelard, D., Artru, A. A., et al. (2002). Brain structural abnormalities in young children with autism spectrum disorder. *Neurology* 59, 184–192. doi: 10.1212/WNL.59.2.184

Sundaram, S. K., Kumar, A., Makki, M. I., Behen, M. E., Chugani, H. T., and Chugani, D. C. (2008). Diffusion tensor imaging of frontal lobe in autism spectrum disorder. *Cereb. Cortex* 18, 2659–2665. doi: 10.1093/cercor/bhn031

Turner, L. M., Stone, W. L., Pozdol, S. L., and Coonrod, E. E. (2006). Follow-up of children with autism spectrum disorders from age 2 to age 9. *Autism* 10, 243–265. doi: 10.1177/1362361306063296

Uddin, L. Q., Supekar, K., and Menon, V. (2013). Reconceptualizing functional brain connectivity in autism from a developmental perspective. *Front. Hum. Neurosci.* 7:458. doi: 10.3389/fnhum.2013.00458

Vissers, M. E., Cohen, M. X., and Geurts, H. M. (2012). Brain connectivity and high functioning autism: a promising path of research that needs refined models, methodological convergence, and stronger behavioral links. *Neurosci. Biobehav. Rev.* 36, 604–625. doi: 10.1016/j.neubiorev.2011.09.003

Walker, L., Gozzi, M., Lenroot, R., Thurm, A., Behseta, B., Swedo, S., et al. (2012). Diffusion tensor imaging in young children with autism: biological effects and potential confounds. *Biol. Psychiatry* 72, 1043–1051. doi: 10.1016/j.biopsych.2012.08.001

Wass, S. (2011). Distortions and disconnections: disrupted brain connectivity in autism. *Brain Cogn.* 75, 18–28. doi: 10.1016/j.bandc.2010.10.005

Weinstein, M., Ben-Sira, L., Levy, Y., Zachor, D. A., Ben Itzhak, E., Artzi, M., et al. (2011). Abnormal white matter integrity in young children with autism. *Hum. Brain Mapp.* 32, 534–543. doi: 10.1002/hbm.21042

Wolff, J. J., Gu, H., Gerig, G., Elison, J. T., Styner, M., Gouttard, S., et al. (2012). Differences in white matter fiber tract development present from 6 to 24 months in infants with autism. *Am. J. Psychiatry* 169, 589–600. doi: 10.1176/appi.ajp.2011.11091447

Xiao, Z., Qiu, T., Ke, X., Xiao, X., Xiao, T., Liang, F., et al. (2014). Autism spectrum disorder as early neurodevelopmental deisorder: evidence from the brain imaging abnormalities in 2-3 years old toddlers. *J. Autism Dev. Disord.* 44, 1633–1640. doi: 10.1007/s10803-014-2033-x

Zhang, K., and Sejnowski, T. J. (2000). A universal scaling law between gray matter and white matter of cerebral cortex. *Proc. Natl. Acad. Sci. U.S.A.* 97, 5621–5626. doi: 10.1073/pnas.090504197

Zwaigenbaum, L., Bryson, S., and Garon, N. (2013). Early identification of autism spectrum disorders. *Behav. Brain Res.* 251, 133–146. doi: 10.1016/j.bbr.2013.04.004

Conflict of Interest Statement: The authors declare that the research was conducted in the absence of any commercial or financial relationships that could be construed as a potential conflict of interest.

frontiers in
HUMAN NEUROSCIENCE

ORIGINAL RESEARCH ARTICLE
published: 17 February 2015
doi: 10.3389/fnhum.2015.00039

The intrahemispheric functional properties of the developing sensorimotor cortex are influenced by maturation

Marika Berchicci[1,2], Gabriella Tamburro[1,3] and Silvia Comani[1,4,5]*

[1] *BIND - Behavioral Imaging and Neural Dynamics Center, University "G. d'Annunzio" of Chieti-Pescara, Chieti, Italy*
[2] *Department of Movement, Human and Health Sciences, University of Rome "Foro Italico," Rome, Italy*
[3] *Department of Medicine and Aging Sciences, University "G. d'Annunzio" of Chieti-Pescara, Chieti, Italy*
[4] *Department of Neuroscience, Imaging and Clinical Sciences, University "G. d'Annunzio" of Chieti-Pescara, Chieti, Italy*
[5] *Casa di Cura Privata Villa Serena, Città Sant'Angelo, Italy*

Edited by:
Sophie Molholm, Albert Einstein College of Medicine, USA

Reviewed by:
Jin Fan, Queens College of The City University of New York and Icahn School of Medicine at Mount Sinai, USA
Julia Stephen, The Mind Research Network, USA
Urs Ribary, Simon Fraser University, Canada

***Correspondence:**
Silvia Comani, BIND - Behavioral Imaging and Neural Dynamics Center, Department of Neuroscience, Imaging and Clinical Sciences, University "G. d'Annunzio" of Chieti-Pescara, Via dei Vestini, 33, 66013 Chieti, Italy
e-mail: comani@unich.it

The investigation of the functional changes in the sensorimotor cortex has important clinical implications as deviations from normal development can anticipate developmental disorders. The functional properties of the sensorimotor cortex can be characterized through the rolandic mu rhythm, already present during infancy. However, how the sensorimotor network develops from early infancy to adulthood, and how sensorimotor processing contributes to the generation of perceptual-motor coupling remains largely unknown. Here, we analyzed magnetoencephalographic (MEG) data recorded in two groups of infants (11–24 and 26–47 weeks), two groups of children (24–34 and 36–60 months), and a control group of adults (20–39 years), during intermixed conditions of rest and prehension. The MEG sensor array was positioned over the sensorimotor cortex of the contralateral hemisphere. We characterized functional connectivity and topological properties of the sensorimotor network across ages and conditions through synchronization likelihood and segregation/integration measures in an individual mu rhythm frequency range. All functional measures remained almost unchanged during the first year of life, whereas they varied afterwards through childhood to reach adult values, demonstrating an increase of both segregation and integration properties. With age, the sensorimotor network evolved from a more random (infants) to a "small-world" organization (children and adults), more efficient both locally and globally. These findings are in line with prior studies on structural and functional brain development in infants, children and adults. We could not demonstrate any significant change in the functional properties of the sensorimotor cortex in the prehension condition with respect to rest. Our results support the view that, since early infancy, the functional properties of the developing sensorimotor cortex are modulated by maturation.

Keywords: sensorimotor cortex, functional organization, connectivity, synchronization likelihood, segregation, integration, rolandic mu rhythm

INTRODUCTION

In the cerebral cortex, functional domains such as visual, cognitive or sensorimotor control rely on the development of distinct and interconnected cortical and subcortical regions (Tau and Peterson, 2009). For instance, the transient loss of face orientation discrimination at 2 months of age may result from a conflict between subcortical and cortical pathways, also known as *transient functional deterioration* (Nakano and Nakatani, 2014). The subsequent recovery by 4–6 months of age can be interpreted as an establishment of coordination between the two systems. U-shaped changes in a given behavior have been observed in reaching (Butterworth, 1989) and cross-modal orientation (Taga et al., 2002). The developmental organization of these circuits is a complex process that begins at early gestational age (Kostovic et al., 1995) and continues until adulthood. The brain development begins with neuronal proliferation and proceeds with migration, apoptosis, synaptogenesis, pruning, myelination and cortical thinning (Giedd et al., 2009). These events are temporally overlapped and are genetically determined, epigenetically directed and environmentally influenced (Tau and Peterson, 2009) by sensorimotor and cognitive experiences.

Investigators working in the pediatric field have been particularly interested in the developmental properties of the mu rhythm, which reflects sensorimotor processing in the fronto-parietal network (Pineda, 2005). The adult mu rhythm, which falls within the alpha frequency range (8–13 Hz), is strongly

Abbreviations: SL_{MEAN}, mean synchronization likelihood; C, mean clustering coefficient; E_{loc}, local efficiency; L, characteristic path length; E_{glob}, global efficiency.

inhibited (i.e., desynchronized, suppressed) before and during the execution of a bodily movement (Cheyne et al., 2014), during the observation (Jarvelainen et al., 2004; Vogt et al., 2007) and the imagination (Grafton et al., 1996; Molnar-Szakacs et al., 2006) of a goal-directed action, and also during sensorimotor stimulation (Cheyne et al., 2003). The mu rhythm modulation is considered a neurophysiological measure of the mirror neuron system (MNS), which is a neuronal mechanism that matches perception and action, allowing goal-directed action understanding (Hari et al., 2000; Hummel et al., 2002; Muthukumaraswamy and Johnson, 2004; Depretto et al., 2006).

A growing body of literature indicates that action experience may also modulate the mu rhythm desynchronization (Calvo-Merino et al., 2006; van Elk et al., 2008; Cannon et al., 2013; Ruther et al., 2014). Recent work on the infant mu rhythm indicates that it is present in infancy (Stroganova et al., 1999; Marshall et al., 2002; Berchicci et al., 2011; Marshall and Meltzoff, 2011), although its peak activity occurs at lower frequency ranges as compared to older children and adults, as it occurs for other brain rhythms, such as the theta and delta rhythms (Orekhova et al., 2006; Cuevas et al., 2014). It has been observed that the infant mu rhythm desynchronizes during the execution of a goal-directed action as well as the observation of a previously learnt action, and that infants' self-experience has an influence on the expectations about others action. These findings support the notion that the action-perception coupling network appears early in life (Marshall and Meltzoff, 2014). However, no general agreement exists on the mechanisms leading to the onset of this network. One of the most popular views claims that perceptual-motor coupling is present at birth and is merely shaped by experience (Lepage and Theoret, 2007; Simpson et al., 2014). An alternative position suggests that sensorimotor experience plays a critical role in the generation of perceptual-motor coupling through general associative learning processes (Heyes, 2001; Cook et al., 2014). Support to this second view comes from studies (Southgate et al., 2009; de Klerk et al., 2014) where the authors showed how visual experience alone increased sensorimotor cortex engagement by activating the previously established visuomotor associations (Greenough et al., 1987; Stiles and Jernigan, 2010).

Indeed, the postnatal period represents a time of dramatic change in the brain structure and function. The brain grows to about 70% of its adult size by 1 year of age, to about 80% by age 2, and to 90% of its adult size between the age of 2 and 5 years, which is known as the "plateau" phase of development (Knickmeyer et al., 2008). With time, local connections within cortical circuits, especially in sensorimotor and visual cortices (Fransson et al., 2007), are fine-tuned, and long-range connections among circuits produce an increasingly unified and functionally organized neural network. Sets of regions that share temporally correlated activity are believed to represent and become functional networks (Damoiseaux et al., 2006), and some studies had provided advanced understanding of the functional architecture of the human brain during early development (Gao et al., 2009; Doria et al., 2010; Dosenbach et al., 2010).

Functional connectivity magnetic resonance imaging (fcMRI) has proved useful in newborn studies. Indeed, it offers insight into the earliest forms of cerebral connectivity in very young infants (Power et al., 2010; Smyser et al., 2011). Damaraju et al. (2014) recently characterized the development of intrinsic connectivity networks (ICNs) in infants aged between 4 and 9 months with resting state MRI (rsMRI) performed while sleeping without sedative medication. They observed that, with age, the connectivity strength decreased within local networks and increased between more distant networks. Other researchers (Gilmore et al., 2011) have shown that, from birth to 2 years of age, cortical thinning proceeds in a back to front direction and occurs first in the sensorimotor areas, followed by association areas and lastly by higher-order cortical areas, such as the prefrontal cortex and the posterior parietal cortex. Two types of age-related changes (from childhood to adulthood) in functional connectivity have been described so far: decreases in local connectivity among anatomically adjacent, but functionally distinct brain regions, because they are integrated in their own brain networks; increases in long-range connectivity among nodes that comprise each network (Fair et al., 2007; Kelly et al., 2009).

In contrast to the high spatial resolution but low temporal resolution of rsMRI and fcMRI, magnetoencephalography (MEG) and electroencephalography (EEG) enable the measurement of functional connectivity with high temporal resolution and medium level spatial resolution. Few studies (Ellingson, 1964; Vanhatalo and Kaile, 2006) have demonstrated the evolution of electro-cortical activity in the infant brain by means of EEG recording, with regional variability and increasingly synchronous activity between bilateral homologous regions. Event related potential (ERP) findings suggested that sensorimotor networks undergo rapid development during the first year of life (Bell and Fox, 1992; Lin et al., 2008). To estimate cortical functioning, Bell and Wolfe (2007) examined the developmental changes of electrical activity during a working memory task in infants and children by means of EEG power and coherence (a spectral measure of the functional coupling between neural generators), and observed similar changes in both measures: the widespread brain electrical activity typical in infancy (8 months of age) became more localized during early childhood (3 years of age). Righi et al. (2014) conducted a longitudinal study in infants at 6 and 12 months of age, and found that infants at risk of autism spectrum disorder had lower functional connectivity between frontal and parietal regions as indexed by linear coherence in gamma frequency band. Other very recent studies (Keehn et al., 2013; Imai et al., 2014) employed the near-infrared spectroscopy (NIRS) to look at the functional connectivity in term, pre-term, and Down syndrome infants, observing increased longer distance functional connectivity over the first year of life in normal developing infants as compared to pathological infants.

MEG was demonstrated to be a suitable method to investigate the function of the developing brain during infancy and childhood due to its non-invasive nature, its excellent temporal resolution and, with recent devices, also good spatial resolution. A technical and practical advantage of MEG systems in pediatric applications is that MEG signals are unaffected by the immature skull features such as fontanels, allowing for longitudinal neuro-developmental studies. In a recent study employing MEG recordings over the contra-lateral hemisphere during a prehension task and power spectrum analysis, Berchicci et al. (2011)

reported the presence of idling mu rhythm at rest and its suppression during prehension in infants (from 11 to 47 weeks of age) and pre-school children (from 2 to 5 years). In particular, they showed that mu rhythm peak frequency increases as a function of age (from 2.75 Hz at 11 weeks of age to 9.5 Hz at 3 years of age), and undergoes a rapid maturation during the first year of life. Based on the time-frequency analysis performed, the specific MEG signal waveform, and the position of the cluster of channels showing maximum mu rhythm desynchronization during prehension over the subject's head, Berchicci et al. (2011) also suggested a sensorimotor generator site for mu oscillatory activity.

Few studies using diffusion tensor imaging based fiber tractography or resting state fMRI have adopted a graph theoretical approach to characterize the developmental properties of the child brain. These studies have focused on the assessment of structural brain maturation (Lebel et al., 2008), on the analysis of intrinsic functional connectivity (Supekar et al., 2009), on the evolution of brain connectivity patterns (Yap et al., 2011), and on the development of neural systems underlying cognition (Fair et al., 2009). In general, they showed that the child brain develops with maturation from strong local connectivity toward a more distributed, predominantly functional based, connectivity pattern characterized by stronger integration.

However, little information is provided on the developmental trajectories of the functional properties of the sensorimotor cortex, and on how sensorimotor processing is modulated by sensorimotor experience. Here we analyzed the MEG data collected in our previous study (Berchicci et al., 2011) using a measure of functional connectivity and graph theoretical concepts to contribute to the understanding of the functional organization of the developing sensorimotor cortex from early infancy to adulthood. In an attempt to verify whether sensorimotor processing contributes to the generation of perceptual-motor coupling, we analyzed the MEG data recorded in two experimental conditions: at rest and during the execution of a prehension task.

We typified the functional organization over the sensorimotor cortex by means of functional connectivity and efficiency measures. Since the developmental properties of the mu rhythm reflect sensorimotor processing (Pineda, 2005), all measures were calculated within an individual mu rhythm frequency band to ensure that all findings referred to the sensorimotor network. Synchronization likelihood (Stam and van Djik, 2002), used in brain studies to quantify the probability for the functional interdependencies between neural signals, was used to reconstruct functional connectivity maps over the sensorimotor cortex. The type of functional efficiency over the sensorimotor network was estimated by means of segregation and integration measures (Stam, 2000) calculated on the functional connectivity maps. Functional segregation measures (i.e., mean clustering coefficient and local efficiency) quantify the specialized information processing occurring within densely interconnected groups of brain regions (Rubinov and Sporns, 2010), whereas functional integration measures (i.e., characteristic path length, Watts and Strogatz, 1998 and global efficiency, Latora and Marchiori, 2001) reckon the ability of a functional network to rapidly combine specialized information processing from distributed brain regions.

We also tried to explore whether any differences could be observed in the functional properties of the sensorimotor cortex during the execution of a prehension task, in order to provide information useful to understand the contribution of sensorimotor processing to the development of perceptual-motor coupling in infants and children. To this aim, we compared the global measures of functional connectivity and efficiency over the sensorimotor cortex at rest with those related to the execution of a prehension task. Prehension is one of the most remarkable examples of perception and action coupling in infants, since reaching for an object is guided by perceptual information on the relation between the self and the environment, which continuously changes as the posture (e.g., the motor system) is adjusted to that information (Hatwell, 1987). Therefore, prehension is a motor task suitable to explore whether sensorimotor processing contributes to the generation of perceptual-motor coupling.

Our investigation adds to prior studies that have considered either the rest condition or the observation of actions (Gilmore et al., 2011; Virji-Babul et al., 2012; Damaraju et al., 2014; Rotem-Kohavi et al., 2014), since we studied the functional properties over the developing sensorimotor cortex not only at rest but also during prehension. Moreover, by including infants below 6 months of age in our study population, we provided a valuable adjunct to studies on the developing brain.

Based on the knowledge that children and young-adults' brains have "small-world" organization at the global level (Supekar et al., 2009), and on the notion that fronto-temporal connections develop more slowly than other regions (Lebel et al., 2008), we expect that the functional properties over the sensorimotor network evolve, from infants to children and adults, toward a more efficient "small-world" organization. As well, based on the hypothesis that sensorimotor processing plays a role in the generation of perceptual-motor coupling, we expect to observe different functional organizations over the sensorimotor cortex for the rest and prehension conditions.

MATERIALS AND METHODS

PARTICIPANTS

Data collection was performed in infants, children and adults following a cross-sectional design. Participants were selected from a larger database of subjects (see Berchicci et al., 2011). Subjects experiencing any serious illnesses or developmental problems since birth (i.e., traumatic brain injury, seizures, and congenital conditions), or receiving any long-term medication were excluded from the study. Out of the 43 healthy infants enrolled (<12 months of age), 25 infants met all inclusion and exclusion criteria. Chronological age at entry in the study ranged between 11 and 47 weeks (mean = 24.9, *SD* = 10.8). The functional development of all infants was examined with the Kent Inventory of Developmental Skills (KIDS; Reuter et al., 1996). All infants were found to function within the normal range for age. Parent report was used to assess Apgar score (Apgar, 1953) at birth, which were all within normal limits (i.e., 8–10). However, due to poor signal quality that prevented a reliable calculation of the functional connectivity and efficiency measures, 11 infants had to be excluded from the study (see details in Section Statistical Analysis). Eighteen healthy children aged between 24 and 60

months were enrolled and met all inclusion and exclusion criteria, but, due to motion artifacts, only 12 children were included in the study population (mean = 37.3, *SD* = 12). Six right-handed adults (mean = 28.3, *SD* = 7.8) participated in the study as control group.

Based on the results of our prior study (see Berchicci et al., 2011), we knew that a large variation of the mu rhythm peak frequency occurred during the first year of life, indicating a rapid functional development. For this reason, we decided to split the group of infants in two age groups, one including the infants <6 months of age, and another including the infants <12 months of age. To have a similar number of subjects in all study groups, we split also the group of children in two age groups, one including the children with an age range of 24–34 months, and another including the children with an age range of 36–60 months. Details on the age groups can be found in Section Statistical Analysis.

The protocol was reviewed and approved by the Human Research Review Committee at the University of New Mexico Health Sciences Center and written informed consent was obtained from participant's guardians or adult participants after the description of the study protocol. Infants and children were recruited at day-care centers and from the community using word of mouth, brochures posted on campus, and social networks.

PROCEDURE AND TASK

The experimental setup is only briefly described herein; details can be found in our previous study (see Berchicci et al., 2011). Neuromagnetic activity was recorded using a multi-channel pediatric magnetoencephalography (MEG) system (Okada et al., 2006) for hemispheric recordings. The sensor array operated in a magnetically shielded room, consisted of 76 first-order axial gradiometers, and had a headrest with a smooth outer surface made of thick fiberglass. Inter-sensor distance was approximately 13 mm center-to-center. The headrest was based on a standard reference for the head size of babies. Since the thickness of the neonatal scalp and skull is about 3–4 mm, brain activity could be measured a few millimeters above the brain surface, providing excellent sensitivity.

Since participants performed the assigned tasks with their right hand, they were positioned on the MEG bed on their left side, and a pillow was used to support their back, if necessary. The left hemisphere of the head was positioned on the MEG headrest in order to cover the sensorimotor areas. To ensure child safety and to promote calmness during acquisition, a parent attended the child inside the magnetically shielded room. For each subject, two 5-min blocks of continuous MEG data were recorded. If the infant/child felt uncomfortable from lying still, or was getting drowsy and needed a break, data collection was stopped.

Two different experimental conditions were intermixed: *rest and prehension*. Under the *rest condition*, the participant remained motionless for about 10 s while the investigator stood in front of him/her at a distance of approximately 40 cm. Infants and children were visually engaged to prevent head motions. During the *prehension condition*, participants were invited (in case of adults and children) or directed (in case of infants) to squeeze a pipette placed at about 5 cm from their right hand. The pipette, small enough to be comfortably held and squeezed by infants and children, was connected to a pressure transducer to record the pressure exerted during prehension. Adults used a similar device with a button trigger. The pressure profile was synchronized with MEG data, hence permitting the identification of the time points at which squeezing started. This was necessary for MEG data post-processing purposes. The shielded room light was kept dim during all acquisition sessions to minimize distractions. The experimental sessions were recorded with a video camera synchronized with MEG recording to observe behavior and take note of any movement that might have occurred during acquisitions.

DATA ACQUISITION AND PRE-PROCESSING

MEG data were recorded with a sampling rate of 500 Hz. Although data acquisition was halted in cases of significant displacement of the child's head, residual artifacts, including small movements due to chewing/sucking and arm displacements, were rejected during MEG data pre-processing.

First, MEG channels not working properly were excluded from further analysis. Second, MEG data were band-pass filtered between 0.5 and 40 Hz using a forward-reverse Butterworth filter of the third order. Filtered MEG data were then processed with PCA for dimension reduction, and Independent Component Analysis (ICA, BinICA algorithm with open source toolbox, EEGlab, www.sccn.ucsd.edu/eeglab) was used to separate the independent components (ICs) of interest and to reject those related to artefactual sources. We allowed for a total of 20 ICs, and retained for further processing only those ICs that satisfied two conditions: a topological distribution compatible with the activation of the contralateral sensorimotor cortex, and a clear mu rhythm peak at the individual frequency of the subject, as identified in our previous study (see Berchicci et al., 2011). In general, we retained 2–4 ICs per subject, since the majority of ICs were related to noise, artifacts, MEG channels not working properly, or were seemingly related to brain activity but with a too high content of noise. An example of ICs separated for an infant at 36 weeks is provided in **Figure 1**, where one can see how ICs with a topological distribution that could be related to the activation of the sensorimotor cortex (e.g., IC6 or IC9), have a frequency content that is mainly due to noise. This type of ICs was not retained to reconstruct the brain signals. The retained ICs (ICs 7, 8, and 14 in the example of **Figure 1**) were re-projected on the sensors' positions to reconstruct the MEG source signals related to the true brain activity.

DATA ANALYSIS

Functional connectivity representations

For each subject, the pre-processed MEG signals were segmented according to the 4-s time intervals of rest and prehension identified in our previous study (see Berchicci et al., 2011) for both spontaneous mu rhythm (rest condition) and mu rhythm desynchronization (prehension condition). The rest time intervals were selected during the resting state far from prehension occurrences. The prehension time intervals were selected around prehension (as identified with the pressure transducer profile and the analysis of the video recordings) to include anticipatory cortical activity.

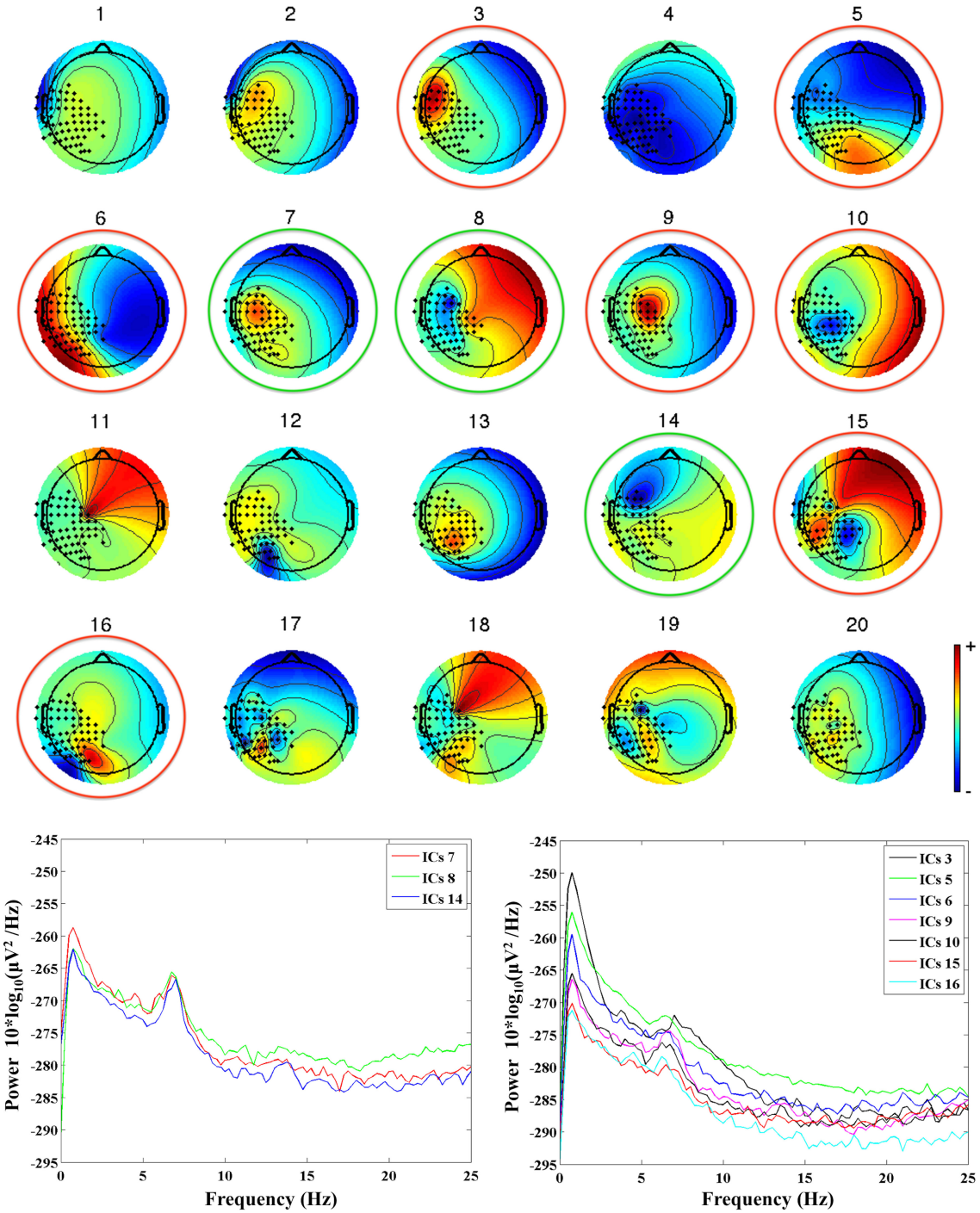

FIGURE 1 | Upper panel: the 20 ICs separated from the MEG recordings in an infant at 36 weeks (G2, mu peak frequency at 7.5 Hz). The ICs retained for further analysis are identified by a green circle, whereas the rejected ICs are identified by a red circle. **Lower panels:** power spectra of the retained ICs (on the left hand side), and of the rejected ICs (on the right hand side).

Hence, prehension time intervals started 1 s before movement onset.

The patterns of functional dependencies between the pre-processed MEG signals were estimated by means of the Synchronization Likelihood (SL) (data were analyzed using Brainwave v0.9.133.1, http://home.kpn.nl/stam7883/brainwave.html). This measure, introduced by Stam and van Djik (2002), gives a straightforward normalized estimate of the dynamical interdependencies between two or more simultaneously recorded time series. Differently from other connectivity measures such as

coherence, this measure, closely related to the concept of generalized mutual information, overcomes the problems related to sub-systems dimensionality, and can be suitable for the analysis of non-stationary data, such as ours. In essence, SL describes how strongly the signal recorded by each channel is synchronized to the signals recorded by the other channels in the array at a given time instant or in a given time span.

For each subject and each experimental conditions (rest and prehension), we calculated one SL matrix for each 4-s time interval within a frequency band centered around the individual mu rhythm peak frequency (IMPF). The IMPF of each subject had been determined in our previous study (see Berchicci et al., 2011), and the frequency band used to calculate the SL matrices had high-pass and low-pass cut-off frequencies at (IMPF − 2 Hz) and (IMPF + 2 Hz) respectively. The SL matrices obtained for all time intervals in each condition were then averaged to obtain one average SL matrix. For each subject we then had two average SL matrices, one for the rest and one for the prehension condition.

To retain only significant functional connections across MEG signals, we thresholded each average SL matrix on the basis of its own SL values distribution, which is expected to be non-Gaussian. We calculated the Median and Median Absolute Deviation (MAD) of the distribution of SL values for each average SL matrix, and defined a new thresholded SL matrix (that we called SL_{MAD} matrix) where only the SL values > (Median + 1 MAD) were retained. All other SL values in the SL_{MAD} matrix were set equal to zero.

Since we analyzed the MEG signals in the sensor space, the SL_{MAD} matrices could still have a bias due to the spatial proximity of adjacent sensors. For this reason, we reconstructed the matrix of Euclidean inter-sensor distances M_{Eu} for all retained MEG channels, and calculated the coefficient of determination r^2 between M_{Eu} and the two SL_{MAD} matrices (one for rest and one for prehension) for each subject. We then retained for further analysis only the subjects for whom both SL_{MAD} matrices satisfied the condition $r^2 < 0.1$, hence ensuring that the SL values in the SL_{MAD} matrices do not depend on the Euclidean distances across neighboring MEG sensors.

To quantify the overall probability for functional connectivity over the sensorimotor areas at rest and during prehension, for each subject and each experimental condition we calculated the mean SL value in the SL_{MAD} matrix as:

$$SL_{MEAN} = \frac{1}{N}\sum_{i,j} SL_{MAD,i,j} \quad (1)$$

where N is the total number of SL values ≠ 0 in the SL_{MAD} matrix.

Measures of functional organization

We used graph theoretical concepts to study the topological features of the functional networks represented by the SL_{MAD} matrices. Within this framework, patterns of functional connections are represented as graphs where nodes (in our case the MEG sensors) are linked with edges (if connected). For each subject, we estimated the level of functional organization over the sensorimotor cortex at rest and during prehension by means of segregation and integration measures described below. To this aim, we calculated the segregation and integration measures on the SL_{MAD} matrices, where each SL value (when different from zero) represents the strength of the functional connection (edge) between two given MEG signals (nodes). As the comparison of graphs derived from brain networks requires a step of normalization, for instance by setting a fixed average degree (K) (van Wijk et al., 2010), prior to calculating segregation and integration measures we checked the degrees of the SL_{MAD} matrices of each subject included in the study population, and considered for further processing only those subjects whose SL_{MAD} matrices had the same degree in both rest and prehension (see also sub-Section Statistical Analysis).

Measures of functional segregation. Functional segregation in the brain refers to specialized information processing occurring within densely interconnected groups of brain regions (Rubinov and Sporns, 2010). In our case, functional connectivity was calculated by SL_{MAD} matrices in the sensor space, hence segregated neural processing will be suggested by statistical dependencies between clustered channels. We calculated two weighted measures of functional segregation:

(1) *Mean clustering coefficient C*. For a given node *i* (in our case, for a given MEG channel *i*), c_i is defined as the fraction of the node's neighbors (other MEG channels) that are directly connected with it (Watts and Strogatz, 1998). At the network level, the *mean clustering coefficient C* reflects the prevalence of clustered connectivity around individual nodes:

$$C = \frac{1}{n}\sum_{i\in N} c_i = \frac{1}{n}\sum_{i\in N}\frac{2t_i^w}{k_i\,(k_i-1)} \quad (2)$$

where N is the set of all nodes in the network, and n is the number of nodes, k_i is the degree of node i (i.e., the number of links connected to node i), and t_i^w is the weighted geometric mean of triangles around *i*. High values of C indicate that a high number of connections exists among neighboring nodes.

(2) *Local efficiency* E_{loc}. The local efficiency is defined as the average efficiency of the local subgraphs. For weighted connectivity matrices, such as SL_{MAD} matrices, it is:

$$E_{loc} = \frac{1}{2}\sum_{i\in N}\frac{\sum_{j,h\in N, j\neq i}\left(w_{i,j}w_{i,h}\left[d_{j,h}^w(N_i)\right]^{-1}\right)^{1/3}}{k_i\,(k_i-1)} \quad (3)$$

where, for a given triangle of vertices *i,j,h*, $w_{i,j}$, and $w_{i,h}$ are the weights between nodes *i* and *j* and nodes *i* and *h* respectively, and $d_{j,h}^w$ is the distance between nodes *j* and *h*, i.e., the minimum number of links connecting node *j* to node *h*. E_{loc} provides an information similar to the mean clustering coefficient C, but adds an indication on how much the system is *fault tolerant*, i.e., how efficient is the communication between the first neighbors of node *i* when it is removed. Local efficiency suggests a connection redundancy that protects the network from local errors and failures (Latora and Marchiori, 2001).

When high functional segregation is found in a functional connectivity matrix, the prevailing functional connections occur across neighboring brain areas (or, as in our case, across signals recorded by neighboring channels).

Measures of functional integration. In the brain, functional integration represents the ability to rapidly combine specialized information from distributed brain regions. Although our MEG recordings refer only to the hemisphere contra-lateral to the moving limb, we calculated two measures of functional integration to estimate how easily different brain regions communicate. The measures of functional integration are based on the concept of a path:

(1) *Characteristic path length L.* In a graph, the lengths of paths connecting two given nodes estimate the potential for functional integration in the network (Watts and Strogatz, 1998). The *characteristic path length L* is defined as the mean of the distances (i.e., the minimum path lengths) among all nodes pairs:

$$L = \frac{1}{n}\sum_{i\in N}\frac{\sum_{j\in N, j\neq i} d^w_{i,j}}{n-1} \quad (4)$$

where $d^w_{i,j}$ is the weighted distance between nodes *i* and *j*, i.e., the minimum number of links connecting node *i* to node *j*. Short paths, corresponding to low values of L, indicate a strong potential for integration within the network.

(2) *Global efficiency* E_{glob}. In functional connectivity data, such as the SL_{MAD} matrices, paths represent sequences of statistical associations between subsequent pairs of channels. The level of functional integration in the network can be represented by the *global efficiency* E_{glob}, which is the average inverse shortest path length (Latora and Marchiori, 2001; Achard and Bullmore, 2007). For weighted connectivity matrices:

$$E_{glob} = \frac{1}{n}\sum_{i\in N}\frac{\sum_{j\in N,\, j\neq i}(d^w_{i,j})^{-1}}{n-1} \quad (5)$$

When high functional integration is found in a functional connectivity matrix, the functional organization of the brain takes advantage of multiple specialized and densely connected areas that are linked with long distance functional connections for a more efficient information processing.

Statistical analysis

Linear regression analysis was performed on the individual measures to assess whether any linear correlation exists between age and/or mu rhythm peak frequency and the functional connectivity/efficiency measures.

Groups analysis was performed for each connectivity/efficiency measure on the age groups defined in Section Participants. In each age group, we retained only those subjects for whom the following two conditions were satisfied: (1) the determination coefficient r^2 between the individual SL_{MAD} matrices at rest and during prehension and the individual M_{Eu} matrix of the euclidean inter-sensor distances was smaller than 0.1, and (2) the degree of the individual SL_{MAD} matrices for rest and prehension was the same. The first condition guarantees that the SL_{MAD} matrices are independent on the inter-sensor distances, and the second condition satisfies the requirement for a reliable comparison of segregation and integration measures. Seven infants (age <6 months) and 4 infants (age <12 months) did not satisfy these conditions and were excluded from further analysis. The characteristics of the age groups are reported in **Table 1**.

Statistical analysis was performed using an ANOVA 5 (age groups) × 2 (conditions: rest, prehension) for each dependent variable, i.e., for the individual measure of functional connectivity (SL_{MEAN}), and for functional segregation (*C* and E_{loc}), and integration (*L* and E_{glob}) measures. Post-hoc comparisons were performed using Bonferroni corrections. Statistical significance was set at $p < 0.05$.

RESULTS

Linear regression analysis on the individual functional connectivity/efficiency measures did not show any significant linear dependence on age or mu rhythm peak frequency. In particular, the coefficient of determination r^2 between age and SL_{MEAN}, *C*, E_{loc}, *L*, and E_{glob} ranged between 0.197 and 0.465, and r^2 between mu rhythm peak frequency and SL_{MEAN}, *C*, E_{loc}, *L*, and E_{glob} ranged between 0.008 and 0.269, indicating no significant linear correlation between any connectivity/efficiency measure and age or mu rhythm peak frequency.

FUNCTIONAL CONNECTIVITY REPRESENTATIONS

The changes of the group-averaged SL_{MEAN} values with age in the two experimental conditions (rest and prehension) are summarized in **Figure 2**. ANOVA results on the individual measures of SL_{MEAN} showed significant differences across age groups [$F_{(4,\ 27)} = 4.546$ $p = 0.006$, $\eta^2_p = 0.402$, power = 0.897], no significant differences between conditions, and no interaction between groups and conditions. During the first year of life (groups G1 and G2), the average SL_{MEAN} values do not differ significantly, whereas around 2 years of age (group G3), SL_{MEAN} values start to increase toward the adult values (group G5). *Post-hoc* analysis showed significant differences only between the

Table 1 | Number of subjects included in each age group (N_{study}) out of those who met all inclusion and exclusion criteria ($N_{incl/excl}$).

Group	$N_{incl/excl}$	N_{study}	Age		Mu peak frequency (Hz) (Mean ± SD)
			Months	Years	
G1	14	7	2.75–6		4.46 ± 1.12
G2	11	7	6.5–11.75	<1	7.41 ± 0.61
G3	6	6	24–34	2–2.8	8.71 ± 0.64
G4	6	6	36–60	3–5	8.50 ± 0.52
G5	6	6		20–39	10.32 ± 1.20

For each age group, the age range and the mu rhythm peak frequency (Mean ± SD) are also reported.

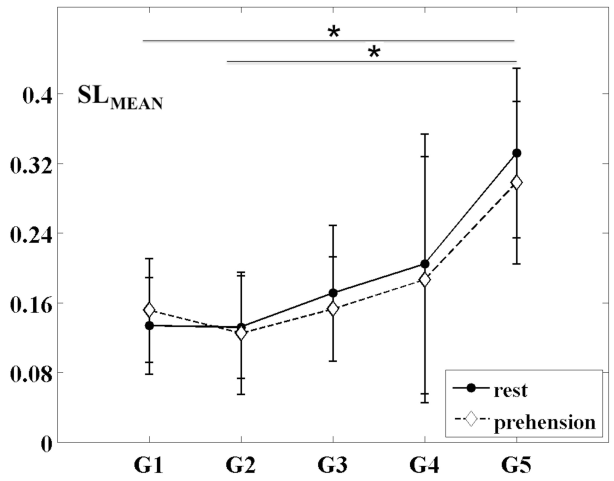

FIGURE 2 | Group-averaged SL_{MEAN} values (mean ± SD) for the five age groups (G1–G5) and the two experimental conditions (rest and prehension). $^*p < 0.05$.

group of adults G5 (0.315 ± 0.093) and the groups of infants G1 (0.143 ± 0.056; $p = 0.015$) and G2 (0.129 ± 0.062; $p = 0.007$).

These results indicate that, during infancy, the likelihood for functional connections over the sensorimotor cortex is much lower than in adulthood, and that it increases with age. Although no statistically significant difference was observed between conditions, it is interesting to observe that, in our group of very young infants (G1), the average SL_{MEAN} is slightly higher during prehension than at rest, whereas in the groups of children and in the group of adults the average SL_{MEAN} slightly decreases during prehension. This fact could deserve further investigation, possibly in larger populations of infants and children. Examples of SL_{MAD} matrices at rest and during prehension for each age group are provided in **Figure 3**. A typical layout of the MEG sensor array over the head is also shown. However, please consider that the same channels in different SL_{MAD} matrices could be positioned over different brain regions, as no information on the relative positions of the MEG channels with respect to the subject's head could be collected.

MEASURES OF FUNCTIONAL SEGREGATION

The changes of the group-averaged C and E_{loc} values with age in the two experimental conditions (rest and prehension) are summarized in **Figures 4A,B**. ANOVA results on the individual measures of C showed significant differences across age groups [$F_{(4,\ 27)} = 4.975$ $p = 0.004$, $\eta_p^2 = 0.424$, power = 0.924], no significant differences between conditions, and no interaction between groups and conditions. During the first year of life (groups G1 and G2), C remains almost unchanged, whereas around 2 years of age (group G3) it starts to increase toward the adult values (group G5). *Post-hoc* analysis showed significant differences between the group of adults G5 (0.231 ± 0.076) and the groups of infants G1 (0.094 ± 0.037; $p = 0.011$), G2 (0.083 ± 0.047; $p = 0.005$). A tendency toward significant difference was also observed between G5 and G3 (0.104 ± 0.041; $p = 0.030$).

Similarly, ANOVA results on the individual measures of E_{loc} showed significant differences across age groups [$F_{(4,\ 27)} = 5.223$ $p = 0.003$, $\eta_p^2 = 0.436$, power = 0.937], no significant differences between conditions, and no interaction between groups and conditions. During the first year of life (groups G1 and G2), E_{loc} remains almost unchanged, and around 2 years of age (group G3) it starts to increase toward the adult values (group G5). *Post-hoc* analysis showed significant differences between the group of adults G5 (0.266 ± 0.084) and the groups of infants G1 (0.112 ± 0.041; $p = 0.008$), G2 (0.100 ± 0.049; $p = 0.004$), whereas a tendency toward significant difference was observed between G5 and G3 (0.125 ± 0.045; $p = 0.026$).

These results indicate that, during infancy, global measures of functional segregation over the sensorimotor cortex are significantly lower than in adulthood, and that they increase with age. Although no statistically significant difference was observed between conditions, in the very young infants (G1), functional segregation seems to be higher during prehension than at rest, whereas in children and in adults it seems to decrease from rest to prehension. As for SL_{MEAN}, this aspect deserves further investigation in larger populations of infants and children.

MEASURES OF FUNCTIONAL INTEGRATION

The changes of the group-averaged L and E_{glob} values with age in the two experimental conditions (rest and prehension) are shown in **Figures 4C,D**. ANOVA results on the individual measures of L showed significant differences across age groups [$F_{(4,\ 27)} = 4.245$ $p = 0.009$, $\eta_p^2 = 0.386$, power = 0.873], no significant differences between conditions, and no interaction between groups and conditions. L tends to decrease with age, although discontinuously. *Post-hoc* analysis showed significant difference between the group of adults G5 (12.975 ± 3.034) and the group of older infants G2 (28.588 ± 7.575; $p = 0.007$), and a trend toward significant difference between G5 and the group of older children G4 (25.739 ± 10.494; $p = 0.047$).

ANOVA results on the individual measures of E_{glob} showed significant differences across age groups [$F_{(4,\ 27)} = 5.594$ $p = 0.002$, $\eta_p^2 = 0.453$, power = 0.952], no significant differences between conditions, and no interaction between groups and conditions. We can see that E_{glob} remains almost unchanged in infancy (groups G1 and G2), and that it increases with age. *Post-hoc* analysis showed significant differences between the group of adults G5 (0.158 ± 0.037) and the groups of infants G1 (0.071 ± 0.022; $p = 0.004$) and G2 (0.068 ± 0.029; $p = 0.003$). A tendency toward significant difference was observed between G5 and G3 (0.085 ± 0.027; $p = 0.030$).

Both measures indicate a significant difference of functional integration over the sensorimotor cortex between infancy and adulthood, and that functional integration over the sensorimotor cortex increases with age. Although no statistically difference was observed between conditions, both L and E_{glob} seem to indicate a higher functional integration during prehension in the very young infants (G1), whereas in children and in adults functional integration seems to decrease from rest to prehension. As for the other connectivity and segregation measures, this aspect deserves further investigation in larger populations of infants and children.

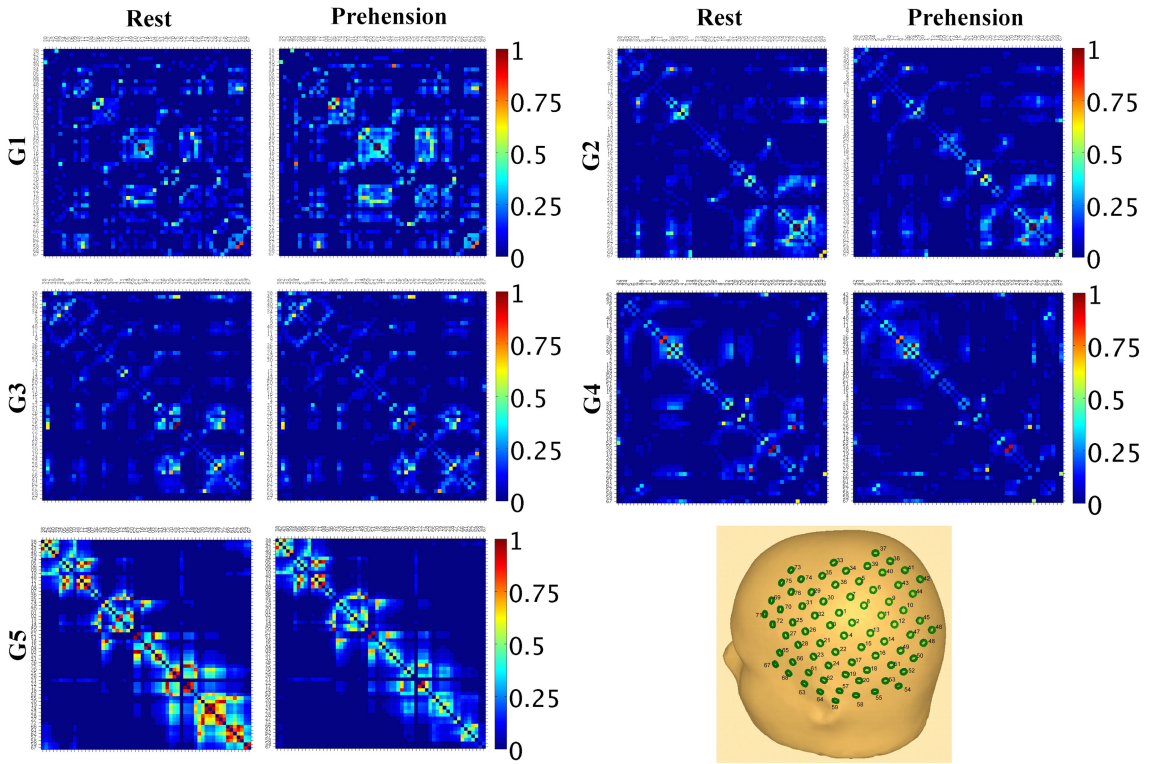

FIGURE 3 | Examples of SL_{MAD} matrices at rest and during prehension (one example per age group). G1: infant, 12 weeks; G2: infant, 36 weeks; G3: child, 34 months; G4: child, 41 months; G5: adult, 28 years. A schematic representation of the sensor array and its approximate placement over the left hemisphere is shown in the lower right hand panel. In the SL_{MAD} matrices, the MEG channels are displayed from the medial to the lateral areas.

DISCUSSION

Our goals were to contribute to the identification of the developmental trajectories of the functional properties over the sensorimotor cortex, and to explore whether any differences could be observed between the rest condition and the execution of a prehension task. To ensure that all findings were related to the sensorimotor cortex, all analyses were performed within a frequency band centered on the individual mu rhythm peak frequency of each subject, as defined in our previous study (Berchicci et al., 2011), since the mu rhythm is known to be the idling rhythm of the sensorimotor cortex. Furthermore, the use of a prehension task for the active condition permitted us to investigate the contribution of sensorimotor processing to the generation of perception and action coupling in infants.

We first observed that the probability of functional connectivity across the sensorimotor areas, estimated by means of SL_{MEAN}, remained almost unchanged during the first year of life, whereas it afterwards increased across groups to reach adult values, significantly different from the infant ones. This increase, occurring after 12 months of age, is in agreement with the suggested pattern of brain maturation in which areas with fronto-temporal connections develop more slowly than other regions (Lebel et al., 2008), and with the notion that motor experience increases the capacity of the whole network to work in an integrated way (Fair et al., 2009; Giedd et al., 2009; Boersma et al., 2011). Unfortunately, no information on the relative position of the MEG sensor array and the subject's head could be collected, therefore we could not precisely ascribe the observed functional connections across MEG signals to specific brain areas. Consequently, our observations on the probability of functional connectivity should be interpreted as global measures over the sensorimotor network.

To support the interpretation of these results, we used graph theoretical concepts to examine the changes occurring in the functional organization of the sensorimotor network across ages, and found that all segregation and integration measures showed a trend similar to SL_{MEAN}: during the first year of life these properties remained almost unchanged, whereas they increased significantly across groups afterwards, as assessed by a marked increase of both segregation parameters (C and E_{loc}), by a tendency of L to decrease, and by a clear increase of E_{glob} across age groups.

The age-related increase of the functional segregation parameters (C and E_{loc}) is compatible with the observation that the widespread brain electrical activity typical of infants (8 months of age) becomes more localized during early childhood (3 years of age) (Bell and Wolfe, 2007). We hypothesize that the increase of functional connections among adjacent cortical areas, which contributes to the functional specialization of the sensorimotor network and to the onset of a connection redundancy that protects the network from local errors and failures (Latora and Marchiori, 2001), is due to brain maturation, a process that involves both physical growth and the intellectual and/or emotional process of

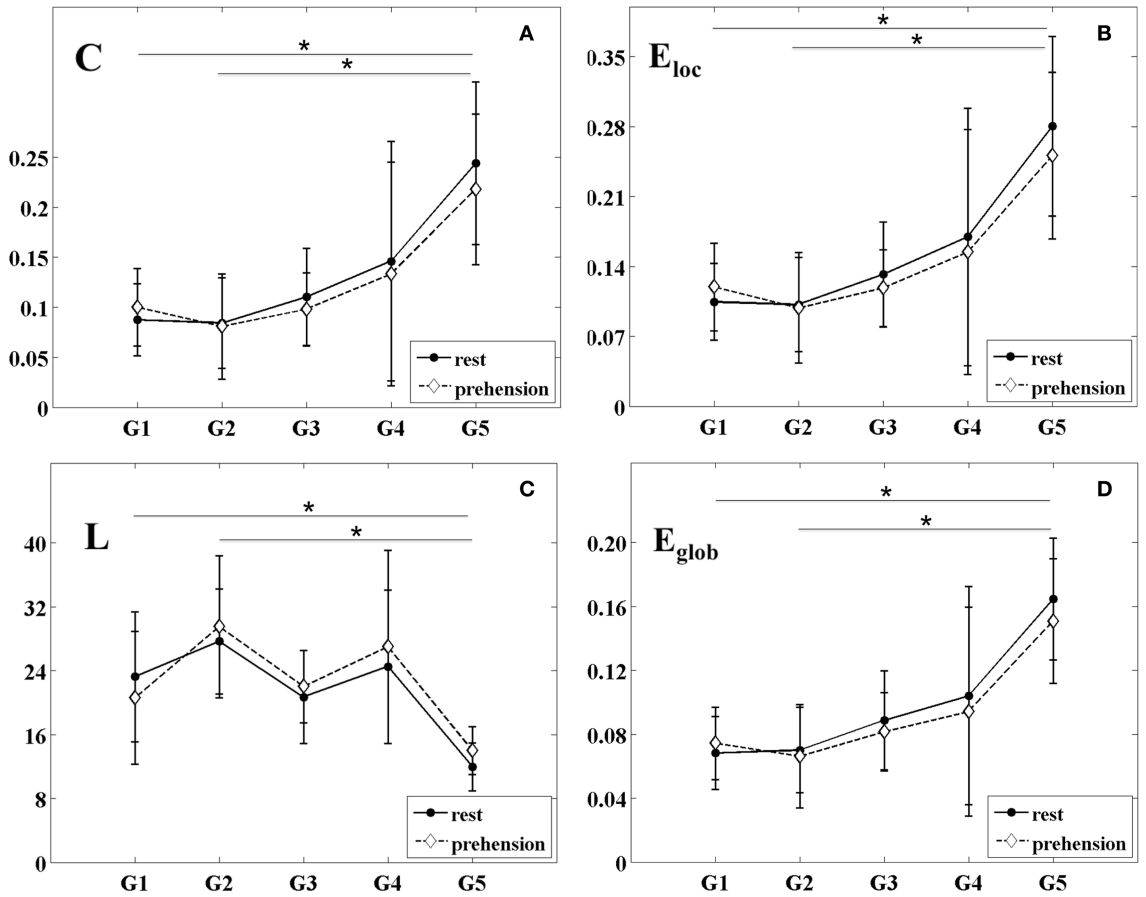

FIGURE 4 | Group-averaged values (mean ± SD) of the segregation and integration measures for the five age groups (G1–G5) and the two experimental conditions (rest and prehension). (A) mean clustering coefficient C; **(B)** local efficiency E_{loc}; **(C)** characteristic path length L; **(D)** global efficiency E_{glob}. $^*p < 0.05$.

development. Also, the increase of local efficiency over the sensorimotor cortex is in line with the findings by Wu et al. (2013), who observed an age-related increase in the local efficiency of the whole functional networks, which may contribute to the development of modular information processing of functional systems.

Although the findings on the functional integration properties over the sensorimotor cortex should be taken with caution because the MEG sensor array covered only one hemisphere, it is interesting to observe that also these properties increased with age after the first year of life, and that the infant values were significantly different from the adult ones. The irregular trend of *L* is also worth noting, as it might be related to the occurrence of growth spurts that coincide with periods of discontinuous development in cognition (van Baal et al., 2001).

Overall, our findings on the functional segregation and integration properties over the sensorimotor cortex support the notion that maturation contributes to both the functional specialization of the sensorimotor network, and the wiring of more efficient long-range connections among different brain circuits. This interpretation is in agreement with the observations by Gao et al. (2011) on the increase of both local and global efficiency at rest from newborns to infants, and with the findings of Damaraju et al. (2014) that the connectivity strength between more distant networks increases with age in infants between 4 and 9 months. Conversely, our results are only partially compatible with the notion that strong local connectivity in the young brain gradually shifts toward stronger long-distance connectivity with maturation (van Baal et al., 2001; Lebel et al., 2008; Fair et al., 2009; Power et al., 2010; Yap et al., 2011).

Our results on the age-related increase of both local and global efficiency are consistent also with the outcome of other studies on the developing brain, which demonstrated a steady increase of global efficiency after 1 year of age (Fransson et al., 2007; Fan et al., 2011), a positive relationship between age and local efficiency throughout the life span (Supekar et al., 2009; Dennis et al., 2013; Wu et al., 2013), and the involvement of both segregation and integration in the development of the adult fronto-parietal network for adaptive online task control (Fair et al., 2007; Sepulcre et al., 2010). Our findings seem to support this interpretation of the functional evolution of the fronto-parietal network, known to host sensorimotor processing (Pineda, 2005). From this perspective, our results seem to fit well also with the suggestion that perceptual and cognitive developments involve

the simultaneous segregation and integration of information-processing streams (Bunge and Wright, 2007), which in turn support the learning processing in infants and children (de Klerk et al., 2014).

Some authors have also suggested that the child brain has a small-world organization that combines the high clustering properties of an ordered network and the short path length of a random network (Fair et al., 2009; Supekar et al., 2009; Power et al., 2010; Boersma et al., 2011). Other authors have observed that, in school children, the brain functional networks evolve from more random toward a more ordered configuration (Smit et al., 2010, 2012; Boersma et al., 2011). Although our hemispheric recordings do not allow for general conclusions on the functional organization of the whole brain, nonetheless our results complement the above mentioned findings by suggesting that, during infancy, the functional properties over the sensorimotor network have a more random organization that, after 1 year of age, shifts toward a more efficient small-world configuration characterized by higher local and global efficiency. It is interesting to observe that this change toward a more efficient functional organization over the sensorimotor network continued throughout childhood until adulthood. The shift from a more random to a small-world configuration could be ascribed to brain maturation, which derives from changes at the structural level, with the thickening of long-range connections among distant brain regions starting during the first year of life (Yap et al., 2011) and with the emergence of inter-hemispheric connectivity earlier than longer-range antero-posterior connections (Bell and Fox, 1992), but is also shaped by experience, which can support the capacity of the network to create long-range connections that are functional to goal-directed actions (Wu et al., 2013; Rotem-Kohavi et al., 2014).

Unfortunately, we could not draw any conclusions on the contribution of sensorimotor processing to the generation of perceptual-motor coupling, since we did not find any significant difference in the functional properties over the sensorimotor cortex between rest and prehension. However, it is worth noting that the pattern of functional organization over the sensorimotor cortex seems to change around 1 year of age. All measures seem to suggest that, during infancy, prehension could be characterized, with respect to rest, by an increased probability of functional connectivity and by increased segregation and integration. This pattern seems to reverse after 1 year of age. These observations, if confirmed in future studies on larger populations of infants and children supported by measurements of motor experience, could indicate that, in young infants, perceptual-motor coupling is accompanied by an increased connectivity within the sensorimotor network to compensate for the lack of functional specialization to accomplish the given task (prehension). The evolution of this functional pattern could be due to the developmental timeline of the infant grasping or to the tight correlation between grasping recognition and execution, which are poor until 6 months of age (Del Giudice et al., 2009), hence requiring the recruitment of more functional resources in early infancy with respect to later ages. On the other hand, the pattern reversal that seems to occur after 1 year of age might indicate that maturation had fostered a more efficient execution of goal-directed actions, in line with the experience-dependent position on perceptual-motor coupling development of the sensorimotor cortex (Heyes, 2001; van Elk et al., 2008; Del Giudice et al., 2009; Cook et al., 2014), and with the concept that sensorimotor experience contributes to the development of more efficient functional networks to support sensorimotor development (Fransson et al., 2011).

We are aware that the impact of our study is limited by a number of factors. First, the shape and size of the MEG sensor array allowed the recording of brain activity originating only from one hemisphere. Consequently, our observations on the small-world topology of the child brain cannot be referred to the whole brain, and the interpretation of the integration measures needs to be cautious. Second, we employed a cross-sectional design for this study. Given that, during infancy and childhood, the brain undergoes a remarkable development at both structural and functional levels, the recorded brain activity could be influenced by the size of the scalp at different ages, which fits differently on the headrest covering the sensor array. Third, the measures of the topological features of the developing sensorimotor network were calculated in the sensor space rather than in the source space, because anatomical information on the baby's head and on its position with respect to the MEG sensor array could not be collected. This condition limits the interpretation of our results in terms of specific cortical areas. Fourth, we are aware of the small sample size of our age groups. However, study protocols like ours are difficult to perform in children and even more so in infants, and the analyses performed are extremely sensitive to noise and to other signal features that further reduced the number of retained subjects. Nonetheless, several research studies in adults and children have been considered reliable even when based on a small number of subjects (Nishitani and Hari, 2000; Simoes et al., 2004; Lepage and Theoret, 2006; van Schie et al., 2008).

In light of these limitations, further work is needed to validate our findings. However, we believe that our results add valuable information to the current knowledge on the functional development of the sensorimotor network during infancy and childhood. The human brain performs its sensory, cognitive and motor functions by dynamically employing highly complex and interwoven neuronal networks, with the first year of life being the most dynamic period of human postnatal brain development. Better understanding of the functional development of these networks during infancy may bring new insights on the pathophysiological mechanisms of neurological development, such as Down syndrome, autism spectrum disorders and cerebral palsy. Further studies employing whole head neuroimaging techniques during motor task execution and complemented with motor experience measurements are therefore needed to support the present findings, and to improve our understanding of the functional development of the sensorimotor network and its contribution to the generation of perceptual-motor coupling in infants.

AUTHOR CONTRIBUTIONS

The study presented here has been conceived and designed by Marika Berchicci and Silvia Comani. The experiments were performed by Marika Berchicci. Data were analyzed by Gabriella Tamburro, Silvia Comani, and Marika Berchicci. Data have been interpreted by Marika Berchicci, Gabriella Tamburro, and Silvia

Comani. The manuscript was written, revised and approved by Marika Berchicci, Gabriella Tamburro, and Silvia Comani.

REFERENCES

Achard, S., and Bullmore, E. (2007). Efficiency and cost of economical brain functional networks. *PLoS Comput. Biol.* 3:e17. doi: 10.1371/journal.pcbi.0030017

Apgar, V. (1953). A proposal for a new method of evaluation of the newborn infant. *Anesth. Analg.* 32, 260–267. doi: 10.1213/00000539-195301000-00041

Bell, M. A., and Fox, N. A. (1992). The relationship between frontal brain electrical activity and cognitive development during infancy. *Child Dev.* 63, 1142–1163. doi: 10.2307/1131523

Bell, M. A., and Wolfe, C. D. (2007). Changes in brain functioning from infancy to early childhood: evidence from EEG power and coherence working memory task. *Dev. Neuropsychol.* 31, 21–38. doi: 10.1207/s15326942dn3101_2

Berchicci, M., Zhang, T., Romero, L., Peters, A., Annett, R., Teuscher, U., et al. (2011). Development of mu rhythm in infants and preschool children. *Dev. Neurosci.* 33, 130–143. doi: 10.1159/000329095

Boersma, M., Smit, D. J. A., de Bie, H. M. A., Van Baal, G. C. M., Boomsma, D. I., de Geus, E. J. C., et al. (2011). Network analysis of resting state EEG in the developing young brain: structure comes with maturation. *Hum. Brain Mapp.* 32, 413–425. doi: 10.1002/hbm.21030

Bunge, S. A., and Wright, S. B. (2007). Neurodevelopmental changes in working memory and cognitive control. *Curr. Opin. Neurobiol.* 17, 243–250. doi: 10.1016/j.conb.2007.02.005

Butterworth, G. E. (1989). "On U-shaped and other transitions in sensorimotor development," in *Transition Mechanisms in Child Development*, ed A. de Ribaupierre (New York, NY: Cambridge University Press), 283–296.

Calvo-Merino, B., Grezes, J., Glaser, D. E., Passingham, R. E., and Haggard, P. (2006). Seeing or doing? Influence of visual and motor familiarity in action observation. *Curr. Biol.* 16, 1905–1910. doi: 10.1016/j.cub.2006.07.065

Cannon, E. N., Yoo, K. H., Vanderwert, R. E., Ferrari, P. F., Woodward, A. L., and Fox, N. A. (2013). Action experience, more than observation, influences mu rhythm desynchronization. *PLoS ONE* 9:e92002. doi: 10.1371/journal.pone.0092002

Cheyne, D., Gaetz, W., Garnero, L., Lachaux, J. P., Ducorps, A., Schwartz, D., et al. (2003). Neuromagnetic imaging of cortical oscillations accompanying tactile stimulation. *Cogn. Brain Res.* 17, 599–611. doi: 10.1016/S0926-6410(03)00173-3

Cheyne, D., Jobst, C., Tesan, G., Crain, S., and Johnson, B. (2014). Movement related neuromagnetic fields in preschool age children. *Hum. Brain. Mapp.* 35, 4858–4875. doi: 10.1002/hbm.22518

Cook, R., Bird, G., Catmur, C., Press, C., and Heyes, C. (2014). Mirror neurons: from origin to function. *Behav. Brain Sci.* 37, 177–192. doi: 10.1017/S0140525X13000903

Cuevas, K., Cannon, E. N., Yoo, K., and Fox, N. A. (2014). The infant EEG mu rhythm: methodological considerations and best practices. *Dev. Rev.* 34, 26–43. doi: 10.1016/j.dr.2013.12.001

Damaraju, E., Caprihan, A., Lowe, J. R., Allen, E. A., Calhoun, V. D., and Phillips, J. P. (2014). Functional connectivity in the developing brain: a longitudinal study from 4 to 9 months of age. *Neuroimage* 84, 169–180. doi: 10.1016/j.neuroimage.2013.08.038

Damoiseaux, J. S., Rombouts, S. A., Barkhof, F., Scheltens, P., Stam, C. J., Smith, S. M., et al. (2006). Consistent resting-state networks across healthy subjects. *Proc. Natl. Acad. Sci. U.S.A.* 103, 13848–13853. doi: 10.1073/pnas.0601417103

de Klerk, C. C. J. M., Johnson, M. H., Heyes, C. M., and Southgate, V. (2014). Baby steps: investigating the development of perceptual-motor couplings in infancy. *Dev. Sci.* 1, 1–11. doi: 10.1111/desc.12226

Del Giudice, M., Manera, V., and Keysers, C. (2009). Programmed to learn? the ontogeny of mirror neurons. *Dev. Sci.* 12, 350–363. doi: 10.1111/j.1467-7687.2008.00783.x

Dennis, E. L., Jahanshad, N., McMahon, K. L., de Zubicaray, G. I., Martin, N. G., Hickie, I. B., et al. (2013). Development of brain structural connectivity between ages 12 and 30: a 4-Tesla diffusion imaging study in 439 adolescents and adults. *Neuroimage* 64, 671–684. doi: 10.1016/j.neuroimage.2012.09.004

Depretto, M., Davies, M. S., Pfeifer, J. H., Scott, A. A., Sigman, M., Bookheimer, S. Y., et al. (2006). Understanding emotions in others: mirror neuron dysfunction in children with autism spectrum disorders. *Nat. Neurosci.* 9, 28–30. doi: 10.1038/nn1611

Doria, V., Beckmann, C. F., Arichi, T., Merchant, N., Groppo, M., Turkheimer, F. E., et al. (2010). Emergence of resting state networks in the preterm human brain. *Proc. Natl. Acad. Sci. U.S.A.* 107, 20015–20020. doi: 10.1073/pnas.1007921107

Dosenbach, N. U. F., Nardos, B., Cohen, A. L., Fair, D. A., Power, J. D., Church, J. A., et al. (2010). Prediction of individual brain maturity using fMRI. *Science* 329, 1358–1361. doi: 10.1126/science.1194144

Ellingson, R. J. (1964). Studies of the electrical activity of the developing human brain. *Prog. Brain Res.* 9, 26–53. doi: 10.1016/S0079-6123(08)63130-1

Fair, D. A., Cohen, A. L., Power, J. D., Dosenbach, N. U. F., Church, J. A., Miezin, F. M., et al. (2009). Functional brain networks develop from a "Local to Distributed" organization. *PLoS Comput. Biol.* 5:e1000381. doi: 10.1371/journal.pcbi.1000381

Fair, D. A., Dosenbach, N. U., Church, J. A., Cohen, A. L., Brahmbhatt, S., Miezin, F. M., et al. (2007). Development of distinct control networks through segregation and integration. *Proc. Natl. Acad. Sci. U.S.A.* 104, 13507–13512. doi: 10.1073/pnas.0705843104

Fan, Y., Shi, F., Smith, J. K., Lin, W., Gilmore, J. H., and Shen, D. (2011). Brain anatomical networks in early human brain development. *Neuroimage* 54, 1862–1871. doi: 10.1016/j.neuroimage.2010.07.025

Fransson, P., Aden, U., Blennow, M., and Lagercrantz, H. (2011). The functional architecture of the infant brain as revealed by resting-state fMRI. *Cereb. Cortex* 21, 145–154. doi: 10.1093/cercor/bhq071

Fransson, P., Skiold, B., Horsch, S., Nordell, A., Blennow, M., Lagercrantz, H., et al. (2007). Resting-state networks in the infant brain. *Proc. Natl. Acad. Sci. U.S.A.* 104, 15531–15536. doi: 10.1073/pnas.0704380104

Gao, W., Gilmore, J. H., Giovanello, K. S., Smith, J. K., Shen, D., Zhu, H., et al. (2011). Temporal and spatial evolution of brain network topology during the first two years of life. *PLoS ONE* 6:e25278. doi: 10.1371/journal.pone.0025278

Gao, W., Zhu, H., Giovanello, K. S., Smith, J. K., Shen, D., Gilmore, J. H., et al. (2009). Evidence on the emergence of the brain's default network from 2-week-old to 2-year-old healthy pediatric subjects. *Proc. Natl. Acad. Sci. U.S.A.* 106, 6790–6795. doi: 10.1073/pnas.0811221106

Giedd, J. N., Lalonde, F. M., Celano, M. J., White, S. L., Wallace, G. L., Lee, N. R., et al. (2009). Anatomical brain magnetic imaging of typically developing children and adolescence. *J. Am. Acad. Adolesc. Psychiatry* 48, 465–470. doi: 10.1097/CHI.0b013e31819f2715

Gilmore, J. H., Shi, F., Woolson, S. L., Knickmeyer, R. C., Short, S. J., Lin, W., et al. (2011). Longitudinal development of cortical and subcortical gray matter from birth to 2 years. *Cereb. Cortex* 22, 2478–2485. doi: 10.1093/cercor/bhr327

Grafton, S. T., Arbib, M. A., Fadiga, L., and Rizzolatti, G. (1996). Localization of action representations in humans by positron emission tomography. 2. Observation compared with imagination. *Exp. Brain Res.* 112, 103–111. doi: 10.1007/BF00227183

Greenough, W. T., Black, J. E., and Wallace, C. S. (1987). Experience and brain development. *Child Dev.* 58, 539–559. doi: 10.2307/1130197

Hari, R., Levanen, S., and Raij, T. (2000). Timing of human cortical functions during cognition: role of MEG. *Trends Cogn. Sci.* 4, 455–462. doi: 10.1016/S1364-6613(00)01549-7

Hatwell, Y. (1987). Motor and cognitive functions of the hand in infancy and childhood. *Int. J. Behav. Dev.* 10, 509–526. doi: 10.1177/016502548701000409

Heyes, C. M. (2001). Causes and consequences of imitation. *Trends Cogn. Sci.* 5, 253–261. doi: 10.1016/S1364-6613(00)01661-2

Hummel, F., Andres, F., Altenmuller, E., Dichgans, J., and Gerloff, C. (2002). Inhibitory control of acquired motor programs in the human brain. *Brain* 125, 404–420. doi: 10.1093/brain/awf030

Imai, M., Watanabe, H., Yasui, K., Kimura, Y., Shitara, Y., Tsuchida, S., et al. (2014). Functional connectivity of the cortex of term and preterm infants and infants with Down's syndrome. *Neuroimage* 85, 272–278. doi: 10.1016/j.neuroimage.2013.04.080

Jarvelainen, J., Schurmann, M., and Hari, R. (2004). Activation of the human primary motor cortex during observation of tool use. *Neuroimage* 23, 187–192. doi: 10.1016/j.neuroimage.2004.06.010

Keehn, B., Wagner, J. B., Tager-Flusberg, H., and Nelson, C. A. (2013). Functional connectivity in the first year of life in infants at-risk for autism: a preliminary near-infrared spectroscopy study. *Front. Hum. Neurosci.* 7:444. doi: 10.3389/fnhum.2013.00444

Kelly, A. M., Di Martino, A., Uddin, L. Q., Shehzad, Z., Gee, D. G., Riss, P. T., et al. (2009). Development of anterior cingulate functional connectivity from

late childhood to early adulthood. *Cereb. Cortex* 19, 640–657. doi: 10.1093/cercor/bhn117

Knickmeyer, R. C., Gouttard, S., Kang, C., Evans, D.,Wilber, K., Smith, J. K., et al. (2008). A structural MRI study of human brain development from birth to 2 years. *J. Neurosci.* 28, 12176–12182. doi: 10.1523/JNEUROSCI.3479-08.2008

Kostovic, I., Judas, M., Petanjek, Z., and Sitlic, G. (1995). Ontogenesis of goal-directed behavior: anatomo-functional considerations. *Int. J. Psychophysiol.* 19, 517–527. doi: 10.1016/0167-8760(94)00081-O

Latora, V., and Marchiori, M. (2001). Efficient behavior of small-networks. *Phys. Rev. Lett.* 87:198701. doi: 10.1103/PhysRevLett.87.198701

Lebel, C., Walker, L., Leemans, A., Phillips, L., and Beaulieu, C. (2008). Microstructural maturation of the human brain from childhood to adulthood. *Neuroimage* 40, 1044–1055. doi: 10.1016/j.neuroimage.2007.12.053

Lepage, J. F., and Theoret, H. (2006). EEG evidence for the presence of an action observation-execution matching system in children. *Eur. J. Neurosci.* 23, 2505–2510. doi: 10.1111/j.1460-9568.2006.04769.x

Lepage, J. F., and Theoret, H. (2007). The mirror neuron system: grasping others' actions from birth? *Dev. Sci.* 10, 513–523. doi: 10.1111/j.1467-7687.2007.00631.x

Lin, W., Zhu, Q., Gao, W., Chen, Y., Toh, C. H., Styner, M., et al. (2008). Functional connectivity MR imaging reveals cortical functional connectivity in the developing brain. *Am. J. Neuroradiol.* 29, 1883–1889. doi: 10.3174/ajnr.A1256

Marshall, P. J., Bar-Haim, Y., and Fox, N. A. (2002). Development of the EEG from 5 months to 4 years of age. *Clin. Neurophysiol.* 113, 1199–1208. doi: 10.1016/S1388-2457(02)00163-3

Marshall, P. J., and Meltzoff, A. N. (2011). Neural mirroring systems: exploring the EEG mu rhythm in human infancy. *Dev. Cogn. Neurosci.* 1, 110–123. doi: 10.1016/j.dcn.2010.09.001

Marshall, P. J., and Meltzoff, A. N. (2014). Neural mirroring mechanisms and imitation in human infants. *Philos. Trans. R. Soc. Lond. B Biol. Sci.* 369:20130620. doi: 10.1098/rstb.2013.0620

Molnar-Szakacs, I., Kaplan, J., Greenfield, P. M., and Iacobini, M. (2006). Observing complex action sequences: the role of fronto-parietal mirror neuron system. *Neuroimage* 33, 923–935. doi: 10.1016/j.neuroimage.2006.07.035

Muthukumaraswamy, S. D., and Johnson, B. W. (2004). Changes in Rolandic mu-rhythm during observation of a precision grip. *Psychophysiol* 41, 152–156. doi: 10.1046/j.1469-8986.2003.00129.x

Nakano, T., and Nakatani, K. (2014). Cortical networks for face perception in two-month-old infants. *Proc. Biol. Soc.* 281:20141468. doi: 10.1098/rspb.2014.1468

Nishitani, N., and Hari, R. (2000). Temporal dynamics of cortical representation for action. *Proc. Natl. Acad. Sci. U.S.A.* 97, 913–918. doi: 10.1073/pnas.97.2.913

Okada, Y., Pratt, K., Atwood, C., Mascarenas, A., Reineman, R., Nurminen, J., et al. (2006). BabySQUID: a mobile, high-resolution multichannel magnetoencephalography system for neonatal brain assessment. *Rev. Sci. Instrum.* 77, 1–9. doi: 10.1063/1.2168672

Orekhova, E. V., Stroganova, T. A., Posikera, I. N., and Elam, M. (2006). EEG theta rhythm in infants and preschool children. *Clin. Neurophysiol.* 117, 1047–1062. doi: 10.1016/j.clinph.2005.12.027

Pineda, J. A. (2005). The functional significance of mu-rhythms: translating "seeing" and "hearing" into "doing." *Brain Res. Brain Res. Rev.* 50, 57–68. doi: 10.1016/j.brainresrev.2005.04.005

Power, J. D., Fair, D. A., Schlaggar, B. L., and Petersen, S. E. (2010). The development of human functional brain networks. *Neuron* 67, 735–748. doi: 10.1016/j.neuron.2010.08.017

Reuter, J., Katoff, L., and Gruber, C. (1996). *Kent Inventory of Developmental Skills (KIDS)*. Los Angeles, CA: Western Psychological Services.

Righi, G., Tierney, A. L., Tager-Flusberg, H., and Nelson, C. A. (2014). Functional connectivity in the first year of life in infants at risk for autism spectrum disorder: an EEG study. *PLoS ONE* 9:e105176. doi: 10.1371/journal.pone.0105176

Rotem-Kohavi, N., Hilderman, C. G. E., Liu, A., Makan, N., Wang, J. Z., and Virji-Babul, N. (2014). Network analysis of perception-action coupling in infants. *Front. Hum. Neurosci.* 8:209. doi: 10.3389/fnhum.2014.00209

Rubinov, M., and Sporns, O. (2010). Complex network measures of brain connectivity: uses and interpretations. *Neuroimage* 52, 1059–1069. doi: 10.1016/j.neuroimage.2009.10.003

Ruther, N. M., Brown, E. C., Klepp, A., and Bellebaum, C. (2014). Observed manipulation of novel tools leads to mu rhythm suppression over sensory-motor cortices. *Behav. Brain Res.* 261, 328–335. doi: 10.1016/j.bbr.2013.12.033

Sepulcre, J., Liu, H., Talukdar, T., Martincorena, I., Yeo, B. T. T., and Buckner, R. L. (2010). The organization of local and distant functional connectivity in the human brain. *PLoS Comput. Biol.* 6:e1000808. doi: 10.1371/journal.pcbi.1000808

Simoes, C., Salenius, S., and Curio, G. (2004). Short-term prediction of perturbation dynamics for 10- and 20-Hz MEG rhythms in human primary sensorimotor hand cortices. *Neuroimage* 22, 387–393. doi: 10.1016/j.neuroimage.2003.12.045

Simpson, E. A., Murray, L., Paukner, A., and Ferrari, P. F. (2014). The mirror neuron system as revealed through neonatal imitation: presence from birth, predictive power and evidence of plasticity. *Philos Trans. R. Soc. Lond. B Biol. Sci.* 369:20130289. doi: 10.1098/rstb.2013.0289

Smit, D. J., Boersma, M., Schnack, H. G., Micheloyannis, S., Boomsma, D. I., Hulshoff, P. H. E., et al. (2012). The brain matures with stronger functional connectivity and decreased randomness of its network. *PLoS ONE* 7:e36896. doi: 10.1371/journal.pone.0036896

Smit, D. J., Boersma, M., van Beijsterveldt, C. E., Posthuma, D., Boomsma, D. I., Stam, C. J., et al. (2010). Endophenotypes in a dynamically connected brain. *Behav. Genet.* 40, 167–177. doi: 10.1007/s10519-009-9330-8

Smyser, C. D., Snyder, A. Z., and Neil, J. J. (2011). Functional connectivity MRI in infants: exploration of the functional organization of the developing brain. *Neuroimage* 56, 1437–1452. doi: 10.1016/j.neuroimage.2011.02.073

Southgate, V., Johnson, M. H., Osborne, T., and Csibra, G. (2009). Predictive motor activation during action observation in human infants. *Biol. Lett.* 5, 769–772. doi: 10.1098/rsbl.2009.0474

Stam, C. J. (2000). Functional connectivity patterns of human magnetoencephalographic recordings: a 'small-world' network? *Neurosci. Lett.* 355, 25–28. doi: 10.1016/j.neulet.2003.10.063

Stam, C. J., and van Djik, B. W. (2002). Synchronization likelihood: an unbiased measure of generalized synchronization in multivariate data sets. *Physica D* 163, 236–251. doi: 10.1016/S0167-2789(01)00386-4

Stiles, J., and Jernigan, T. L. (2010). The basics of brain development. *Neuropsychol. Rev.* 20, 327–348. doi: 10.1007/s11065-010-9148-4

Stroganova, T. A., Orekhova, E. V., and Posikera, I. N. (1999). EEG alpha rhythm in infants. *Clin. Neurophysiol.* 110, 997–1012. doi: 10.1016/S1388-2457(98)00009-1

Supekar, K., Musen, M., and Menon, V. (2009). Development of large-scale functional brain networks in children. *PLoS Biol.* 7:e1000157. doi: 10.1371/journal.pbio.1000157

Taga, G., Ikejiri, T., Tachibana, T., Shimojo, S., Soeda, A., Takeuchi, K., et al. (2002). Visual feature binding in early infancy. *Perception* 31, 273–286. doi: 10.1068/p3167

Tau, G. Z., and Peterson, B. S. (2009). Normal development of brain circuits. *Neuropsychopharmacol* 35, 147–168. doi: 10.1038/npp.2009.115

van Baal, G. C., Boomsma, D. I., and de Geus, E. J. (2001). Longitudinal genetic analysis of EEG coherence in young twins. *Behav. Genet.* 31, 637–651. doi: 10.1023/A:1013357714500

van Elk, M., van Schie, H. T., Hunnius, S., Vesper, C., and Bekkering, H. (2008). You'll never crawl alone: neurophysiological evidence for experience-dependent motor resonance in infancy. *Neuroimage* 43, 808–814. doi: 10.1016/j.neuroimage.2008.07.057

Vanhatalo, S., and Kaile, K. (2006). Development of neonatal EEG activity: from phenomenology to physiology. *Semin. Fetal Neonatal Med.* 11, 471–478. doi: 10.1016/j.siny.2006.07.008

van Schie, H. T., Koelewijn, T., Jensen, O., Oostenveld, R., Maris, E., and Bekkering, H. (2008). Evidence for fast, low-level motor resonance to action observation: an MEG study. *Soc. Neurosci.* 3, 213–228. doi: 10.1080/17470910701414364

van Wijk, B. C., Stam, C. J., and Daffertshofer, A. (2010). Comparing brain networks of different size and connectivity density using graph theory. *PLoS ONE* 5:e13701. doi: 10.1371/journal.pone.0013701

Virji-Babul, N., Rose, A., Moiseeva, N., and Makan, N. (2012). Neural correlates of action understanding in infants: influence of motor experience. *Brain Behav.* 2, 237–242. doi: 10.1002/brb3.50

Vogt, S., Buccino, G., Wohlschlager, A. M., Canessa, N., Shah, N. J., Zilles, K., et al. (2007). Prefrontal involvement in imitation learning of hand actions: effects of practice and expertise. *Neuroimage* 37, 1371–1383. doi: 10.1016/j.neuroimage.2007.07.005

Watts, D. J., and Strogatz, S. H. (1998). Collective dynamics of 'small-world?' networks. *Nature* 393, 440–442. doi: 10.1038/30918

Wu, K., Taki, Y., Sato, K., Hashizume, H., Sassa, Y., Takeuchi, H., et al. (2013). Topological organization of functional brain networks in healthy children: differences in relation to age, sex, and intelligence. *PLoS ONE* 8:e55347. doi: 10.1371/journal.pone.0055347

Yap, P. T., Fan, Y., Chen, Y., Gilmore, J. H., Lin, W., and Shen, D. (2011). Development trends of white matter connectivity in the first years of life. *PLoS ONE* 6:e24678. doi: 10.1371/journal.pone.0024678

Conflict of Interest Statement: The authors declare that the research was conducted in the absence of any commercial or financial relationships that could be construed as a potential conflict of interest.

Received: 24 November 2014; accepted: 14 January 2015; published online: 17 February 2015.

Citation: Berchicci M, Tamburro G and Comani S (2015) The intrahemispheric functional properties of the developing sensorimotor cortex are influenced by maturation. Front. Hum. Neurosci. ***9****:39. doi: 10.3389/fnhum.2015.00039*

This article was submitted to the journal Frontiers in Human Neuroscience.

frontiers in Human Neuroscience

ORIGINAL RESEARCH
published: 25 March 2015
doi: 10.3389/fnhum.2015.00153

Mothers say "baby" and their newborns do not choose to listen: a behavioral preference study to compare with ERP results

Christine Moon[1]*, *Randall C. Zernzach*[2] *and Patricia K. Kuhl*[3]

[1] Department of Psychology, Pacific Lutheran University, Tacoma, WA, USA, [2] Wilford Hall Ambulatory Surgical Center, 59th MDW, JBSA-Lackland, TX, USA, [3] Institute for Learning and Brain Sciences, University of Washington, Seattle, WA, USA

Previously published results from neonatal brain evoked response potential (ERP) experiments revealed different brain responses to the single word "baby" depending on whether it was recorded by the mother or an unfamiliar female. These results are consistent with behavioral preference studies in which infants altered pacifier sucking to contingently activate recordings of the maternal vs. an unfamiliar female voice, but the speech samples were much longer and information-rich than in the ERP studies. Both types of neonatal voice recognition studies imply postnatal retention of prenatal learning. The preference studies require infant motor and motivation systems to mount a response in addition to voice recognition. The current contingent sucking preference study was designed to test neonatal motivation to alter behavior when the reward is the single word "baby" recorded by the mother or an unfamiliar speaker. Results showed an absent or weak contingent sucking response to the brief maternal voice sample, and they demonstrate the complementary value of electrophysiological and behavioral studies for very early development. Neonates can apparently recognize the maternal voice in brief recorded sample (previous ERP results) but they are not sufficiently motivated by it to alter sucking behavior.

Keywords: auditory, behavior, fetal, learning, motivation, neonatal, non-nutritive sucking, preference

OPEN ACCESS

Edited by:
Marika Berchicci, University of Rome "Foro Italico" - Rome, Italy

Reviewed by:
Christine Parsons, University of Oxford, UK
Theofanis Panagiotaropoulos, Max Planck Institute for Biological Cybernetics, Germany

***Correspondence:**
Christine Moon, Department of Psychology, Pacific Lutheran University, 12180 Park Ave. S., Tacoma, WA 98447, USA
mooncm@plu.edu

Received: *24 November 2014*
Accepted: *06 March 2015*
Published: *25 March 2015*

Citation:
Moon C, Zernzach RC and Kuhl PK (2015) Mothers say "baby" and their newborns do not choose to listen: a behavioral preference study to compare with ERP results. Front. Hum. Neurosci. 9:153. doi: 10.3389/fnhum.2015.00153

Recent electrophysiological and brain imaging studies have advanced our understanding of the development of very early perception and learning through measurement of brain activity in response to specific events (May et al., 2011; Partanen et al., 2013; Kuhl et al., 2014). When there are differential responses to familiar vs. novel stimuli, learning and memory can be inferred. These methods permit localization to specific brain areas, and they are valuable for mapping the immature brain as it undergoes rapid development. It is, of course, ideal when brain activity can be linked to behavior, and the perception-action circuit is illuminated. Documenting the link can be difficult in early development because the competence-performance distinction (Chomsky, 1965) is particularly relevant. If the brain shows that a stimulus is recognized, there may be no corresponding measurable behavior because the individual cannot yet execute a motor response. A second consideration is that the path to behavior includes not only motor competence but also motivation. The newborn brain may detect an event, recognize it, and may be capable of rendering a motor response, but if the event is not sufficiently motivating, the infant will not mount the response.

Results of several experiments show that the newborn brain responds differentially to even a brief snippet of the maternal vs. a stranger female voice (Deregnier et al., 2000; deRegnier et al., 2002; Siddappa et al., 2004; Therien et al., 2004). In several studies, scalp recordings of brain activity in sleeping newborns using evoked response potentials (ERPs) used the brain's mismatch detection response to show this discrimination. This procedure requires that the stimuli be brief so the brain's rapid response can be time-locked to stimulus presentation. In the newborn ERP studies, the mother and stranger voice recordings were each limited to a brief sample of the word "baby" that averaged 750 ms. The midline brain response to both the maternal and novel voices was a positive wave appearing at 290 ms and that has been interpreted as reflecting auditory stimulus detection of both types of stimuli. For the novel voices only, the positive wave was accompanied by a negative slow wave that was interpreted as a response to novelty (deRegnier, 2005). The lack of a similar response to the maternal voice implies recognition of a familiar sound. The recognition response has been detected in newborns from uncomplicated pregnancies and births, whereas in newborns of iron-deficient (Siddappa et al., 2004) mothers and in extremely premature newborns (Therien et al., 2004), the differences are attenuated or absent. These ERP differences were interpreted as showing compromised recognition memory development in the infants of complicated pregnancies or deliveries.

Prior to these ERP results, it was not known whether newborns could even recognize their mothers' voices without the prosodic information present in lengthy and acoustically rich samples of talking or reading. Doubt about the limits of newborn voice recognition arose from analysis of intrauterine voice recordings (Querleu et al., 1988) and from behavioral experiments using only lengthy and acoustically rich voice samples. For a review, see Moon and Fifer (2000). It is now apparent that brief and relatively uninformative voice samples are sufficient for a differential brain response.

There have been several behavior-based investigations of maternal voice recognition. DeCasper and Fifer showed that neonates alter their behavior to selectively activate the sound of the mother reading a nursery rhyme (DeCasper and Fifer, 1980). Because the results were based on infants who had had no more than 12 h postnatal experience with their mother, their selective response to the maternal voice implied postnatal retention of prenatal learning. In the experiment, sound presentations of the maternal voice were contingent on infants altering their sucks on a pacifier. The authors compared the observed behavior to that of non-human infants who express "perceptual preference" and "proximity-seeking behavior" p.1176 (DeCasper and Fifer, 1980). Developmental psychobiologists and cognitive development researchers have described this kind of behavior as a "listening bias" (Vouloumanos and Werker, 2004), "operant choice" (Granier-Deferre et al., 2011), "operant learning" (Floccia et al., 1997) and "operant-choice preference" (Aldridge et al., 2001). The latter terms presuppose differential reinforcing value of the stimuli and motivation to respond. A contingent sound-sucking experiment using yoked-control methodology showed that the contingency is important in increasing sucking rates (Floccia et al., 1997). Thus, a measurable difference in neonatal preference or choice offers the opportunity to study motivation at the beginning of life.

Since 1980, experiments using contingent pacifier sucking have replicated and extended two main ideas: (i) humans learn before birth; and (ii) prenatal learning can affect postnatal behavior. The maternal voice preference has been robust in demonstrating learning in the womb. It has held whether the voice samples were highly melodic and rhythmic recordings of mothers reading nursery rhymes (DeCasper and Fifer, 1980) or relatively monotone adult conversation (Fifer and Moon, 1989). Although neonates respond to a simple maternal voice recording, they prefer a version that has been low pass filtered to simulate the voice *in utero* (Fifer and Moon, 1995; Spence and Freeman, 1996). A newborn experiment with fathers' and comparison male voices failed to show a preference, despite newborn discrimination of the two voices (DeCasper and Prescott, 1984). During the neonatal period, infants have expressed preferences for other sounds available *in utero* such as the mother's native vs. a foreign language (Mehler et al., 1988; Moon et al., 1993). The native over foreign language preference was replicated and extended in a study showing that, for infants of bilingual mothers, her two languages receive equivalent responses (Byers-Heinlein et al., 2010). Perhaps the most convincing example of prenatal learning's effect on postnatal preference are the results of an exposure study in which mothers read a nursery rhyme out loud during pregnancy. Newborns sucked more to activate the familiar rhyme vs. a novel rhyme, regardless of whether the voice was maternal (DeCasper and Spence, 1986). Thus, there is converging evidence from 35 years of laboratory research that shortly after birth infants are capable of employing prenatal experience, motor control, and the motivational system to mount a behavioral response when the consequence is hearing a familiar sound.

What has not been known up to now is whether the brief and recognizable sample of the maternal voice saying a single word is sufficiently motivating for newborns to mount a preference response. What follows is a description of an experiment using the preference procedure in which the consequence of infant sucking on a pacifier was the delivery through headphones of brief maternal and non-maternal voice samples of the word "baby". Thirty-six infants were in the experimental group of Mother-Stranger (MS) infants for whom the stimuli were the maternal vs. a stranger female voice. Twenty-four infants were in the Stranger-Stranger (SS) control group who heard two different non-maternal female voices. If the brief snippets of mother's voice are sufficiently motivating for newborns to alter sucking behavior to show a preference, then (Kuhl et al., 2014) sucking during opportunities to produce the maternal voice should exceed those for the stranger voice, and (May et al., 2011) sucking by the MS group should exceed that of the SS group.

Materials and Methods

Participants

Sixty term neonates (*M* age = 31 h, SD = 10.3) each completed an experimental session prior to discharge from the mother-baby

postpartum unit of a military medical center. They had no documented antenatal or birth complications, no risk factors for hearing loss (American Academy of Pediatrics Joint Committee on Infant Hearing, 2007), and English was the primary language spoken in the home. Infants were assigned to one of two conditions. In the MS Condition (N = 36), the stimuli were mother's and a stranger female's voice. In the Stranger-Stranger Condition (N = 24), the stimuli were two voices of unfamiliar females. In order to be included in the analysis, infants were required to complete a 10 min session with no more than two consecutive or three non-consecutive minutes in which no sucking occurred. Study sessions were terminated immediately if the infant became excessively fussy or cried. The data from 29 infants were excluded from analysis due to drowsiness (n = 18), crying/fussiness (n = 3), inconsistent sucking not apparently due to arousal state (n = 7), or experimenter error/equipment problems (n = 1).

Apparatus and Stimuli

Infants sucked on a Gerber Little Suzy Zoo pacifier fitted with a plastic tube connected to a Becton-Dickinson P23 × L pressure transducer that provided input to a Grass Telefactor CP122 Strain Gage Amplifier. The analogue output of the amplifier was converted to a digital signal by a Data Translation DT2814 data acquisition board that was connected to a Gateway 486 PC equipped with a ProAudio 16 sound card. Custom software recorded sucking pressure, controlled stimulus delivery, and created a summary data file. Analog pressure changes were converted into digital signals and served as input for a Gateway 486 PC. The computer delivered stimuli to the infants via Grado SR225 earphones suspended from a custom-made adjustable plexiglass frame that fit into the infant's bassinet. Voice stimuli were recorded using an Electro-Voice PL88H Microphone on a laptop computer. Analysis of the recorded speech samples was conducted using Signalyze Speech and Sound Analysis software on an Apple computer.

Each of 53 stimuli consisted of one naturalistic token of the word "baby" spoken in a woman's voice. Talkers had been instructed to say the declarative sentence, "He's/she's a baby" with a falling intonation contour. The statement was followed by four repetitions of the word "baby" using the same intonation contour. One voice token for each speaker was chosen on the basis of absence of background sound, clarity, loudness and presence of falling intonation contour. The mean duration of voice stimuli was 480.0 ms (s.d. 92.3). For the MS group, the Mother and Stranger stimuli did not significantly differ in duration, nor did the two voices in the SS condition. Pairs of stimuli were matched for loudness by two adult listeners and were presented at about 66 dBA as measured by a sound level meter (Bruel and Kjaer Model 2235) placed midway between the headphones.

Design and Procedure

The study was conducted according to a protocol that was approved by the medical center and university (PLU) ethics boards. For the MS infants, the stimuli were available during five one-minute periods of stimulus voice alternations for a total of 10 min (Cowan et al., 1982; Sansavini et al., 1997; Vouloumanos and Werker, 2007). The MS stimuli were counterbalanced for order of presentation (Mother First, N = 17, Stranger First, N = 19) and were delivered on a partial reinforcement schedule of a minimum of two qualifying sucks in quick succession for reinforcement. The Stranger-Stranger infants (SS) heard two different unfamiliar female voices, the availability of which alternated in one-minute intervals for 10 min. Each voice was thus available for five one-minute periods.

Parental informed consent was obtained in the mother-infant hospital room according to university- and medical center-approved protocols. For infants in the MS group, a recording of maternal voice was obtained at the bedside for subsequent editing. Each mother received a walkie-talkie to call when her infant appeared to be in a quiet and alert state. Infants were transported to the study room in the mother-baby unit where the headphone frame was placed in the bassinette and headphones were fitted next to the infants' ears. Prior to the beginning of the session, an experimenter swaddled the infant either snugly or loosely, based on the best judgment about supporting a quiet and alert state for 10 min. The experimental pacifier was given to infants and was held in place by an experimenter who listened to masking music through headphones during the session. After subjects demonstrated consistent sucking on the pacifier, usually no more than two to three minutes, the study session began by recording 1 min of baseline sucking data at the conclusion of which a threshold was established for stimulus delivery. The threshold was set at the 30th percentile of sucking amplitudes produced during the baseline minute. That is, sucks that were above the lowest 30% of baseline suck amplitudes resulted in stimulus activation. This is consistent with previous neonatal contingent sucking studies in which amplitude threshold has ranged from the 20th (Floccia et al., 2000; Vouloumanos and Werker, 2007) to the 50th (Floccia et al., 1997) percentiles of baseline.

Results

The dependent measure was the number of qualifying (above threshold) sucks per minute. Analyses included the factor of time (sequential minutes of the session) because previous studies have shown the emergence of a preference response over time (Sansavini et al., 1997; Vouloumanos and Werker, 2004, 2007). A D'Agostino-Pearson test of normality was conducted on the mean number of sucks per minute for the sample of 60 newborns, and results were consistent with a normal distribution, K^2 = 2.21, $p > 0.05$. A preliminary independent samples t-test was conducted on sucks during baseline for stimulus conditions MS vs. SS. There was a significant difference with greater mean sucks per minute of baseline for the MS group, M = 43.0, SD = 17.6 compared to the SS group, M = 31.9, SD = 19.2, $t_{(58)}$ = 2.3, p = 0.025. Baseline sucks were entered as a covariate in subsequent analyses.

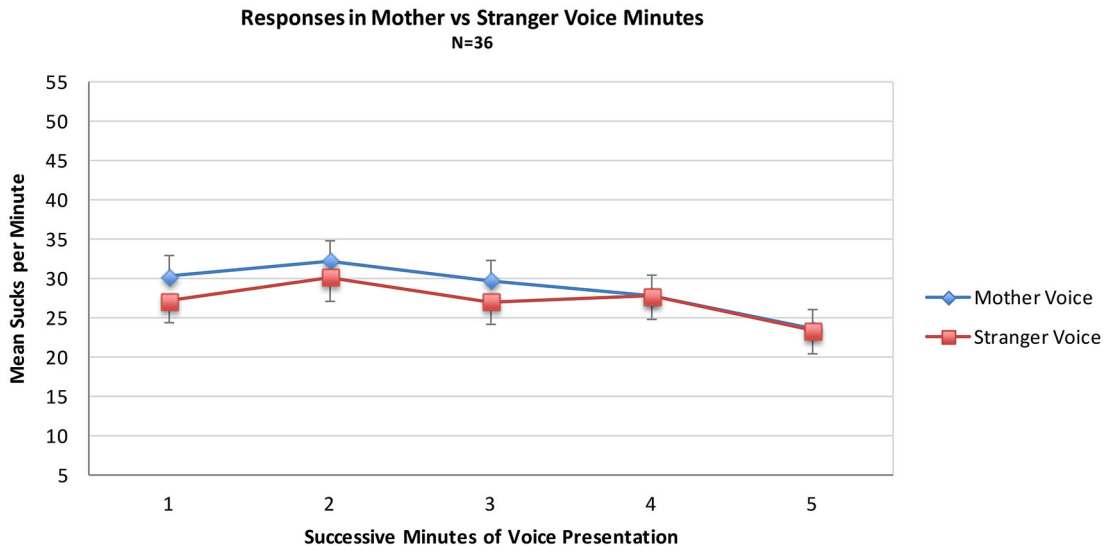

FIGURE 1 | Mean sucks per minute to the maternal vs. the stranger female voice. Voice stimuli were contingent on sucking, and the maternal and stranger voices alternated in five one-minute intervals of a 10 min presentation period.

TABLE 1 | Analysis of variance results for the Mother-Stranger group (*N* = 36).

Source	*Df*	*F*	η^2	*p*
Voice	1,33	0.36	0.01	0.55
Minutes	4,132	0.59	0.02	0.67
Order	1,33	2.63	0.07	0.11
Voice × Minutes	4,132	0.49	0.01	0.75
Voice × Order	1,33	2.28	0.07	0.14
Mins × Order	4,132	1.32	0.04	0.27
Voice × Min × Ord	4,132	0.93	0.03	0.45

Data from the MS group were used to test the hypothesis that sucks during minutes of opportunity to hear mother's voice would exceed those of stranger voice minutes. For the MS group (N = 36) a mixed 2 (**Voice**) × 2 (**Order** of voice presentation) × 5 (**Minutes**) ANOVA was conducted. There were no statistically significant main effects of the within-subjects variable Voice (Mother Voice sucks per minute: Mean = 28.7, SD = 16.3, Stranger Voice Mean = 27.0, SD = 14.4 or the between-subjects variable of Order. There was no main effect of Minutes nor were there any significant interaction effects. See **Figure 1**; **Table 1**.

An analysis was conducted with the entire sample comparing the MS (N = 36) and SS (N = 24) groups to test whether infant opportunities to suck to activate the maternal voice would result in more sucking overall during the 10 min session, whether or not a higher sucking frequency was confined to the maternal voice periods. A mixed two factor ANOVA included Stimulus Group (2) × Minutes (10). There was no main effect of Stimulus Group ($F_{(1,57)}$ = 1.9, p = 0.18, η_p^2 = 0.03), no main effect of Minutes ($F_{(1,513)}$ = 1.33, p = 0.22, η_p^2 = 0.02) and no interaction effect of Group X Minutes ($F_{(9,513)}$ = 0.89, p = 0.22, η_p^2 = 0.12). See **Figure 2**.

Discussion

Neither the direct comparison of responses to the maternal vs. stranger voices nor the indirect comparison in present vs. absent maternal voice provides statistically significant evidence for a preference for the maternal voice. Visual inspection of the pattern of the two MS sub-groups in **Figure 2** provides some evidence for a preference response in the transitions mother-to-stranger (Mother First group) and stranger-to-mother (Stranger First group) over 10 min.

One possible explanation for the absent or weak behavioral response to mother's voice that can be ruled out is that infants could not recognize the maternal voice in the brief sample. Previously published ERP studies demonstrate otherwise, at least in infants without complicated prenatal and birth histories. Moreover, previous sucking experiments have shown that neonates can respond differentially to brief speech samples such as syllables or vowels (Moon and Fifer, 1990; Moon et al., 1992, 1993; Floccia et al., 2000).

Although the newborns were able to discriminate the maternal and the stranger voices, the brief, repetitive sample of the maternal voice was apparently not sufficiently motivating for them to suck to activate it significantly more frequently than the alternative. There are other published reports of newborn failure to show a voice preference in contingent sucking procedures. For example, infants did not differentially suck to activate a recording of father's vs. a stranger male voice although they could discriminate the voices (DeCasper and Prescott, 1984). Newborns did not show a maternal voice preference when mother's and stranger voices were whispered (Spence and Freeman, 1996) and they showed no preference when hearing recordings of their bilingual mothers' two languages (Byers-Heinlein et al., 2010).

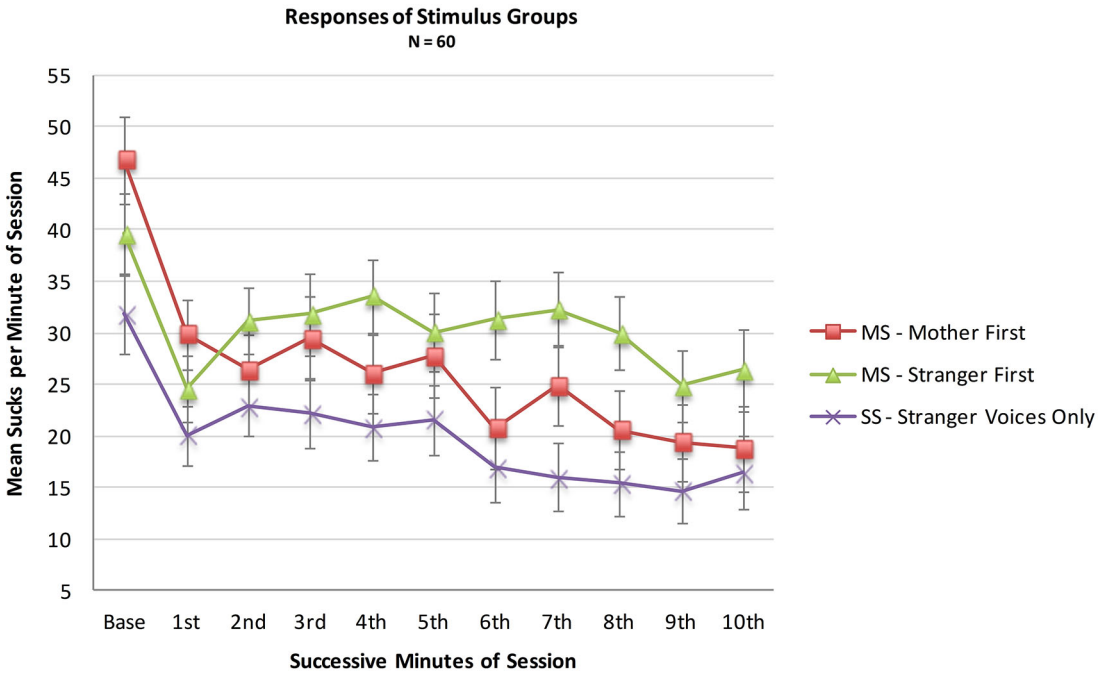

FIGURE 2 | Mean sucks per minute in the 10 min presentation period of the two MS groups (*N* = 36 total) and the Stranger-Stranger Group (*N* = 24). For the MS-Mother first group, the maternal voice was presented in minutes 1, 3, 5, 7, and 9. For the MS-Stranger first group, the maternal voice was presented in minutes 2, 4, 6, 8, and 10.

Collecting behavioral data from neonates has limitations. There are many sources of variability that are difficult to control such as rapid changes in infant state, competing infant behaviors, and internal perceptual events that are often unspecifiable. In the current study, the attrition rate was 33 per cent. Although this rate is typical or even low for contingent sucking experiments (Floccia et al., 1997, 2000; Vouloumanos and Werker, 2007), it is an indicator of the inherent variability in behavior-based data collection with neonates. Although the current study was conducted by experienced neonatal researchers using a standard contingent sucking protocol, it certainly merits replication, at best with extension to other forms of familiar and unfamiliar stimuli, especially those of caregivers over time as newborns adjust to postnatal life.

Taken all together, the current results add to the literature on neonatal behavioral preferences for sounds, and they complement previously published, electrophysiological results. They inform us about incipient capacities in very early development. In the absence of robust behavioral evidence for discrimination and therefore recognition of mother's voice, the presence of differential ERP responses confirms that the two auditory signals are, in fact, processed differently by the neonatal brain, at least for infants with uncomplicated pre- and early postnatal histories. Mother's voice is recognized, even in the impoverished form. The presence or, in this case, the absence of overt behavior informs about the relative salience of the signal and, perhaps, its hedonic valence, something that electrophysiological measures do not provide at present. Mother's familiar talking or reading voice with its unique and characteristic changes over time in pitch, rhythm and loudness is sufficiently salient and positively valenced that neonates are motivated to act to produce more of it (DeCasper and Fifer, 1980; Fifer and Moon, 1989). Without these characteristics in the sound of the maternal voice, they apparently are not. As newborn brain imaging techniques advance, more will be known about the development of brain organization for perception, memory, motivation and motor control. It will be important to complement this understanding with increasing knowledge about the actions that result.

Acknowledgments

We thank the families and staff at Madigan Army Medical Center for their support of the study. The views expressed in the article are those of the authors and do not reflect the official policy of the Department of the Army, the Department of Defense or the U.S. Government. This research was supported by a National Institutes of Health Grant HD 37954 to PKK. Software was generously provided by Anne Christophe of the Centre National de la Recherche Nationale, Paris, France. Student research assistants were: Jung Chong, R. Todd Davis, and Scott Nguy.

References

Aldridge, M. A., Stillman, R. D., and Bower, T. G. R. (2001). Newborn categorization of vowel-like sounds. *Dev. Sci.* 4, 220–232. doi: 10.1111/1467-7687.00167

American Academy of Pediatrics Joint Committee on Infant Hearing (2007). Year 2007 position statement: principles and guidelines for early hearing detection and intervention programs. *Pediatrics* 120, 898–921. doi: 10.1542/peds.2007-2333

Byers-Heinlein, K., Burns, T. C., and Werker, J. F. (2010). The roots of bilingualism in newborns. *Psychol. Sci.* 21, 343–348. doi: 10.1177/0956797609360758

Chomsky, N. (1965). *Aspects of the Theory of Syntax*. Oxford, England: M.I.T. Press.

Cowan, N., Suomi, K., and Morse, P. A. (1982). Echoic storage in infant perception. *Child Dev.* 53, 984–990. doi: 10.2307/1129138

DeCasper, A. J., and Fifer, W. P. (1980). Of human bonding: newborns prefer their mothers' voices. *Science* 208, 1174–1176. doi: 10.1126/science.7375928

DeCasper, A. J., and Prescott, P. A. (1984). Human newborns' perception of male voices: preference, discrimination and reinforcing value. *Dev. Psychobiol.* 17, 481–491. doi: 10.1002/dev.420170506

DeCasper, A. J., and Spence, M. J. (1986). Prenatal maternal speech influences newborns' perception of speech sounds. *Infant Behav. Dev.* 9, 133–150. doi: 10.1016/0163-6383(86)90025-1

deRegnier, R. A. (2005). Neurophysiologic evaluation of early cognitive development in high-risk infants and toddlers. *Ment. Retard. Dev. Disabil. Res. Rev.* 11, 317–324. doi: 10.1002/mrdd.20085

Deregnier, R. A., Nelson, C. A., Thomas, K. M., Wewerka, S., and Georgieff, M. K. (2000). Neurophysiologic evaluation of auditory recognition memory in healthy newborn infants and infants of diabetic mothers. *J. Pediatr.* 137, 777–784. doi: 10.1067/mpd.2000.109149

deRegnier, R. A., Wewerka, S., Georgieff, M. K., Mattia, F., and Nelson, C. A. (2002). Influences of postconceptional age and postnatal experience on the development of auditory recognition memory in the newborn infant. *Dev. Psychobiol.* 41, 216–225. doi: 10.1002/dev.10070

Fifer, W. P., and Moon, C. (1989). Psychobiology of newborn auditory preferences. *Semin. Perinatol.* 13, 430–433.

Fifer, W. P., and Moon, C. M. (1995). "The effects of fetal experience with sound," in *Fetal Development: A Psychobiological Approach*, eds J. P. Lecanuet, N. A. Krasnegor, W. P. Fifer and W. P. Smotherman (Hillsdale, NJ: Lawrence Erlbaum), 351–366.

Floccia, C., Christophe, A., and Bertoncini, J. (1997). High-amplitude sucking and newborns: the quest for underlying mechanisms. *J. Exp. Child Psychol.* 64, 175–198. doi: 10.1006/jecp.1996.2349

Floccia, C., Nazzi, T., and Bertoncini, J. (2000). Unfamiliar voice discrimination for short stimuli in newborns. *Dev. Sci.* 3, 333–343. doi: 10.1111/1467-7687.00128

Granier-Deferre, C., Ribeiro, A., Jacquet, A.-Y., and Bassereau, S. (2011). Near-term fetuses process temporal features of speech. *Dev. Sci.* 14, 336–352. doi: 10.1111/j.1467-7687.2010.00978.x

Kuhl, P. K., Ramírez, R. R., Bosseler, A., Lin, J. F., and Imada, T. (2014). Infants' brain responses to speech suggest analysis by synthesis. *Proc. Natl. Acad. Sci. U S A* 111, 11238–11245. doi: 10.1073/pnas.1410963111

May, L., Byers-Heinlein, K., Gervain, J., and Werker, J. F. (2011). Language and the newborn brain: does prenatal language experience shape the neonate neural response to speech? *Front. Psychol.* 2:222. doi: 10.3389/fpsyg.2011.00222

Mehler, J., Jusczyk, P. W., Lambertz, G., Halsted, N., Bertoncini, J., and Amiel-Tison, C. (1988). A precursor of language acquisition in young infants'. *Cognition* 29, 143–178. doi: 10.1016/0010-0277(88)90035-2

Moon, C. M., Bever, T. G., and Fifer, W. P. (1992). Canonical and non-canonical syllable discrimination by two-day-old infants. *J. Child Lang.* 19, 1–17. doi: 10.1017/S030500090001360X

Moon, C., and Fifer, W. P. (1990). Syllables as signals for 2-day-old infants. *Infant Behav. Dev.* 13, 377–390. doi: 10.1016/0163-6383(90)90041-6

Moon, C. M., and Fifer, W. P. (2000). Evidence of transnatal auditory learning. *J. Perinatol.* 20, S37–S44. doi: 10.1038/sj.jp.7200448

Moon, C., Panneton Cooper, R., and Fifer, W. P. (1993). Two-day-olds prefer their native language. *Infant Behav. Dev.* 16, 495–500. doi: 10.1016/0163-6383(93)80007-u

Partanen, E., Kujala, T., Naatanen, R., Liitola, A., Sambeth, A., and Huotilainen, M. (2013). Learning-induced neural plasticity of speech processing before birth. *Proc. Natl. Acad. Sci. U S A* 110, 15145–15150. doi: 10.1073/pnas.1302159110

Querleu, D., Renard, X., Versyp, F., Paris-Delrue, L., and Crèpin, G. (1988). Fetal hearing. *Eur. J. Obstet. Gynecol. Reprod. Biol.* 28, 191–212. doi: 10.1016/0028-2243(88)90030-5

Sansavini, A., Bertoncini, A., and Giovanelli, G. (1997). Newborns discriminate the rhythm of multisyllabic stressed words. *Dev. Psychol.* 33, 3–11. doi: 10.1037//0012-1649.33.1.3

Siddappa, A. M., Georgieff, M. K., Wewerka, S., Worwa, C., Nelson, C. A., and Deregnier, R. A. (2004). Iron deficiency alters auditory recognition memory in newborn infants of diabetic mothers. *Pediatr. Res.* 55, 1034–1041. doi: 10.1203/01.pdr.0000127021.38207.62

Spence, M. J., and Freeman, M. S. (1996). Newborn infants prefer the maternal low-pass filtered voice, but not the maternal whispered voice. *Infant Behav. Dev.* 19, 199–212. doi: 10.1016/s0163-6383(96)90019-3

Therien, J. M., Worwa, C. T., Mattia, F. R., and deRegnier, R. A. (2004). Altered pathways for auditory discrimination and recognition memory in preterm infants. *Dev. Med. Child Neurol.* 46, 816–824. doi: 10.1111/j.1469-8749.2004.tb00447.x

Vouloumanos, A., and Werker, J. F. (2004). Tuned to the signal: the privileged status of speech for young infants. *Dev. Sci.* 7, 270–276. doi: 10.1111/j.1467-7687.2004.00345.x

Vouloumanos, A., and Werker, J. F. (2007). Listening to language at birth: evidence for a bias for speech in neonates. *Dev. Sci.* 10, 159–164. doi: 10.1111/j.1467-7687.2007.00549.x

Conflict of Interest Statement: The authors declare that the research was conducted in the absence of any commercial or financial relationships that could be construed as a potential conflict of interest.

frontiers in Human Neuroscience

ORIGINAL RESEARCH
published: 23 April 2015
doi: 10.3389/fnhum.2015.00189

Objective differentiation of neonatal EEG background grades using detrended fluctuation analysis

Vladimir Matic[1,2]*, *Perumpillichira Joseph Cherian*[3], *Ninah Koolen*[1,2], *Amir H. Ansari*[1,2], *Gunnar Naulaers*[4], *Paul Govaert*[5], *Sabine Van Huffel*[1,2], *Maarten De Vos*[6] and *Sampsa Vanhatalo*[7]

[1] Department of Electrical Engineering (ESAT), STADIUS Centre for Dynamical Systems, Signal Processing and Data Analytics, KU Leuven, Leuven, Belgium, [2] iMinds Medical IT Department, Leuven, Belgium, [3] Section of Clinical Neurophysiology, Department of Neurology, Erasmus MC, University Medical Center, Rotterdam, The Netherlands, [4] Neonatal Intensive Care Unit, University Hospital Gasthuisberg, Leuven, Belgium, [5] Section of Neonatology, Department of Pediatrics, Erasmus MC-Sophia Children's Hospital, University Medical Center, Rotterdam, Netherlands, [6] Department of Engineering, Institute of Biomedical Engineering, University of Oxford, Oxford, UK, [7] Department of Children's Clinical Neurophysiology, HUS Medical Imaging Center and Children's Hospital, Helsinki University Central Hospital and University of Helsinki, Helsinki, Finland

A quantitative and objective assessment of background electroencephalograph (EEG) in sick neonates remains an everyday clinical challenge. We studied whether long range temporal correlations quantified by detrended fluctuation analysis (DFA) could be used in the neonatal EEG to distinguish different grades of abnormality in the background EEG activity. Long-term EEG records of 34 neonates were collected after perinatal asphyxia, and their background was scored in 1 h epochs (8 h in each neonate) as mild, moderate or severe. We applied DFA on 15 min long, non-overlapping EEG epochs ($n = 1088$) filtered from 3 to 8 Hz. Our formal feasibility study suggested that DFA exponent can be reliably assessed in only part of the EEG epochs, and in only relatively short time scales (10–60 s), while it becomes ambiguous if longer time scales are considered. This prompted further exploration whether paradigm used for quantifying multifractal DFA (MF-DFA) could be applied in a more efficient way, and whether metrics from MF-DFA paradigm could yield useful benchmark with existing clinical EEG gradings. Comparison of MF-DFA metrics showed a significant difference between three visually assessed background EEG grades. MF-DFA parameters were also significantly correlated to interburst intervals quantified with our previously developed automated detector. Finally, we piloted a monitoring application of MF-DFA metrics and showed their evolution during patient recovery from asphyxia. Our exploratory study showed that neonatal EEG can be quantified using multifractal metrics, which might offer a suitable parameter to quantify the grade of EEG background, or to monitor changes in brain state that take place during long-term brain monitoring.

Keywords: asphyxia, detrended fluctuation analysis, multifractal, background EEG, brain monitoring

OPEN ACCESS

Edited by:
Silvia Comani, Università degli Studi "G. d'Annunzio," Italy

Reviewed by:
Luc Berthouze, University of Sussex, UK
Pål Gunnar Larsson, Oslo University Hospital, Norway

***Correspondence:**
Vladimir Matic, Division STADIUS-BIOMED, Department of Electrical Engineering, KU Leuven, Kasteelpark Arenberg 10 - bus 2446, 3000 Leuven, Belgium
maticvl@gmail.com; vladimir.matic@esat.kuleuven.be

Received: *25 November 2014*
Accepted: *20 March 2015*
Published: *23 April 2015*

Citation:
Matic V, Cherian PJ, Koolen N, Ansari AH, Naulaers G, Govaert P, Van Huffel S, De Vos M and Vanhatalo S (2015) Objective differentiation of neonatal EEG background grades using detrended fluctuation analysis. Front. Hum. Neurosci. 9:189. doi: 10.3389/fnhum.2015.00189

Introduction

Development of neonatal care has led to an increasing interest in continuous brain monitoring for individually optimized neurological treatment. Scalp electroencephalography (EEG) is the most

commonly used, non-invasive method in the continuous monitoring of brain function in the neonatal intensive care units (NICU). While neonatal EEG monitoring is becoming a standard of care in many NICUs, the interpretation of continuous EEG records in a 24/7 mode remains a global challenge, especially because of shortage of the special expertise required for an adequate visual reading (Boylan et al., 2010). One solution to this over the past decade has been the use of compressed displays, especially the amplitude integrated EEG (aEEG, a.k.a. CFM; De Vries and Hellström-Westas, 2005), which enables easier review of selected EEG features at bedside. However, it is now well recognized that aEEG trends are susceptible to artifacts that require special expertise in aEEG reading, and yet, the aEEG interpretation is qualitative and subjective.

The current main challenge in the EEG interpretation is to objectively and quantitatively characterize the spontaneous, ongoing brain activity, often called "background activity" in the EEG nomenclature. It has been shown that the EEG background is most informative when it comes to assessing acute state or predicting future outcome of the brain (Monod et al., 1972; Watanabe et al., 1999; Menache et al., 2002). Several background grading systems have been published over the years (Watanabe et al., 1999; Murray et al., 2009; Cherian et al., 2011; Walsh et al., 2011), and they combine visually (i.e., subjectively) observed EEG properties to yield one, holistic EEG grade. Perhaps due to the high interindividual variability and ambiguity in visual assessments, the clinically used EEG grading is remarkably rough. For instance, ranges of interburst intervals (IBI) between mild and moderate EEG grades go in 5 s increments from <5 to 5–10 s till >10 s, respectively (Murray et al., 2009; Cherian et al., 2011).

It is intuitively obvious, that so rough EEG grading cannot adequately reflect the time-varying physiological state of the brain, although it allows a technically straightforward translation of the criteria into automated classifiers. Intriguingly, classifiers based on these same criteria are not able to fully emulate the visual grading (Murray et al., 2009; Korotchikova et al., 2011; Stevenson et al., 2013), which indirectly calls for identification of novel EEG features with clinical relevance.

Recent work in basic neuroscience has provided ample evidence that many brain behaviors exhibit scale-free properties where dynamics of a given feature have no distinct spatial or temporal scale (Beggs and Plenz, 2003; Fransson et al., 2013; Iyer et al., 2014; Roberts et al., 2014). This was also recently shown to be the case for the EEG activity of full-term neonates that recover from perinatal asphyxia (Iyer et al., 2014; Roberts et al., 2014), one of the most common reasons for continuous EEG monitoring in the NICUs.

Scale-free dynamics in a complex system can give rise to self-similarity over temporal scales, i.e., long-range temporal correlations (LRTC), which may be assessed from the EEG using detrended fluctuation analysis (DFA; Peng et al., 1994; Hardstone et al., 2012). Recent work has shown that LRTC in brain function is significantly affected by various clinical conditions (Linkenkaer-Hansen et al., 2001; Parish et al., 2004; Stam et al., 2005; Monto et al., 2007). Compared to the conventional, visually defined EEG features, LRTC reaches beyond the visually perceived time scales, while it also integrates multiple time scales (from seconds to minutes) into one mathematically and conceptually transparent estimate. Moreover, DFA as a paradigm is very strongly supported by theoretical, experimental and clinical studies (for review, see Hardstone et al., 2012). In addition, a small number of neonates have been studied and long-range temporal correlations have been explored (Berthouze et al., 2010). Recent development of signal analysis methods has extended DFA to multifractal DFA (MF-DFA), which characterizes time series with multiple co-existent dynamic processes that may give rise to temporally local fluctuations including both extreme small and large magnitudes. Several studies have reported MF-DFA to offer additional insight in experimental and clinical neuroscience contexts (Kantelhardt et al., 2002; Zorick and Mandelkern, 2013). The neonatal EEG is, indeed, an example of signal with extreme, apparently erratic fluctuations in signal amplitudes, making it potentially suitable for MF-DFA paradigm as well. Notably, a recent study provided evidence of fractal behavior in time series of interburst intervals in preterm babies (Hartley et al., 2012).

The present study was set out to examine the possibility that neonatal EEG exhibits LRTC, which can be used as a feature to assess brain condition in a clinically relevant context. This entails answering the following questions: First, is it possible to assess reliable DFA exponents from the neonatal EEG at clinically relevant time scales from seconds to tens of minutes? Second, if DFA is suboptimal, can metrics from an existing MF-DFA paradigm reflect neonatal EEG in a meaningful way? Third, is it possible to use these measures to distinguish background grades of the neonatal EEG? The last question offers a benchmark to the existing analysis paradigms, while it is also directly relevant for development of novel features for automated background EEG classifiers.

Materials and Methods

The present study was designed to proceed sequentially. We first examined the mathematical and physiological feasibility of the DFA approach in neonatal EEG analysis, and we studied the DFA fluctuation plots for differences in our clinical populations (different EEG grades). After observing mathematical limitations with the DFA paradigm, the work was continued to test MF-DFA paradigm, and finally to benchmark MF-DFA metrics with clinical EEG grading.

Dataset

We used altogether 1088 15 min epochs (total 272 h) from 34 neonates that were recorded for clinical reasons at Sophia Children's Hospital, Erasmus MC (Rotterdam, the Netherlands). These neonates were part of a larger cohort of term asphyxiated neonates who were monitored from March 2003 till August 2007. Other results from this cohort have been published previously (Deburchgraeve et al., 2008; Cherian et al., 2011; De Vos et al., 2011; Matic et al., 2014). The clinical inclusion criteria for EEG monitoring were: gestational age of 37–43 weeks with clinical features of encephalopathy, and having at least one of the following features of birth asphyxia: (a) arterial pH of umbilical cord blood ≤ 7.1, (b) Apgar score ≤ 5 at 5 min, and (c) high clinical suspicion (like fetal distress, umbilical cord prolapse, difficult

labor, or a history of convulsions). Exclusion criteria were: congenital cardiac abnormalities or other multiple anomalies, inborn errors of metabolism, and constantly isoelectric (<5 μV) EEG activity. The study had the approval of the Erasmus MC Medical Ethical Review Board. Informed consent was obtained from the parents/guardians prior to the onset of the registration. The EEG recordings started 2–48 (median 19) h post-partum. The median duration of EEG was 31 (range 20–96) h. Seizures were recorded in 18 patients, however this clinical information was not considered in the later analyses further than confirming that distribution of DFA/MF-DFA metrics was not statistically significantly different between babies with vs. without seizures (calculated separately for each background category).

EEG Sampling

The EEG was recorded with NicOne EEG recorder (Cardinal Healthcare, Madison, WI, USA) at sampling frequency of 256 Hz and our current data analysis was performed using bipolar montage with 12 derivations. Four epochs of 2 h continuous EEG recordings were selected per neonate with a minimal distance between them longer than 4 h.

Feasibility of DFA in the Neonatal EEG

Detrended Fluctuation Analysis (DFA), originally introduced by Peng et al. (1994), is a widely applied method to quantify LRTC in various biological time series that exhibit self-similarity over multiple time scales. In the context of EEG analysis, DFA is typically computed by measuring amplitude dynamics of selected frequency bands (cf. Hardstone et al., 2012). In the first step, after band-specific amplitude extraction, the DFA procedure splits the signal into time windows (time scale—*s*), detrends the EEG segment, and computes the variance of amplitude fluctuations. In the second step, a DFA plot is generated by plotting the average signal variance per each window size on log-log coordinates (time scale—*s*, Fluctuation function—*F* in **Figures 1C,E**). Finally, a linear fit of this fluctuation function gives the DFA output, the scaling exponent α (cf. Appendix A; Hardstone et al., 2012).

Use of DFA paradigm requires defining several parameters so that they comply with the *a priori* known characteristics of the given biological signal. These include definitions of (1) the frequency band which is used for the signal envelope extraction (2) the epoch lengths, *time scales,* that are used to calculate the fluctuation function as well as (3) the range of time windows over which the slope of the linear fit (exponent α) is calculated (see **Figure 1C**).

Epoch Length

We analyzed data epochs of 300, 600, 900, and 3600 s duration, but the final analysis was then carried out using 900 s (15 min) epochs. The choice was to strike a practical compromise between obtaining enough data for a reliable DFA plot, yet having likely a consistent background state in the given window. Our clinical background grading was performed initially in 15 min epochs, hence 900 s was practical for benchmarking purposes.

Frequency Band

Neonatal EEG, especially in the acute state after asphyxic injury as in our data series, is dominated by intermittent bursting activity that consists of oscillations mostly at about 0.1–10 Hz. The lowest frequencies may be unpredictably contaminated by movement and other artifacts, so they were filtered out using a FIR high-pass filter at 3 Hz. We chose to use a lowpass FIR filter at 8 Hz to maximally limit our analysis to the previously described 3–8 Hz band (Palmu et al., 2010; Tokariev et al., 2012; Omidvarnia et al., 2014). However, we also examined other frequency bands (1–3 and 1–5 Hz), and we got qualitatively comparable findings (data not shown).

Time Scale (DFA Window)

Feasibility of the DFA method requires that the signal does exhibit genuine LRTC, which in an ideal case could be seen over all time scales up to the limits of the recording time. The shortest time scale is defined by the need to include multiple fluctuation cycles of interest to really assess its temporal correlations (cf. Hardstone et al., 2012). In the present context, the amplitude fluctuations in the early recovering neonatal EEG consist of intermittent bursting at multi-second scale. The selected frequency band (3–8 Hz) gives slowest fluctuations with a duration of around 1 s (Tokariev et al., 2012), which suggested to use the lowest time scale of 10 s. The upper range can be physiologically limited by the spontaneous changes in the brain state over time, especially vigilance state cycling that occurs 1–3 times per hour in the neonatal brain (Stevenson et al., 2014). However, the upper limit of feasible scales can also be reasoned mathematically, since estimation of the DFA exponent α is based on linear fitting in the DFA plot over the given time scale (see below; **Figure 1C**).

Next, we continued quantitatively by analysing how well the linear fitting suits to different ranges of windows (5–60, 10–60, 10–100, and 10–300 s) in the fluctuation functions. Two independent techniques were used: The first method was developed by Botcharova et al. (2013) based on the maximum likelihood approach that compares a set of alternative models: linear, polynomial, root, exponential, logarithmic, and spline functions. This paradigm identifies the best fit model when the involved number of parameters is minimal and over-fitting is penalized. The second method was less strict, and adopted from prior studies (e.g., Linkenkaer-Hansen et al., 2001), based on computing the standard linear regression fit, R^{2}·, and using a predefined threshold of 0.97 to indicate acceptance of the epochs for DFA analysis. More details about both results are shown in the Supplemental Data and they confirm that results obtained with the maximum likelihood based approach are valid.

Feasibility Of MF-DFA in the Neonatal EEG

Various complex systems and physiological time series may show LRTC although they cannot be characterized with a single parameter (monofractal; for a review, see Ihlen, 2012). For instance, there may be clear monofractal dynamics at distinct, narrow time scales bounded by deflections in the log-log fluctuation plot (so called "crossover points"; Kantelhardt et al., 2002). Then, instead of a single linear approximation, the fluctuation function can be better described as a set of linear approximations, yielding different scaling exponents for different time scales. They are called multifractal time series, where the set of scaling exponents,

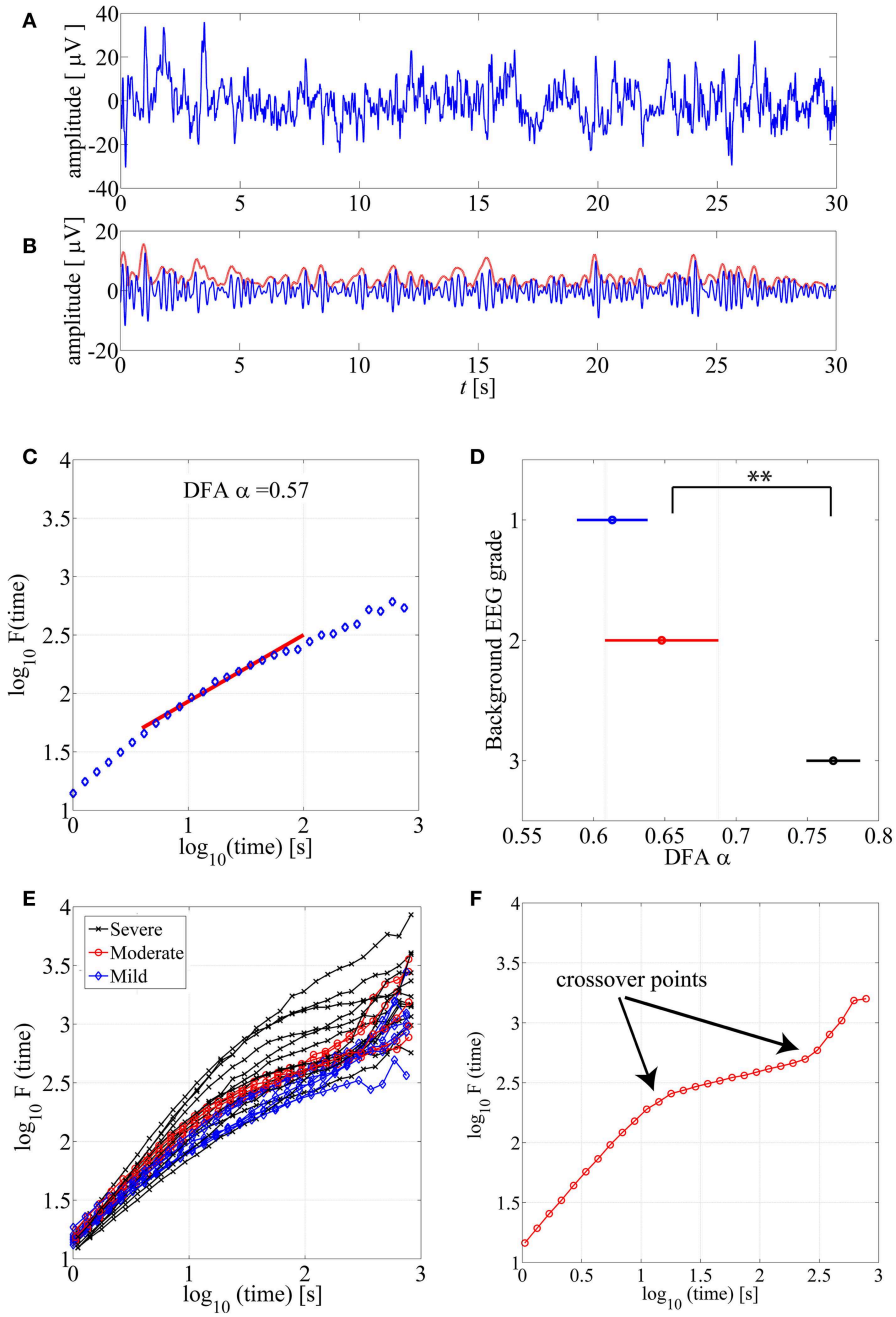

FIGURE 1 | (A) An example of normal neonatal EEG signal with continuous background pattern. **(B)** The signal is band-pass filtered between 3–8 Hz (blue), and the instantaneous amplitude envelope (red) is calculated using Hilbert transform. **(C)** The DFA fluctuation function is presented along the Y axis, whereas the size of the windows analyzed in the DFA method are displayed in the X axis. The red line presents an example of linear fluctuation function that is here fitted for the time scale 10–60 s to obtain its slope, the DFA scaling exponent α. **(D)** DFA fluctuation functions are plotted for 15 min EEG epochs from different background EEG abnormalities (Mild-blue, Moderate-red, Severe-black). Statistically significant differences can be observed between different background EEG classes (**$p < 0.01$). This figure only shows examples of such EEG epochs where linear fit ($R^2 > 0.97$) was confirmed. **(E)** Comparison of scaling exponent α between different background EEG grades shows a significant difference between grades 2 and 3. **(F)** An example of the DFA fluctuation function (moderate EEG grade) where clear existence of the crossover points are illustrated.

or parameters, are called *q*-order (generalized) Hurst exponents (Ihlen, 2012). For monofractal time series, the *q*-order Hurst exponents will have equal values, whereas in multifractal time series, the *q*-order Hurst exponents will be significantly diversified. A common reason for multifractality is that the signal may exhibit different LRTC for temporally *local* small and large

fluctuations. In contrast, monofractal time series are mainly noise like (e.g., white noise; cf. Ihlen, 2012) and they do not show *local* periods of either extremely small or large fluctuations. Hence, the known non-stationarity of the fluctuations in the neonatal EEG does, indeed, suggest that MF-DFA may offer better handling of the temporal EEG dynamics (e.g., local suppression and burst periods). Mathematically, MF-DFA differs from the DFA only in the calculation of the q-order fluctuation functions, F_q (**Figures 2B1,B2**), which is followed with the extraction of the q-order Hurst exponents (**Figures 2C1,C2**; see also Appendix A). Next, MF-DFA can be plotted as a so called multifractal spectrum, which can be quantified with mathematically robust metrics. The conventional MF-DFA metrics included *mean* h_q, *width* h_q, *mean* D_q, and *height* D_q (see **Figure 3D** for their graphical presentation). The *width*_h_q is calculated as the difference between maximal and minimal h_q values, whereas *height*_$D_q$is calculated as the difference between maximal and minimal $D_q$values (as suggested in Zorick and Mandelkern (2013). Mean $h_q$and mean D_q are calculated by averaging all data points across spectra and across 12 channels. The statistical results are presented in **Figures 3E–H**.

In addition, the difference between DFA and MF-DFA can be observed only within the relatively short time scales (e.g., less than 100 s) and within MF-DFA concept the linear fitting from 1 s till 128 s was applied in this work.

Benchmarking with EEG Grades

The ultimate goal in the present study was to establish the applicability of DFA or MF-DFA metrics in quantification of background EEG abnormalities. To this end, we had two benchmarking methods, visual and automated background classification.

Both DFA exponent and four MF-DFA metrics were calculated exactly the same way for each 15 min EEG epochs that also had a known visually scored background EEG grade inherited jointly for all four 15 min epochs within the given hour of EEG.

The visual background grading was performed by an experienced clinical neurophysiologist (PJC), blinded to the clinical details of the neonates. A three level EEG grading was adapted from Murray et al. (2009) as follows: (a) normal/mild (IBIs $<$ 5 s; poorly organized sleep-wake cycle; recovered, continuous background EEG), (b) moderate (5 s $\leq$ IBIs $<$ 10 s), and (c) severe (10 s $\leq$ IBI s$<$ 60 s; dominated by prolonged and marked suppressions).

The automated background grading was taken from the automatically computed inter-burst intervals (IBI). This was generated using the automated IBI detection method described in Matic et al. (2012). The main steps of this algorithm are summarized in the Appendix B. Subsequently, we used mean IBI values and compared them with MF-DFA based parameters. All data points were extracted from 15 min cEEG epochs, thereby providing for every neonate 32 data values = 4 (epochs of 2 h) $\times$ 2 (h) $\times$ 4 (15 min segments in 1h cEEG).

Statistical Analysis

Group comparisons between background grades were performed with the Kruskal-Wallis test, and we applied Bonferroni correction for multiple comparisons for the *post-hoc* tests. There were always three comparisons, hence the corrected significance level were $p = 0.05/3 = 0.01$ and $p = 0.005/3 = 0.001$. Correlations between MF-DFA metrics and IBI values were computed using Spearman correlation coefficient, and here we used more stringent significance level set to 0.01. Binomial statistics were used to evaluate whether significant findings in individual subjects can be considered statistically significant on the group level (see also Vanhatalo et al., 2004; Palva et al., 2005).

Results

DFA

Visual Observations

DFA fluctuation function plots (an example shown in **Figure 1C**) were computed and examined first visually from hundreds of EEG segments. As a general observation, the ranges of window lengths with possible linear relationships were variable and limited. Our systematic qualitative comparison of window lengths ranging from 5–60 to 10–300 s (data not shown) suggested that linear fit should preferably be attempted at time scales of up to about 60 s. Then, we also reasoned that the lowest feasible limit should be around 10 s to avoid measuring trivial autocorrelations in the amplitude fluctuations (for further reasoning regarding the choice of minimum length, please see Hardstone et al., 2012). A direct comparison of hundreds of DFA fluctuation plots from EEG epochs with different EEG backgrounds showed that they all follow the same overall course, however, they also appear to differ in the segment corresponding to the shorter time windows (**Figure 1E**).

Testing the Feasibility of DFA

In above, we had defined the epoch length to 900 s, which was a partly theoretical, partly practical choice. It is known that the DFA fluctuation plots provide more stable estimates of variance when longer epochs are analyzed. The practical reasoning was that the epoch length could be chosen as a multiple of our manual EEG grade classification that was set to 1 h. Obviously, a 900 s long, fixed epoch lengths cannot follow the more rapid dynamic changes known to take place in brain state of these babies (see also Berthouze and Farmer, 2012). Hence, other epoch lengths may be worth trying in future neonatal applications.

The actual feasibility of conventional DFA was tested by examining whether linear fit can adequately characterize the fluctuation plot within the tested range of time scales.

First, our analysis of 1088 epochs using the "maximum likelihood"-based technique suggested that only minority of them could be modeled with a linear fit. This finding was consistent even when we systematically varied frequency band (1–3, 1–5, and 3–8 Hz) or the range of fitting scale (5–60, 10–60, 10–100 and 10–300 s). The best set of parameters, which we fixed and consistently used in the study, was 3–8 Hz frequency band and 10–60 s window fitting size, and even then, only 200 out of 1088 15 min cEEG epochs (18%) were successfully modeled as linear. We also found that continuous background EEG (grade 1)

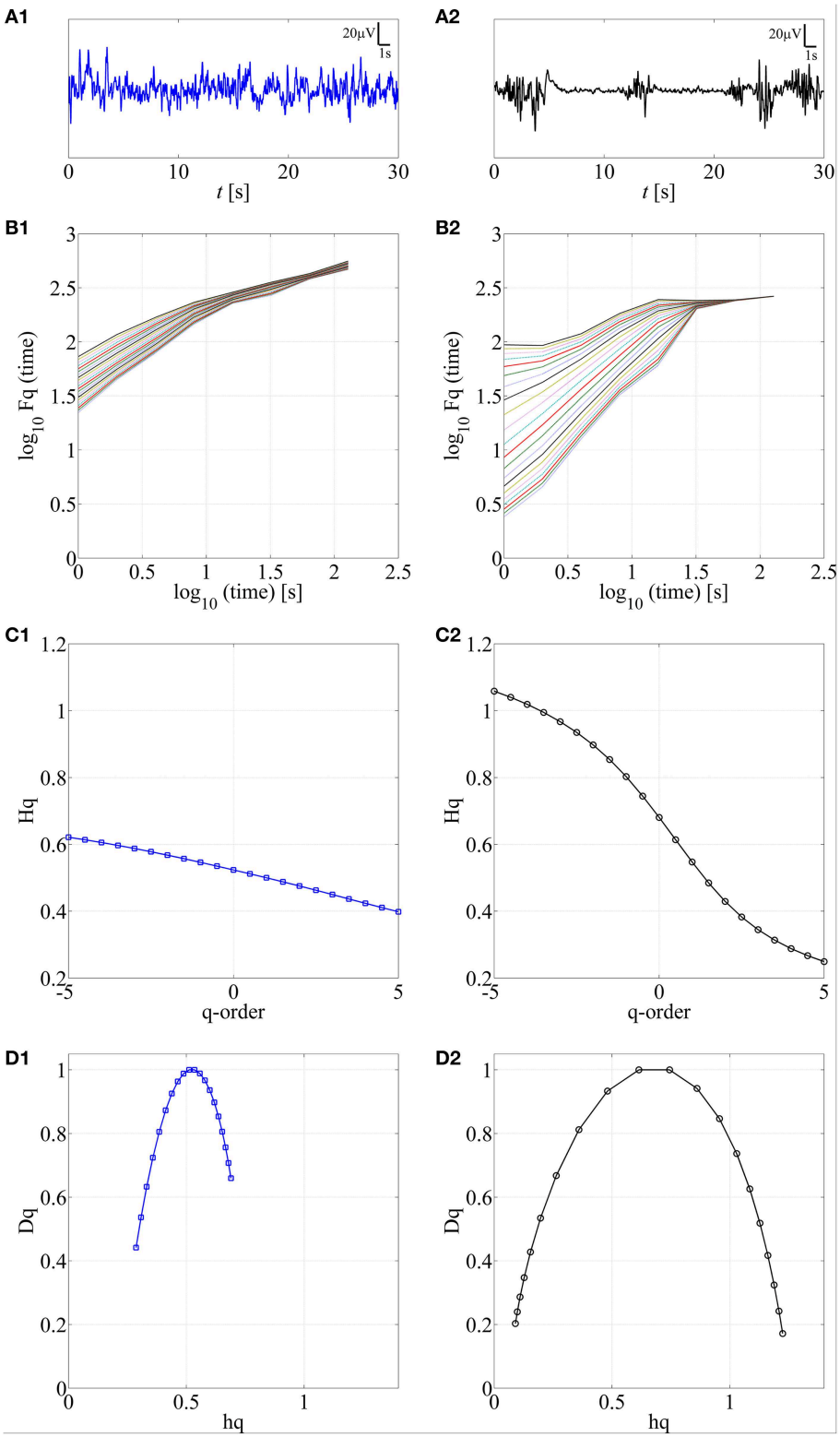

FIGURE 2 | Application of MF-DFA on two different neonatal EEG signals, continuous (A1) and burst-suppression (A2), respectively. In **B1,B2**, the q-order fluctuation function, F_q, is shown for two processes. **C1,C2** q-order Hurst exponent, H_q, is obtained as the linear fitting coefficient of the F_q fluctuation lines from **B1,B2**. Wider range of H_q values is associated with the larger multifractal dimension. In contrast, a constant line is expected for monofractal time series. **D1,D2**. Multifractal spectra are displayed for continuous and burst-suppression neonatal EEG periods. Longer tails and wider width between the tails in **D2** compared to **D1** are associated with a higher degree of multifractality.

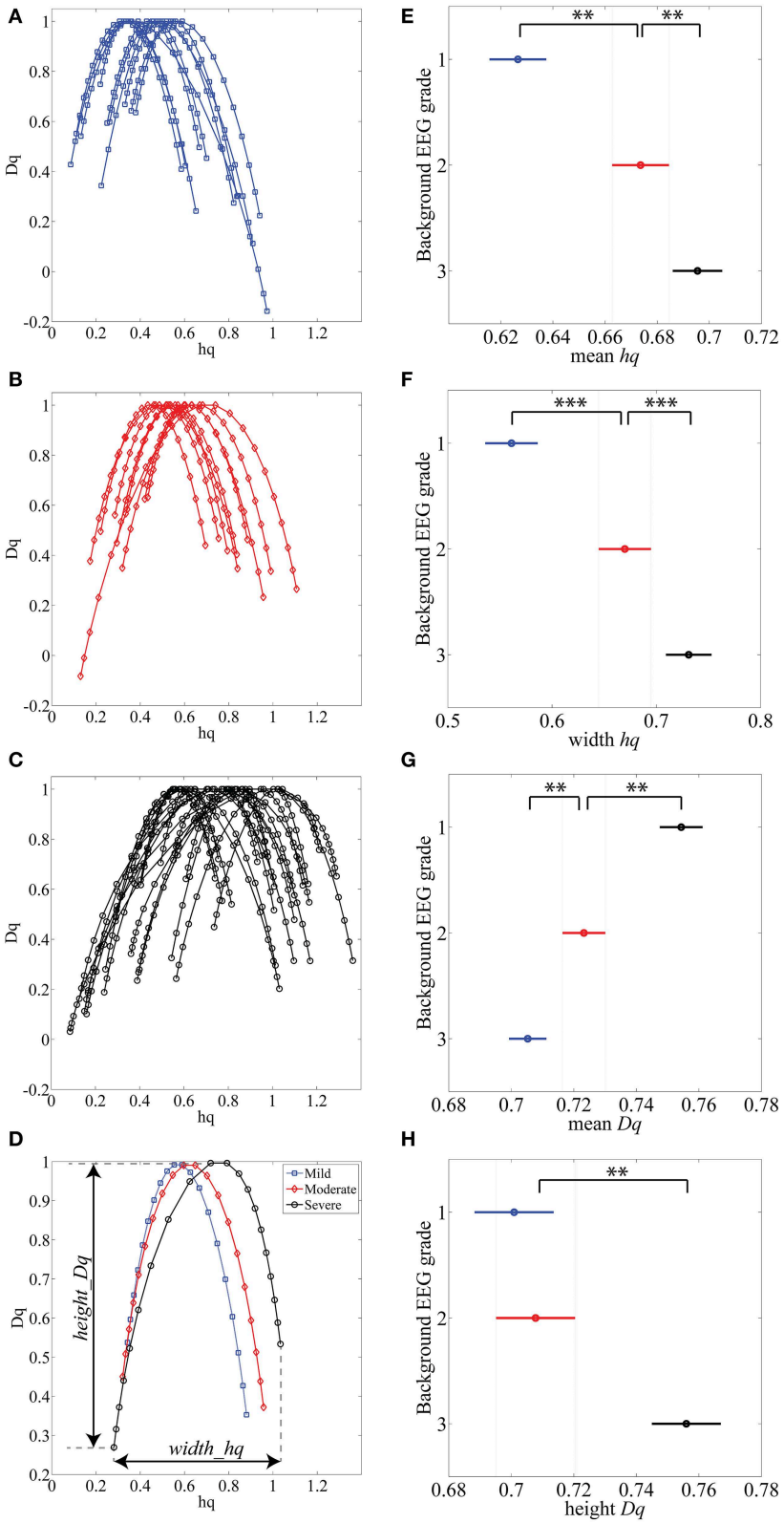

FIGURE 3 | (A–C) MF-DFA spectra lines are randomly selected and displayed for various background EEG degrees of abnormality: A-mild (blue), B-moderate (red) and C-severe (black). **(D)** Average of all 1088 multifractal spectra lines is displayed for three background EEG classes. **(E–H)** Results of Kruskal-Wallis mean value group comparisons are displayed for *mean* h_q ($p < 0.01$), *width* h_q ($p < 0.001$), *mean* D_q ($p < 0.01$) and *height* D_q(not significant). $^{**}p < 0.01$, $^{***}p < 0.001$.

is most likely to fit linear model (data not shown). The detailed results are presented in the Supplemental Figure S1.

Second, we also studied the more commonly applied measure, the linear fit R^2 using the previously adopted threshold of $R^2 = 0.97$. We found that about two thirds (68%; 731 out of 1088) of EEG epochs passed this test. For detailed comparison of R^2 values and maximum likelihood—based models, please see Supplemental Figure S4.

Benchmarking with Clinical EEG Grades

For benchmarking with clinical EEG grades, we chose only those EEG epochs that had passed our linear fitting test ($R^2 > 0.97$), and we computed their DFA exponents (α). Group-wise comparison of α shows a wide variation within all EEG grades, while the mean α increases toward more severe EEG background. Notably, the normal/mild EEG grade (continuous EEG activity) was close to $\alpha = 0.5$, **Figure 1D**, (an "uncorrelated" process; cf. Hardstone et al., 2012), while the most severe EEG background approached 1.0. Statistical group comparison of α shows that group 3 is significantly different from the other two groups ($p < 0.01$ after *post-hoc* correction; Kruskal-Wallis test).

Crossover Points

Finally, we visually inspected a large number of DFA plots to observe possible systematic differences between EEG grades. **Figure 1E** shows an example where the plots have different overall forms: Those computed from the severe EEG grade epochs (black) are at the top, and the plots from the mild EEG grades (blue) are on the bottom of the group. It was also apparent, that the range of linear-appearing trends varied between EEG grades, and that they were often clearly multiphasic: short time scales with steep rise, middle window lengths with flatter rise, and again steep rise at the longest time scales. An example of an EEG epoch with very clear "crossover points," i.e., change of slope in the fluctuation function (Hardstone et al., 2012) is shown in **Figure 1F**. Finding such crossover points, suggests that the signal might exhibit multifractal behavior (Kantelhardt et al., 2002; Ihlen, 2012; however, see Hu et al., 2001). Describing such signal with one exponent, as in the conventional monofractal DFA, will overlook key dynamic properties, and the results will be particularly sensitive to chance factors in the conventional DFA analysis.

In our dataset, the crossover point in the burst-suppression background (red and black DFA fluctuation functions in **Figure 1E**) was usually encountered within 30–60 s time scale [1.5–2 in $\log_{10}$(time) s]. Continuous EEG background (blue DFA fluctuation functions) were successfully modeled as linear for longer window sizes [up to 100 s or 2 in $\log_{10}$(time) s], and the crossover points mainly appeared in the interval of 100–300 s [2–2.5 in $\log_{10}$(time) s]. In comparing different EEG grades, the different crossover points hence preclude use of single, monofractal DFA exponent, and supports exploration of MF-DFA metrics.

Multifractal DFA (MF-DFA)

We next studied the feasibility of MF-DFA in neonatal EEG by applying a previously published method (Kantelhardt et al., 2002; Ihlen, 2012). The special clinical attraction in MF-DFA comes from its clear metrics that have been recently shown to aid discrimination of brain states (Zorick and Mandelkern, 2013) and pathologies (Zheng et al., 2005).

Feasibility of MF-DFA

The first step here was to show that neonatal EEG signal is characterized by multiple rather than single exponents. The presence of multifractal behavior in at least some neonatal EEG data becomes apparent when comparing the temporal behavior of two common neonatal EEG patterns in asphyxiated infants, the normal continuous EEG signal and the severely abnormal EEG with marked intermittency called burst-suppression (see **Figures 2A1,A2**). For those signals, we calculated the *q-order* fluctuation functions F_q (**Figures 2B1,B2**) with q values from −5 till 5, equidistantly sampled with a 0.5 unit-step as suggested by Ihlen (2012), notably, different range could be examined as well. The q factor is able to detect mixed occurrence of large fluctuations with periods of negligible fluctuations, which in our case characterizes the burst-suppression background. In contrast, the continuous EEG consists of neither very large nor very small fluctuations (**Figure 2A1**).

Comparison of q-order fluctuation functions (F_q) taken from these two different EEG patterns shows their fundamental difference. In the normal, continuous EEG activity, the slopes of the fluctuation functions appear comparable to each other. Hence, they could also be reasonably described with only one DFA fluctuation function (**Figure 2B1**; $q = 2$), and be considered as monofractal process. In contrast to this, EEG periods with burst-suppression are much more variable, and different time epochs exhibit a notably wide spread of F_q (**Figure 2B2**), suggestive of an underlying multifractal process (see also Ihlen, 2012). Taken together, these observations suggest that measuring LRTC in neonatal EEG datasets like ours should require quantification of multifractal dynamics.

Subsequently, we calculated q-order Hurst exponents, H_q (Ihlen, 2012), which returns linear approximation of the F_q fluctuation functions (**Figures 2C1,C2**). This again discloses a clear difference between background EEG activity grades. In the continuous EEG, the relation between H_q and q factor shows a monotonic decrease (characteristic of a monofractal process; Ihlen, 2012), whereas the H_q plot of burst-suppression EEG (**Figure 2C2**) shows a relatively sharp and nonlinear decline (characteristic of a multifractal process). These q-order Hurst exponent functions can be readily transformed into a multifractal spectrum (**Figures 2D1,D2**), which outlines the relation of local temporal changes of the H_q and the distribution of its probability density function (see Ihlen, 2012). Multifractal spectrum represents two measurable dimensions, the D_q (q-order singularity/fractal dimension) and the h_q (q-order singularity exponent). In the visual assessment of multifractal spectra, differences can be noticed in a horizontal and vertical positioning (h_q, D_q values), a width ($width\_h_q$), as well as in the general shape of the multifractal spectra reflecting temporal variations of local Hurst exponents.

The MF-DFA spectra were then computed for each ($n = 1088$) of the 15 min long EEG epochs. Example of these spectra

are plotted from each EEG background grade (**Figures 3A–C**). Visual inspection of the spectra shows that worsening of EEG background (from mild to severe) is associated with a shift to the right (higher h_q value). Grand averages of the spectra are shown in **Figure 3D** (1088 epochs from 12 channels: total 13056 spectra).

Other differences among EEGs were also observed visually within the tails of the spectra: the left tails, corresponding to positive q values, are longer in the EEG with local large fluctuations, i.e., the severe EEG grade with IBIs > 10 s (**Figure 3C**). Moderate and milder EEG background traces do not have such pronounced structural differences and the corresponding tails are respectively shorter (**Figures 3A,B**). On the other hand, the right tails, reflect the amplitude fluctuations within local periods of low activity (e.g., suppressed EEG periods).

Benchmarking with Clinical EEG Grades

Comparison of MF-DFA metrics between EEG grades showed highly significant differences between the three EEG grades. The mean height of spectra, *mean* h_q, was significantly ($p < 0.01$; Kruskall-Wallis test) increased with EEG severity (mild 0.63 ± 0.10; moderate 0.67 ± 0.09; severe 0.70 ± 0.09). The width of the spectra, *width* h_q, was also significantly ($p < 0.001$) increased with increasing severity of EEG background (mild 0.56 ± 0.13; moderate 0.67 ± 0.16; severe 0.73 ± 0.19). At the same time, the *mean* D_q decreased significantly ($p < 0.01$) with increasing severity of EEG background (mild 0.75 ± 0.05; moderate 0.72 ± 0.05; severe 0.70 ± 0.06). Height of the MF-DFA spectra, *height*_D_q, was significantly ($p < 0.01$) different between moderate and severe EEG grades (moderate 0.70 ± 0.09; severe 0.76 ± 0.11). These findings together suggest that MF-DFA is superior to the conventional DFA in distinguishing between neonatal EEG grades.

A further inspection of the shapes of MF-DFA spectra shows additional qualitative spectral features that are different between background grades. Namely, the mild/normal EEG grade does typically correspond to asymmetric spectra with a longer right side tail, whereas the spectra of severe EEG grade are more asymmetric with longer left side tail. This asymmetry is not measured by the currently used, established MF-DFA metrics. It may, however, readily explain the lesser differences between groups seen in *mean*_D_q and *height*_D_q, which are insensitive to asymmetry. To examine this further in a quantitative manner, we also computed the metrics from the right side tail only (see below).

Benchmarking and Application into Intraindividual Context

While the group level findings above are by themselves strong, clinical applicability of any novel study paradigm requires performance at individual level as well (see discussion in Ahtola et al., 2014). In order to preliminarily probe this issue, we studied those 34 neonates in our dataset that had four EEG epochs of 2 h duration randomly selected at time points with at least 4 h intervals. We then computed MF-DFA metrics from 15 min segments within each 2 h epochs (total 32 epochs in each infant). The long intervals between epochs yielded us datasets where EEG grade, or at least the mean IBI, was changing due to variation in the clinical state of the patient. As a benchmark to MF-DFA metrics, we calculated the mean IBI for each 15 min epoch using our previously described automated detector (Matic et al., 2012). Nine patients were excluded because their range of IBIs was too narrow to reasonably compute correlation coefficients with another parameter, i.e., IBI range was only within 3 to 6 s interval. This left 25 babies for our analysis. Finally, non-parametric, ranking correlation (Spearman) was computed between mean IBI levels and MF-DFA spectra metrics in each patient.

Measures of the full MF-DFA spectra

Individual results are shown in Supplementary Table 1, Supplemental Data. We observed that in 10 out of 25 babies there was a significant ($p < 0.01$) correlation at the individual level, which finding is statistically very significant at the group level ($p <$ 1e–10; Binomial statistics). As shown in **Figure 4**, for an example infant ($n = 21$), a visually apparent temporal relationship was observed between decreasing IBI trend and changes in at least three of the MF-DFA parameters (*mean_hq*, *width_hq*, and *mean_Dq*).

Measures of the right side tail of MF-DFA spectra

Closer inspection showed that the signs of correlation coefficients (ρ) were inconsistent even for infants with statistically significant correlations (Supplementary Table 1, Supplemental Data). To search for reasons we inspected further the shapes of MF-DFA spectra, and observed their asymmetry, especially in the severe EEG grades. For instance, visual comparison of individual MF-DFA spectra shown in **Figure 4B** from different time epochs during recovery shows that the shape of spectra changes over time, most notably as a shift from longer left tail to longer right tail as well as the shift of the right tail to the left when going from severe to normal EEG background, respectively. Since the current MF-DFA metrics are insensitive to asymmetry of the multifractal spectra, it is possible that change in symmetry with EEG grades would confound the correlations. Hence, we investigated the parameterization of the right tail of the MF-DFA spectra, and we found these metrics to exhibit much stronger relationship to the mean IBI values. In particular, for 13 out of 25 patients, we found that at least 3 metrics namely *width hq* ($\rho = -0.70 \pm 0.15$), *mean Dq* ($\rho = 0.68 \pm 0.13$) and *height Dq* ($\rho = -0.67 \pm 0.11$), were significantly correlated with the mean IBI values, showing consistent range of correlation coefficient values (ρ) as detailed at subject level in Supplementary Table 2, Supplemental Data.

Additionally, we illustrate how the MF-DFA parameters (extracted from the right tail of the spectra) are correlated with IBI values for five infants that showed higher Spearman correlation p-values (selected from the Supplementary Table 2, Supplemental Data) (**Figure 5**).

Discussion

Our study shows that changes in long range temporal dynamics in the early neonatal EEG may be characterized with the DFA paradigm, however the conventional DFA is compromised and the recently introduced multifractal DFA can better disclose

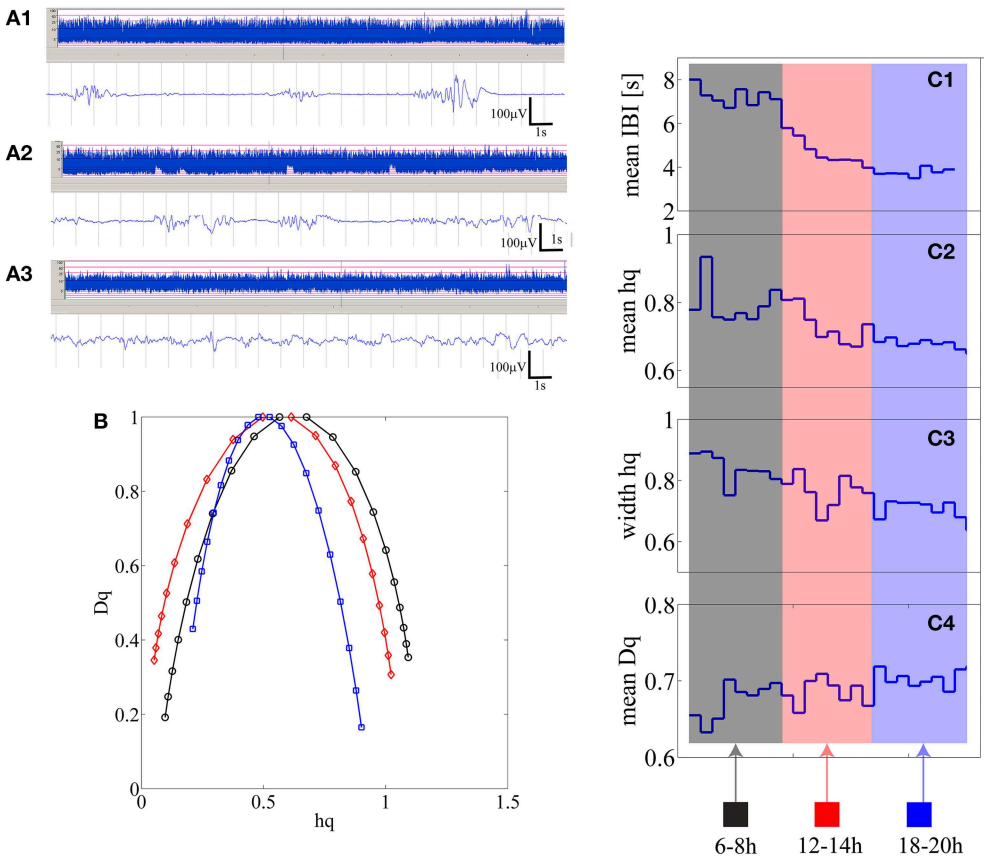

FIGURE 4 | (A1–A3) Three examples of burst-suppression, tracé discontinue, and continuous EEG periods are shown as aEEG trends and EEG epoch in an infant who is showing recovery from initial severe hypoxic insult. **(B)** Three multifractal spectra lines are shown for the corresponding three states quantifying 15 min of burst-suppression (black-recorded at 6 h post-partum), tracé discontinu (red-recorded at 12 h post-partum) and continuous EEG period (blue-recorded at 18 h post-natal age). (**C1–C4**) from 15 min segments mean IBI, *mean* h_q, *width* h_q and *mean* D_q values are represented as one data point [24 in total; 2 h × 4 (15 min epochs in 1 h) × 3 epochs].

neonatal EEG dynamics in a way that correlates with the current clinical EEG grading systems. Our clinical benchmarking of DFA feasibility extends prior literature to include full-term neonatal EEG as a potential application of DFA/MF-DFA paradigms. The present findings corroborate earlier reports that DFA or MF-DFA metrics can quantify brain dynamics associated with prematurity (Hartley et al., 2012) and neurological conditions (Linkenkaer-Hansen et al., 2001; Parish et al., 2004; Monto et al., 2007). We also suggest a novel MF-DFA metric for EEG analysis based on observing asymmetric change in MF-DFA spectra between clinically relevant brain states.

The physiological underpinnings of multifractal behavior in the neonatal brain remain elusive, and our dataset is suboptimal for a tour de force exploration of the phenomenon of multifractality in the neonatal brain activity. However, our observations provide some tentative ideas to how MF-DFA may be suitable in such data: The well-known hallmark of both the early preterm EEG and the severely abnormal EEG of a term newborn is a salient intermittency (Vanhatalo and Kaila, 2006; André et al., 2010): seemingly erratic ruptures of transient cortical activity alternate with periods of relative quiescence. Considering the structural immaturity of underlying brain networks (Kostović and Judaš, 2010) and/or the pathological mechanisms related to resource constraints (Roberts et al., 2014), it is conceivable that they would readily compromise the extreme long range temporal correlations previously shown in the adult brain (Linkenkaer-Hansen et al., 2001). There is ample evidence from the neonatal EEG studies that cortical activity may continue even after extensive structural lesions that lead to physical disconnection of cortical areas. The multifractality could hence reflect a spatial and/or temporal fragmentation of large scale brain activity, resulting in multiple partly independent mechanisms in brain activity. Nevertheless, more rigorous confirmation with more extensive datasets and stringent mathematical testing of alternative models will be necessary to confirm fundamental behaviors of this kind (for instance, see Clauset et al., 2009; Roberts et al., 2014).

In addition to showing the significant discrimination of background grades with the established MF-DFA metrics, our closer visual inspection of MF-DFA spectra suggested further differences. The highest difference between grades was achieved for the relatively small window size values [<30 s or 1.5 in $\log_{10}$(time)s]

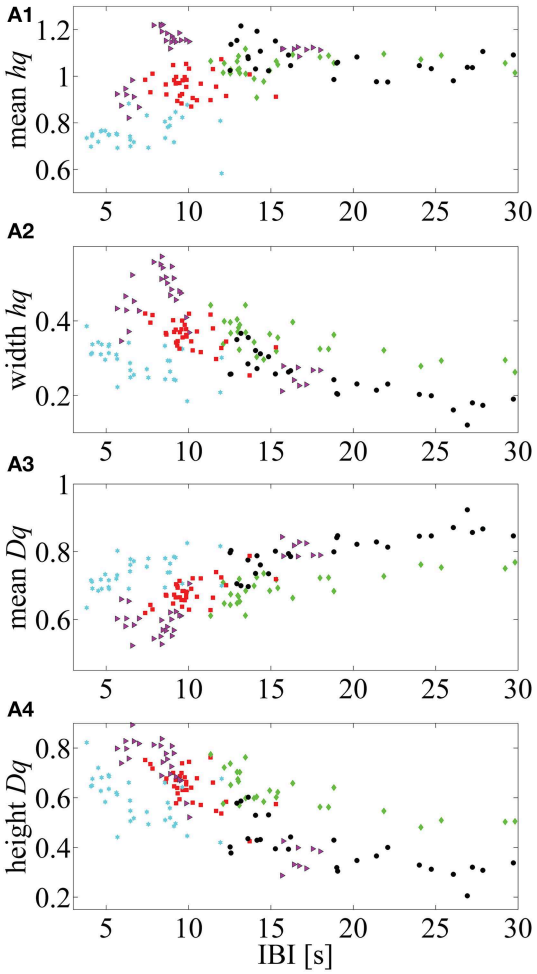

FIGURE 5 | Five neonates in which mean IBI values are highly correlated with the MF-DFA metrics (calculated from the right part of the multifractal spectra). (A1–A4) respectively, represent the correlation between *mean* h_q, *width* h_q, *mean* D_q and *height* D_q values with the mean IBIs. This approach for calculation of MF-DFA based metrics avoids insensitivity to the asymmetry which affects the originally proposed parameters calculated for the complete spectra (see Zorick and Mandelkern, 2013).

(**Figure 2B2**), which is most sensitive to temporally *local* variations in signal fluctuations. We also observed that the different background grades yield saliently different shapes, especially the asymmetry, in their corresponding MF-DFA spectra. This is not quantified by the established MF-DFA metrics (cf. Zorick and Mandelkern, 2013), hence we proposed quantification of the right side tail of the spectra for an improved sensitivity. These measures were, indeed, significantly correlating with IBIs in a large proportion of infants. It is possible that the prominent intermittency of the burst suppression signal has an important effect on the MF-DFA metrics. Conceivably, burst suppression EEG consists of two overlaid, but at least partly independent physiological processes: intermittent bursting behavior and the varying levels of spontaneous activity between the bursts, both with unique scaling properties (Roberts et al., 2014). A similar situation is also found during the early intermittent EEG activity of preterm babies where two mechanistically different brain activities are superimposed on each other (Vanhatalo and Kaila, 2006), giving rise to unique long range temporal correlations in the inter-event time series (Hartley et al., 2012). The physiological meaning of asymmetry remains to be established in simulations and experimental studies, however our data suggests that it relates to continuity and perhaps the relative shapes of bursts that interrupt the interburst silence.

In search of clinical relevance, we benchmarked the MF-DFA metrics with both visual and automated background EEG grading, and show that all our four metrics (*mean* h_q, *width* h_q, *mean* D_q, *height* D_q) do significantly co-vary with the visually scored EEG background grades. Three (*mean* h_q, *width* h_q, *mean* D_q) of our metrics were significantly different between all EEG groups. In addition, the application within patients showed that MF-DFA metrics might even reflect temporal change of background EEG states at individual level as suggested by the significant correlations with IBI levels in 10 out of 25 infants. These correlations suggest that MF-DFA metrics and IBI would at least partly reflect similar pathological brain dynamics, or at least the amplitude fluctuations of burst suppression are reflected in the MF-DFA spectra. However, despite the general correspondence with IBI levels and its evolution, the match between IBI and MF-DFA metrics is neither fully consistent nor complete. Such partial mismatch are consistent with the idea that MF-DFA metrics reflect some as yet latent EEG signal dynamics.

Beyond the physiological interest, our present findings have potential implications in future construction of computational classifiers for neonatal EEG. A number of studies have reported development of various automated EEG background classifiers. Some of them are designed to directly replicate the visual criteria. Using this approach, the recent study by Korotchikova et al., 2011, combined a larger set of quantified EEG features and found them indiscriminative with respect to background EEG classes, with special challenges in distinguishing mild vs. moderate grades. A more recent attempt along this line was able to discriminate normal vs. abnormal EEG backgrounds as a dichotomous choice (Stevenson et al., 2013), which does not yet support its use in EEG monitoring or for more refined needs. Another approach has been to optimize a learning algorithm with a smaller dataset to detect extreme classes of EEG background, such as severe burst-suppression patterns (Löfhede et al., 2010), which is further used to output IBI detections. The design of such classifier will ideally allow accurate quantitation of IBIs (Flisberg et al., 2011), however, it will not allow constructing methods that can monitor evolution of EEG activity over background grade boundaries, which obviously happens among a majority of clinical patients during their brain monitoring.

Prior extensive engineering works have mostly focused on identifying discrete EEG states (e.g., burst suppression), or on discrimination of normal from abnormal backgrounds as benchmarked with visual criteria. One of the shortcomings in benchmarking with visual EEG grading is its temporal coarseness. Visual grades are commonly assigned hourly for slow changes such as sleep-wake cycling (Murray et al., 2009; Matic et al., 2014; Stevenson et al., 2014). Other EEG grading systems have

been developed to include even longer term evolution, up to over 24 h, to characterize recovery from hypoxic insults (Cherian et al., 2011), which as a principle reminds of the conventional approach used in the aEEG assessment (Hellström-Westas and Rosén, 2006). We are not aware of objective computational, graded measures of background EEG activity although the clinical experience shows that the key part of brain monitoring is the follow-up of patients through different stages over hours. Our findings suggest that measures based on MF-DFA metrics may offer an advantage here: for instance, these metrics may distinguish moderately abnormal EEG from the severe and normal backgrounds, which is clinically very important. Brain states change more rapidly in the real life, hence we wanted to compare MF-DFA-based metrics also with the automated algorithm that detects IBI levels in 15 min epochs. This showed that MF-DFA metrics do co-vary with IBI, and they do evolve over time. A systematic characterization and benchmarking with existing trend paradigms, especially aEEG (Hellström-Westas and Rosén, 2006) will help to identify the clinical added value of MF-DFA measures.

We consider our study as exploratory, providing only proof of concept. Further prospective and larger studies are needed to determine the clinical robustness and added value obtained from the proposed method, as well as to validate its use in the prospective clinical context. The first practical consideration is the age range of infants. Our dataset was limited to full-term neonates, but we do not see any *a priori* physiological or technical reason why the same temporal dynamics could not be clinically meaningful in the preterm babies as well. The second practical consideration is the unknown relative sensitivity of our metrics to artifacts that are unavoidably present in real life recordings from intensive care units. This can be assessed formally by simulated addition of real EEG artifacts (cf. Matic et al., 2009; De Vos et al., 2011; Räsänen et al., 2013). The future artifact avoidance strategies may include rejection by amplitude criteria (cf. Palmu et al., 2013), although missing data segments may also introduce confounders. The third practical consideration is the added clinical value relative to existing measures, especially the aEEG paradigm. It is conceivable that our metrics provide a theoretically and functionally complementary view on neonatal brain dynamics, yet the actual added bedside value needs to be determined in future clinical studies. There are also technical considerations for future studies. First, the known alternative ways in the MF-DFA analysis, such as wavelet transform modus maxima (Muzy et al., 1993), might be useful to further improve the robustness and consistency (Zorick and Mandelkern, 2013). Second, our study demonstrate as yet uncharacterized changes in the spectral shape, which suggests that further theoretical and practical studies are needed to define spectral measures that optimally reflect changes in the neurophysiological and/or clinical state of the brain.

Acknowledgments

We thank our patients and their parents for their cooperation and the neurotechnologists who made the high quality EEG recordings.VM, AA, NK, and SV are supported by: Research Council KUL: CoE PFV/10/002 (OPTEC); PhD/Postdoc grants Flemish Government: FWO: projects: G.0427.10N (Integrated EEG-fMRI), G.0108.11 (Compressed Sensing) G.0869.12N (Tumor imaging) G.0A5513N (Deep brain stimulation); PhD/Postdoc grants IWT: projects: TBM 080658-MRI (EEG-fMRI), TBM 110697-NeoGuard; PhD/Postdoc grants. iMinds Medical Information Technologies SBO 2015, ICON: NXT_Sleep. Belgian Federal Science Policy Office: IUAP P7/19/(DYSCO, "Dynamical systems, control and optimization," 2012–2017). Belgian Foreign Affairs-Development Cooperation: VLIR UOS programs. EU: The research leading to these results has received funding from the European Research Council under the European Union's Seventh Framework Programme (FP7/2007–2013)/ERC Advanced Grant: BIOTENSORS (n° 339804). This paper reflects only the authors' views and the Union is not liable for any use that may be made of the contained information. Other EU funding: RECAP 209G within INTERREG IVB NWE program, EU MC ITN TRANSACT 2012 (n° 316679), ERASMUS EQR: Community service engineer (n° 539642-LLP-1-2013) SV was supported by the Academy of Finland grant 253130, Finnish Cultural Foundation, Päivikki ja Sakari Sohlberg Foundation, and Juselius Foundation.

Supplementary Material

The Supplementary Material for this article can be found online at: http://journal.frontiersin.org/article/10.3389/fnhum.2015.00189/abstract

Figure B1 | Steps of the automated IBI detection method are illustrated. First, EEG signal is segmented using an adaptive segmentation algorithm **(A1)** Next, the segments are classified into the low amplitude class (approximately $<10\,\mu V$) and depicted in blue. **(A2)** The temporal profile signal counts the prevalence of low amplitude segments and it is used to detect IBI patterns **(A3)**. The time that the temporal profile signal exceeds the threshold determines the IBI duration and the IBI is detected.

References

Ahtola, E., Stjerna, S., Yrttiaho, S., Nelson, C. A., Leppänen, J. M., and Vanhatalo, S. (2014). Dynamic eye tracking based metrics for infant gaze patterns in the face-distractor competition paradigm. *PLoS ONE* 9:e97299. doi: 10.1371/journal.pone.0097299

André, M., Lamblin, M. D., d'Allest, A. M., Curzi-Dascalova, L., Moussalli-Salefranque, F., Nguyen The Tich, S., et al. (2010). Electroencephalography in premature and full-term infants. Developmental features and glossary. *Neurophysiol. Clin.* 40, 59–124. doi: 10.1016/j.neucli.2010.02.002

Beggs, J. M., and Plenz, D. (2003). Neuronal avalanches in neocortical circuits. *J. Neurosci.* 23, 11167–11177.

Berthouze, L., and Farmer, S. F. (2012). Adaptive time-varying detrended fluctuation analysis. *J. Neurosci. Methods* 209, 178–188. doi: 10.1016/j.jneumeth.2012.05.030

Berthouze, L, James, L. M., and Farmer, S. F. (2010). Human EEG shows long-range temporal correlations of oscillation amplitude in Theta, Alpha and

Beta bands across a wide age range. *Clin. Neurophysiol.* 121, 1187–1197 doi: 10.1016/j.clinph.2010.02.163

Botcharova, M., Farmer, S. F., and Berthouze, L. (2013). A maximum likelihood based technique for validating detrended fluctuation analysis (ML-DFA). *arXiv preprint arXiv:*1306.5075.

Boylan, G. B., Burgoyne, L., Moore, C., O'Flaherty, B., and Rennie, J. M. (2010). An international survey of EEG use in the neonatal intensive care unit. *Acta Paediatr.* 99, 1150–1155. doi: 10.1111/j.1651-2227.2010.01809.x

Cherian, P. J., Deburchgraeve, W., Swarte, R. M., De Vos, M., Govaert, P., Van Huffel, S., et al. (2011). Validation of a new automated neonatal seizure detection system: a clinician's perspective. *Clin. Neurophysiol.* 122, 1490–1499. doi: 10.1016/j.clinph.2011.01.043

Clauset, A., Shalizi, C. R., and Newman, M. E. (2009). Power-law distributions in empirical data. *SIAM Rev.* 51, 661–703. doi: 10.1137/070710111

Deburchgraeve, W., Cherian, P. J., De Vos, M., Swarte, R. M., Blok, J. H., Visser, G. H., et al. (2008). Automated neonatal seizure detection mimicking a human observer reading EEG. *Clin. Neurophysiol.* 119, 2447–2454. doi: 10.1016/j.clinph.2008.07.281

De Vos, M., Deburchgraeve, W., Cherian, P. J., Matic, V., Swarte, R. M., Govaert, P., et al. (2011). Automated artifact removal as preprocessing refines neonatal seizure detection. *Clin. Neurophysiol.* 122, 2345–2354. doi: 10.1016/j.clinph.2011.04.026

De Vries, L. S., and Hellström-Westas, L. (2005). Role of cerebral function monitoring in the newborn. *Arch. Dis. Child. Fetal Neonatal Ed.* 90 F201–FF207. doi: 10.1136/adc.2004.062745

Flisberg, A., Kjellmer, I., Löfhede, J., Lindecrantz, K., and Thordstein, M. (2011). Prognostic capacity of automated quantification of suppression time in the EEG of post−asphyctic full−term neonates. *Acta Paediatr.* 100, 1338–1343. doi: 10.1111/j.1651-2227.2011.02323.x

Fransson, P., Metsäranta, M., Blennow, M., Åden, U., Lagercrantz, H., and Vanhatalo, S. (2013). Early development of spatial patterns of power-law frequency scaling in fMRI resting-state and EEG data in the newborn brain. *Cereb. Cortex* 23, 638–646. doi: 10.1093/cercor/bhs047

Hardstone, R., Poil, S. S., Schiavone, G., Jansen, R., Nikulin, V. V., Mansvelder, H. D., et al. (2012). Detrended fluctuation analysis: a scale-free view on neuronal oscillations. *Front. Physiol.* 3:450. doi: 10.3389/fphys.2012.00450

Hartley, C., Berthouze, L., Mathieson, S. R., Boylan, G. B., Rennie, J. M., Marlow, N., et al. (2012). Long-range temporal correlations in the EEG bursts of human preterm babies. *PLoS ONE* 7:e31543. doi: 10.1371/journal.pone.0031543

Hellström-Westas, L., and Rosén, I. (2006). Continuous brain-function monitoring: state of the art in clinical practice. *Semin. Fetal Neonatal. Med.* 11, 503–511. doi: 10.1016/j.siny.2006.07.011

Hu, K., Ivanov, P. C., Chen, Z., Carpena, P., and Stanley, H. E. (2001). Effect of trends on detrended fluctuation analysis. *Phys. Rev. E* 64:011114. doi: 10.1103/PhysRevE.64.011114

Ihlen, E. A. (2012). Introduction to multifractal detrended fluctuation analysis in Matlab. *Front. Physiol.* 3:141. doi: 10.3389/fphys.2012.00141

Iyer, K. K., Roberts, J. A., Metsäranta, M., Finnigan, S., Breakspear, M., and Vanhatalo, S. (2014). Novel features of early burst suppression predict outcome after birth asphyxia. *Ann. Clin. Transl. Neurol.* 1, 209–214. doi: 10.1002/acn3.32

Kantelhardt, J. W., Zschiegner, S. A., Koscielny-Bunde, E., Havlin, S., Bunde, A., and Stanley, H. E. (2002). Multifractal detrended fluctuation analysis of nonstationary time series. *Phys. A Stat. Mech. Appl.* 316, 87–114. doi: 10.1016/S0378-4371(02)01383-3

Korotchikova, I., Stevenson, N. J., Walsh, B. H., Murray, D. M., and Boylan, G. B. (2011). Quantitative EEG analysis in neonatal hypoxic ischaemic encephalopathy. *Clin. Neurophysiol.* 122, 1671–1678. doi: 10.1016/j.clinph.2010.12.059

Kostović, I., and Judaš, M. (2010). The development of the subplate and thalamocortical connections in the human foetal brain. *Acta Paediatr.* 99, 1119–1127. doi: 10.1111/j.1651-2227.2010.01811.x

Krajča, V., Petránek, S., Patáková, I., and Värri, A. (1991). Automatic identification of significant graphoelements in multichannel EEG recordings by adaptive segmentation and fuzzy clustering. *Int. J. Biomed. Comput.* 28, 71–89. doi: 10.1016/0020-7101(91)90028-D

Linkenkaer-Hansen, K., Nikouline, V. V., Palva, J. M., and Ilmoniemi, R. J. (2001). Long-range temporal correlations and scaling behavior in human brain oscillations. *J. Neurosci.* 21, 1370–1377.

Löfhede, J., Thordstein, M., Löfgren, N., Flisberg, A., Rosa-Zurera, M., Kjellmer, I., et al. (2010). Automatic classification of background EEG activity in healthy and sick neonates. *J. Neural Eng.* 7:016007. doi: 10.1088/1741-2560/7/1/016007

Matic, V., Cherian, P. J., Jansen, K., Koolen, N., Naulaers, G., Swarte, R. M., et al. (2012). "Automated EEG inter-burst interval detection in neonates with mild to moderate postasphyxial encephalopathy," in *Engineering in Medicine and Biology Society (EMBC), 2012 Annual International Conference of the IEEE* (IEEE), 17–20.

Matic, V., Cherian, P. J., Koolen, N., Naulaers, G., Swarte, R. M., Govaert, P., et al. (2014). Holistic approach for automated background EEG assessment in asphyxiated full-term infants. *J. Neural Eng.* 11:066007. doi: 10.1088/1741-2560/11/6/066007

Matic, V., Deburchgraeve, W., and Van Huffel, S. (2009). "Comparison of ICA algorithms for ECG artifact removal from EEG signals," in *Proceedings of the 4th Annual Symposium of the IEEE-EMBS Benelux Chapter* (IEEE-EMBS), 137–140.

Menache, C. C., Bourgeois, B. F., and Volpe, J. J. (2002). Prognostic value of neonatal discontinuous EEG. *Pediatr. Neurol.* 27, 93–101. doi: 10.1016/S0887-8994(02)00396-X

Monod, N., Pajot, N., and Guidasci, S. (1972). The neonatal EEG: statistical studies and prognostic value in full-term and pre-term babies. *Electroencephalogr. Clin. Neurophysiol.* 32, 529–544. doi: 10.1016/0013-4694(72)90063-6

Monto, S., Vanhatalo, S., Holmes, M. D., and Palva, J. M. (2007). Epileptogenic neocortical networks are revealed by abnormal temporal dynamics in seizure-free subdural EEG. *Cereb. Cortex* 17, 1386–1393. doi: 10.1093/cercor/bhl049

Murray, D. M., Boylan, G. B., Ryan, C. A., and Connolly, S. (2009). Early EEG findings in hypoxic-ischemic encephalopathy predict outcomes at 2 years. *Pediatrics* 124, e459–e467. doi: 10.1542/peds.2008-2190

Muzy, J. F., Bacry, E., and Arneodo, A. (1993). Multifractal formalism for fractal signals: the structure-function approach versus the wavelet-transform modulus-maxima method. *Phys. Rev. E* 47:875. doi: 10.1103/PhysRevE.47.875

Omidvarnia, A., Fransson, P., Metsäranta, M., and Vanhatalo, S. (2014). Functional bimodality in the brain networks of preterm and term human newborns. *Cereb. Cortex* 24, 2657–2668. doi: 10.1093/cercor/bht120

Palmu, K., Kirjavainen, T., Stjerna, S., Salokivi, T., and Vanhatalo, S. (2013). Sleep wake cycling in early preterm infants: comparison of polysomnographic recordings with a novel EEG-based index. *Clin. Neurophysiol.* 124, 1807–1814. doi: 10.1016/j.clinph.2013.03.010

Palmu, K., Wikström, S., Hippeläinen, E., Boylan, G., Hellström-Westas, L., and Vanhatalo, S. (2010). Detection of 'EEG bursts' in the early preterm EEG: visual vs. automated detection. *Clin. Neurophysiol.* 121, 1015–1022. doi: 10.1016/j.clinph.2010.02.010

Palva, J. M., Palva, S., and Kaila, K. (2005). Phase synchrony among neuronal oscillations in the human cortex. *J. Neurosci.* 25, 3962–3972. doi: 10.1523/JNEUROSCI.4250-04.2005

Parish, L. M., Worrell, G. A., Cranstoun, S. D., Stead, S. M., Pennell, P., and Litt, B. (2004). Long-range temporal correlations in epileptogenic and non-epileptogenic human hippocampus. *Neuroscience* 125, 1069–1076. doi: 10.1016/j.neuroscience.2004.03.002

Peng, C. K., Buldyrev, S. V., Havlin, S., Simons, M., Stanley, H. E., and Goldberger, A. L. (1994). Mosaic organization of DNA nucleotides. *Phys. Rev. E* 49:1685. doi: 10.1103/PhysRevE.49.1685

Räsänen, O., Metsäranta, M., and Vanhatalo, S. (2013). Development of a novel robust measure for interhemispheric synchrony in the neonatal EEG: activation Synchrony Index (ASI). *Neuroimage* 69, 256–266. doi: 10.1016/j.neuroimage.2012.12.017

Roberts, J. A., Iyer, K. K., Finnigan, S., Vanhatalo, S., and Breakspear, M. (2014). Scale-free bursting in human cortex following hypoxia at birth. *J. Neurosci.* 34, 6557–6572. doi: 10.1523/JNEUROSCI.4701-13.2014

Stam, C. J., Montez, T., Jones, B. F., Rombouts, S. A. R. B., Van Der Made, Y., Pijnenburg, Y. A. L., et al. (2005). Disturbed fluctuations of resting state EEG synchronization in Alzheimer's disease. *Clin. Neurophysiol.* 116, 708–715. doi: 10.1016/j.clinph.2004.09.022

Stevenson, N. J., Korotchikova, I., Temko, A., Lightbody, G., Marnane, W. P., and Boylan, G. B. (2013). An automated system for grading EEG abnormality in term neonates with hypoxic-ischaemic encephalopathy. *Ann. Biomed. Eng.* 41, 775–785. doi: 10.1007/s10439-012-0710-5

Stevenson, N. J., Palmu, K., Wikström, S., Hellström-Westas, L., and Vanhatalo, S. (2014). Measuring brain activity cycling (BAC) in long term EEG monitoring of preterm babies. *Physiol. Meas.* 35:1493. doi: 10.1088/0967-3334/35/7/1493

Tokariev, A., Palmu, K., Lano, A., Metsäranta, M., and Vanhatalo, S. (2012). Phase synchrony in the early preterm EEG: development of methods for estimating synchrony in both oscillations and events. *Neuroimage* 60, 1562–1573 doi: 10.1016/j.neuroimage.2011.12.080

Vanhatalo, S., and Kaila, K. (2006). Development of neonatal EEG activity: from phenomenology to physiology. *Semin. Fetal Neonatal. Med.* 11, 471–478. doi: 10.1016/j.siny.2006.07.008

Vanhatalo, S., Palva, J. M., Holmes, M. D., Miller, J. W., Voipio, J., and Kaila, K. (2004). Infraslow oscillations modulate excitability and interictal epileptic activity in the human cortex during sleep. *Proc. Natl. Acad. Sci. U.S.A.* 101, 5053–5057. doi: 10.1073/pnas.0305375101

Walsh, B. H., Murray, D. M., and Boylan, G. B. (2011). The use of conventional EEG for the assessment of hypoxic ischaemic encephalopathy in the newborn: a review. *Clin. Neurophysiol.* 122, 1284–1294. doi: 10.1016/j.clinph.2011.03.032

Watanabe, K., Hayakawa, F., and Okumura, A. (1999). Neonatal EEG: a powerful tool in the assessment of brain damage in preterm infants. *Brain Dev.* 21, 361–372. doi: 10.1016/S0387-7604(99)00034-0

Zheng, Y., Gao, J. B., Sanchez, J. C., Principe, J. C., and Okun, M. S. (2005). Multiplicative multifractal modeling and discrimination of human neuronal activity. *Phys. Lett. A* 344, 253–264. doi: 10.1016/j.physleta.2005.06.092

Zorick, T., and Mandelkern, M. A. (2013). Multifractal detrended fluctuation analysis of human EEG: preliminary investigation and comparison with the wavelet transform modulus maxima technique. *PLoS ONE* 8:e68360. doi: 10.1371/journal.pone.0068360

Conflict of Interest Statement: The authors declare that the research was conducted in the absence of any commercial or financial relationships that could be construed as a potential conflict of interest.

frontiers in
HUMAN NEUROSCIENCE

ORIGINAL RESEARCH ARTICLE
published: 23 December 2014
doi: 10.3389/fnhum.2014.01030

Interhemispheric synchrony in the neonatal EEG revisited: activation synchrony index as a promising classifier

Ninah Koolen[1,2]*†, Anneleen Dereymaeker[3†], Okko Räsänen[4], Katrien Jansen[3], Jan Vervisch[3], Vladimir Matic[1,2], Maarten De Vos[5,6], Sabine Van Huffel[1,2], Gunnar Naulaers[3] and Sampsa Vanhatalo[7]

[1] Division STADIUS, Department of Electrical Engineering (ESAT), University of Leuven, Leuven, Belgium
[2] iMinds-KU Leuven Medical IT Department, Leuven, Belgium
[3] Department of Development and Regeneration, University of Leuven, Leuven, Belgium
[4] Department of Signal Processing and Acoustics, Aalto University, Espoo, Finland
[5] Department of Psychology, University of Oldenburg, Oldenburg, Germany
[6] Department of Engineering Science, Institute of Biomedical Engineering, University of Oxford, Oxford, UK
[7] Department of Children's Clinical Neurophysiology, HUS Medical Imaging Center and Children's Hospital, Helsinki University Central Hospital and University of Helsinki, Helsinki, Finland

Edited by:
Silvia Comani, Università degli Studi "G. d'Annunzio," Italy

Reviewed by:
Simon Farmer, National Hospital for Neurology and Neurosurgery and University College London, UK
Andrea Guzzetta, University of Pisa, Italy

***Correspondence:**
Ninah Koolen, Division STADIUS-BIOMED, Department of Electrical Engineering, University of Leuven, Kasteelpark Arenberg 10 - Bus 2446, 3000 Leuven, Belgium
e-mail: ninah.koolen@esat.kuleuven.be

† *These authors are joint first authors.*

A key feature of normal neonatal EEG at term age is interhemispheric synchrony (IHS), which refers to the temporal co-incidence of bursting across hemispheres during trace alternant EEG activity. The assessment of IHS in both clinical and scientific work relies on visual, qualitative EEG assessment without clearly quantifiable definitions. A quantitative measure, activation synchrony index (ASI), was recently shown to perform well as compared to visual assessments. The present study was set out to test whether IHS is stable enough for clinical use, and whether it could be an objective feature of EEG normality. We analyzed 31 neonatal EEG recordings that had been clinically classified as normal ($n = 14$) or abnormal ($n = 17$) using holistic, conventional visual criteria including amplitude, focal differences, qualitative synchrony, and focal abnormalities. We selected 20-min epochs of discontinuous background pattern. ASI values were computed separately for different channel pair combinations and window lengths to define them for the optimal ASI intraindividual stability. Finally, ROC curves were computed to find trade-offs related to compromised data lengths, a common challenge in neonatal EEG studies. Using the average of four consecutive 2.5-min epochs in the centro-occipital bipolar derivations gave ASI estimates that very accurately distinguished babies clinically classified as normal vs. abnormal. It was even possible to draw a cut-off limit (ASI∼3.6) which correctly classified the EEGs in 97% of all cases. Finally, we showed that compromising the length of EEG segments from 20 to 5 min leads to increased variability in ASI-based classification. Our findings support the prior literature that IHS is an important feature of normal neonatal brain function. We show that ASI may provide diagnostic value even at individual level, which strongly supports its use in prospective clinical studies on neonatal EEG as well as in the feature set of upcoming EEG classifiers.

Keywords: interhemispheric synchrony, biomarker, preterm infant, brain monitoring, neonatal EEG

INTRODUCTION

Recent progress in basic neuroscience, neuroimaging, and neonatal care has raised interest in the understanding of physiological and pathological processes in the preterm and neonatal brain. Electroencephalography (EEG) is a non-invasive and sensitive tool for evaluating brain function in the neonatal period. A key component in early brain functional development is the emergence of functional networks, the long range connectivity between and within brain hemispheres, which lay the basis for the development of neurocognitive capabilities (Uhlhaas et al., 2010; Lubsen et al., 2011; Omidvarnia et al., 2014). In this context, it is intriguing that synchrony between hemispheres has been considered as an important feature of normal neonatal brain function since the seminal studies in the late 1970s (Lombroso, 1979).

Clinical classification of spontaneous neonatal EEG is traditionally based on visual assessment of multiple features: continuity, quality of sleep wake organization, interhemispheric synchrony (IHS), symmetry and amplitude. However, visual EEG interpretation requires expertise, and there are no objective standards for classification schemes, nor any other established method to yield appropriate diagnostic accuracy to support modern neuroscience or evidence based medicine. This has greatly compromised comparisons of results between different studies. A quantitative analysis of EEG activity, including automated analysis of selected features of cortical function, could create

an objective and appropriate classification scheme for neonatal EEG. Moreover, it could also support and accelerate visual EEG analyses in medical centers without access to highly skilled EEG interpretation.

Visual estimation of IHS is based on observation of co-incidence of bursts in spontaneous background EEG activity during tracé alternant/discontinue (Holmes and Lombroso, 1993). IHS is interpreted as a sign of connectivity or functional interaction between hemispheres and is hence considered an important feature of normal brain function, resulting from the development of callosal connections (Kostovic and Jovanov-Milosevic, 2006; Dudink et al., 2008).

Despite the long and widespread clinical use of IHS, there is no physiologically plausible definition of IHS for visual EEG reading (for more details, please see Räsänen et al., 2013). A quantitative measure for IHS, the activation synchrony index (ASI), was recently developed by Räsänen et al. (2013). The ASI is based on statistically measuring the temporal delay between two signal energies, and was shown to correlate with visually rated IHS grades. It was also shown to clearly outperform other methods proposed for the same purpose in the recent literature (Räsänen et al., 2013).

Our ultimate aim is to use ASI more widely as a clinical biomarker or as a feature in EEG classifiers, which poses special requirements for individual stability. In addition, the analysis settings such as the epoch lengths need to be practical with respect to clinical reality, where obtaining longer high quality epochs is often challenging due to intermittent, trivial artifacts. The aim of this study was to test the ability of the ASI to distinguish normal and abnormal neonatal EEG recordings. Therefore, we first defined the optimal ASI parameters to maximize its intraindividual and technical stability, and then tested ASI as an input for a classifier to identify abnormal EEG activity.

MATERIALS AND METHODS

The present study consisted of two discrete phases (see **Figure 1**). First, we optimized the intraindividual stability of ASI. The earlier development of ASI had aimed to optimize parameter settings for maximal distinction between asynchrony grades as well as robustness against artifacts. Our present study continued ASI optimization by searching for EEG epoch lengths and channel derivations that would strike a balance between technical reliability and clinical practice. For clinical practice, an important consideration is that the algorithm should work equally well on EEG samples either with longer continuous epochs or with multiple shorter epochs. In addition, we tested our optimized ASI protocol on a new EEG dataset that had been classified using conventional clinical criteria, with the aim of seeing how well ASI alone is able to distinguish normal and abnormal EEG recordings. This latter aim is also a rigorous test of the conventional, albeit quantitatively untested assumption, that interhemispheric asynchrony would be an essential property in the abnormal EEG near term age.

SUBJECTS AND EEG RECORDINGS

A total of 31 neonatal EEG traces [postmenstrual age (PMA) 36–42 weeks], were retrospectively selected by an expert (A.D.) to assess the spontaneous background EEG activity. These EEG recordings were collected from a larger EEG dataset, recorded for clinical purposes. All EEG data were recorded at 256 Hz with a video-synchronized EEG device (BRAIN RT, OSG equipment, Mechelen, Belgium). After skin preparation (Nuprep Gel), 10–17 Ag/AgCl cup electrodes were placed according to the international 10–20 standard locations. The reference electrode was Cz. Electrode impedance was below 10 kΩ at the start, and the signal quality was monitored visually throughout the recording. The minimum recording time was 4 h to record multiple vigilance states. The protocol was reviewed and approved by the relevant Ethics Committee of the University Hospitals of Leuven, Belgium.

The EEG records were reviewed for clinical purposes by two independent raters (A.D. and K.J.) who were not aware of the later use of the EEG for this study. Hence, they were fully blinded to both the overall design as well as the numerical ASI results. The clinical assessment is based on holistic, conventional visual criteria (see Table 1 in Supplementary Material). If there was any difference in the interpretation of an EEG, a consensus was reached after re-evaluation (2 patients, Table 1 in Supplementary Material). The following parameters were assessed on the whole measurement, according to standard developmental features in preterm and term EEG (Scher et al., 2005; André et al., 2010; Shellhaas et al., 2011; Hayashi-Kurahashi et al., 2012): (1) brain activity cycling as being normal or abnormal for the age; (2) grade of continuity; (3) age-specific landmarks: amplitude, disorganization, and dysmaturation patterns; and (4) qualitative synchrony in quiet sleep. The overall clinical classification of the EEG recording as normal ($n = 14$) vs. abnormal ($n = 17$) was based on observing at least two features that were not appropriate for age.

ACTIVATION SYNCHRONY INDEX

The ASI algorithm implemented in Matlab is described in full detail in the original publication (Räsänen et al., 2013). It takes two EEG-signals (e.g., bipolar derivations in left and right hemispheres, respectively) as inputs to be processed through four main stages (**Figure 1C**): (1) preprocessing; (2) computation of signal amplitude envelope; (3) quantization of the amplitude envelope; and (4) calculation of the ASI value, a single scalar value, from the temporal relationship of the two quantized signals. Technical details of the algorithm can be found in the Supplementary Material. For as long as the peaks in energy envelopes are temporally co-incident (clinically perceived as "synchronized"), their dependency is highest at zero lag and diminishes with increasing relative lag between the two channels, thereby leading to a high ASI value. On the other hand, lack of temporal co-incidence, the signature of low-synchrony, will result in low ASI (for example signals, see **Figure 1B** or Räsänen et al., 2013).

PARAMETER OPTIMIZATION

The prior work on ASI development defined the main parameter settings, the most important of which appeared to be the definition of the frequency band, and the weighting of higher frequencies (a.k.a. "pre-emphasis"). These yielded an ASI that can discriminate between different visually rated IHS grades, and which clearly outperforms the other methods proposed earlier in

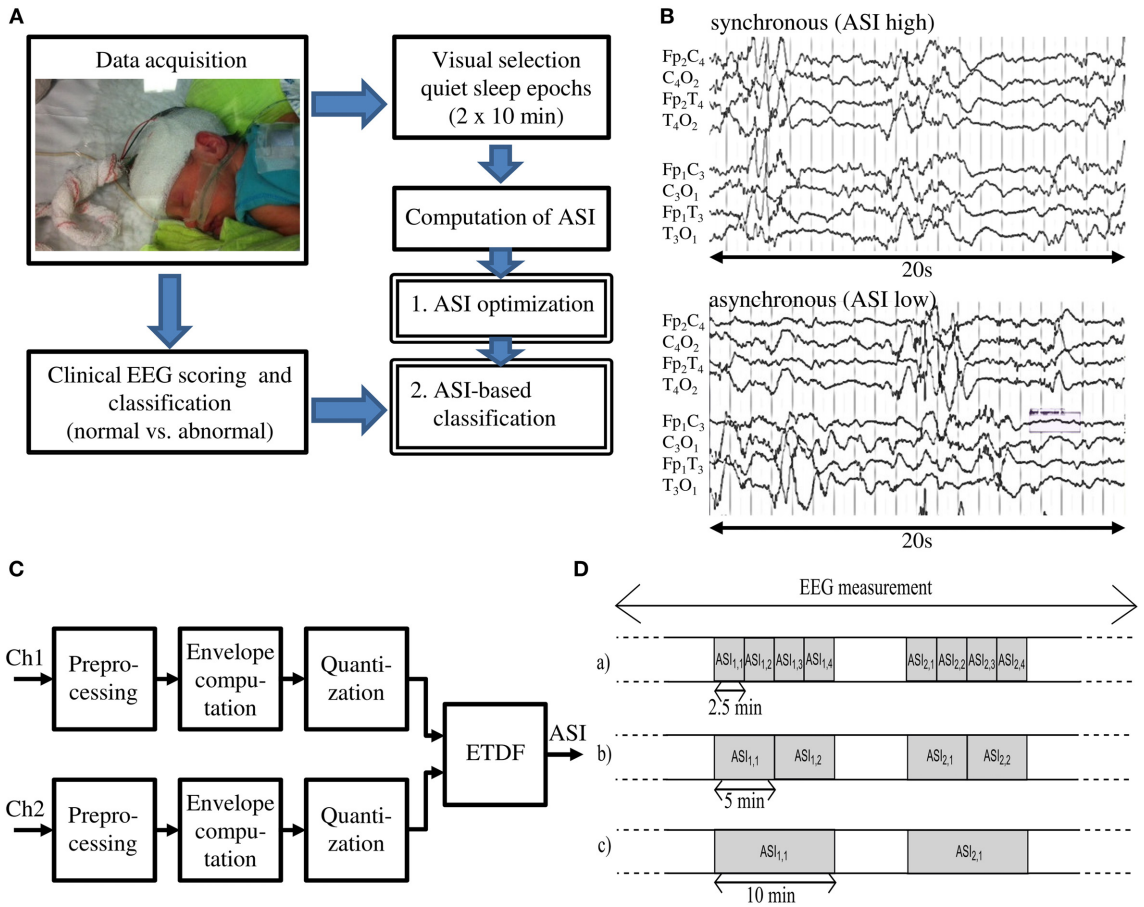

FIGURE 1 | (A) Schematic overview of the presented method. **(B)** EEG tracks with Normal and Abnormal synchrony. **(C)** Schematic view of the ASI algorithm (Räsänen et al., 2013). **(D)** Two 10-min quiet sleep epochs are subdivided into shorter epochs of 2.5, 5, and 10 min for analysis, which gives respectively *ASI2.5, ASI5,* and *ASI10* values.

the literature (Räsänen et al., 2013). However, it was not shown (1) how stable the ASI is technically and physiologically within an individual; (2) what window length would allow the most practical setting in clinical practice where selecting longer data epochs is always challenged by the intermittent, trivial artifacts; and (3) which of the bipolar EEG derivations would produce the best results.

Stability over time

It is commonly assumed by clinicians that IHS is a fairly stable property of a given brain function, at least at the scale of multiple hours. Thus, the IHS measure should be comparable between successive sleep cycles, and at least between few-minute epochs within a given QS period. Theoretically and physiologically thinking, it is also possible, and may even be more likely, that subtle fluctuations occur in the IHS over time. The clinically required intraindividual stability of our measure by a test-retest paradigm is technically straightforward, but the differences to be seen in repeated measures are affected by multiple factors. First, there is a numerical uncertainty in the measure itself when recorded from typically noisy neonatal recordings. Second, the feature quantified by ASI may change due to subtle fluctuations in brain state at multi-minute scale. The former possibility is typically tackled by using longer data epochs, while the latter possibility is better assessed by looking at multiple shorter data epochs. Hence, we decided to study the whole range of epoch lengths and numbers that we felt could be practical in future clinical implementations.

To this end, we divided the original 10-min data epochs into 10, 5, and 2.5-min epochs, and examined ASI in each. The aim was to define the epoch length with the smallest possible intra-patient deviations. This was assessed by searching for the lowest mean-squared difference (MSD) between the (average) ASI value of the first 10-min epoch (ASI_1) and the (average) ASI value of the second 10-min epoch (ASI_2). In formula 1 this difference is squared, summed and averaged over all patients, with n representing the number of patients.

$$MSD = \frac{1}{n}\sum_{i=1}^{n}(ASI_{1,i} - ASI_{2,i})^2 \quad (1)$$

MSD measures the difference between the different ASI values within an individual. The optimal ASI parameters were expected

to give the lowest MSD. In this way, a MSD minimization problem is solved as a function of different channel pair combinations and different ASI window lengths.

A further issue to investigate was the stability of ASI between different quiet sleep epochs. In clinical practice, it may not always be possible to find long epochs of undisturbed and good signal quality epochs of quiet sleep. Therefore, more data could be readily gathered from successive sleep cycles. Hence, we analyzed either continuous 20-min epochs from one cycle or two 10-min epochs from successive cycles.

ASI window length

ASI is a statistical estimate of synchrony, and its numerical accuracy ("technical reliability") will increase when the analysis epochs get longer. Our earlier work showed that an ASI estimate becomes more stable when the epochs grow longer than about 2 min (Räsänen et al., 2013). Longer EEG epochs are needed to statistically quantify temporal co-incidence of pseudoperiodic, intermittent cortical activity. In this work, we searched for the optimal window by calculating the ASI feature for window lengths of 2.5, 5, and 10 min. To have a fair comparison between different window lengths, we studied two manually-selected epochs of 10 min. First, we divided each epoch into 4 equal parts of 2.5 min from which we separately computed the ASI value (*ASI2.5*), and then averaged them (**Figure 1D** upper part). Similarly, the 10-min epoch was split into two equal parts of 5 min and the ASI values (*ASI5*) were estimated and averaged (**Figure 1D** middle part). These average ASI values were compared to the single ASI value from the 10-min analysis (*ASI10*) (**Figure 1D** lower part).

Channel pair combination

IHS is traditionally analyzed from bipolar derivations (Lombroso, 1979) rather than from individual EEG signals (Omidvarnia et al., 2014). To comply with this idea, we also analyzed ASI from symmetric bipolar derivations. We wanted to define the derivation with least intraindividual variability. Hence, we computed ASI from the following symmetric combinations; Fp_1C_3-Fp_2C_4, C_3O_1-C_4O_2, Fp_1O_1-Fp_2O_2, Fp_1T_3-Fp_2T_4, T_3O_1-T_4O_2.

CLASSIFICATION

After optimization of the ASI parameters, we examined the ability of ASI to distinguish normal and abnormal EEG recordings classified by clinical criteria. To this end, we used 20 min of data, channel pair combination C_3O_1-C_4O_2, and 2.5-min ASI analysis windows *(ASI2.5)*. This gave us two average ASI estimates in each patient, derived from the two 10-min epochs (**Figure 1D** upper part). The lower of these was used to represent the lowest possible synchrony level in the given patient (ASI_{class}).

$$ASI_{class} = minimum\,(mean_1\ ASI2.5,\ mean_2\ ASI2.5) \quad (2)$$

Next, we searched for a threshold that could distinguish normal and abnormal EEG records. The optimal ASI settings were found to yield nearly non-overlapping distributions of ASI values in the two groups, so the ASI threshold can be readily drawn between the distributions. However, we then wanted to see how much ASI-based classification would be compromised if the user has only a limited amount of data available for the ASI computation. In this situation, distributions between ASI values in the two groups are overlapping. Hence, all thresholds will have their own classifier performance, i.e., levels sensitivity and specificity. Their dependence on the threshold can be readily visualized using receiver operating characteristic (ROC) curves that were computed to assess the classifier performance as a function of thresholds.

AGE DEPENDENCE OF ASI

Finally, we studied the dependence of ASI on PMA to know whether it should be taken as a confounder in babies near term age. It is known that both anatomical and electrical cortico-cortical connectivity increases toward term age (Kostovic and Judas, 2010; Omidvarnia et al., 2014). The previous study with ASI showed a modest age-dependence in a much younger group of preterm babies compared to our present group of fullterm newborns (Räsänen et al., 2013). This could be a biological confounder when using ASI on babies with a wider age range.

RESULTS

OPTIMAL PARAMETERS FOR ASI STABILIZATION

In **Figure 2**, we show the ASI comparison of 10-min epochs for two clinically relevant channel pair combinations (Fp_1C_3-Fp_2C_4 and C_3O_1-C_4O_2). Visual inspection of the scatter plots shows that least scatter is found for C_3O_1-C_4O_2 in combination with smaller ASI windows (2.5 min). Quantitation of the scatter with MSD is summarized in **Table 1** for all channel pair combinations and ASI window lengths. Out of all channel pairs tested, C_3O_1-C_4O_2 yielded the lowest MSD values. Out of all combinations of ASI windows tested, the average over 4 windows of 2.5 min led to the lowest MSD.

Next, we tested how stable the ASI value is for different selections of epochs in the whole EEG recording. We could find uninterrupted 20-min epochs of "artifact-free" quiet sleep in only a few patients, while in most of them the EEG was interrupted by arousals, movements or care procedures. Therefore, a scatter plot is shown for the analysis of an epoch of the same quiet sleep period (20 min) and of two epochs of different quiet sleep periods (2×10 min) (**Figure 3**). There is no significant difference in the MSDs between the epochs taken from the same vs. different quiet sleep epochs (mean MSD_subsequent = 1.061 and mean MSD_separated = 1.066, respectively; $p = 0.12$; Mann–Whittney *U*-test).

CLASSIFICATION

Using the two epochs of 10 min, we plotted the ASI values using the best channel pair (C3O1-C4O2) and window lengths (4×2.5 min), and labeled them according to clinical EEG judgments. As shown in **Figure 4**, the distributions of ASI values in the two groups are distinct. Comparison of the smaller of the two ASI values in each baby shows that the difference is highly significant ($p < 0.001$, *t*-test). A tentative cut-off set at ASI = 3.6 gives only one misclassified normal baby (pt #28) having an ASI below that limit, yielding a very high classification accuracy (96.77%). This patient was clinically classified as normal due to age-specific transients interpreted as "borderline" for the PMA

age of 37.6 weeks (i.e., "immaturity"), which as a clinical finding does not need to be associated with globally abnormal function detected by ASI.

After observing such high classification accuracy using 2 × 10 min EEG epochs, we finally wanted to do a *post-hoc* analysis to see how the classification accuracy is affected by reduction in EEG data. This is important for clinical studies where the ideal 20 min of good quality EEG from quiet sleep is usually not available. Hence, we systematically examined a range of EEG lengths (5, 10 or 20 min), ASI window lengths (2.5, 5, and 10 min), as well as the way of combining the ASI values from multiple windows. Instead of attempting formal statistical comparisons, we aimed to provide useful practical answers by visually analyzing how the ROC curves change when the underlying data and analysis settings are changed. As an expected finding in the visual comparison of ROC curves, using more EEG data led to a generally better overall classification (**Figure 5**). We also observed that the length of the ASI window made a difference such that shorter ASI windows tended to yield higher classification accuracy. Moreover, the way of combining ASI estimates of multiple windows (mean vs. minimum vs. maximum) also appeared to affect the classification accuracy. Taking the mean ASI value from several windows seemed to produce more accurate classifications. However, qualitative comparison of ROC curves based on subsequent 5-min epochs showed that the classification accuracy varies considerably.

AGE DEPENDENCE OF ASI

ASI was not found to significantly correlate with PMA in infants near term age (PMA >36 weeks) (**Figure 6**), and the slopes of the linear regression lines are very small. Hence, the same cut-off can

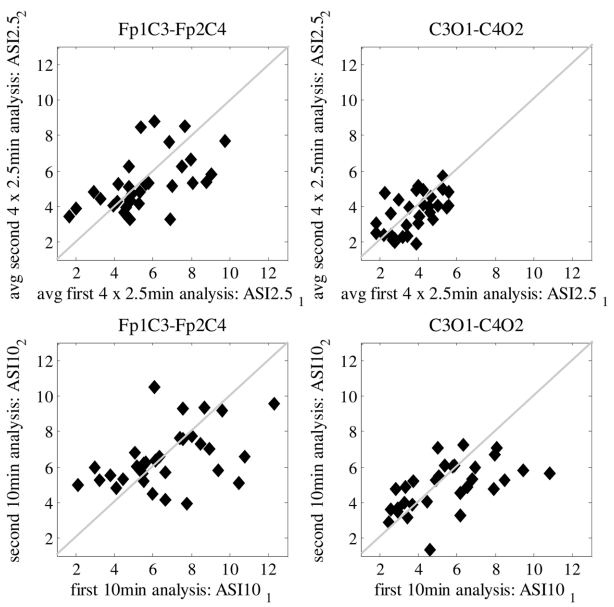

FIGURE 2 | Difference in mean-squared difference (MSD) between two analyzed periods of 10-min EEG, every dot representing a different patient. Results are shown for Frontal-Centro (Fp-C) and Centro-Occipital (C-O) derivations for different analyzing window lengths (2.5/10 min). Best result with lowest MSD is shown in the upper right plot, obtained for average ASI values over 4 × 2.5 min analysis on C-O derivations.

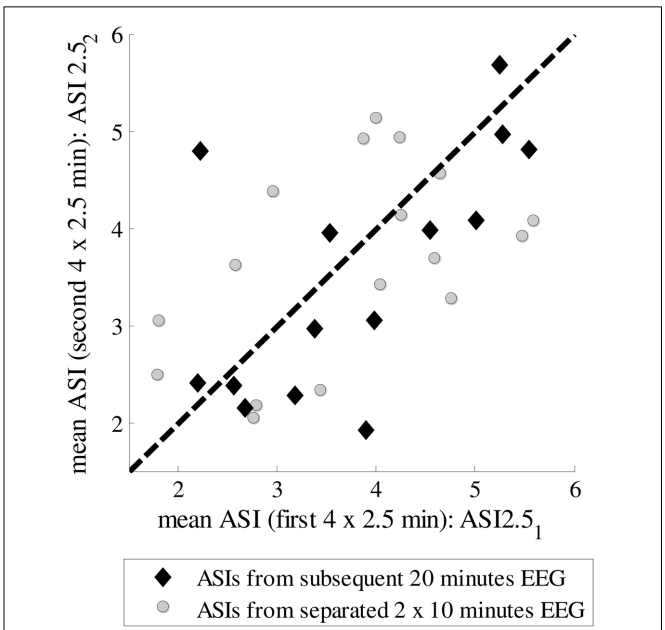

FIGURE 3 | ASIs for subsequent 10-min epochs from the same quiet sleep period or for separate 10-min epochs from two different quiet sleep periods.

Table 1 | Mean squared difference (MSD) for different channel pairs and different ASI analyzing window lengths shown as an average for all 31 patients.

	Fp_1C_3-Fp_2C_4	C_3O_1-C_4O_2	Fp_1O_1-Fp_2O_2	Fp_1T_3-Fp_2T_4	T_3O_1-T_4O_2	Mean MSD_ch
ASI_10 min	4.84	3.58	6.05	4.76	5.22	4.89
ASI avg_4 × 2.5min	2.99	1.06	1.63	1.15	2.02	1.77
ASI avg_2 × 5 min	9.90	4.23	8.60	5.51	5.25	6.70
ASI avg_2 × 2.5 min	3.21	2.22	3.82	2.91	3.74	3.18
ASI_5 min	7.59	4.71	5.71	5.38	9.05	6.49
Mean_MSD ASIwindows	5.71	316	5.16	3.94	5.06	

*Grand averages of the MSD values over all channel pair combinations and window lengths are shown as well. Examples shown in **Figure 2** are underlined in this table.*

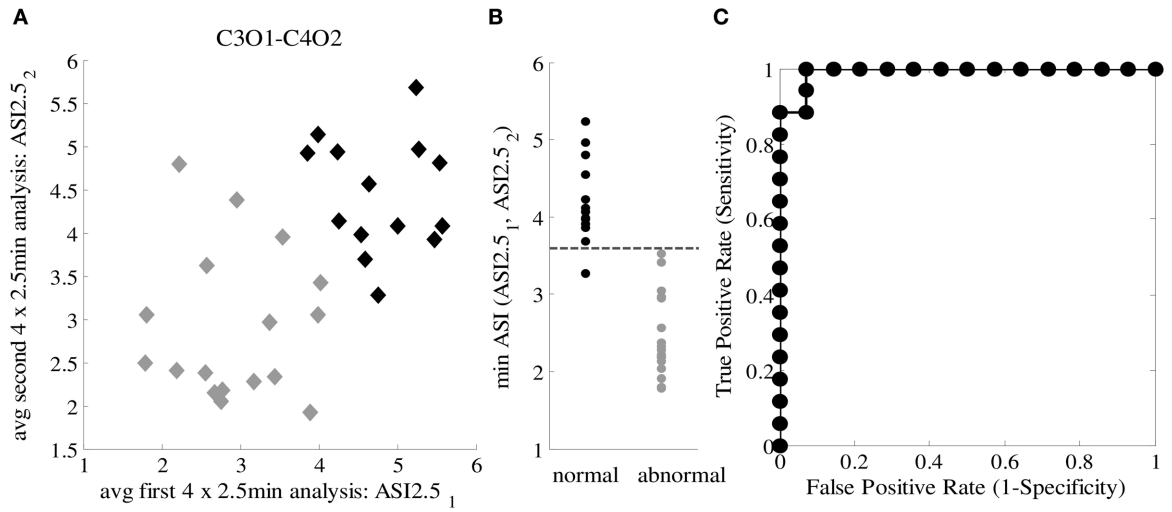

FIGURE 4 | (A) ASI2.5$_1$ and ASI2.5$_2$ for both 10-min EEG segments from 31 patients for C-O derivation with the lowest MSD value. Two groups are specified: normal patients (black labels) and abnormal patients (gray labels). **(B)** Discrimination between normal and abnormal ASI taking the minimum ASI of ASI2.5$_1$ and ASI2.5$_2$ and thresholding (Th_ASI = 3.6). **(C)** ROC curve for classification, AUC = 0.971.

be applied to distinguish normal and abnormal EEG throughout this age range, and no correction for PMA is needed.

DISCUSSION

Our study shows that IHS is a very robust feature of normal neonatal EEG, and that it can be readily quantified by using the novel metric ASI. We further show that ASI is able to reach the same classification that has been traditionally reached by a skilled EEG clinician when combining multiple visually-identified signal features. To the best of our knowledge, this study provides the first quantitative evidence in support of the old clinical thinking that disturbance of neonatal brain function is readily reflected in the interaction between hemispheres. We extend the earlier work with ASI by providing detailed assessment of how ASI performance is affected by variations in data length or analysis settings. As a conclusion, the results provide guidance for future employment of ASI in clinical work and research as well as in the development of automated EEG classifiers.

INTRAINDIVIDUAL STABILITY AND MEASUREMENT STABILITY: SELECTION OF SMALL EPOCHS

We found that the most stable ASI value was obtained by using the mean of multiple short-term ASI values, each estimated from a 2.5-min epoch. Physiologically, this observation suggests that long-range temporal correlations in the IHS are limited over time. Temporal correlations in amplitude fluctuations over several minutes have been shown in the adult brain (Linkenkaer-Hansen et al., 2001). Our recent observations in neonatal EEG datasets suggest, however, that only limited temporal correlations can be seen in the neonatal EEG signals (Matic et al., submitted), indirectly supporting the idea that ASI analyses may also best operate when using limited window lengths. Clinically and methodologically, using short segments offers several advantages in future studies and for possible implementation in brain monitoring algorithms. It is relatively easy to find several 2.5-min long undisturbed and sufficiently high quality (cf. Räsänen et al., 2013) EEG segments from neonatal recordings, while requesting longer (e.g., 10 min) continuous and undisturbed EEG epochs would pose a serious limitation in the future use of ASI. We suggest that the minimum duration of the recordings should be long enough to improve the statistical value and to overcome technical artifacts and subtle fluctuations in brain state at the multi-minute level. To this end, one should aim to collect a total of up to 20 min of quiet sleep data, which may come from successive sleep cycles. Reduction of the total data to 10 min will compromise individual diagnostic accuracy; however, it would only moderately decrease the utility of ASI at group level analyses (e.g., as an early biomarker).

CHANNEL PAIR COMBINATION AND CUT-OFF VALUE

We found that the best intraindividual stability is obtained from using central-occipital derivation. Despite decades of clinical visual assessment of IHS, there are no established practices as to which derivations should be used. A common clinical experience is that temporal co-incidence of activity bursts varies between brain areas, especially when the IHS is decreased in sick babies. It is also common to have disturbing movement and muscle artifacts in the frontal and temporal channels. Our finding suggests that ASI is optimally measured from a derivation that, by co-incidence, also happens to be usually clean of artifacts. This helps implementation of ASI in future studies. Physiologically, this finding is compatible with current knowledge of neonatal brain networks. It is well established that anatomical neonatal networks grow first in post-central regions (Kostovic and Judas, 2010), and that neonatal EEG activity mostly occurs in posterior regions (André et al., 2010). It was also shown recently that there is a prominent posterior-parietal network in the newborn brain created by long-range amplitude

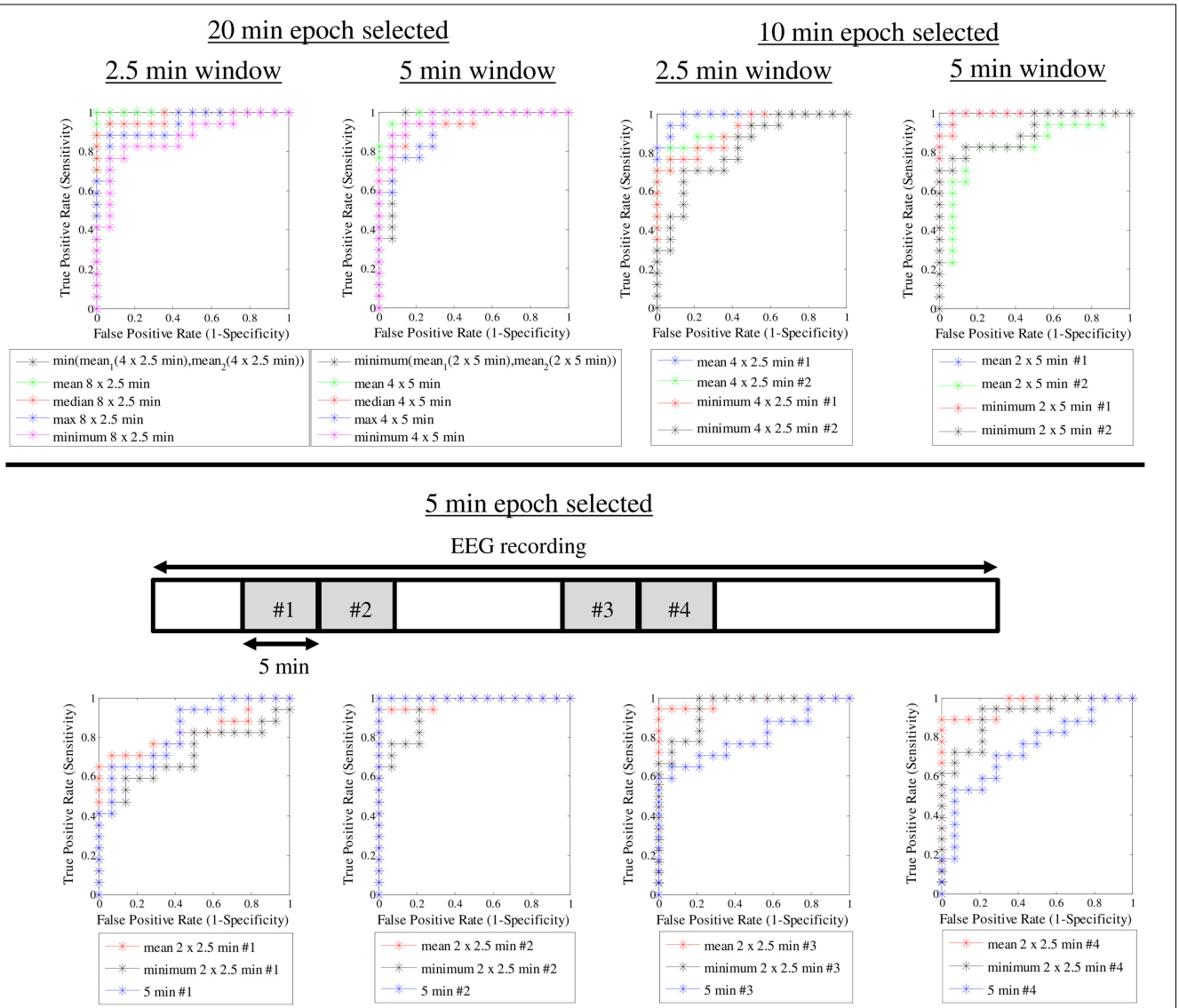

FIGURE 5 | ROC curves for different ASI window lengths and different epoch lengths.

correlations (Omidvarnia et al., 2014), which as a coupling mechanism comes close to what is measured by ASI. Taking these together, our observations suggest that the post-central networks may be the key driver of interhemispheric connectivity, and the traditionally observed loss of IHS in sick babies is probably due to changes in these posterior networks. Further studies are warranted to study whether different structural pathologies could give rise to altered IHS in a spatially selective manner.

AGE INDEPENDENCY OF ASI

We found a clear cut-off across the whole age range of babies, which suggests that future ASI implementation can disregard PMA when studying babies near term age. The younger infants in our group (PMA 36–38 weeks) showed more interindividual variability, which may reflect the as yet poorly established brain networks at that age. It has been shown that both the anatomical growth of callosal connections (Kostovic and Judas, 2010) and the appearance of visually observed IHS (Tharp et al., 1989; André et al., 2010) take place only a few weeks earlier, up to the 35th week of gestation. It is commonly seen in the clinic in these younger babies (data not shown) that the onset of quiet sleep may be markedly asynchronous and that synchrony increases within the quiet sleep period. Such dynamics could arise from functional instability in the young networks, which would readily explain a larger variability both within and between individuals.

FUTURE DIRECTIONS

Finding a high correlation between ASI and the traditional clinical visual EEG classification suggests that ASI may provide an objective and quantified global biomarker for neonatal

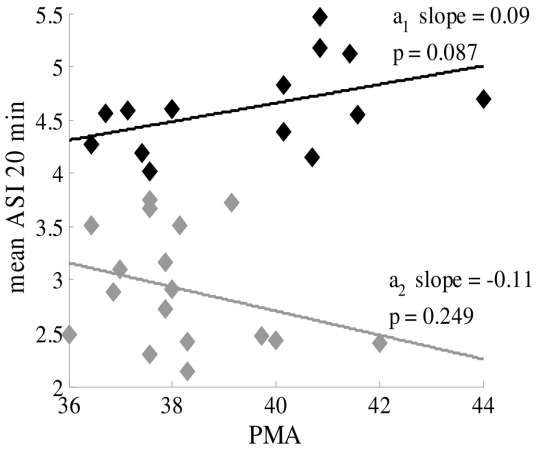

FIGURE 6 | ASI value is independent of postmenstrual age of the term infant (PMA >36 weeks). Black labels represent healthy patients with synchronous patterns; gray labels are patients with asynchronous patterns. The mean ASI value is calculated for manually-selected 20-min periods (8 × 2.5 min).

brain function. Its design makes it physiologically reasoned; our current work makes it clinically benchmarked; and its technical properties make it transparent and straightforward to implement. Hence, it holds promise for becoming a useful feature in future clinical work and research, as well as in the construction of automated classifiers of neonatal EEG. In this context, finding quiet sleep periods in an automated way would be beneficial.

This research has potential value, as prematurity-associated injury of the subplate, early extrauterine environmental stimulation, and acquired brain lesions may induce a structural adaptation of synapses and, consequently, alter the normal differentiation of cortical connectivity or even disruption of the cortical network development. These altered brain functions, expressed as levels of inter- and intrahemisperic synchrony, may reflect transiently or permanently disturbed connectivity of the cortico-cortical and cortico-basal ganglia connections, even in the absence of standard neuroimaging abnormalities. Further work for clinical research may include ASI as an outcome parameter in standardized neurodevelopment follow-up data and may also include quantitative analyses of synchrony in preterm and term infants, to identify normative and altered patterns of development.

ACKNOWLEDGMENTS

Research supported by Research Council KUL: GOA/10/09 MaNet, CoE PFV/10/002 (OPTEC); PhD/Postdoc grants; Flemish Government: FWO, IWT: projects: TBM 110697-NeoGuard; PhD/Postdoc grants; IWT project 110697; Belgian Federal Science Policy Office: IUAP P7/19/ (DYSCO); EU: ERC Advanced Grant: BIOTENSORS (n° 339804). Sampsa Vanhatalo and Okko Räsänen were supported by the Academy of Finland. Sampsa Vanhatalo was also supported by the European Community's Seventh Framework Programme European Community (FP7-PEOPLE-2009-IOF, grant agreement n°254235, as well as FP7-HEALTH-2009-4·2-1, grant agreement no. 241479, The NEMO Project).

SUPPLEMENTARY MATERIAL

The Supplementary Material for this article can be found online at: http://www.frontiersin.org/journal/10.3389/fnhum.2014.01030/abstract

REFERENCES

André, M., Lamblin, M.-D., d'Allest, A. M., Curzi-Dascalova, L., Moussalli-Salefranque, F. S., Nguyen The, T., et al. (2010). Electroencephalography in premature and full-term infants. Developmental features and glossary. *Clin. Neurophysiol.* 40, 59–124. doi: 10.1016/j.neucli.2010.02.002

Dudink, J., Kerr, J. L., Paterson, K., and Counsell, S. J. (2008). Connecting the developing preterm brain. *Early Hum. Dev.* 84, 777–782. doi: 10.1016/j.earlhumdev.2008.09.004

Hayashi-Kurahashi, N., Kidokoro, H., Kubota, T., Maruyama, K., Kato, Y., Kato, T., et al. (2012). EEG for predicting early neurodevelopment in preterm infants: an observational cohort study. *Pediatrics* 130, 891–897. doi: 10.1542/peds.2012-1115

Holmes, G. L., and Lombroso, C. T. (1993). Prognostic value of background patterns in the neonatal EEG. *Clin. Neurophysiol.* 10, 323–352.

Kostovic, I., and Jovanov-Milosevic, N. (2006). The development of cerebral connections during the first 20-45 weeks' gestation. *Semin. Fetal Neonatal Med.* 11, 415–422. doi: 10.1016/j.siny.2006.07.001

Kostovic, I., and Judas, M. (2010). The development of the subplate and thalamocortical connections in the human foetal brain. *Ácta Paediatr.* 99, 1119–1127. doi: 10.1111/j.1651-2227.2010.01811

Linkenkaer-Hansen, K., Nikouline, V. V., Palva, J. M., and Ilmoniemi, R. J. (2001). Long-range temporal correlations and scaling behavior in human brain oscillations. *J. Neurosci.* 21, 1370–1377.

Lombroso, C. T. (1979). Quantified electrographic scales on 10 pre-term healthy newborns followed up to 40-43 weeks of conceptional age by serial polygraphic recordings. *Electroencephalogr. Clin. Neurophysiol.* 46, 460–474.

Lubsen, J., Vohr, B., Myers, E., Hampson, M., Lacadie, C., Schneider, K. C., et al. (2011). Microstructural and functional connectivity in the developing preterm brain. *Semin. Perinatol.* 35, 34–43. doi: 10.1053/j.semperi.2010.10.006

Omidvarnia, A., Fransson, P., Metsäranta, M., and Vanhatalo, S. (2014). Functional bimodality in the brain networks of preterm and term human newborns. *Cereb. Cortex* 24, 2657–2668. doi: 10.1093/cercor/bht120

Räsänen, O., Metsäranta, M., and Vanhatalo, S. (2013). Development of a novel robust measure for interhemispheric synchrony in the neonatal EEG: activation synchrony index (ASI). *Neuroimage* 69, 256–266. doi: 10.1016/j.neuroimage.2012.12.017

Scher, M. S., Turnbull, J., Loparo, K., and Johnson, M. W. (2005). Automated state analyses: proposed applications to neonatal neurointensive care. *Clin. Neurophysiol.* 22, 256–270. doi: 10.1097/01.WNP.0000161418.87923.10

Shellhaas, R. A., Chang, T., Tsuchida, T., Scher, M. S., Riviello, J. J., Abend, N. S., et al. (2011). The American clinical neurophysiology society's guideline on continuous electroencephalography monitoring in neonates. *Clin. Neurophysiol.* 28, 611–617. doi: 10.1097/WNP.0b013e31823e96d7

Tharp, B. R., Scher, M. S., and Clancy, R. R. (1989). Serial EEGs in normal and abnormal infants with birth weights less than 1200 grams–a prospective study with long term follow-up. *Neuropediatrics* 20, 64–72. doi: 10.1055/s-2008-1071267

Uhlhaas, P. J., Roux, F., Rodriguez, E., Rotarska-Jagiela, A., and Singer, W. (2010). Neural synchrony and the development of cortical networks. *Trends Cogn. Sci.* 14, 72–80. doi: 10.1016/j.tics.2009.12.002

Conflict of Interest Statement: The authors declare that the research was conducted in the absence of any commercial or financial relationships that could be construed as a potential conflict of interest.

Received: 15 October 2014; paper pending published: 12 November 2014; accepted: 07 December 2014; published online: 23 December 2014.
Citation: Koolen N, Dereymaeker A, Räsänen O, Jansen K, Vervisch J, Matic V, De Vos M, Van Huffel S, Naulaers G and Vanhatalo S (2014) Interhemispheric synchrony in the neonatal EEG revisited: activation synchrony index as a promising classifier. Front. Hum. Neurosci. ***8****:1030. doi: 10.3389/fnhum.2014.01030*
This article was submitted to the journal Frontiers in Human Neuroscience.